Development of original strategies for the electrochemical detection of cell-penetrating peptides and for the electrochemical bleaching of fluorescent probes : an entry to the monitoring of translocation in phospholipid membranes

Ana Isabel Perez Jimenez

THÈSE DE DOCTORAT

de l'Université de recherche Paris Sciences et Lettres
PSL Research University

Ecole Normale Supérieure

Development of original strategies for the electrochemical detection of cell-penetrating peptides and for the electrochemical bleaching of fluorescent probes: an entry to the monitoring of translocation in phospholipid membranes

Ecole doctorale 388

Chimie Physique et Chimie Analytique de Paris-Centre

Spécialité : Chimie

COMPOSITION DU JURY :

M. SOJIC Neso
ENSCPB, Rapporteur

M. DE OLIVEIRA Pedro
PARIS SUD, Rapporteur

Mme. LAVIELLE Solange
UPMC, Membre du jury

M. BEDIOUI Fethi
CHIMIE PARIS TECH, Membre du jury

M. AMATORE Christian
ENS, Membre du jury

M. LABBE Eric
ENS, Membre du jury

M. BURIEZ Olivier
ENS, Membre du jury

Soutenue par Ana Isabel **PEREZ JIMENEZ**
le 19 Septembre 2016

Dirigée par Olivier BURIEZ

Département de CHIMIE

Acknowledgements

First and foremost, I would like to extend my deepest gratitude to Professor Christian Amatore for welcoming me in his group and for his insight and guidance over the course of my Ph.D. studies.

I would also like to express my sincere thanks to my thesis advisor, Olivier Buriez, and Eric Labbé for the opportunity to work with them, fostering my development as a scientist, and sharing their knowledge.

To my reviewers, Neso Sojic and Pedro de Oliveira, thank you for your time and attention in reading and considering my thesis work. And to my jury, Solange Lavielle and Fethi Bedioui, thank you for evaluating this work.

I would like to acknowledge Lylian Challier and Margherita Di Pisa for training me at the beginning of my project, as well as Gerard Chassaing for helpful discussions.

I would like, in particular, to thank Jérôme Delacotte not only for training me, but also for his scientific input and career advice. It has been a pleasure working with you.

To Laurence Grimaud, thank you for your moral support in and outside of lab.

Thank you to all the members of the laboratory for creating an enjoyable and productive work environment, as well as to all those in neighboring labs for the collegial environment and scientific discussions. In no particular order: Xiaoqing, Lihui, Indira, Alexandra S, Rachel, Martina, Baptiste, Adnan, Luca, Damian, Thomas, Hakin, Marie Aude, Alexandra C, and the rest of biophysical group.

To my dear family, thanks for trusting me. This accomplishment is for you.

To my foolish friends: Marina, Monserrat, Manel, Alison, Xiaoqing, Isabel, Margherita, LiZhi, Miguel, Luca, Lylian, Baptiste Adnan …

Thanks to The Mexican National Council of Science and Technology for funding my Ph.D. work.

Contents

Abbreviations

Ag/AgCl	Silver/Silver Chloride (Pseudo-reference electrode)
AMP	Antimicrobial Peptides
Au	Gold
CPP	Cell-Penetrating Peptide
CV	Cyclic Voltammetry
D_L	Lateral Diffusion
DMF	Dimethylformamide
DOPC	1,2-dioleoyl-*sn*-glycero-3-phosphocholine
DOPG	1,2-dioleoyl-sn-glycero-3-phosphoglycerol
DPhPC	1,2-diphytanoyl-sn-glycero-3-phosphocholine
DPPG	1,2-dipalmitoyl-*sn*-glycero-3-phospho-(1'-*rac*-glycerol)
D_R	Rotational Diffusion
Fc-$(Arg)_9$	Ferrocene-Arginine 9
Fc	Ferrocenyl unit
FLAP	Fluorescence Localization After Photobleaching
FLIM	Fluorescence Lifetime Imaging Microscopy
FLIP	Fluorescence Loss In Photobleaching
FRAP	Fluorescence Recovery After Photobleaching
FRET	Förster or Fluorescence resonance energy transfer
GUV	Giant unilamellar vesicles
ITO	Indium Tin Oxide
LUV	Large unilamellar Vesicle
NBD	4-nitrobenzo-2-oxa-1,3-diazol-4-yl
NBD-G	NBD-glycine
NBD-PE	1,2-dipalmitoyl-sn-glycero-3-phosphoethanolamine-N-(7-nitro-2-1,3-benzoxadiazol-4-yl)
NO	Nitrogen Oxide
PBS	Phosphate buffer saline
PC	Phosphatidylcholine
PDMS	Polydiméthylsiloxane
PE	Phosphatidylethanolamine
PG	Phosphatidylglycerol
PS	Phosphatidylserine
RE	Reference Electrode
ROI	Region of interest
ROS	Reactive Oxygen Species
SCE	Saturated Calomel Electrode
SEM	Scanning Electrochemical Microscopy
SUV	Small Unilamellar Vesicles
T	Temperature
T_m	Phase transition temperature
UME	Ultramicroelectrode
W	Working Electrode
µRE	Microscale reference electrodes

Résumé

I) Introduction

L'électrochimie est un outil puissant pour détecter, activer, étudier la réactivité et les mécanismes impliquant des molécules à haute valeur ajoutée. Dans ce cadre, une utilisation judicieuse des techniques et approches électrochimiques peut conduire à de nouvelles perspectives dans des domaines fondamentaux comme la chimie analytique et la biologie moléculaire. Pour atteindre cet objectif, il est important d'adapter nos méthodes électrochimiques aux phénomènes étudiés et non l'inverse. Ainsi, la miniaturisation des électrodes permet d'étudier de nombreux mécanismes de réactions catalysées par des métaux de transition et réalisées dans des milieux organiques résistifs [1]. En outre, le développement d'ultra-microélectrodes a permis d'ouvrir un nouveau champ d'investigations dénommé bio-électrochimie dans lequel les méthodes électrochimiques sont particulièrement utiles pour l'analyse *in vitro* de biomolécules [2]. Ainsi, les électrodes de tailles micrométriques sont très pratiques pour étudier les mécanismes conduisant à la libération de biomolécules au niveau d'une cellule vivante unique comme, par exemple, le stress oxydant (libération d'espèces réactives oxygénées (ROS) et azotées (RNS)) et l'exocytose vésiculaire (sécrétion de neurotransmetteurs par des cellules endocriniennes) [3]. Parfois, l'électrochimie doit être combinée avec d'autres techniques pour s'attaquer à ce type de questions importantes. Ainsi, la combinaison de techniques électrochimiques et de fluorescence a permis de mieux appréhender des phénomènes biologiques comme l'exocytose [4].

Bien que l'électrochimie soit déjà très utilisée pour apporter de nouvelles perspectives dans de nombreuses questions d'ordre biologique, il en reste encore beaucoup ainsi que des controverses où les techniques électrochimiques peuvent être très utiles. Le passage transmembranaire de peptides cationiques tels que les peptides pénétrants (Cell-Penetrating Peptides (CPPs) en anglais) en est un exemple frappant/important. L'intérêt de la communauté scientifique pour cette classe originale de peptides n'a cessé de croître ces dernières années en raison de leur capacité à traverser les membranes plasmiques de cellules de mammifères permettant ainsi de transporter efficacement et avec une faible cytotoxicité des molécules biologiquement actives [5, 6]. Cependant, la pénétration de ces peptides cationiques au travers des membranes cellulaires est un processus complexe dont la description et la représentation restent encore incomplètes notamment au niveau des aspects dynamiques. Malgré le développement de nombreuses études à la fois *in vitro* et *in vivo*, basées notamment sur des techniques de fluorescence, la nature des mécanismes impliqués pendant les passages transmembranaires de peptides cationiques fait encore débat [7]. Pourtant, la

compréhension de tels mécanismes est cruciale notamment pour le développement de stratégies pour la vectorisation *in vivo* de molécules thérapeutiques ainsi que le développement de nouveaux agents thérapeutiques. En réalité, l'origine de la controverse vient essentiellement du fait qu'il est très difficile, voire impossible, de distinguer, sans ambigüité, la fluorescence émise par les peptides réellement internalisés de celle émise par ceux restés au niveau de la membrane externe.

Des protocoles ont été développés pour contourner ce problème. Le plus commun consiste à éteindre la fluorescence émise par des peptides non internalisés portant un fluorophore.

Cette difficulté est généralement contournée via l'extinction de la fluorescence émise par les peptides non internalisés et marqués avec le fluorophore NBD (4-nitrobenzo-2-oxa-1,3-diazol-4-yl) par le dithionite ($S_2O_4^{2-}$) qui agit comme un réducteur chimique [8, 9]. Néanmoins, il a été récemment démontré que ce réducteur chimique est capable de traverser les membranes vésiculaires [10]. Cette propriété peut ainsi remettre en cause toutes les études basées sur l'extinction de la fluorescence par le dithionite.

Tenant compte de cet « état de l'art » et mettant à profit les méthodes électrochimiques, un programme de recherche original avait été lancé, il y a quatre ans environ, pour essayer de rationaliser les paramètres clés qui contrôlent le transport des CPPs au travers des membranes cellulaires qui constitue une problématique biologique et pharmacologique importante. Dans ce contexte, l'électrochimie avait déjà été utilisée une première fois, un an avant le démarrage de ma thèse (en 2012), pour détecter des CPPs portant une sonde redox (le ferrocène) à des concentrations micromolaires [11]. Bien que le travail réalisé à cette époque avait permis de valider le principe de détection de CPPs par voie électrochimique, il a également montré que le développement de stratégies plus adéquates était nécessaire dans le but d'obtenir des propriétés analytiques plus rationnelles et de réduire la « consommation » de ces composés à haute valeur ajoutée. En effet, les expériences réalisées à cette époque nécessitaient l'utilisation de grandes quantités de CPPs dû à la taille centimétrique des cellules électrochimiques utilisées. A la même époque, une méthode électro-analytique originale permettant de détecter, en temps réel, le passage de molécules au travers de membranes suspendues réelles ou artificielles avait été développé [12]. Cette méthode est basée sur la combinaison des techniques de « patch-clamp » et d'ampérométrie. D'un côté, la technique du « patch-clamp » permet de tendre un morceau de membrane réelle ou artificielle (par excision d'une cellule réelle ou artificielle type vésicule) sur la pointe d'une micropipette; d'un autre côté, la présence d'une ultra-microélectrode en fibre de carbone positionnée en face de la membrane suspendue permet une détection électrochimique efficace d'une molécule sortant de la micropipette au-travers de la membrane suspendue. Néanmoins, cette méthode qui a été validée avec des sondes redox

classiques (ferrocene-méthanol, benzoquinone, hydroquinone, $[Fe(CN)_6]^{3-}$, $[Ru(NH_3)_6]^{+}$) en présence de bicouches lipidiques suspendues (DPhPC, DOPC, DOPG) obtenues par excision de vésicules géantes uni-lamellaires (GUVs) n'a jamais été utilisée jusqu'à avec des biomolécules.

Dans ce contexte, au moment de démarrer ma thèse, j'avais deux objectifs principaux. Le premier visait le développement d'un dispositif électrochimique miniaturisé permettant l'analyse de composés à haute valeur ajoutée tels que les CPPs. Le second était d'utiliser le dispositif combinant les techniques de « patch-clamp » et d'ampérométrie pour étudier le transport de CPPs au travers de membranes artificielles suspendues. Comme décrit ci-après, le premier objectif a été atteint mais pas le second pour des raisons de sensibilité. Ce résultat inattendu nous a conduits à se tourner vers une technique plus sensible comme la fluorescence et d'utiliser l'électrochimie non plus comme un moyen de détection mais comme un moyen de contrôler la fluorescence. Plus spécifiquement, j'ai été amené à développer une approche originale combinant l'électrochimie et la microscopie confocale en vue d'étudier la translocation de peptides au travers de vésicules géantes. Les principaux résultats obtenus dans le cadre de ces travaux sont résumés ci-après.

II) Apport de l'électrochimie pour la détection de peptides pénétrants en milieux confinés

1) Développement d'un dispositif électrochimique miniaturisé permettant l'analyse de microgouttelettes

Comme montré dans la Figure 1, l'originalité du concept repose sur la suspension, par forces capillaires, d'une microgoutte de solvant (50 µL) au niveau du fritté d'une électrode de référence au calomel saturé (Figure 1A).

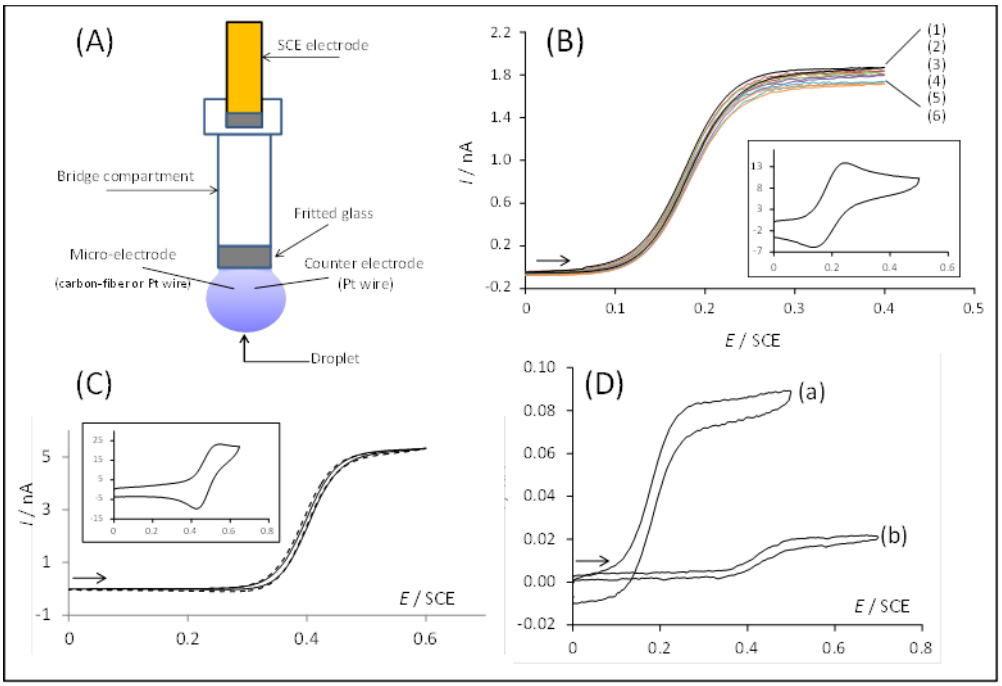

Figure 1. ***(A)*** *Dispositif expérimental permettant de réaliser des études voltammétriques et des électrolyses à potentiel contrôlé dans des gouttes micro-volumiques (50 µL).* ***(B)*** *Voltamogramme du ferrocène méthanol (0.5 mM) réalisée en milieu H_2O + KCl (0.1 M), à une électrode en fibre de carbone (v= 20 mV/s). Le même voltamogramme (1) a été obtenu dans une goutte et dans une cellule électrochimique classique de grand volume (3 mL). Les voltamogrammes numérotés de (2) à (6) ont été réalisés successivement après 2, 3, 8, 13, et 15 minutes dans la micro-goutte. Le voltamogramme transitoire montré en insert a été obtenu à v = 20 V/s dans la goutte.* ***(C)*** *Voltamogrammes du ferrocène (1 mM) réalisée en milieu DMF + nBu_4PF_6 (0.1 M), à une électrode de platine (diamètre : 25 µm), soit dans la goutte après un temps d'attente de 15 minutes (trait pointillé), soit dans une cellule électrochimique classique de grand volume (3 mL – trait plein) ; dans les deux cas : v = 20 mV/s. Le voltamogramme transitoire montré en insert a été obtenu à v = 20 V/s dans la goutte.* ***(D)*** *Voltamogrammes du (a) ferrocène méthanol (25 µM) et (b) du peptide $Fc\text{-}(Arg)_9$ (50 µM) réalisés en milieu tampon phosphate (PBS), à une électrode en fibre de carbone (diamètre : 10 µm) immergée dans une goutte (50 µL) et à v=20 mV/s.*

La détection électrochimique de peptides pénétrants marqués par une sonde redox de type ferrocène a déjà été réalisée [11]. Néanmoins, ces expériences réalisées à l'aide d'un dispositif électrochimique classique (cellule de taille centimétrique) requièrent l'utilisation de quantités non négligeables de peptides. Dans ce contexte, un dispositif électrochimique «de poche» permettant d'analyser de petites quantités de produits a été développé. Cette cellule électrochimique miniaturisée est constituée d'une microgouttelette de solvant suspendue par capillarité au niveau du verre fritté d'une électrode de référence conventionnelle (électrode au calomel saturé (ECS)). Ceci permet de contrôler avec une grande finesse le potentiel électrochimique comparativement aux autres dispositifs miniatures existants mettant en jeu des «pseudo» électrodes de référence (e.g. Ag, Ag/AgCl, Pt) et dont le potentiel peut être instable en présence de certains composés [13-15].

Ce dispositif a été testé et validé par des études voltammétriques réalisées dans des conditions stationnaire et transitoire non seulement dans l'eau mais aussi en milieu solvant organique. Le ferrocène méthanol a d'abord été étudié à une électrode en fibre de carbone (10 µm de diamètre) immergée dans une goutte d'eau (50 µL).

La Figure 1B montre les voltamogrammes typiques obtenus en conditions stationnaire (obtention d'un plateau de courant – v = 20 mV/s) et transitoire (obtention d'un pic de courant – v = 20 V/s). Les mêmes voltammogrammes ont été obtenus dans une cellule classique de taille centimétrique (V = 3 mL) et dans les mêmes conditions (solvant, concentration, électrodes, vitesse de balayage) démontrant que dans des volumes microlitres les réponses électrochimiques ne sont pas affectées par un possible phénomène d'épuisement du composé comme observé dans des cellules picolitres [16]. Par ailleurs, l'absence d'augmentation de l'intensité de courant en fonction du temps démontre l'absence d'évaporation du solvant dans nos conditions. Au contraire, on peut observer une baisse sensible du plateau de courant dû vraisemblablement à une légère passivation de la surface d'électrode. D'ailleurs, l'intensité de pic initiale était à nouveau obtenue après polissage de l'électrode.

Des résultats similaires ont été obtenus en milieu solvant organique (diméthylformamide et acétonitrile). Dans ces conditions, il est toutefois nécessaire de placer une « chambre » autour de la goutte permettant de travailler sous atmosphère inerte et de prévenir l'évaporation du solvant. Comme montré en Figure 1, des voltammogrammes transitoire et stationnaire obtenus respectivement à 20 V/s et à 20 mV/s ont pu être réalisés dans ces conditions. Là encore, les mêmes réponses électrochimiques ont été obtenues dans une cellule contenant 3 millilitres de solution.

Après avoir validé le dispositif, ce dernier a été utilisé pour la détection électrochimique de peptides pénétrants. Dans ce cadre, un peptide composé de neuf arginines et marqué par un groupement ferrocène a été spécialement synthétisé dans le groupe du Prof. Solange Lavielle (LBM – UMR 7203) (Figure 2). Comme montré en Figure 1, un voltammogramme de forme sigmoïdale a pu être obtenu à basse vitesse de balayage pour une concentration micromolaire en peptide Fc-$(Arg)_9$. A noter que l'oxydation de ce peptide apparaît à un potentiel plus positif que celui du ferrocèneméthanol indiquant un effet électroattracteur des acides aminés [17].

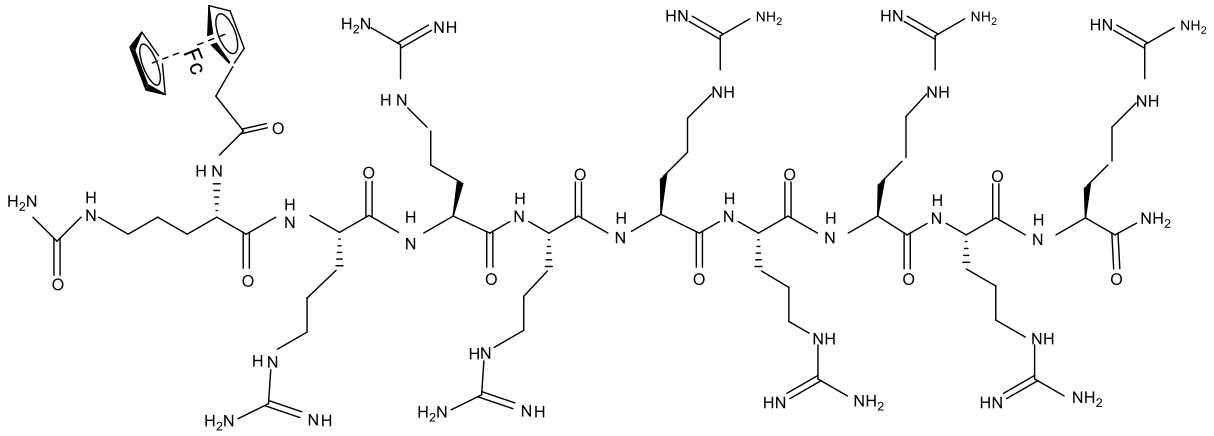

Figure 2. Structure moléculaire du peptide arginine neuf tagué avec la sonde redox ferrocène.

Parallèlement à la détection de produits à haute valeur ajoutée comme les peptides pénétrants, ce dispositif nous a permis également de réaliser des électrolyses à potentiel contrôlé pour électro-déposer du platine et des nano-cristaux d'or à la surface de fibres de carbone (10 µm de diamètre) (Figure 3). Ces électrodes modifiées, généralement préparées dans des conditions mettant en jeu des quantités non négligeables de réactifs et de solvant, sont très utilisées dans le domaine de la bio-électrochimie notamment pour la détection de petites molécules comme les "ROS" ("Reactive Oxygen Species"). Ici, les fibres de carbones ont été modifiées dans une goutte d'eau (50 µL) par réduction de H_2PtCl_6 ou $KAuCl_4$.

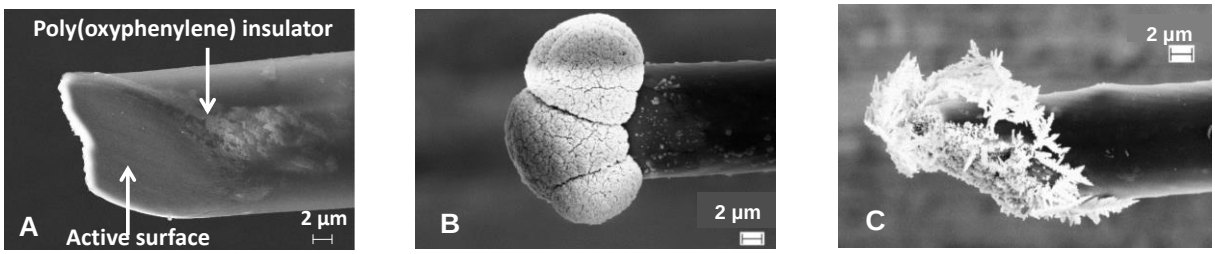

Figure 3. *Images obtenues à l'aide d'un microscope électronique à balayage montrant une fibre de carbone avant (A), et après électrodéposition de platine (B) et de nanocristaux d'or (C).*

A l'avenir, l'usage de cet outil électro-analytique miniaturisé pourrait être intéressant non seulement pour l'étude de composés à haute valeur ajoutée ne pouvant être fournis en grande quantité, mais aussi pour des raisons économiques et écologiques évidentes (réduction des déchets, consommation de faibles quantités de solvants et réactifs précieux/coûteux).

Ce travail a été récemment publié : ***Electrochem. Commun***. 54 (2015) 41. "Three-electrode analytical and preparative electrochemistry in micro-volume hanging droplets".

2) Détection électrochimique de peptides pénétrants via la combinaison des techniques de « patch-clamp » et d'ampérométrie

Parallèlement à la mise au point d'un dispositif permettant de réduire considérablement la consommation de composés à haute valeur ajoutée, un autre objectif était la détection électrochimique de peptides pénétrants traversant une membrane suspendue. Pour ce faire, je me suis appuyée sur une méthodologie originale développée récemment au sein du groupe et qui repose sur la combinaison des techniques de «patch-clamp» et d'ampérométrie [12] (Figure 4).

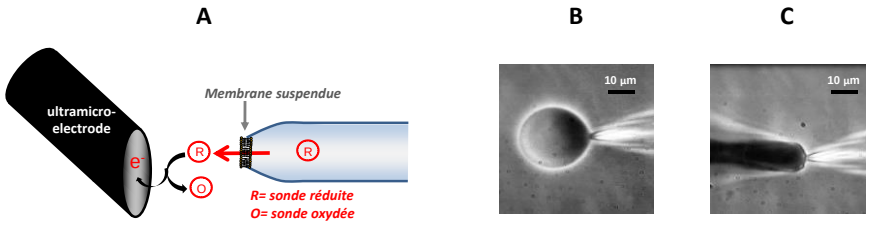

Figure 4. *A) Montage mis au point pour la détection et la quantification de molécules traversant une membrane, réelle ou artificielle, suspendue. B) Image obtenue avec un microscope à contraste de phase montrant la formation d'un "giga seal" entre la pipette et une vésicule géante. C) Configuration ampérométrique typique montrant une micro-électrode en fibre de carbone (à gauche) positionnée à proximité d'une micropipette (à droite) maintenant une membrane suspendue à son extrémité obtenue par excision de la vésicule géante montrée en B).*

D'un côté, la technique du «patch-clamp» permet de tendre un morceau de membrane réelle ou artificielle (par excision d'une cellule réelle ou artificielle type vésicule); d'un autre côté, la détection des molécules/sondes rédox ayant traversé la membrane ainsi suspendue est assurée par une mesure ampérométrique sur une ultramicroélectrode positionnée en face de la membrane.

Dans le but d'apprendre à utiliser ce dispositif nécessitant diverses compétences (préparation de vésicules géantes par électro-formation ; excision de vésicules géantes à l'aide d'une micropipette ; utilisation de micromanipulateurs sous microscope inversé), je me suis tout d'abord intéressée au transport passif du ferrocène-methanol au travers d'une membrane suspendue composée du phospholipide DPhPC (1,2-diphytanoyl-sn-glycero-3-phosphocholine) (Figure 5)

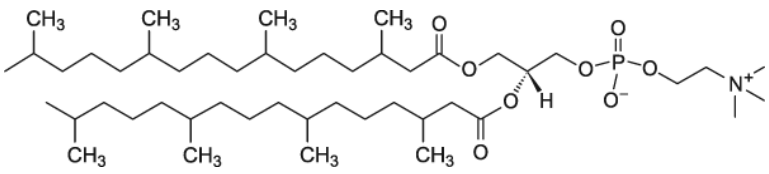

Figure 5*. 1,2-diphytanoyl-sn-glycero-3-phosphocholine (DPhPC).*

Pour ce faire, des vésicules géantes ont d'abord été préparées par electroformation [18] dont le principe est schématisé en Figure 6.

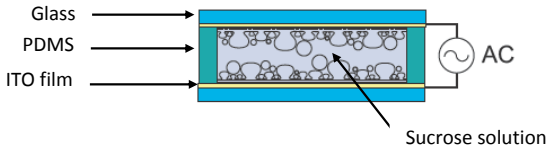

Figure 6. *Chambre d'électroformation en PDMS associant 2 électrodes d'ITO parallèles et séparées par une épaisseur de 2 mm (PDMS: polydiméthylsiloxane).*

Le principe consiste à appliquer un champ électrique entre deux lamelles de verre recouvertes d'une fine couche d'Indium Tin Oxide (ITO) et sur lesquelles ont été préalablement déposés les phospholipides en solution dans le chloroforme. Cette technique permet d'obtenir des vésicules uni-lamellaires géantes (GUVs) ayant des diamètres compris entre 10 et 100 µm et pouvant être facilement «patchées», sous microscope, à l'aide d'une micropipette en verre préalablement remplie avec le composé à détecter (1 à 2 µm de diamètre) (Figure 7).

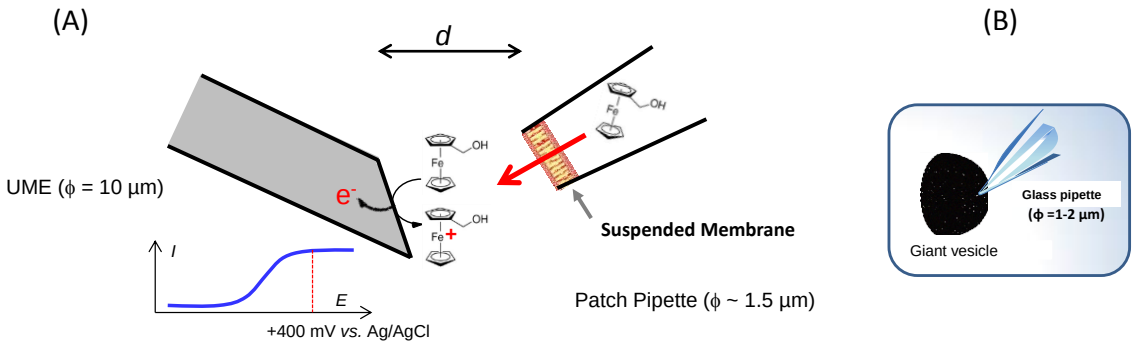

Figure 7. (A) Configuration utilisée pour la detection ampérométrique du ferrocene methanol traversant une membrane de PPhPC patchée à partir d'une vésicule géante. (B)Excision (« patch ») d'une vésicule géante.

Après l'excision de la vésicule géante, la membrane suspendue à la pointe de la pipette est amenée, à l'aide d'un micromanipulateur et sous microscope, en face d'une fibre de carbone utilisée comme électrode détectrice (Figure 7). Le potentiel de l'électrode est fixée à +400 mV/Ag/AgCl de façon à détecter, en temps réel, le flux de ferrocène méthanol traversant la membrane suspendue. La réponse en courant est ainsi étudiée, en temps réel, en fonction de la distance électrode/membrane (Figure 8).

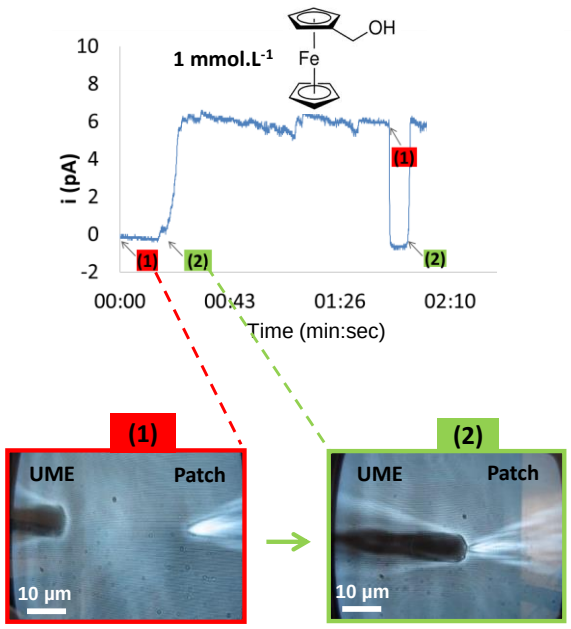

Figure 8. Réponse ampérométrique caractéristique obtenue pour le ferrocèneméthanol (C = 1 mM) en fonction de la distance d de l'électrode para rapport à la membrane (d > 100 µM (1); d < 1 µm (2)).

Comme le montre la Figure 8, et en accord avec les résultats déjà publiés par ailleurs [12] le courant est nul au début de l'expérience car la membrane est trop éloignée de la surface d'électrode. Par contre, dès que la membrane se situe à une distance raisonnable de l'électrode (typiquement moins de 5µm) le courant (dû à l'oxydation du ferrocène méthanol) augmente rapidement et atteint un état stationnaire reflétant une diffusion spontanée et constante du ferrocène méthanol au travers de la membrane suspendue. Dans ces conditions, on peut dire que l'efficacité de collection est quasiment quantitative. Inversement, le courant diminue très rapidement dès que la pipette est éloignée de l'électrode.

Dans le but d'étudier le passage transmembranaire de CPPs au travers d'une membrane suspendue, l'objectif suivant était la préparation d'une membrane suspendue composée non plus de DPhPC mais de DOPG. Le DOPG est un phospholipide chargé négativement (au niveau de la tête lipidique) souvent utilisé dans l'étude de la translocation de CPPs cationiques. Néanmoins, contrairement au DPhPC qui est un phospholipide neutre, il est impossible de « patcher » des vésicules constituées de DOPG à cause des répulsions électrostatiques entre les têtes lipidiques et la micropipette de patch également chargée négativement. Cet inconvénient a pu être contourné grâce à l'introduction dans le milieu d'espèces dicationiques, comme le calcium (Ca^{2+}) et le mégnésium (Mg^{2+}), assurant une liaison « électrostatique » entre la vésicule et la pipette.

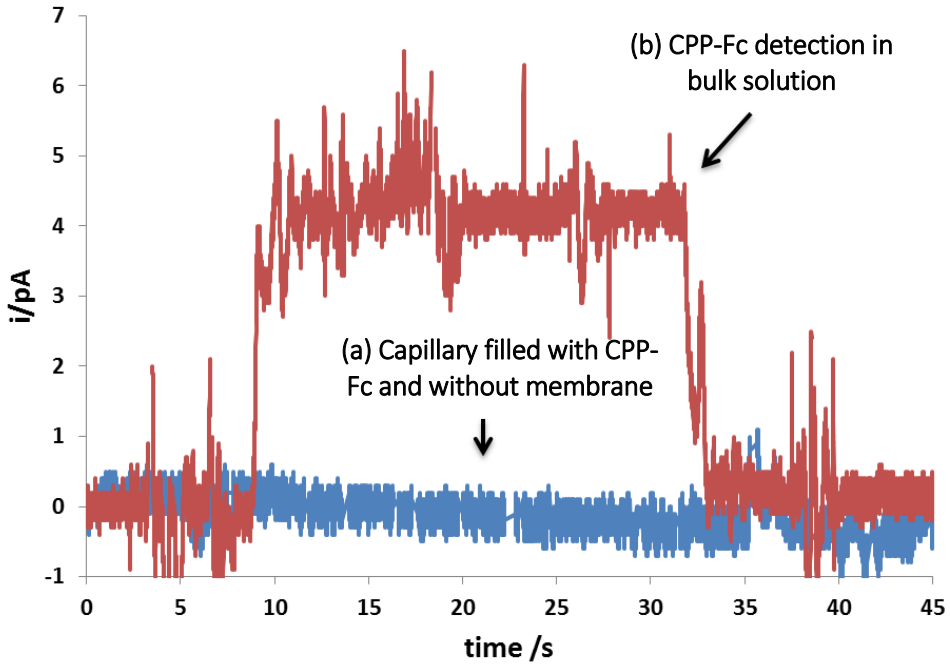

Figure 9. *Current/time response obtained at a carbon fiber microelectrode (10 µm in diameter) positioned either (a) in front of a glass micropipette tip filled with a solution of Fc-$(Arg)_9$ (C = 50 µM), or (b) immersed in a solution containing Fc-(Arg)9 at a concentration of 50 µM.*

Suite à cela, et avant la détection de CPP traversant une membrane suspendue de DOPG, il était important de tester la détection électrochimique d'un CPP sortant de la micropipette de patch en absence de membrane. Pour ce faire, le CPP Fc-$(Arg)_9$ utilisé pour la détection dans une microgoutte a été utilisé ici aussi. Dans le but d'éviter l'agrégation du CPP il est important de travailler avec des concentrations ne dépassant pas 50 µM. Dans ces conditions, aucun courant n'a pu être détecté. Pourtant, l'immersion de la même électrode dans une solution contenant Fc-$(Arg)_9$ à la même concentration que précédemment a conduit à une réponse électrochimique (comparer a) et b) dans la Figure 9).

Contrairement à l'expérience mettant en jeu du ferrocèneméthanol à une concentration de 1 mM, ceci montre qu'à 50 µM le flux de Fc-$(Arg)_9$ sortant de la pipette de patch est trop faible pour être détecté par voie électrochimique.

Comme attendu, aucune détection du peptide Fc-$(Arg)_9$ n'a pu être obtenue en présence d'une membrane de DOPG suspendue à la pointe de la micropipette. Cependant, cela ne signifie pas que le peptide Fc-$(Arg)_9$ est incapable de diffuser à l'intérieur de ce type de membrane. En effet, récemment, il a été montré (résultats non encore publiés) qu'il était possible de détecter le peptide Fc-$(Arg)_9$, mis en solution à une concentration de 50 µM, en présence d'une électrode supportant une bicouche lipidique de DOPG. Ce résultat démontre que Fc-$(Arg)_9$ est capable de diffuser jusque la surface de l'électrode au travers de la membrane. En outre, ceci confirme que la non détection de Fc-$(Arg)_9$ sortant d'une micropipette est dû à un flux trop petit.

En conclusion, les résultats obtenus dans le cadre de ce second chapitre montrent que l'électroanalyse de produits à haute valeur ajoutée comme les CPPs peut être réalisée dans des gouttes micro-volumiques en présence d'une électrode conventionnelle. Ce dispositif peut être utilisé non seulement pour l'étude de composés à haute valeur ajouté comme les CPPs, mais aussi pour n'importe quel type de composé difficile à obtenir en grande quantité. D'un autre côté, nous avons pu montrer que la combinaison des techniques de patch-clamp et d'ampérométrie n'est pas assez sensible pour détecter des petits flux de composés traversant une membrane suspendue. Ce résultat inattendu nous a conduits à se tourner vers une technique plus sensible comme la fluorescence et d'utiliser l'électrochimie comme un moyen de contrôler la fluorescence.

III) Extinction sélective de la fluorescence émise par des phospholipides ou des peptides marqués par un fluorophore

1) Développement d'un dispositif permettant de coupler l'électrochimie et la microscopie confocale à fluorescence

Comme démontré dans la partie précédente, l'utilisation de l'électrochimie pour détecter des concentrations micro-molaires de CPPs traversant une membrane suspendue de taille micrométrique paraît difficile, voire impossible, pour des raisons de sensibilité. D'un autre côté, l'étude des processus de passages transmembranaires impliquant des CPPs met classiquement en jeu des techniques très sensibles comme la fluorescence. Malgré cela, les mécanismes mis en jeu font toujours débat. L'origine de cette controverse vient principalement du fait que les techniques de fluorescence ne sont pas capables de discriminer entre les peptides internalisés et externalisés à cause de résolutions spatiales limitées. Typiquement, la méthode utilisée pour étudier le passage transmembranaire de CPPs au travers de vésicules, ou de cellules, consiste à greffer une fluorophore du type nitrobenzoxadiazolyl (NBD) sur le peptide, puis de comparer la fluorescence émise avant et après la pénétration des peptides dans la cellule artificielle ou réelle. En pratique, il est très difficile voire impossible de faire la distinction entre les peptides réellement internalisés de ceux qui se trouvent complexés côté externe de la membrane. Pour remédier à cet inconvénient majeur, de nombreux protocoles ont été développés pour éteindre la fluorescence émise par les peptides non internalisés. Ces protocoles consistent à réduire chimiquement le groupe "nitro" du NBD à l'aide de dithionite ($S_2O_4^{2-}$). Malheureusement, il a été démontré que le dithionite peut traverser les membranes et conduire ainsi à l'extinction des peptides internalisés et donc à des résultats erronés (Figure 10).

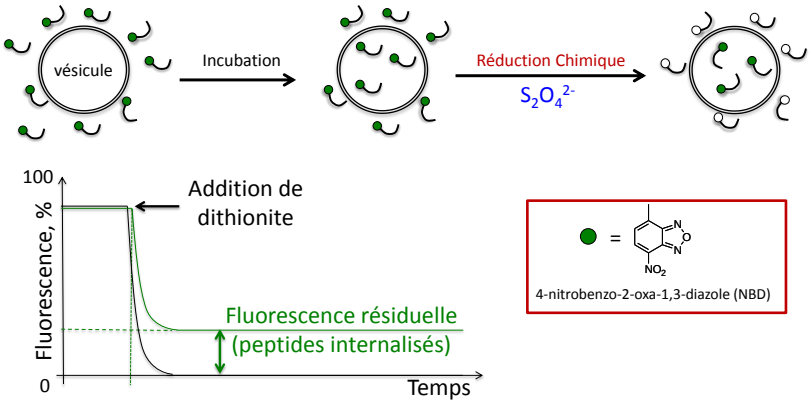

Figure 10. *Méthode typique permettant d'étudier l'internalisation de peptides pénétrants (CPPs) au travers de vésicules de type LUV (Large Unilamellar Vesicle).*

Dans ce contexte, il a été décidé de remplacer la réduction chimique par une réduction électrochimique. Pour ce faire, il a été développé un outil totalement original consistant à combiner l'électrochimie avec une technique de fluorescence comme la microscopie confocale. Ici, l'électrochimie n'est pas utilisée comme un outil de détection mais comme un moyen de contrôler la fluorescence de façon sélective. Par rapport à d'autres techniques de fluorescence comme la spectroscopie, la microscopie confocale possède l'avantage de pouvoir visualiser des objets de taille micrométriques et de suivre les variations d'intensité de fluorescence en temps réel.

Ainsi, le dispositif montré en Figure 11 a été conçu pour (i) la préparation in situ de vésicules géantes unilamellaires (GUVs), (ii) la visualisation des GUVs fluorescentes, (iii) la réduction électrochimique des groupes "nitro" du NBD portés soit par les phospholipides du feuillet externe des GUVs, soit par des peptides incapables de traverser la membrane.

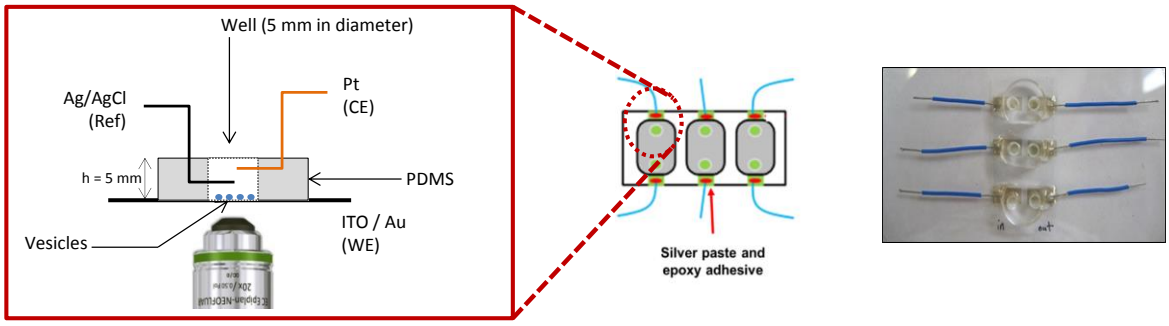

Figure 11. *A gauche : schéma du dispositif permettant de coupler l'électrochimie et la microscopie confocale à fluorescence. A droite : photo du dispositif montrant 6 puits.*

Ce dispositif est constitué d'un puit en polydiméthylsiloxane (PDMS) collé sur une lamelle de verre recouverte d'oxyde d'indium-étain (ITO) et d'une fine couche d'or servant d'électrode de travail. Les vésicules sont fabriquées directement dans le puit en faisant passer une émulsion de phospholipides au travers d'une monocouche phospholipidique déposée à la surface du puit. Les différences de densités des solutions à l'intérieur (sucrose) et l'extérieur (glucose) des vésicules font que ces dernières tombent par gravimétrie au fond du puit. Afin d'augmenter la stabilité des GUVs et d'éviter leur éclatement, la surface d'or est recouverte d'une monocouche de biotine. La contre électrode et l'électrode de référence sont introduites dans la cellule par transpercement du puit.

Notre approche a été validée en présence de GUV composées de 1,2-dioleoyl-sn-glycero-3-phosphoglycerol (DOPG), classiquement utilisé pour modéliser les endosomes, et d'une petite quantité (5 mol. %) de NBD-PE (1,2-dipalmitoyl-sn-glycero-3-phosphoethanolamine-N-(7-nitro-2-1,3-benzoxadiazol-4-yl)) utilisé comme phospholipide fluorescent. Trois type de vésicules géantes ont été préparées en fonction de la localisation de la sonde fluorescente NBD : (i) sur le feuillet externe, (ii) sur le feuillet interne, (iii) à la fois sur les feuillets externe et interne.

Une première série d'expériences réalisée en présence de vésicules marquées sur leurs feuillets externes a permis de valider qualitativement notre approche. Typiquement, après avoir vérifié l'intégrité de la vésicule et le contact de cette dernière avec la surface de l'électrode une première image montrant la fluorescence au niveau du plan équatorial de la vésicule est enregistrée. L'électrode est ensuite polarisée à un potentiel égal à -0.9 V/Ag/AgCl (la réduction du groupe "nitro" du NBD se situe à -0.7 V) pendant 30 secondes puis une nouvelle image de la fluorescence est enregistrée. Cette séquence est répétée une vingtaine de fois de façon à suivre la variation de la fluorescence au niveau du plan équatorial de la vésicule en fonction du temps. La Figure 12 montre une série d'images enregistrées en fonction du temps et montrant clairement l'extinction de la fluorescence au fur et à mesure des réductions électrochimiques. En outre, il a été démontré que cette extinction de fluorescence provient bien de la réduction du fluorophore et non pas d'un processus de "photobleaching" ou d'une espèce électro-générée en solution.

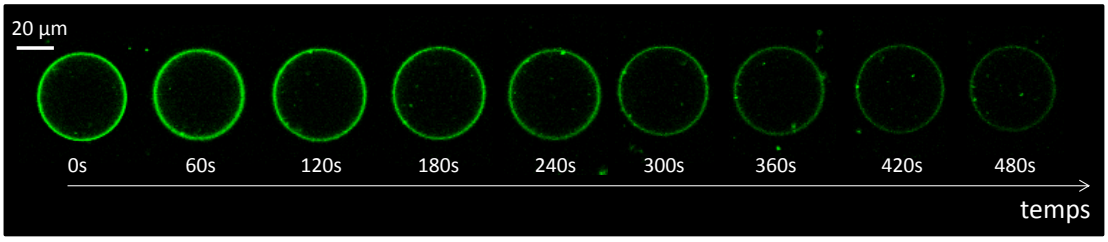

Figure 12. *Extinction de fluorescence observée au niveau de l'équateur d'une vésicule géante marquée sur son feuillet externe par une sonde NBD en fonction du temps. Vésicule posée sur une lamelle de verre recouverte d'ITO, d'or, et d'une monocouche de biotine. Polarisation à -0.9 V/Ag/AgCl.*

Par analogie aux techniques de FRAP et de FLIP, ce processus peut être apparenté à un blanchiment électrochimique où le faisceau laser est remplacé par une électrode. L'acronyme FLIE, pour « Fluorescence Loss In Electrobleaching », pourrait ainsi être introduit pour qualifier cette méthode. De la même manière ce blanchiment électrochimique crée un gradient de concentration déclenchant la diffusion des phospholipides fluorescents vers la région appauvrie de la vésicule c'est-à-dire celle en contact avec l'électrode. En outre, il a été montré qu'une réduction électrochimique réalisée de façon

continue (comme en FLIP) conduits aux mêmes résultats obtenus via une réduction séquencée. Ceci démontre qu'en réduction séquencée la fluorescence observée au niveau du plan équatorial ne subit pas de fortes variations entre l'arrêt du potentiel et la prise de photo.

En outre, les mêmes résultats ont été obtenus en présence d'une réduction électrochimique réalisée de façon continue (comme en FLIP) et non plus séquencée. Si l'on tient compte de (i) la surface de la zone électro-blanchie et de (ii) la taille de la vésicule ceci indique que la fluorescence observée au niveau du plan équatorial ne subit pas de fortes variations durant le temps écoulé pour prendre chacune des photos.

2) Extinction sélective de la fluorescence émise par le feuillet externe d'une vésicule

Notre approche a été ensuite validée quantitativement en fonction de la localisation du fluorophore NBD : (i) principalement sur le feuillet externe, (ii) principalement sur le feuillet interne, (iii) à la fois sur les feuillets externe et interne. Les résultats obtenus sont regroupés dans la Figue 13 ou F^0 et F sont respectivement les intensités de fluorescence initiale (t = 0) et à chaque instant t.

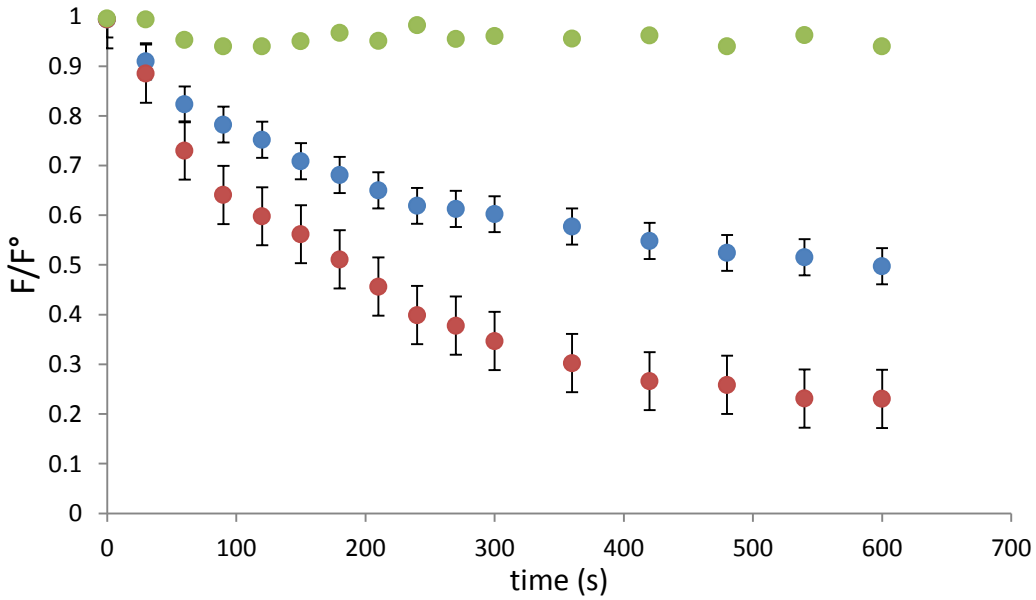

Figure 13. *Variations de fluorescence en fonction du temps de polarisation (E = -0.9 V/Ag/AgCl) obtenues, à une électrode modifiée avec de la biotine, pour des vésicules géantes possédant des phospholipides marqués par le fluorophore NBD au niveau (●) du feuillet interne (5 GUVs), (●) du feuillet externe (5 GUVs), (●) des feuillets interne et externe (13 GUVs). Les diamètres, au niveau du plan équatorial, des vésicules étudiées sont compris entre 42 et 120 µm. Les barres d'erreur représentent l'erreur standard.*

Comme le montre la Figure 13, trois comportements différents ont été obtenus en fonction de la localisation du fluorophore. Tout d'abord, quasiment aucune extinction n'est obtenue quand les vésicules sont marquées uniquement au niveau du feuillet interne de la vésicule. Ceci démontre que la réduction électrochimique des fluorophores situés à l'intérieur de la vésicule est impossible. Comme vérifié par ailleurs, la faible perte de fluorescence (environ 10%) n'est pas dû à un phénomène de "photobleaching". Ceci est vraisemblablement lié au mode de préparation des vésicules qui ne peut totalement exclure l'incorporation de phospholipides fluorescent du côté externe de la vésicule [19-21].

Inversement, une forte diminution d'intensité de fluorescence est observée en présence de vésicules marquées au niveau du feuillet externe des vésicules. Environ 80% de la fluorescence est éteinte après 600 secondes de blanchiment électrochimique. Là encore, en accord avec la littérature, les 20% restant seraient liées au mode de préparation des vésicules qui aurait conduit à internaliser 20% des phospholipides fluorescents [21].

Enfin, comme montré en Figure 13, 50% d'extinction sont obtenus lorsque les vésicules sont marquées à la fois au niveau des feuillets externe et interne. Comme précédemment, la répartition des phospholipides fluorescents est très vraisemblablement dissymétrique entre les deux feuillets mais doit être compensée dans le cas présent. Surtout, cette série de résultats confirme clairement que le blanchiment électrochimique ne concerne que les phospholipides localisés au niveau du feuillet externe des vésicules permettant ainsi de faire la distinction entre les deux côtés de la membrane.

La forte analogie entre les techniques FLIE et FLIP nous a conduits à pousser plus loin la comparaison entre ces deux techniques *via* la détermination du coefficient de diffusion des phospholipides. Quelle que soit la technique employée, nous avons montré que la vitesse d'extinction de la fluorescence dépend essentiellement du rapport des tailles de la zone blanchie et de la vésicule (diamètre). Ce rapport, défini par a_{bleach} / a, où les termes a_{bleach} et a représentent respectivement le rayon de la zone blanchie (celle au contact de l'électrode) et celui de la vésicule n'est malheureusement pas constant d'une vésicule à l'autre. En effet, bien que la plupart des vésicules posées sur la surface de l'électrode possède des formes sphéroïdales aplaties (Figure 14), l'aplatissement dépend fortement des conditions expérimentales.

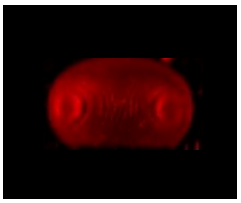

Figure 14. Image « Z stacking » d'une vésicule (50 µM de diamètre) contenant des phospholipides DOPG et une petite fraction de phospholipides fluorescentes (rhodamine-PE , 5 mol.% - Avanti Polar Lipids) sur les deux feuillets extérieurs et intérieurs.

Par conséquent, si l'on veut comparer différentes méthodes de blanchiment il est important de travailler avec des vésicules ayant des rapports a_{bleach} / a similaires. C'est dans ce cadre que nous avons tout d'abord réalisé une expérience de FLIP sur une vésicule marquée au niveau des deux feuillets. Le photo-blanchiment a été réalisé dans une zone située au niveau du pôle nord de la vésicule tandis que les variations de fluorescence sont observées au niveau du plan équatorial (a_{bleach} / a= 0.66). La Figure 15 montre une décroissance similaire à celles obtenues précédemment (Figure 13). Cependant, l'extinction de fluorescence est supérieure à 50% dans le cas présent en accord avec le fait qu'en FLIP le faisceau laser photo-blanchit les deux feuillets de la membrane sans distinction. Cette décroissante a ensuite été comparée à une simulation basée sur un modèle dont la solution numérique repose sur la résolution de l'équation de diffusion de vésicules sphéroïdales aplaties. Dans ces conditions, et comme le montre la bonne adéquation entre les valeurs expérimentales et simulées (Figure 15), une valeur de 4 $\mu m^2/s$ a été trouvée pour le coefficient de diffusion du DOPG. Cette valeur, en parfait accord avec celles données dans la littérature, a ainsi permis de valider notre modèle [22-24].

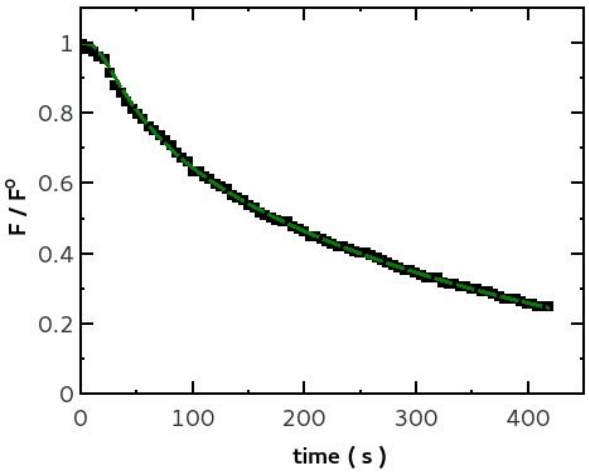

Figure 15. Diminution de l'intensité de fluorescence obtenue lors d'une expérience du FLIP réalisé dans une vésicule géante tagué à l'intérieur et à l'extérieur avec de l'NBD *(65 µm de diamètre – a_{bleach} / a = 0.66) – des points noirs avec des barres d'erreurs correspondant à la taille des points- et modélisation correspondent (ligne verte pointillée) à la diminution de la fluorescence causé par la diffusion; D = 4 $\mu m^2/s$, µ=0.8, α=0.8, écart moyen 7x10^{-4} par point.*

Le modèle numérique présenté en Figure 15, obtenu pour des vésicules marquées au niveau des deux feuillets de la membrane, a ensuite été comparé avec des données obtenues par la technique du FLIE pour des vésicules marquées uniquement au niveau du feuillet externe puisque seuls les fluorophores externes peuvent être blanchis par cette dernière technique. Comme précisé précédemment, pour que la comparaison soit pertinente nous avons travaillé avec des vésicules ayant des rapports a_{bleach} / a similaires (0.66 en FLIP et 0.71 en FLIE). Du point de vue qualitatif, un bon accord a été obtenu en termes de vitesse d'extinction de fluorescence confirmant ainsi que la technique FLIE est également liée à la diffusion des fluorophores (Figure 16).

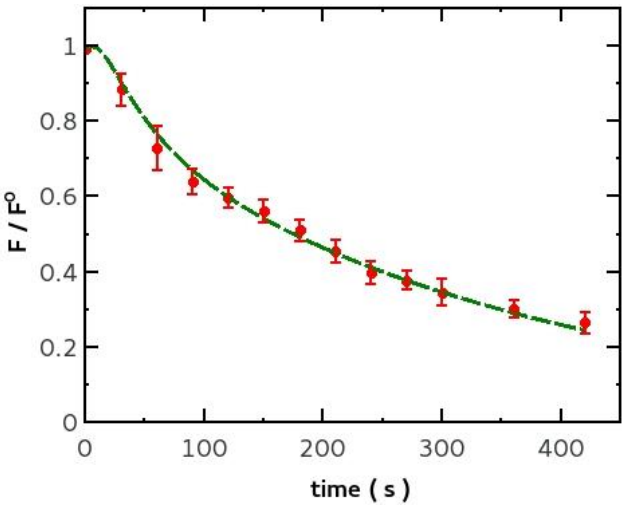

Figure 16. Comparaison entre le modèle numérique de décroissance de l'intensité de fluorescence obtenue par la méthode de FLIP (ligne verte pointillé) et la décroissance de la fluorescence obtenue lors des expériences FLIE impliquant GUVs tagué avec NBD (point rouges) également présenté dans la Figure 13.

3) Extinction sélective de la fluorescence émise par des peptides localisés au niveau du feuillet externe d'une vésicule

Pour terminer, la stratégie d'extinction électrochimique a été utilisée avec des vésicules (non marquées) mises en présence de peptides marqués par le fluorophore NBD. Cette étude a été menée en laissant incuber le peptide NBD-R6/W3 pendant 5 min en présence de GUVs de DPPG soit en phase gel (22°C), soit en phase fluide (45°C). La figure 17 montre l'évolution de la fluorescence obtenue:

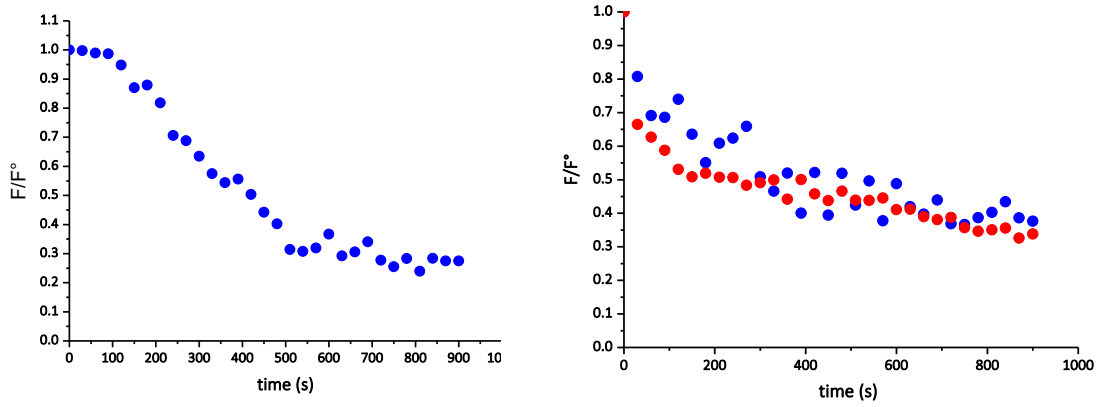

Figure 17. Fluorescence relative de vésicules de DPPG (12 µm de diamètre) en présence de peptide NBD-R6/W3 lorsque l'électrode ITO/Au est polarisée à E = -0.9 V vs Ag/AgCl. Figure de gauche = expérience réalisée à 22 °C (phase gel). Figure de droite = expérience réalisée à 45 °C (phase fluide) / points bleus = vésicule de 12 µm de diamètre, points rouges = vésicule de 40 µm de diamètre.

Ces expériences montrent que l'extinction électrochimique de la fluorescence affecte les peptides localisés sur le feuillet externe de la vésicule géante de DPPG. En phase gel, l'extinction est plus quantitative (moins de peptides sont internalisés). En phase fluide, l'extinction est plus rapide au début de la polarisation de l'électrode, en accord avec une mobilité accrue des lipides (réorganisation par diffusion latérale) dans cette phase.

IV) Conclusions et Perspectives

Le premier objectif de mon travail de thèse visait le développement d'une cellule électrochimique miniaturisée permettant l'analyse de petites quantités de molécules à haute valeur ajoutée comme les peptides pénétrants. Dans ce cadre, une cellule à trois électrodes, mettant en jeu une goutte de solvant suspendue au niveau du fritté d'une électrode de référence conventionnelle, a pu être développée. Cette approche originale, simple, peu couteuse et versatile présente également des avantages pour des raisons économiques et écologiques évidentes (consommation de petites quantités de composés précieux, faible production de déchets). Bien que non développé dans ce travail, ce dispositif expérimental pourrait être facilement modifié pour séparer les électrodes de travail et auxiliaire permettant ainsi de réaliser des électrolyses préparatives de composés à haute valeur ajouté.

Le second objectif consistait à combiner les techniques du « patch-clamp » et d'ampérométrie pour suivre, en temps réel, le transport de peptides pénétrants au travers de membranes artificielles suspendues. Tout d'abord, nous avons pu montrer que l'excision de vésicules géantes constituées de phospholipides chargés négativement comme le DOPG peut être réalisée en présence d'espèces dicationiques (Ca^{2+}, Mg^{2+}) via des interactions électrostatiques qui permettent également de stabiliser la membrane au niveau de la micropipette. Malgré tout, il a été démontré que ce dispositif combinant le « patch » et l'ampérométrie n'est pas adapté pour caractériser la translocation de CPPs à cause de flux d'espèces trop faibles. Néanmoins, ce dispositif peut offrir de nouvelles perspectives pour l'étude de peptides antimicrobiens (AMPs) qui ne traversent pas les membranes mais qui provoque la formation de pores au travers de celle-ci. Ce type de dispositif permettrait ainsi de développer une méthode originale et rapide pour cribler des familles de peptides afin de différencier les deux propriétés extrêmes que sont (a) la translocation de peptides cationiques au travers de membranes (CPP) et (b) altération de la perméabilité membranaire *via* la formation de pores (AMP)).

Compte tenu de la difficulté à détecter, par voie électrochimique, des concentrations micromolaires de peptides pénétrants traversant une bicouche lipidique suspendue, nous avons développé une autre approche consistant à combiner la fluorescence et l'électrochimie. Comparé aux dispositifs développés jusqu'ici, l'électrochimie est utilisée non plus comme un outil de détection mais comme un moyen de contrôler la fluorescence. Dans ce cadre, l'utilisation de la microscopie confocale avec une commande électrochimique est apparue judicieuse pour éteindre sélectivement la fluorescence émise par des phospholipides ou des peptides marqués par un fluorophore et situés au niveau du feuillet externe de vésicules unilamellaires géantes. Par rapport aux techniques classiques de photo-blanchiment (ex : FRAP, FLIP), le processus électrochimique n'affecte pas les sondes fluorescentes localisées à l'intérieur des vésicules permettant ainsi une discrimination entre les feuillets interne et externe. L'utilisation d'un processus électrochimique permet également de s'affranchir de l'utilisation de réducteurs chimiques qui peuvent induire des changements de force ionique et/ou être internalisés dans les vésicules. Cette procédure originale apparaît versatile et parfaitement adaptée pour suivre précisément le processus d'internalisation de molécules actives. En résumé, l'étude des mécanismes liés au transport, à la distribution, à l'internalisation, et au relargage de molécules thérapeutiques marquées par un fluorophore peut substantiellement bénéficier de l'introduction d'une commande électrochimique permettant le contrôle de la fluorescence.

Références

[1] A. Jutand. Chem. Rev. 2008, 108, 2300-2347.

[2] K.L. Adams, M. Puchades, A.G. Ewing. Annu. Rev. Anal. Chem. 2008 (1) 329–355.

[3] C. Amatore, S. Arbault, M. Guille, F. Lemaître. Chem. Rev. 2008, 108, 2585-2621.

[4] Meunier, A; Jouannot, O; Fulcrand, R; Fanget, I; Bretou, M; Karatekin, E; Arbault, S; Guille, M; Darchen, F; Lemaitre, F; Amatore, C. Angew.Chem. Int. Ed. 2011, 50, 5081-5084.

[5] P. Järver, Ü. Langel, Biochimica et Biophysica Acta, 2006, 1758, 260.

[6] S. El-Andaloussi, T. Holm, Ü. Langel, Current Pharmaceutical Design, 2005, 11, 3597.

[7] C. Bechara, S. Sagan. FEBS Letters 587 (2013) 1693-1702.

[8] J.-M. Swiecicki, M. Di Pisa, F. Lippi, S. Chwetzoff, C. Mansuy, G. Trugnan, G. Chassaing, S. Lavielle, F. Burlina, Chem. Commun., 51 (2015) 14656-14659.

[9] J.-M. Swiecicki, A. Bartsch, J. Tailhades, M. Di Pisa, B. Heller, G. Chassaing, C. Mansuy, F. Burlina, S. Lavielle, ChemBioChem, 2014, 15, 884.

[10] M. J. Moreno, L. M. B. B. Estronca, W. L. C. Vaz, Biophysical Journal 91, 873-881 (2006).

[11] P. Messina, G. Hallais, E. Labbé, M. Béranger, G. Chassaing, S. Lavielle, C. Mansuy, O. Buriez, C. Amatore. Electrochimica Acta 80 (2012) 180.

[12] P. Messina, F. Lemaître, F. Huet, K. A. Ngo, V. Vivier, E. Labbé, O. Buriez, C. Amatore. Angew. Chem. Int. Ed. 53 (2014) 3192.

[13] R. A. B. da Silva, A.C. Rabelo, R.A.A. Munoz, E.M. Richter, Electroanalysis. 22 (2010) 2167-2171.

[14] M.W. Shinwari, D. Zhitomirsky, I.A. Deen, P.R. Selvaganapathy, M.J. Deen, D. Landheer, Sensors. 10 (2010) 1679-1715.

[15] M.E. Clark, J.L. Ingram, E.E. Blakely, W.J. Bowyer, J. Electroanal. Chem. 385 (1995) 157-162.

[16] R. Kashyap, M. Gratzl, Anal. Chem. 70 (1998) 1468-1476.

[17] H.-B. Kraatz, D. M. Leek, A. Houman, G.D. Enright, J. Lusztyk, D.D.M. Wayner, J. Organomet. Chem. 589 (1999) 38-49.

[18] M. Le Berre, A. Yamada, L. Reck, Y. Chen, D. Baigl, Langmuir 2008, 24, 2643-2649

[19] A. Yamada, T. Yamanaka, T. Hamada, M. Hase, K. Yoshikawa, D. Baigl. Langmuir 22 (2006) 9824-9828.

[20] A. Yamada, M. Le Berre, K. Yoshikawa, D. Baigl. Chem.Bio.Chem. 8 (2007) 2215-2218.

[21] S. Pautot, B.J. Frisken, D.A. Weitz, PNAS, 2003 100 (19) 10718-10721.

[22] K. Bacia, C. G. Schuette, N. Kahya, R. Jahn, P. Schwille, J Biol Chem 2004, 279, 37951.

[23] Y. a Domanov, S. Aimon, G. E. S. Toombes, M. Renner, F. Quemeneur, A. Triller, M. S. Turner, P. Bassereau, Proc. Natl. Acad. Sci. U. S. A. 2011, 108, 12605.

[24] Pincet F, Adrien V, Yang R, Delacotte J, Rothman JE, Urbach W, et al. (2016) FRAP to Characterize Molecular Diffusion and Interaction in Various Membrane Environments. PLoS ONE 11(7): e0158457. doi:10.1371/journal.pone.0158457.

General Introduction

Electrochemistry is a powerful tool to detect, to activate, and to investigate reactivity as well as mechanisms involving high value-added molecules. In order to achieve this goal, it is important to adapt the electrochemical methods to the very reality of the phenomena investigated rather than adapting the phenomena to our methods. For instance, miniaturization of electrodes has been allowing investigations of numerous mechanisms of transition metal-catalyzed reactions in resistive media [1]. The development of ultra-microelectrodes also opened a new field called bio-electrochemistry in which electrochemical methods are useful for *in vitro* analysis of biomolecules [2]. For instance, micrometric electrodes are very convenient for the understanding of biomolecules release mechanisms at the single cell level, namely oxidative stress (Reactive Oxygen and Nitrogen Species –ROS and RNS- releases) and vesicular exocytosis (neurotransmitters secretion by endocrine cells) to name a few [3]. Sometimes, electrochemistry must be combined with other techniques to tackle these major issues. Combination of electrochemistry and fluorescence allowed to gain further insight into biological investigations such as exocytosis [4]. Though electrochemistry has already been widely used to bring new insight in a number of important biological issues, it still remains a lot of questions and/or controversies in which electrochemical techniques could be helpful. The translocation of cationic peptides such as the cell-penetrating peptides (CPP) belongs to this category. The interest of the scientific community for this original class of peptides has been growing these last-years owing to their ability to cross the plasma membrane of mammalian cells and to deliver biologically active molecules with high efficiency and low cytotoxicity [5, 6]. Nevertheless, the penetration of these cationic peptides across cell membranes is a complex process, the description and representation of which being still incomplete especially in its dynamic aspects. Despite the development of numerous *in vivo* and *in vitro* investigations, based notably on fluorescence techniques, the nature of the mechanism(s) involved in the cationic peptides uptake is still under debate [7]. Yet, the comprehension of the mechanisms involved in cationic peptides uptake is a crucial step especially for the development of strategies for the *in vivo* delivery of therapeutic molecules as well as the development of novel therapeutic agents. Actually, the origin of the controversy comes essentially from the poor discrimination between internalized and surface-bound CPPs bearing a fluorescent probe. This drawback is generally overcome via the fluorescence quenching of surface-bound CPPs tagged with 4-nitrobenzo-2-oxa-1,3-diazol-4-yl (NBD) by dithionite ($S_2O_4^{2-}$), which act as a chemical reducing agent [8, 9]. However, this physiologically compatible chemical quencher has recently been found to permeate membrane vesicles [10]. This permeation property could therefore

severely affect translocation investigations based on the fluorescence monitoring after dithionite quenching.

Based on this "state of the art" and taking advantage of electrochemical methods, an original research program was launched, about four years ago, to provide new entries in the rationalization of key parameters, which control the CPP transport through cellular membranes that is an important biological and pharmacological issue. Within this context, and one year before I started my PhD thesis, electrochemistry was first tested to detect CPP at micromolar concentrations. Accordingly, a cationic cell-penetrating peptide was modified with ferrocene (used as the redox probe) and electrochemically detected for the first time in 2012. At that time, although the reported work established the validity of the principle of electrochemical detection of CPP, it also showed that more adequate strategies needed to be developed to provide correct analytical properties and to reduce "consumption" of such high added value compounds. Indeed, these experiments required large CPP amounts due to the electrochemical device used (milliliter electrochemical cell and millimetric sized electrodes).
At about the same time, a new advancement, based on the combination of the patch-clamp principle and amperometry, was done in view of probing and quantifying, in real time, the passive transport of biomolecules through suspended real and model cell membranes [11]. On the one hand, the patch-clamp technique consisted in sealing a patch of real or artificial cell membrane at the tip of a glass micropipette (by excision of a real cell or of an artificial vesicle, respectively); on the other hand, the electrochemical detection of molecules crossing the suspended membrane was performed by amperometry with a carbon-fiber electrode placed in front of the glass micropipette tip. Nevertheless, this method which was validated with typical redox probes (ferrocene-methanol, benzoquinone, hydroquinone, $[Fe(CN)_6]^{3-}$, $[Ru(NH_3)_6]^{+}$) and lipid bilayers (DPhPC, DOPC, DOPG) patched from single-wall giant unilamellar vesicles (GUV) had not been used with biomolecules.

Within this framework, I had therefore two main objectives when I started my PhD work: (a) miniaturization of the electrochemical cell allowing analysis of poorly available compounds such as CPPs, and (b) development of an electrochemical method aimed at monitoring CPP translocation, with a first attempt combining patch-clamp and amperometry. As shown in the following, the first objective was reached, but not the second one for sensitivity reasons. This unexpected result led us to turn to a more sensitive technique such as fluorescence. More specifically, an original synergistic association between electrochemistry and confocal fluorescence microscopy was successfully developed in view of investigating peptides translocation through giant unilamellar vesicles. In this original approach fluorescence was under electrochemical control.

Accordingly, I decided to outline my PhD work in three main chapters:

-The First Chapter is aimed to provide some examples describing how electrochemistry has emerged as a valuable tool for investigating dynamical biological processes. Particularly, those related with the release or internalization of species displaying redox activity. In this context, the monitoring of exocytosis and oxidative stress is addressed at the beginning of the Chapter. It continues with an explanation of some strategies to overcome the electrochemical limitations responsible for hindering the study of other biologically-relevant species, especially, when these molecules are non-redox, present at low concentrations or difficult to spatially localize. Then, a brief introduction to the subject of Cell-penetrating peptides is given, which comprises their characteristics, mechanisms of uptake and some techniques used to investigate their uptake. At the end of the Chapter, a first electrochemical strategy to detect a CPP labeled with a redox probe is presented. This approach was successfully proposed in the biomolecular electrochemistry group where I pursued my Ph D. The results were at the onset of the present work aimed to design and implement feasible electrochemical setups for CPP monitoring.

- The second chapter will be first dedicated to the conception of an original three-electrode micro-cell equipped with a conventional reference electrode (Saturated Calomel Electrode) allowing classical electrochemistry of high value-added compound such as CPPs to be readily performed in minute samples. This original device is based on micro-volume droplets suspended by capillary forces to the fritted glass of the SCE bridge (Figure 1). Concomitantly, a patch clamp methodology was tested for a direct amperometry detection of redox-labeled CPPs, revealing limitations that prompted us to use the redox properties of fluorophores to achieve an electrochemical bleaching of their fluorescence (Chapter 3).

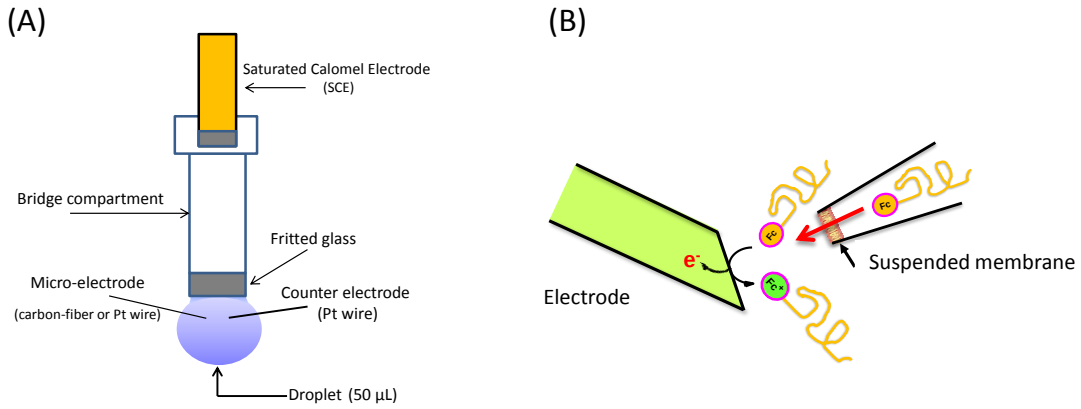

Figure 1. (A) Experimental device developed for the investigation of high value-added compound such as Cell-Penetrating Peptides [12]. (B) Experimental device used to attempt the electrochemical detection of a ferrocene-labeled CPP crossing a suspended artificial membrane.

- In Chapter three, we will show how the combination of electrochemistry and confocal fluorescence microscopy is a very promising original approach for the investigation of CPP translocation. Particularly, it will be shown that combination of these techniques is helpful for monitoring, in real time, the selective fluorescence extinction of either outer leaflet NBD-labeled giant liposomes (GUV) or NBD-labeled CPP localized on the outer leaflet of GUVs (Figure 2).

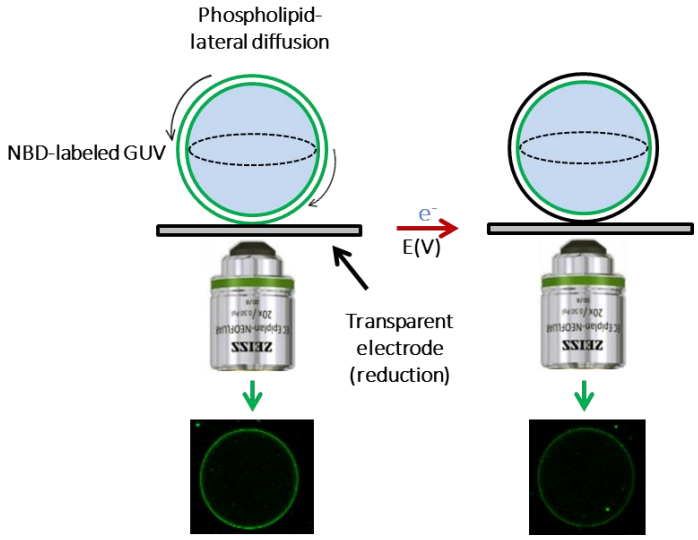

Figure 2. Selective electrochemical bleaching of outer leaflet fluorophore-labeled giant liposomes. Manuscript submitted to Chemical Science, September 2016.

Sections 4 and 5 summarized the materials and experimental procedures used in the Second and Third Chapter, respectively. Finally, Section 6 contains the appendixes of this manuscript.

References

1. Jutand, A., *Contribution of Electrochemistry to Organometallic Catalysis.* Chemical Reviews, 2008. **108**, 2300-2347.
2. Adams, K.L., M. Puchades, and A.G. Ewing, *In Vitro Electrochemistry of Biological Systems.* Annual Review of Analytical Chemistry, 2008. **1**, 329-355.
3. Amatore, C., S. Arbault, M. Guille, and F. Lemaître, *Electrochemical Monitoring of Single Cell Secretion: Vesicular Exocytosis and Oxidative Stress.* Chemical Reviews, 2008. **108**, 2585-2621.

4. Meunier, A., O. Jouannot, R. Fulcrand, I. Fanget, M. Bretou, E. Karatekin, S. Arbault, M. Guille, F. Darchen, F. Lemaître, and C. Amatore, *Coupling Amperometry and Total Internal Reflection Fluorescence Microscopy at ITO Surfaces for Monitoring Exocytosis of Single Vesicles.* Angewandte Chemie International Edition, 2011. **50**, 5081-5084.
5. Järver, P. and Ü. Langel, *Cell-penetrating peptides—a brief introduction.* Biochimica et Biophysica Acta (BBA)-Biomembranes, 2006. **1758**, 260-263.
6. El-Andaloussi, S., T. Holm, and U. Langel, *Cell-Penetrating Peptides: Mechanisms and Applications.* Current Pharmaceutical Design, 2005. **11**, 3597-3611.
7. Bechara, C. and S. Sagan, *Cell-penetrating peptides: 20 years later, where do we stand?* FEBS letters, 2013. **587**, 1693-1702.
8. Swiecicki, J.M., M. Di Pisa, F. Lippi, S. Chwetzoff, C. Mansuy, G. Trugnan, G. Chassaing, S. Lavielle, and F. Burlina, *Unsaturated acyl chains dramatically enhanced cellular uptake by direct translocation of a minimalist oligo-arginine lipopeptide.* Chemical Communications, 2015. **51**, 14656-14659.
9. Swiecicki, J.-M., A. Bartsch, J. Tailhades, M. Di Pisa, B. Heller, G. Chassaing, C. Mansuy, F. Burlina, and S. Lavielle, *The Efficacies of Cell-Penetrating Peptides in Accumulating in Large Unilamellar Vesicles Depend on their Ability To Form Inverted Micelles.* ChemBioChem, 2014. **15**, 884-891.
10. Moreno, M.J., L.M.B.B. Estronca, and W.L.C. Vaz, *Translocation of Phospholipids and Dithionite Permeability in Liquid-Ordered and Liquid-Disordered Membranes.* Biophysical journal, 2006. **91**, 873-881.
11. Messina, P., F. Lemaître, F. Huet, K.A. Ngo, V. Vivier, E. Labbé, O. Buriez, and C. Amatore, *Monitoring and Quantifying the Passive Transport of Molecules Through Patch–Clamp Suspended Real and Model Cell Membranes.* Angewandte Chemie International Edition, 2014. **53**, 3192-3196.
12. Perez-Jimenez, A.I., L. Challier, M. Di Pisa, M. Guille-Collignon, F. Lemaître, S. Lavielle, C. Mansuy, C. Amatore, E. Labbé, and O. Buriez, *Three-electrode analytical and preparative electrochemistry in micro-volume hanging droplets.* Electrochemistry Communications, 2015. **54**, 41-45.

First Chapter:

How electrochemistry addresses biological issues

1. First Chapter: How electrochemistry addresses biological issues

1.1. General context

During the past few decades, electrochemistry has grown as a key methodology to investigate life sciences beyond usual bioelectrochemistry [1]. The experimental and technological bases of electroanalytical chemistry can be traced back a century ago, from the introduction of the glass electrode by Max Cremer[2] and the invention of polarography by Jaroslav Heyrovsky in the early 1920's [3-6], a major contribution for which he was awarded the Nobel Prize of Chemistry in 1959. Interestingly, Cremer pioneered the field of potentiometric sensors, *viz.* those showing a Nernstian dependence of their potential value with the activity of analytes in a state of thermodynamic equilibrium between the sensing electrode and the solution/phase under study. In polarographic methods, the current intensity flowing through the electrode is proportional to the flux of species which undergo electrochemical oxidation or reduction, a property opening avenues for the amperometric determination/monitoring of concentrations. The principles of recent electrochemical sensors and setups remain rooted in – and inspired by – these initial works, although considerable improvements have been brought in terms of sensitivity, selectivity and reliability. Incidentally, it is somehow amazing to recall that apart from his ownership regarding the invention of the glass electrode, Max Cremer was primarily a physiologist whose research field is nowadays explored by a variety of electrochemical techniques (ion sensing, electrophysiology, amperometry, etc.). In this respect, Cremer remains a visionary for the upcoming evolutions in bioanalytical chemistry.

The analytical applications of electrochemical probes/sensors have found a natural interest for environmental and biological issues [7, 8]. Some developments related to biology are described in the following paragraphs in order to establish how electrochemistry brings significant insights in this field, with a focus on the developments which inspired this work.

1.1.1. Direct electrochemical detection/monitoring

1.1.1.1. Monitoring exocytosis

Electrochemistry in ultra-small environments has emerged as an increasingly important technique for fundamental studies of diffusional restricted reactions, low sample volume analysis, and single cell neurochemistry [9-15]. In neuroscience, knowledge of the chemical composition and dynamics of single nerve cells should lead to better models of the cellular neurotransmission process [10]. One key dynamic event in neuronal communication is exocytosis. The process of exocytosis can be described as the docking of vesicles (storage compartments) into the cell membrane and subsequent release of their content by fusion of the vesicle and cell membranes. This process allows the conversion of an electrical signal (action potential) to a chemical signal (messenger release and receptor recognition), which is necessary for exocytotic communication between cells [10]. The electrochemical monitoring of exocytosis has been studied by Amatore and co-workers during the last two decades, within a cell configuration mimicking an artificial synapse [9-13]. Accordingly, the receptor cell is replaced by an ultramicroelectrode (UME) which allows the real-time collection of neurotransmitters release at the level of a single cell (Figure 1). This analysis is possible since neurotransmitters are catecholamines which can be easily oxidized at carbon surface (E = 650 mV versus Ag/AgCl) [9]. The study is accomplished using either a basic UME, or a total micro-sized electrochemical cell. The interest in using UMEs for the exocytosis investigation relies on the proximity between the size of such electrodes and that of nerve cells. Moreover, the short duration of a vesicular release event (from a few milliseconds to several hundred milliseconds) requires electrochemical setups to allow an accurate and very fast acquisition of the current [9-13]. The most commonly used UMEs are micrometric (5-10 µm diameter) carbon fiber electrode, which decrease the capacitive current. This carbon fiber is beveled a 45 ° and then placed at few micrometers from the analyzed cell, restricting so the release volume (Figure 1.1).

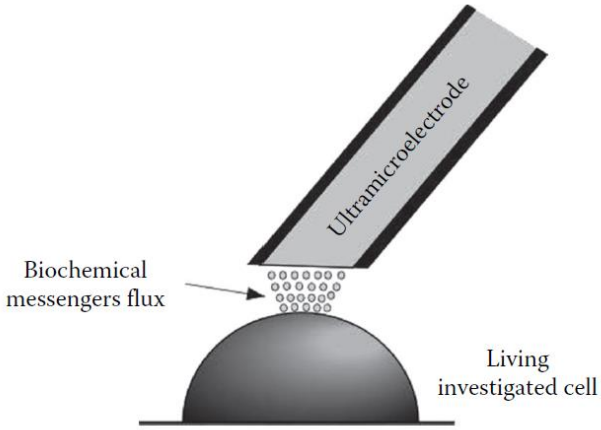

Figure 1.1 Configuration for measuring exocytotic release by using a carbon fiber UME. The electrode is positioned at the top of a living cell that releases electroactive species.

Here, it is important to understand why the electrode is placed so near to the cell surface. Since a large concentration does not mean a large quantity, a small number of molecules may correspond to a large concentration by restricting the volume in which these molecules are released. For instance, one femtomole delivered into a volume of a thousand μm^3 creates a millimolar concentration rise. Such variation in concentration can be monitored kinetically via electrochemical techniques with an excellent signal-to-noise ratio, provided that the electrode does not pick up too much noise through its surface [13]. Electrodes pick up electrical noise through their capacitance (through their overall conducting surface area) while the analytical information (the faradaic current) may arise only from the surface area exposed to the cell release. Thus, using an electrode with an active surface matching that of the examined cell decreases the noise, while no affecting the quality and intensity of the analytical information. This increases the signal-to-noise ratio and ensures quantitative collection efficiency, since the microelectrode covers the whole cell emitting surface [13].

The electrochemical detection of exocytosis is generally carried out either by fast-scan voltammetry (FSCV) or constant potential amperometry. When working in amperometric mode, the electrode is held at high enough potentials to oxidize the released molecules. This recording allows detecting in real time zepto to attomoles of released neurotransmitters with submillisecond precision. The resulting plot displays a series of current spikes that correspond to the detection of successive exocytotic events. Each current spike represents one exocytotic event, which allows the quantification of released neurotransmitters through integration of the current generated by an individual event (Figure 1.2).

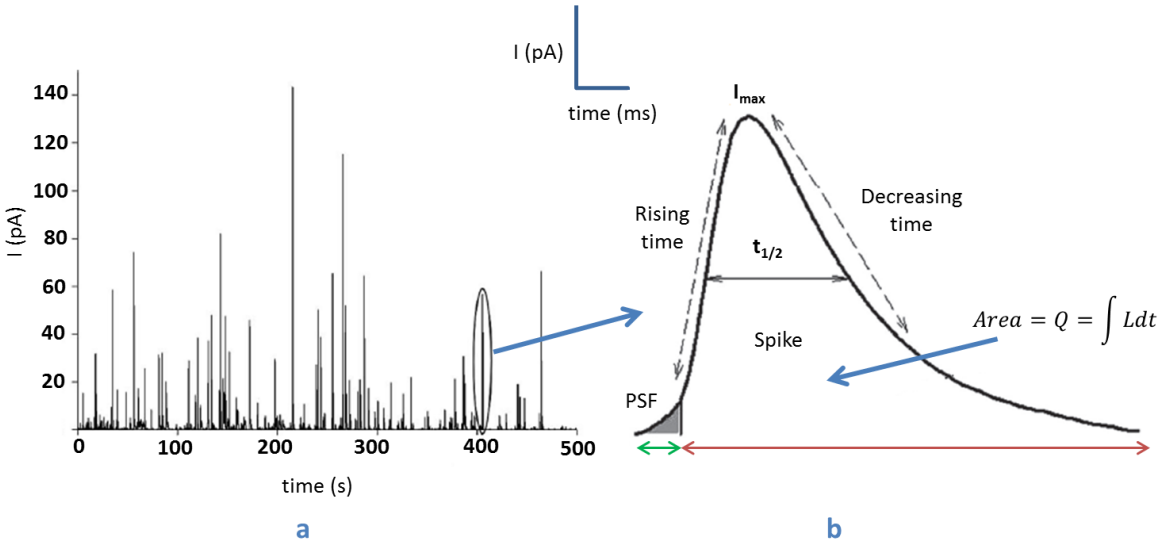

Figure 1.2 (a) Amperometric trace obtained during exocytosis of a single chromaffin cell. (b) Usual amperometric analysis of an exocytotic event: major relevant quantitative and kinetic parameters extracted from amperometric spike. PSF: prespike feature. Figure adapted from references [9, 13].

On the other hand, FSCV is a method that allows identifying and quantifying the neurotransmitter released or discerning between species within a mixture [13]. For instance, species as dopamine, norephinephrine and serotonin have been detected by using FSCV [16, 17]. However, the distribution of exocytotic activity is a spatially heterogeneous at the cell surface. This subcellular heterogeneity motivated the design of systems having carbon fiber UME array. In such approach, the exocytotic events were measured using electrodes of 1 µm of radius separated a distance of 15 µm. Under these conditions, it was possible to simultaneously measure the dopamine release in single cells, at multiple spatially separated sites [18]. Similarly, another approach for spatially resolve heterogeneous events of exocytosis was given by Ewing and co-workers [19]. The main difference with the former method lies in the complete miniaturization of the electrochemical cell. Here, the electrode array consists of a set of platinum thin-film micro well-based UMEs, fabricated on glass substrate by photolithography, thin film deposition, and reactive etching. Because of several UMEs can cover a single cell, the approach success on electrochemically imaging heterogeneous exocytosis events.

1.1.1.2. Detection of oxidative stress

Oxidative stress is a metabolic disturbance in the balance due to an overproduction of reactive oxygen species (ROS) and antioxidant defenses [20]. The primary species of oxidative stress are the superoxide anion (O_2^-) and the nitric oxide radical (NO) [13]. Nitric oxide (NO) has been implicated in the pathogenesis of several diseases. A deficiency of NO may play a role in some diseases such as hypertension, hyperglycemia, atherosclerosis, Parkinson's disease and Alzheimer's disease. Conversely, an increase of NO may participate in others: arthritis, reperfusion injury and cancer [21]. Thus from a biochemical as well as a medical perspective, it is important to quantify the amount of NO produced in cell tissues. NO is stable in oxygen-free solutions. However, NO reacts rapidly with several components in vitro or in vivo, producing protein nitrosylation as well as reacting with hemoglobin and oxygen [20]. In the presence of superoxide, NO is rapidly converted into peroxynitrite. Indeed, as this reaction undergo extremely fast (about 3-19x10^9 $M^{-1}s^{-1}$) [22], the detection of NO in biological systems has been proven to be technically difficult (especially, because it is found at extremely low concentrations: in the range of 0.1 uM to 5 nM) [23]. The currently used instrumental techniques for NO measurements are spectroscopic and electrochemical methods. Moreover, electrochemical methods for NO determination offer several features that are not available with spectroscopic approaches. For instance, the relative ease fabrication and miniaturization of electrochemical systems (addressed in section 2.2). In fact, electrochemical measurements using modified ultramicroelectrodes is the only approach allowing direct monitoring of NO in real time [24] and without using label strategies [23]. The detection can be achieved by either electro reduction or oxidation of NO. However, the strategy of electroreduction faces interferences such as the electroreduction of molecular oxygen, thus this approach is no longer used. Some features of miniaturized electrochemical systems are: (i) sensitivity in the nanomolar order or above; (ii) good selectivity to NO despite the presence of interfering species (iii) it is often a non-invasive and non-destructive strategy; (iv) fast acquisition time (millisecond range), among others [23]. One crucial point for the success in the electrochemical analysis of NO concerns the modification of the electrode surface, to allow a detection selective towards NO species [23]. In this context, Malinski and co-workers demonstrated the suitability of electrochemistry to detect NO release in single cells (and thus in close proximity to the NO source) by using a porphyrinic-based microsensor [25, 26]. Lantoine et al reported the first example of calibration of this nickel porphyrin and Nafion electrochemical sensor, for the detection of NO in the range of 1.5 nM to 40 µM [27]. Other strategies of NO detection by direct oxidation involves the use of platinum electrodes mimicking the Clark electrode [28, 29], detection by scanning electrochemical microscopy [30, 31], among others (see references [9, 13]). On the other hand,

Amatore and co-workers proposed a large series of works to study in real-time the fundamental mechanisms of oxidant release at the single cell level [32]. These studies were performed at platinized carbon fiber UME and by using either chronoamperometry [33-36] or triple-potential step chronoamperometry [37]. The first example consisted of positioning a platinized carbon fiber UME (which improves the sensing of reactive oxygen and nitrogen species released by macrophages or fibroblasts) above an isolated single cell cultured in a Petri dish to measure oxidative stress release by stimulation with a microcapillary. The following release of ROS and reactive nitrogen species (RNS) was detected by chronoamerometry (Figure 1.3a) and the accurate chemical nature of the compounds was obtained through comparison with in vitro electrochemical oxidation of H_2O_2, $ONOO^-$, NO, and NO_2^- solutions (Figure 1.3b). These data enabled the calculation of time variations of emission flux for each species and the reconstruction of the original flux of the production of the two primary species, O_2^- and NO [33].

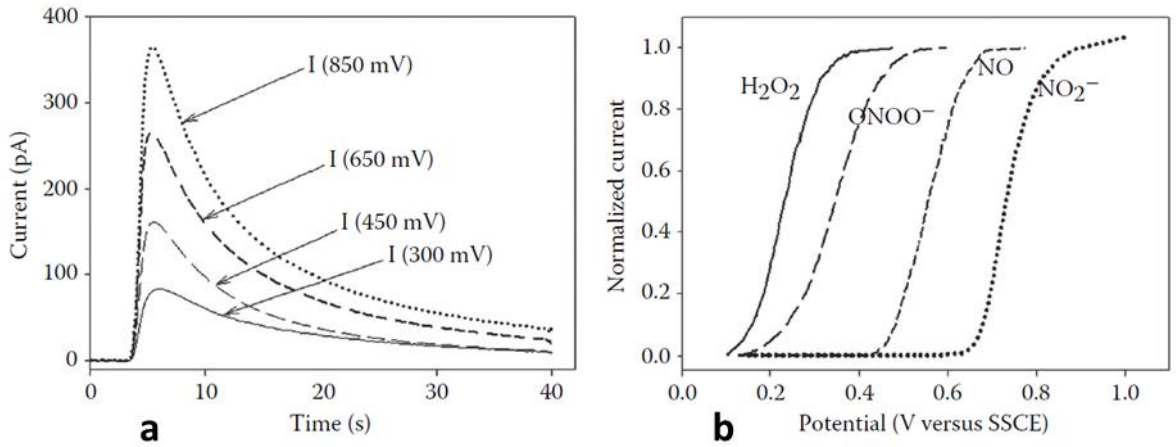

Figure 1.3 (a) Typical amperograms recorded as a function of the potential at a single macrophage stimulated by microcapillary. (b) Normalized steady-state voltammograms of some electroactive species (working electrode = platinized carbon fiber UME, C = 1 mM, v = 20 mVs^{-1}) that help to select the appropriate potential values in chronoamperometry. Figure from Ref [13].

The application of UMEs has largely contributed in the detection of both reactive oxygen (ROS) and nitrogen (RNS) at the single cell level. However, there are some limitations when working with these electrodes, such as the difficulty to ascertain the exactly localization of the emitted compound within the cell [13]. Thus, similarly to the case of exocytosis, this can be achieved by the use of micro electrochemical arrays (MEAs), which are devices comprising of numerous individual electrodes appropriately separated, designed and functionalized with the appropriate chemistry to allow multianalyte detection [13].

One of the first approaches of NO detection by using MEAS was given by the group of Bedioui [38], who developed a sensor array to detect NO released from a group of HUVEC cells (Figure 1.4). The device was composed of three individually addressable electrodes, each of them were modified with different NO-sensing materials. Thus, each electrode surface was modified by electrodepositing films of nickel tetrasulfonated phthalocyanine (NiTSPc), pyrrole-substituted manganese porphyrin (MnTriOMePyP) and nickel tetramethylpyridyl porphyrin (NiTmPyP) enclosed in a polymer capsule. The cells were grown on Collagen discs which in turn were fitted approximately 0.1 µm above the electrodes. This strategy avoid the direct contact of cells with the electrode surface, and their potentially death. This approach successfully depicted the feasibility of modifying individual electrodes to achieve multiple analyte detection from cell populations [38, 39].

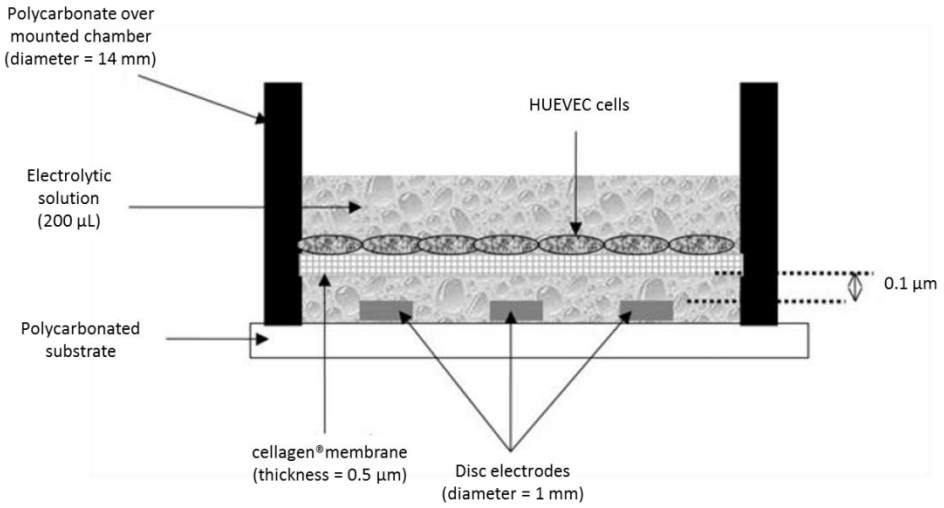

Figure 1.4 Scheme of the MEA developed in Ref [34] .

An example of MEA for the simultaneous amperometry detection of peroxynitrite and nitric oxide was proposed by Quinton et al. The device consisted of gold electrodes of 50 µm of diameter and divided in two sets, each one having its own reference and counter electrode [40]. A set of electrodes modified by electrodeposition with poly(eugenol) and poly(phenol) was devoted to the detection of the NO oxidation. Meanwhile, another set, aimed at monitoring peroxynitrite reduction was used without modification. This allowed the simultaneous detection of NO and ONOO- in physiological buffer, validating in this manner the concept.

There are several examples of ROS and RNS detection involving the use of MEAs, which reflect the progress in this field and the importance of monitoring such oxidative stress species. In conclusion, performing amperometric recordings at carbon fiber UME or microelectrode arrays is a suitable

method for characterizing very fast processes (as the neurotransmitters release), allowing the detection of a large amount of small (then fast-diffusing) molecules in a very restricted portion of space. Here, as the local concentration is high, the real challenges are i) to collect fast and ii) to connect the amperometric response to a biological event and to perform a signal processing accurate enough to provide information on the different steps of exocytosis.

1.1.2. Coupling Electrochemistry and Fluorescence

1.1.2.1. General context

In the previous section, electrochemical methods was evidenced to be a reliable method to monitor the release of metabolites displaying a redox activity, and we focused on catecholamines involved in synapse communication as well as reactive oxygen/nitrogen species resulting from oxidative stress. However, their extension to study the transport of other biologically-relevant species faces several limitations, namely:

- Non-redox metabolites cannot be monitored electrochemically.
- Amperometric techniques performed at solid electrodes under general biological conditions have limits of detection above 1µM, a value corresponding to the upper concentration limit of some biological species, e.g. cell penetrating peptides.
- Electrochemistry does not give readily interpretable information on the spatial localization/distribution of a species that undergoes reduction or oxidation.

The amperometric detection of non-redox species can be resolved through their functionalization by electroactive groups. One of the most popular redox probe is ferrocene, which presents numerous advantages related to i) its small size poorly affects the steric hindrance once grafted on the molecule ii) there are some commercially available derivatives like ferrocene carboxaldehyde which constitute reliable and versatile precursors for functionalization iii) ferrocene generally undergoes fast/reversible electron transfer, which is the promise of an “uncomplicated” probe behavior, a quality for analytical applications. We have used this strategy as an entry to the detection of cell penetrating peptides, as described later in this chapter.

A potential improvement of the limitations of electrochemical methods can be brought by their coupling with other techniques. Generally, a coupled technique is introduced in order to bring complementary information on those brought by oxidation or reduction at the electrode surface or in a thin layer (film) in contact with the electrode surface. Accordingly, NMR [41] or mass spectrometry

[42] have been used with electrochemistry to characterize a specific function or a specific electrogenerated metabolite/residue. Electrochemical Surface-Enhanced Raman Spectroscopy (SERS) has also been increasingly developed over the past two decades and to allow the characterization of transient intermediates generated at electrodes, a very interesting feature in oxidative metabolism studies [43-45].

The monitoring of low-concentrated metabolites and their localization puts fluorescence in the spotlight of the most sensitive and reliable techniques to achieve such objectives. The way electrochemical and fluorescence methods synergistically interact to monitor a specific species in biological medium relies on the complementarity of both techniques, as exposed in the following.

1.1.2.2. Combining electrochemical detection and fluorescence: detection of exocytotic events

Exocytosis involves secretion of vesicles, their docking and fusion to the inner cell membrane and the release of the vesicle content (a neurotransmitter, a peptide, and a hormone) at the exterior of the cell. Such events have been widely explored in our group through amperometric methods at ultramicroelectrodes [9, 46-48], which provide a time resolution accurate enough to allow a reconstruction of the fusion event during exocytosis, after a thorough analysis of the current spikes recorded [49-52]. However, some events remain difficult to detect by amperometry, such as the fusion of empty vesicles or “kiss and run” cases, i.e. when the vesicle finally goes back to the cytosol with no release. In that perspective, fluorescence may bring complementary information on the localization of either the vesicle itself or its content, independently. A first introduction of fluorescence in this field was brought using acridine orange stained chromaffin cells at ITO electrodes [53], which brought a proof of concept and the possibility to run experiments with evanescent waves used in Total Internal Reflection (TIRF) Microscopy. A more complete investigation has been realized and published in recent years on the association of amperometry and TIRF microscopy to monitor exocytosis [54].

Another interesting strategy for exocytosis exploration is provided by false fluorescent neurotransmitters (FFN), which may produce fluorescent spikes during the release if contained in the vesicle. Concomitant amperometric detection would allow the association of light events (release of FFN) with amperometric events (release of catecholamines). Accordingly, a recent paper has described the combination of amperometric and optical analysis of false fluorescent neurotransmitters to characterize the modulation of dopamine release upon interaction with cocaine and methylphenidate in mouse striatum [55].

1.1.3. Electrochemically switchable fluorescent probes

The introduction of an electrochemical command in the emission or extinction of fluorescence is another strategy featuring the association of electrochemical and optical techniques. In such a configuration, electrochemistry is not used to collect independent (amperometric) information but triggers fluorescence emission on and off. F. Miomandre has successfully used tetrazines as electrochemically-switchable fluorescent dyes [56, 57]. In these studies, the electrochemical setup is completed by a TIRF microscope and the region concerned by the electrochemical switching of the fluorescent probe is the *electrochemically-attainable* portion of solution in contact with the ITO electrode, viz. the one corresponding to the dimension of the diffusion layer. These electrochemically switchable fluorescent probes are naturally interesting for applications in confined environments (such as thin layers in contact with the electrode) where all fluorophore molecules can be oxidized or reduced. The development of such reversible optical switches to address biological issues related to the release or internalization of species is currently an important topic in our group and in the next chapters of this work we will report examples of electrochemical detection quenching of NBD-labelled peptides and phospholipids.

1.2. Monitoring the translocation of CPPs

1.2.1. What are Cell Penetrating Peptides?

Cell-Penetrating Peptides (CPPs) are short peptides sequences of less than 40 amino acids, possessing the ability to gain access to the interior of cells. They are cationic and usually rich in arginine and lysine. The identification of proteins that can enter cells was first reported for the Trans-Activator of Transcription (Tat) protein of the Human Immunodeficiency Virus which was found to internalize in tissue-cultured cells and promote the viral gene expression [58, 59]. Additionally, Antennapedia homeodomain, a transcription factor of *Drosophilia melanogaster*, was also shown to enter nerve cells and regulate neural morphogenesis [60]. These observations, apparently in contradiction with the "at the time established" conception that charged species/fragments could not cross hydrophobic barriers such as lipidic membranes, triggered increased research activities aimed at identifying the shortest peptide sequence capable of entering cells, leading to the characterization of respectively the Tat peptide (a domain of the HIV-1 Tat protein) [61, 62] and Penetratin (a fragment of Antennapedia homeodomain) [63]. The state-of-the-art on CPP origins, properties and internalization mechanisms

has recently been reviewed by C. Bechara and S. Sagan [64] and we will develop some aspects related to the specific issue of the uptake mechanism in the following.

1.2.2. Cell-penetrating peptides: why are they important to investigate?

The internalization of Tat and Penetratin opened avenues for the uptake of other CPPs and introduced the possibility to use these peptides for the intracellular delivery of covalently or non-covalently conjugated bioactive cargos, namely the delivery of therapeutic agents [65, 66].

Indeed, targeting and delivering a drug into a cell is not an easy task. Setting aside recurrent problems such as solubility and aggregation, crossing the cell membrane represents a major hurdle for drug delivery [67]. Currently, strategies involve vector-based methods, electroporation, micro-injection and chemical methods with liposomes and polymers [68]. However, these methods present drawbacks regarding the specificity, the toxicity, the efficiency and bioavailability. Conversely, the overall characteristics of CPPs, *viz.* low cytotoxicity for a variety of cell lines, ability to be taken up by a variety of cell types [67], dose-dependent efficiency, and no restriction with respect to the size or type of cargo [67]. Thus, CPPs offer great potential as future therapeutics [69].

1.2.3. Applications of CPPs

1.2.3.1. CPPs for medical and biological applications

Although the high ability of internalization of CPPs makes them promising candidates for cargo translocation, they can also possess specific biological activity. There is not a real distinction between inherently bioactive CPPs and CPPs fused with a bioactive sequence. This is a consequence of the difficulty to determine which part of a CPP sequence is responsible for the cellular internalization and which one is responsible of the biological activity.

As a representative example of therapeutic application, the discovery of the pro-apoptotic activity of a peptide derived from tumor suppressor protein p14ARf [70], led the development of a variety of apoptotic CPPs. An example is given by a Bcl-2 family protein. The BH3 apoptotic domain of these proteins is confined to their α-helical conformation, which is a domain known for inducing apoptosis.

Then, the secondary structure is altered, making the peptides cell permeable. Thus, a bioactive cell-penetrating peptide is obtained [71].

Another important therapeutic use of CPPs relies on their cytotoxicity, although this property is not generally associated with CPPs. However, in a determinate dose threshold, they provoke membrane disruption as antimicrobial peptide does [72].

1.2.3.2. CPPs as transporters

A variety of transporters may favor cargo translocation. Among them, CPPs stand out as one of the most efficient techniques for achieving cellular access. The application of CPPs as carriers have succeeded in delivering small interfering RNA (siRNA), involved in the modulation of gene expression, anionic biomolecules such as nucleic acids, small molecules for chemotherapeutics and large molecules such as proteins [73, 74]. Recent applications of CPPs encompass the development of cellular imaging, nuclear localization, pH sensitivity and thermally targeted delivery [75, 76], and so on (Figure 1.5).

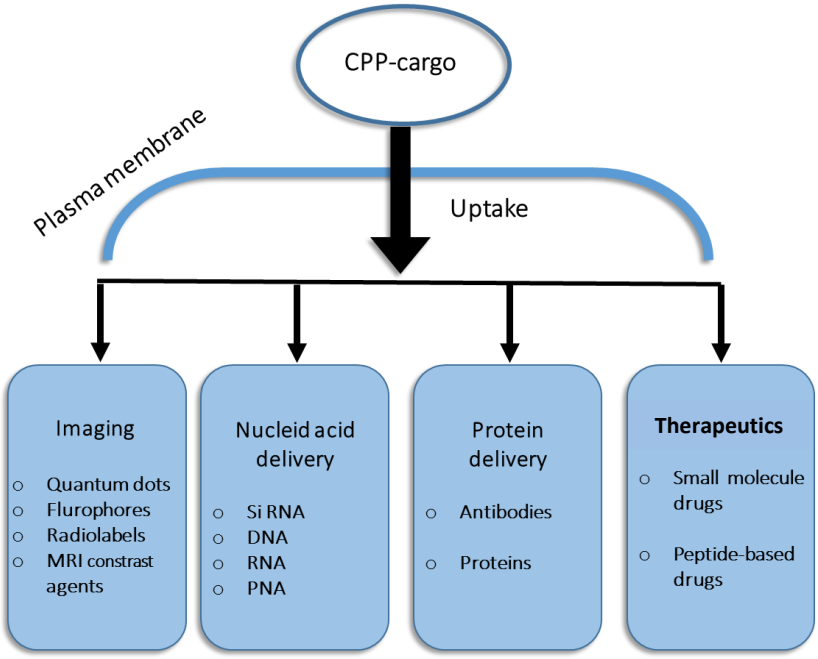

Figure 1.5 Applications of CPPs as molecular delivery vehicles adapted from Ref [76].

CPPs have contributed to help imaging agents, as quantum dots, crossing the blood-brain barrier (a series of tight junctions between endothelial cells) [77]. Other molecules that have been delivered by CPPs to intracellular targets are monoclonal antibodies, extensively used for radio immunotherapy and radio immunodetection [78]. In addition to delivering imaging agents and radiolabels, CPPs can be used to deliver light –emitting biosensors. For instance, the ratiometric-fluorescence zinc biosensor, developed to detect zinc levels as low as 5-10 pM into the nucleus and cytoplasm cell [79].

CPPs are attached to their cargo via either a covalent or noncovalent bond (Figure 1.6). Covalent complexes are neutral cargo, such as phosphorodiamidate morpholino oligomers, peptide nucleic acids, and small drugs molecules. Neutral cargos are coupled to a CPP by a disulfide bond, an amide bond, or other specific linkers [71]. On the other hand, noncovalent CPP/cargo assemblies are formed by electrostatic and/hydrophobic interactions between negatively charged cargo (nucleic acids i.e.), and a positively charged CPP.

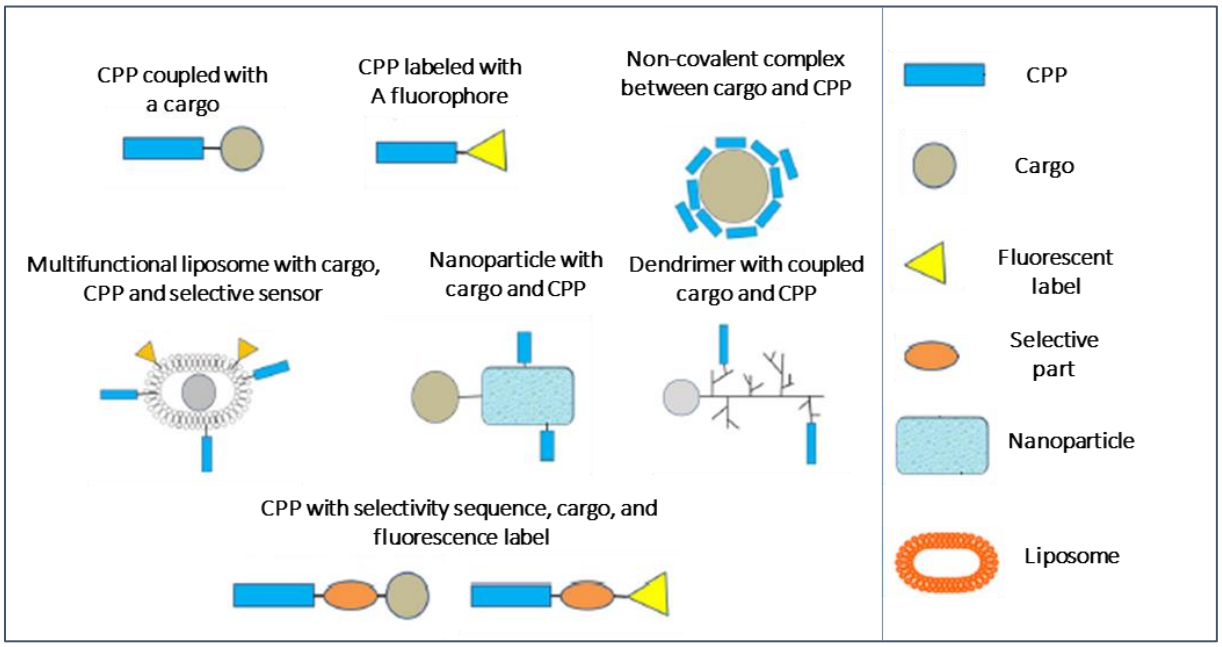

Figure 1.6 Assembly of cell-penetrating peptide (CPP) structures. Adapted from Ref [74].

1.2.4. Mechanisms of uptake

Despite of numerous studies performed on a wide variety of cell types and artificial phospholipid bilayers, the pathways through which CPPs cross the cell membrane remain, in some degree, unresolved [64, 80]. Actually, a specific CPP may undergo two or more uptake mechanisms depending

on its structure, the cell line and membrane composition, the nature of the cargo, concentration, temperature, and time of incubation [74, 80]. In general, the modes of uptake are broadly categorized into two groups: energy-dependent (endocytosis) and energy-independent pathways [72].

Energy-dependent active internalization occurs when a CPP triggers uptake via endocytosis [72]. Endocytosis is the conventional internalization mode of extracellular hydrophilic macromolecules, involves absorption to the plasma membrane or a membrane-bound receptor, followed by energy-dependent formation of endosomes. Endosomes that are generated by endocytosis can be recycled back to the plasma membrane, targeted to another subcellular location, or sent to multivesicular bodies for degradation [81].

1.2.4.1. Energy-independent pathways: passive membrane translocation

Energy-independent passive internalization is the process by which a peptide-cargo conjugate directly crosses the cell membrane. This can occur via transient membrane disruption or spontaneous translocation. The last phenomenon neither causes nor requires membrane disruption [72].

The main differences between these pathways lie in the membrane permeation and release step. In non-endocytotic uptake, CPPs localize directly in the cytoplasm and nucleus, lacking of cell-selectivity. On the contrary, endocytotic pathways rarely release CPPs into the cytosol, making this process non-ideal for the delivery of material into the cytoplasmic or nuclear compartments [82]. The possible CPPs uptake pathways are outlined in Figure 1. 7.

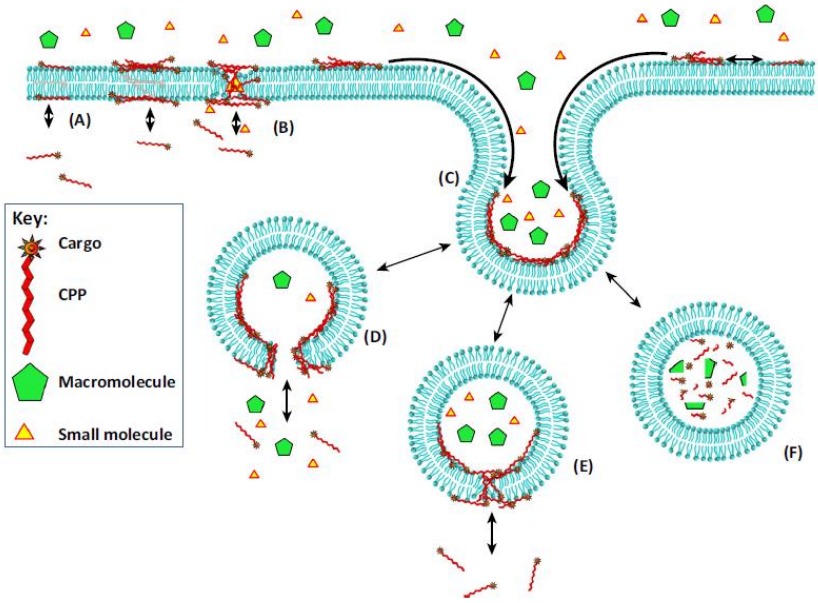

Figure 1.7 Schematic illustration of some pathways by which CPPs and attached cargo may internalize into the cell. Also, it is shown the ending of an unattached small and macro molecule. (A) Spontaneous membrane translocation, which occurs without peptide self-assembly or membrane disruption. (B) Transient plasma membrane permeabilization. (C) Endocytosis of membrane-bound peptide-cargo complex, along with an unattached small and large molecule cargo. (D) Endosomal membrane lysis releases the CPP-cargo conjugate and all co-encapsulated cargoes. (E) Translocation across the endosomal membrane delivers CPP and attached cargo, but not co-encapsulated cargo. (F) Degradation or recycling of CPP and all cargoes will occur rapidly if the other mechanisms do not enable delivery to the cytosol. The mechanisms depicted are not mutually exclusive; they can occur simultaneously. Taken from Ref [72].

1.2.5. Structural parameters and conditions controlling CPP internalization

Although several results report contradictory observations about the mechanisms of CPP uptake, they agree concluding that the initial CPP-cell membrane contact is favored by electrostatic interactions [72]. Afterwards, the cellular uptake is driven by several parameters as (i) the nature and secondary structure of the CPP; (ii) the ability to interact with cell surface and membrane lipid components; (iii) the nature, type and active concentration of the cargo; and (iv) the cell type and membrane composition [71].

1.2.5.1. Positive charge: a key feature

Cationic peptides possess a positive net charge at physiological pH resulting from the sequence of positively charged amino acids (arginine, lysine) that constitute them. The initial step of internalization is the formation of tight electrostatics interactions between cationic CPPS and anionic cell surface molecules (glycosaminoglycans) [64]. However, efficient internalization has been detected even in the absence of these anionic molecules as already demonstrated by a vast number of experiments performed using artificial model cell-membranes [83].

Although effective CPPs are known to possess positive charges, the evidence of a higher degree of internalization on CPPs involving arginine residues rather than lysine, indicates the contribution of additional parameters in the uptake [71]. See below.

1.2.5.2. Hydrophobicity

Peptides containing only apolar residues are considered as hydrophobic, including stapled peptides, prenylated peptides, and pepducins [76]. The presence of hydrophobic residues in the CPP sequence enhances the degree of uptake [64]. The peptide's positive charge appears responsible for the initial interaction with the membrane while the hydrophobicity is crucial for insertion. However, it is important to optimize the level of hydrophobicity. For instance, when the hydrophobic interactions are too high, CPPs are stuck in the membrane and no internalization occurs [64, 71].

1.2.5.3. Peptide secondary structure

CPPs are generally unstructured in aqueous solution, but they adopt various structures once in interaction with lipids. This variability for the same sequence arises from different experimental conditions as peptide/lipid concentration, temperature, buffer, etc., applied during the tests. It has been envisioned that the "membranolytic" properties of a given peptide could be governed by its secondary structure, specifically helicity. Nevertheless, no clear dependence has been evidenced between peptide secondary structure and translocation [64].

1.2.6. State of the art on the methods aimed at studying the mechanisms of CPP uptake

As mentioned previously, despite the number of studies on CPPs, their uptake mechanism(s) appear multiple, sometimes controversial or not completely solved. A mechanistic framework of their modes of internalization is essential to identify the structural features which control the interaction of CPPs and lipids all along the uptake process, in order to rationalize the design of these promising cellular delivery vectors. At least, three mechanisms should be envisioned: direct penetration across the membrane, translocation through formation of a transient structure, and endocytosis-mediated entry [84].

In this context, several methods have been developed to evaluate the uptake mechanisms in both biological and biophysical systems. For instance, transport studies are generally performed on living cells by microscopic techniques. However, the complexity/fragility of real cells and their handling make the application of some biophysical methods difficult or impossible. Since passive transport does not involve specific interactions with membrane receptors, model membranes have soon be envisioned for mechanistic investigations [85]. This section summarizes, in a non-exhaustive manner, some representative methods described in the literature to study the mechanisms of CPP uptake.

1.2.6.1. CPP-membrane interactions: biophysical approaches

Understanding the interactions of CPPs with model membranes contributes to the understanding of the mechanisms of CPPs translocation. Techniques such as atomic force microscopy (AFM) and polarized total internal reflection fluorescence microscopy (pTIRFM) can describe the morphological changes induced by peptides on model membranes. AFM allows the observation of nanometer-sized particles and provides information on surfaces, but cannot image structures having insufficient topographical contrast, like CPPs inserted into a membrane. Meanwhile, fluorescence microscopy has a large sensitivity, but is a diffraction-limited technique. However, the combination of both strategies was successful to evidence the formation of domains on bilayers induced by antimicrobial peptides [84]. Nevertheless, this approach is limited to supported phospholipids bilayers.

On the other hand, techniques like circular dichroism (CD) and nuclear magnetic resonance (NMR) can determine the secondary and tertiary structures of CPPs interacting with different model membranes. CD spectroscopy detects the chirality of molecules as the small difference in absorptivity for right –and left hand- circularly polarized light [85]. CD spectroscopy gives information about the overall secondary structures of the peptides in solution as well as their conformational changes in different environments. However, CD has some drastic constraints proper to spectroscopic techniques. For instance, it is unable to work in turbid solutions. Except for few synthetic examples, most phospholipids form vesicles leading to milky solutions or suspensions with high scattering power. It is possible to overcome this problem by using either lysophospholipids or detergents, which form non-scattering micelles. However, in some cases misleading results are obtained since micelle has geometrical constrains which do not exist for membranes, therefore the system does not reflect a membrane situation [84]. In contrast to CD, NMR spectroscopy provides molecular structure information at the atomic level. ^{1}H is the most commonly studied nucleus for the characterization of proteins and peptides, but the isotope-labeled nuclei ^{13}C and ^{15}N are also involved. Employing NMR spectroscopy is possible to analyze properties of the CPP and their localization (i.e. depth) in a model membrane. There are several studies reporting the structure of CPPs both in solution and in the presence of model membranes. But, it is not simple to identify any correlation between the particular structure induced by the model membrane, and the observed mechanism of internalization for different CPPs. Additionally, despite CD and NMR give information regarding the mechanistic aspects of CPPs, they are difficult or impossible to use for an intact biological cell membrane [85].

Another way to analyze the interactions CPPs/membrane concerns the “peptide-induced vesicle leakage”. This method uses the fluorescence spectroscopy technique to measure the degree of membrane perturbation generated by different CPPs. The principles rely on the preparation of LUVs in a buffer containing a high concentration of the fluorophore. In this manner, LUVs encapsulate some volume of the fluorophore, and the non-encapsulated volume outside the vesicle is removed carefully.

However, self-quenching occurs due to the high concentration of fluorophore, decreasing the fluorescence intensity. Addition of the CPP outside of the LUVs may induce a leakage and dilution of the fluorophore. The results show that primary amphipathic CPPs have higher degree of membrane perturbation and leakage than non-amphipathic or hydrophilic CPPs. These results indicate that the potential effects of other components present in real cell membranes may be important and suggest the occurrence of mechanisms more related to a receptor-protein-mediated uptake [85].

1.2.6.2. Localization and quantification: fluorescence-based methods

The quantification of the translocation of a CPP is possible by attaching a reporter group to the active amino acid sequence. This is the most frequent approach so far, referred to as "the fluorescence-based method". By labeling a peptide with a fluorophore (Figure 1.6-b) is possible to measure the fluorescent emission of treated cells. In theory, this method should easily allow discerning between energy-independent and energy-dependent pathways. For instance, an uptake driven by direct translocation/penetration should yield a uniform and diffuse labeling into the cells, while endocytosis results in a granular or punctuate pattern due to entrapment of peptide and label in vesicles organelles [85].

There is a variety of fluorophores used to evaluate the uptake of CPPs. Generally, the fluorescent probe is covalently linked to the N-terminal α-amino group or ε-amino group of Lys of the peptide. The fluorophore should be photoresistant, unable to significantly alter the peptide's hydrophobicity, and relatively small in size. Some examples of fluorophores used for labeling are fluorescein, 2-aminobenzoic acid fluorophore, rhodamine, and 7-nitrobenz-2-oxo-1,3 diazol (NBD). Methods applied to quantify the content of fluorescently labeled peptide involve: fluorescence-assisted cell sorting (FACS), fluorimetry, and confocal microscopy. FACS uses a cell sorted apparatus that classifies cells according to their fluorescence intensity, and then measures the amount of cells that have taken up the CPPs. Fluorimetry enables the indirect quantification of labeled CPPs. Finally, confocal microscopy maps the distribution of CPPs or associated cargoes molecules within the cell. This mapping allows distinguishing the extracellular from internalized peptides inside, for instance, endosomes or the nucleus. The described methods are appropriate for detecting the uptake ability of CPPs. However, fluorescence-based analysis cannot discriminate between surface-bound labeled peptide and translocated-labeled peptide. This is especially problematic with cationic CPPs, which can bind either to the inner (if translocated) or the outer leaflet (if not) of a membrane, leading to a misleading interpretation of the obtained results.

Some protocols have been introduced to reduce signals from surface bound CPPs. For instance, Langel *et al* reported a quantitative fluorescence assay where fluorescent-CPPs bound to the cell surface are removed by trypsin [86]. Nevertheless, this method has a limitation since trypsin is ineffective against extracellular peptide aggregates, therefore additional analysis need to be performed. Another approach performs the fluorescence quenching of surface bound fluorescent-CPPs. A well-known example is the quenching of the NBD – labeled CPPs. Besides the essential NBD properties detailed hereafter, this fluorescent group is sensitive to reducing agents such as dithionite. The fluorescence

emitted by the NBD group can be chemically quenched by dithionite (Figure 1.8). Treatment with dithionite consists in incubating real cells or artificial membranes under a relatively high concentrated solution of this quencher (about 3 mM or 1 M). The surface bound NBD-CPPs exposed to dithionite therefore undergo irreversible fluorescence extinction. However, the main disadvantage of using dithionite lies in its slow permeability across membranes [87]. Therefore, this method could alter the real amount of uptake of the analyzed NBD-CPPs. To solve this problem, we proposed a strategy for analyzing the uptake of NBD-labelled CPPs, introducing an electrochemical reduction of NBD.

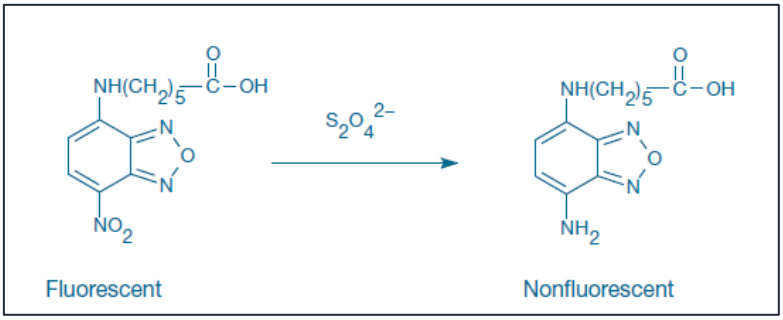

Figure 1.8. Scheme of the quenching of NBD by dithionite reduction of the NO_2 moiety

1.2.7. Electrochemical detection of a ferrocene –labelled cationic cell-penetrating peptide

A first attempt to achieve an electrochemical characterization of a CPP was carried out in our group in collaboration with Christelle Mansuy, Gérard Chassaing and Solange Lavielle at the Laboratoire des Biomolécules (UMR 7203), who prepared a cationic cell-penetrating peptide (CPP) labeled with both a ferrocenyl (Fc) unit and a biotin moiety (B) [88]. This original CPP derivative, noted Fc-CPP-B (Fc for the ferrocene redox probe, B for Biotin), could be electrochemically detected at a bare gold bead electrode, at a low concentration (17 µM). The presence of a biotin moiety in the Fc-CPP-B complex allowed its complexation by avidin, which was itself tethered to a thiolated biotin-self-assembled monolayer. Such a modified gold surface, characterized by atomic force microscopy, allowed the immobilization of Fc-CPP-B at the electrode surface and the improvement of the electrochemical detection of the latter (Figure 1.9).

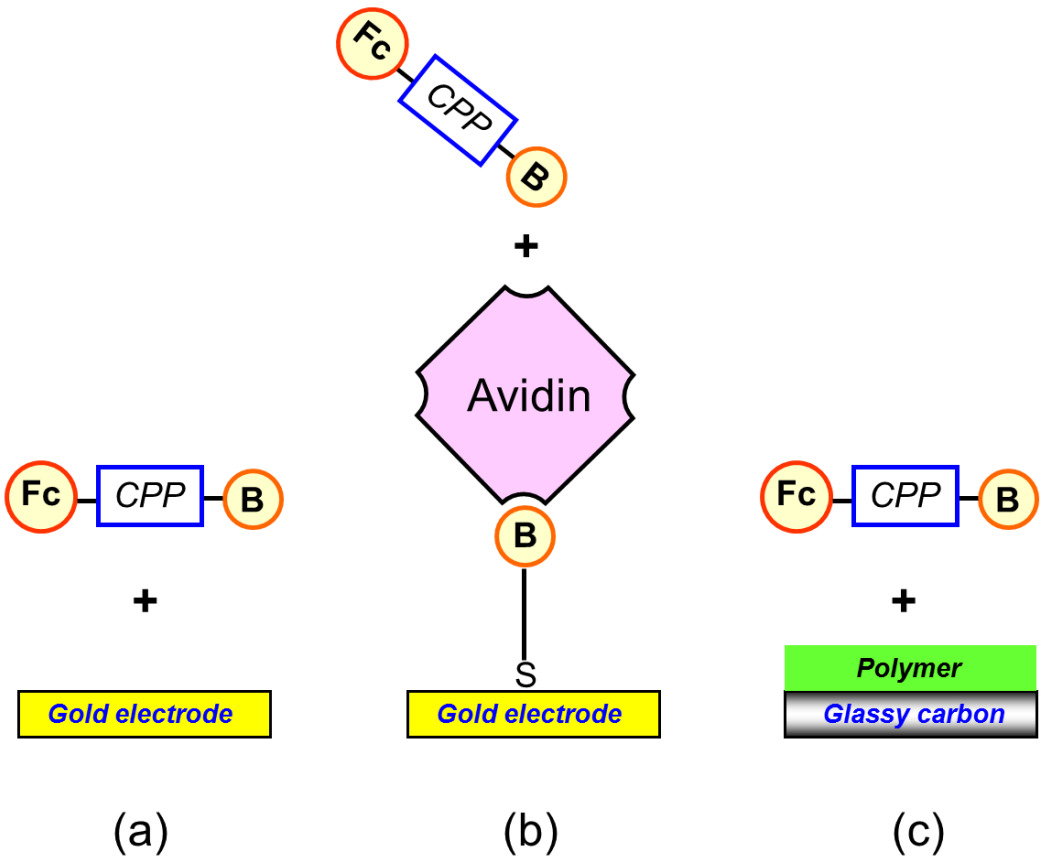

Figure 1.9 Representation of the three strategies developed in [88]. (a) A gold bare electrode; (b) a biotin-avidin self-assembled monolayer over gold substrate and (c) a glassy carbon electrode modified with a cation exchanger polymer. Figure taken from Ref [88].

However, when using the Fc-CPP-B/Avidin method, the electrogenerated ferrocenium cation could not be reduced during the backward scan thus preventing the recovery of the redox probe. This was presumably due to polar interactions between the Fc^+ cation and the avidin environment. In terms of detection and redox probe regeneration, the best results were obtained at a glassy carbon electrode modified with cation exchange polymers such as the poly(estersulfonate) ionomer Eastman AQ55. The ion-exchange voltammetry performed under these conditions allowed the pre-concentration of the peptide at the electrode surface thanks to the net positive charge of the CPP. Interestingly, the anionic character of the polymer contributed to retain the electrogenerated cation Fc^+ in the film so that it could be reduced into its original neutral form (Figure 1.10).

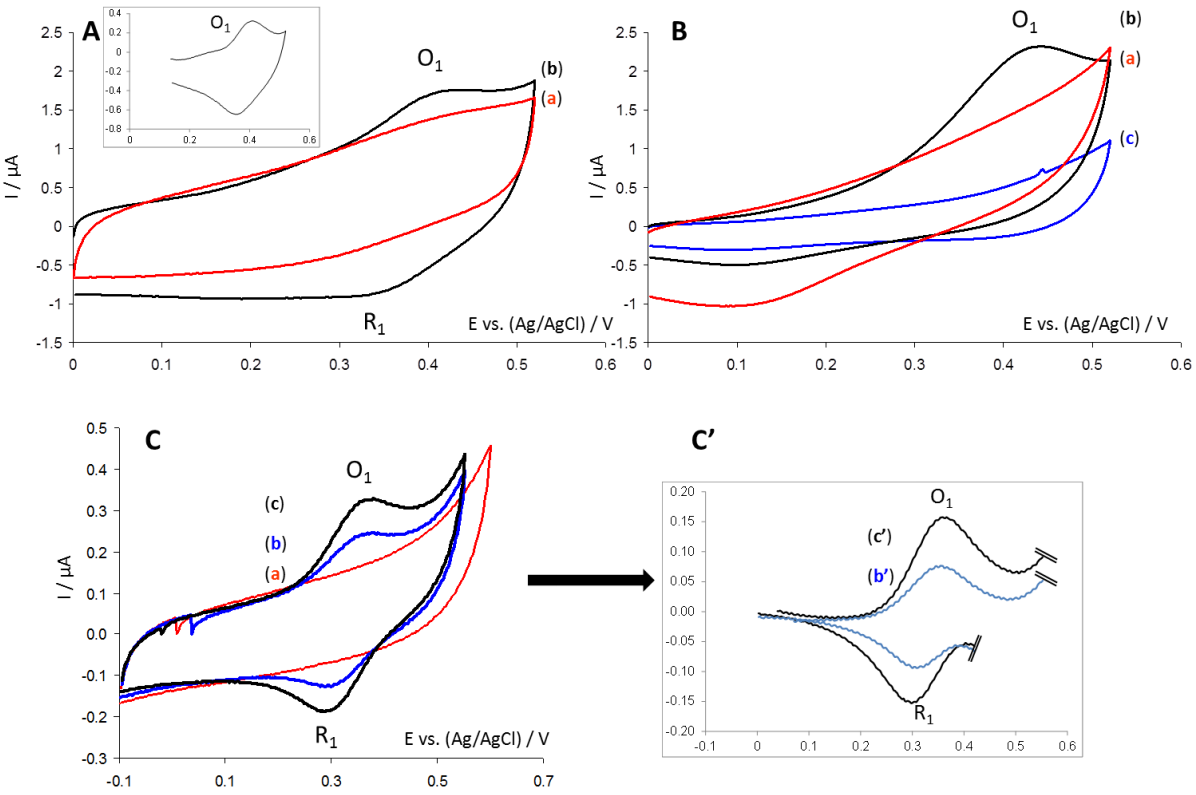

Figure 1.10 (A) Voltametry of the Fc-CPP-biotin derivative at gold bare lelectrode, (B) at gold bead electrode modified with a biotin-avidin self-assembled monolayer and (C) at AQ55 modified glassy carbon electrode. Figure from Ref [88].

This work was aimed at developing a "purely electrochemical" methodology for the detection of cationic CPPs. Although innovating, this strictly electrochemical detection did not provide sufficient sensibility compared to fluorescent techniques and required the formation of avidin-biotin complexes immobilized in a film coating the electrode, an electrochemical configuration poorly adapted to the monitoring of dynamic processes like translocation. However, these results were the starting/launching point of the work described in the next chapters, devoted to the design and implementation of suitable electrochemical setups for CPP monitoring.

References

1. Adams, K.L., Puchades, M., and Ewing, A.G., *In Vitro Electrochemistry of Biological Systems.* Annual Review of Analytical Chemistry, 2008. **1**, 329-355.

2. Cremer, M., *Origin of electromotor properties of tissues, and instructional contribution for polyphasic electrolyte chains.* Zeitschrift Fur Biologie., 1906. **47**, 562-608.
3. Heyrovsky, J., *XXIX. Electrolysis with a dropping mercury cathode. Part I. Deposition of alkali and alkaline earth metals.* Philosophical Magazine, 1923. **45**, 303-315.
4. Heyrovsky, J., *The processes at the mercury dropping cathode. Part I. The deposition of metals.* Transactions of the Faraday Society, 1924. **19**, 692-702.
5. Heyrovsky, J., *The processes at the mercury dropping cathode. Part II. The hydrogen overpotential.* Transactions of the Faraday Society, 1924. **19**, 785-788.
6. Heyrovsky, J., and Shikata, M., *Researches with the dropping mercury cathode: Part II. The Polarograph.* Recueil des Travaux Chimiques des Pays-Bas, 1925. **44**, 496-498.
7. Hart, J.P. and. Wring, S.A., *Recent developments in the design and application of screen-printed electrochemical sensors for biomedical, environmental and industrial analyses.* TrAC Trends in Analytical Chemistry, 1997. **16**, 89-103.
8. Hart, J.P., Crew, A., Crouch, E., Honeychurch, K.C., and Pemberton, R.M., *Some Recent Designs and Developments of Screen-Printed Carbon Electrochemical Sensors/Biosensors for Biomedical, Environmental, and Industrial Analyses.* Analytical Letters, 2004. **37**, 89-830.
9. Amatore, C., Arbault, S.,. Guille, M., and Lemaître, F., *Electrochemical Monitoring of Single Cell Secretion: Vesicular Exocytosis and Oxidative Stress.* Chemical Reviews, 2008. **108**, 2585-2621.
10. Wittenberg, N., Maxson, M., Eves, D., Cans A.S., and Ewing. A. G., *Electrochemistry at the Cell Membrane/Solution Interface*, in *Electrochemical Methods for Neuroscience.* 2006, CRC Press. p. 285-314.
11. Schulte, A. and Schuhmann, W., *Single-Cell Microelectrochemistry.* Angewandte Chemie International Edition, 2007. **46**, 8760-8777.
12. Robinson, D.L., Hermans, A., Seipel, A.T., and Wightman, R.M., *Monitoring Rapid Chemical Communication in the Brain.* Chemical Reviews, 2008. **108**, 2554-2584.
13. Amatore, C., Guille-Collignon, M., and Lemaître, F., *Recent Investigations of Single Living Cells with Ultramicroelectrodes*, in *Nanoelectrochemistry.* 2015, CRC Press. p. 439-468.
14. Schulte, A., Nebel, M., and Schuhmann, W., *Scanning Electrochemical Microscopy in Neuroscience.* Annual Review of Analytical Chemistry, 2010. **3**, 299-318.
15. Bucher, E.S., and Wightman, R.M., *Electrochemical Analysis of Neurotransmitters.* Annual Review of Analytical Chemistry, 2015. **8**, 239-261.
16. Park, J., Takmakov, P., and Wightman, R.M., *In vivo comparison of norepinephrine and dopamine release in rat brain by simultaneous measurements with fast-scan cyclic voltammetry.* Journal of Neurochemistry, 2011. **119**, 932-944.

17. Bunin, M.A., Prioleau, C., Mailman, R.B., and Wightman, R.M., *Release and Uptake Rates of 5-Hydroxytryptamine in the Dorsal Raphe and Substantia Nigra Reticulata of the Rat Brain.* Journal of Neurochemistry, 1998. **70**, 1077-1087.
18. Dressman, S.F., Peters, J.L., and Michael, A.C., *Carbon fiber microelectrodes with multiple sensing elements for in vivo voltammetry.* Journal of Neuroscience Methods, 2002. **119**, 75-81.
19. Wang, J., Trouillon, R., Lin, Y., Svensson, M.I., and Ewing, A.G., *Individually Addressable Thin-Film Ultramicroelectrode Array for Spatial Measurements of Single Vesicle Release.* Analytical Chemistry, 2013. **85**, 5600-5608.
20. Hybertson, B.M., Gao, B., Bose, S.K., and McCord, J.M., *Oxidative stress in health and disease: The therapeutic potential of Nrf2 activation.* Molecular Aspects of Medicine, 2011. **32**, 234-246.
21. Bard, A.J., Wilson, G.S., and Stratmann, M., *Encyclopedia of Electrochemistry, Bioelectrochemistry.* 2002, Wiley.
22. Trujillo, M., Naviliat, M., Alvarez, M., Peluffo, N.G., and Radi, R., *Nitrogen monoxide and oxidative stress: composition and intensity of cellular oxidative bursts cocktail. A study through artificial electrochemical synapses on single human fibroblasts.* Analusis, 2000. **28**, 518-527.
23. Bedioui, F. and Griveau, S., *Electrochemical Detection of Nitric Oxide: Assessement of Twenty Years of Strategies.* Electroanalysis, 2013. **25**, 587-600.
24. Bedioui, F. and N. Villeneuve, *Electrochemical Nitric Oxide Sensors for Biological Samples – Principle, Selected Examples and Applications.* Electroanalysis, 2003. **15**, 5-18.
25. Malinski, T. and Taha, Z., *Nitric oxide release from a single cell measured in situ by a porphyrinic-based microsensor.* Nature, 1992. **358**, 676-678.
26. Malinski, T., Taha, Z., Grunfeld, S., Patton, S., Kapturczak, M., and Tomboulian, P., *Diffusion of Nitric Oxide in the Aorta Wall Monitored in Situ by Porphyrinic Microsensors.* Biochemical and Biophysical Research Communications, 1993. **193**, 1076-1082.
27. Lantoine, F., Trévin, S., Bedioui, F., and Devynck, J., *Selective and sensitive electrochemical measurement of nitric oxide in aqueous solution: discussion and new results.* Journal of Electroanalytical Chemistry, 1995. **392**, 85-89.
28. Shibuki, K., *An electrochemical microprobe for detecting nitric oxide release in brain tissue.* Neuroscience Research, 1990. **9**, 69-76.
29. Shibuki, K., and Okada, D., *Endogenous nitric oxide release required for long-term synaptic depression in the cerebellum.* Nature, 1991. **349**, 326-328.
30. Isik, S., Etienne, M., Oni, J., Blöchl, A., Reiter, S., and Schuhmann, W., *Dual Microelectrodes for Distance Control and Detection of Nitric Oxide from Endothelial Cells by Means of Scanning Electrochemical Microscope.* Analytical Chemistry, 2004. **76**, 6389-6394.

31. Isik, S., and Schuhmann, W., *Detection of Nitric Oxide Release from Single Cells by Using Constant-Distance-Mode Scanning Electrochemical Microscopy.* Angewandte Chemie International Edition, 2006. **45**, 7451-7454.

32. Amatore, C., and Arbault, S., *Oxidative Stress at the SingleCell Level*, in *Electrochemical Methods for Neuroscience.* 2006, CRC Press. p. 261-284.

33. Amatore, C., Arbault, S., Bouton, C., Coffi, K., Drapier, J.-C., Ghandour, H., and Tong, Y., *Monitoring in Real Time with a Microelectrode the Release of Reactive Oxygen and Nitrogen Species by a Single Macrophage Stimulated by its Membrane Mechanical Depolarization.* ChemBioChem, 2006. **7**, 653-661.

34. Amatore, C., Arbault, S., and Erard, M., *Triangulation Mapping of Oxidative Bursts Released by Single Fibroblasts by Amperometry at Microelectrodes.* Analytical Chemistry, 2008. **80**, 9635-9641.

35. Amatore, C., Arbault, S., Bouton, C., Drapier, J.-C., Ghandour, H., and Koh, A.C.W., *Real-Time Amperometric Analysis of Reactive Oxygen and Nitrogen Species Released by Single Immunostimulated Macrophages.* ChemBioChem, 2008. **9**, 1472-1480.

36. Hu, R., Guille, M., Arbault, S., Lin, C.J., and Amatore, C., *In situ electrochemical monitoring of reactive oxygen and nitrogen species released by single MG63 osteosarcoma cell submitted to a mechanical stress.* Physical Chemistry Chemical Physics, 2010. **12**, 10048-10054.

37. Amatore, C., Arbault, S., and Koh, A.C.W., *Simultaneous Detection of Reactive Oxygen and Nitrogen Species Released by a Single Macrophage by Triple Potential-Step Chronoamperometry.* Analytical Chemistry, 2010. **82**, 1411-1419.

38. Oni, J., Pailleret, A., Isik, S., Diab, N., Radtke, I., Blöchl, A., Jackson, M., Bedioui, F., and Schuhmann, W., *Functionalised electrode array for the detection of nitric oxide released by endothelial cells using different NO-sensing chemistries.* Analytical and Bioanalytical Chemistry, 2004. **378**, 1594-1600.

39. Griveau, S., and Bedioui, F., *Overview of significant examples of electrochemical sensor arrays designed for detection of nitric oxide and relevant species in a biological environment.* Analytical and Bioanalytical Chemistry, 2013. **405**, 3475-3488.

40. Quinton, D., Girard, A., Thi Kim, L.T., Raimbault, V., Griscom, L., Razan, F., Griveau, S., and Bedioui, F., *On-chip multi-electrochemical sensor array platform for simultaneous screening of nitric oxide and peroxynitrite.* Lab on a Chip, 2011. **11**, 1342-1350.

41. Yano, H., Inukai, J., Uchida, H., Watanabe, M., Babu, P.K., Kobayashi, T., Chung, J.H., Oldfield, E., and Wieckowski, A., *Particle-size effect of nanoscale platinum catalysts in oxygen reduction reaction: an electrochemical and 195Pt EC-NMR study.* Physical Chemistry Chemical Physics, 2006. **8**, 4932-4939.

42. Karst, U., *Electrochemistry/Mass Spectrometry (EC/MS)—A New Tool To Study Drug Metabolism and Reaction Mechanisms.* Angewandte Chemie International Edition, 2004. **43**, 2476-2478.

43. Tian, Z.-Q. and Ren, B., *ADSORPTION AND REACTION AT ELECTROCHEMICAL INTERFACES AS PROBED BY SURFACE-ENHANCED RAMAN SPECTROSCOPY.* Annual Review of Physical Chemistry, 2004. **55**, 197-229.

44. Wu, D.-Y., Li, J.-F., Ren, B., and Tian, Z.-Q., *Electrochemical surface-enhanced Raman spectroscopy of nanostructures.* Chemical Society Reviews, 2008. **37**, 1025-1041.

45. Abdelsalam, M.E., Bartlett, P.N., Baumberg, J.J., Cintra, S., Kelf, T.A., and Russell, A.E., *Electrochemical SERS at a structured gold surface.* Electrochemistry Communications, 2005. **7**, 740-744.

46. Amatore, C., S. Arbault, I. Bonifas, Y. Bouret, M. Erard, and M. Guille, *Dynamics of Full Fusion During Vesicular Exocytotic Events: Release of Adrenaline by Chromaffin Cells.* ChemPhysChem, 2003. **4**, 147-154.

47. Amatore, C., S. Arbault, I. Bonifas, Y. Bouret, M. Erard, A.G. Ewing, and L.A. Sombers, *Correlation between Vesicle Quantal Size and Fusion Pore Release in Chromaffin Cell Exocytosis.* Biophysical journal, 2005. **88**, 4411-4420.

48. Sombers, L.A., H.J. Hanchar, T.L. Colliver, N. Wittenberg, A. Cans, S. Arbault, C. Amatore, and A.G. Ewing, *The Effects of Vesicular Volume on Secretion through the Fusion Pore in Exocytotic Release from PC12 Cells.* The Journal of Neuroscience, 2004. **24**, 303-309.

49. Amatore, C., A.I. Oleinick, and I. Svir, *Reconstruction of Aperture Functions during Full Fusion in Vesicular Exocytosis of Neurotransmitters.* ChemPhysChem, 2010. **11**, 159-174.

50. Li, Y.-T., S.-H. Zhang, X.-Y. Wang, X.-W. Zhang, A.I. Oleinick, I. Svir, C. Amatore, and W.-H. Huang, *Real-time Monitoring of Discrete Synaptic Release Events and Excitatory Potentials within Self-reconstructed Neuromuscular Junctions.* Angewandte Chemie International Edition, 2015. **54**, 9313-9318.

51. Oleinick, A., F. Lemaitre, M.G. Collignon, I. Svir, and C. Amatore, *Vesicular release of neurotransmitters: converting amperometric measurements into size, dynamics and energetics of initial fusion pores.* Faraday Discussions, 2013. **164**, 33-55.

52. Oleinick, A., R. Hu, B. Ren, Z.-Q. Tian, I. Svir, and C. Amatore, *Theoretical Model of Neurotransmitter Release during In Vivo Vesicular Exocytosis Based on a Grainy Biphasic Nano-Structuration of Chromogranins within Dense Core Matrixes.* Journal of The Electrochemical Society, 2016. **163**, H3014-H3024.

53. Amatore, C., S. Arbault, Y. Chen, C. Crozatier, F. Lemaître, and Y. Verchier, *Coupling of Electrochemistry and Fluorescence Microscopy at Indium Tin Oxide Microelectrodes for the Analysis of Single Exocytotic Events.* Angewandte Chemie International Edition, 2006. **45**, p. 4000-4003.

54. Meunier, A., O. Jouannot, R. Fulcrand, I. Fanget, M. Bretou, E. Karatekin, S. Arbault, M. Guille, F. Darchen, F. Lemaître, and C. Amatore, *Coupling Amperometry and Total Internal Reflection Fluorescence Microscopy at ITO Surfaces for Monitoring Exocytosis of Single Vesicles.* Angewandte Chemie International Edition, 2011. **50**, 5081-5084.

55. Federici, M., E.C. Latagliata, A. Ledonne, F.R. Rizzo, M. Feligioni, D. Sulzer, M. Dunn, D. Sames, H. Gu, R. Nisticò, S. Puglisi-Allegra, and N.B. Mercuri, *Paradoxical Abatement of Striatal Dopaminergic Transmission by Cocaine and Methylphenidate.* Journal of Biological Chemistry, 2014. **289**, 264-274.

56. Miomandre, F., R. Meallet-Renault, J.-J. Vachon, R.B. Pansu, and P. Audebert, *Fluorescence microscopy coupled to electrochemistry: a powerful tool for the controlled electrochemical switch of fluorescent molecules.* Chemical Communications, 2008, 1913-1915.

57. Miomandre, F., E. Lépicier, S. Munteanu, O. Galangau, J.F. Audibert, R. Méallet-Renault, P. Audebert, and R.B. Pansu, *Electrochemical Monitoring of the Fluorescence Emission of Tetrazine and Bodipy Dyes Using Total Internal Reflection Fluorescence Microscopy Coupled to Electrochemistry.* ACS Applied Materials & Interfaces, 2011. **3**, 690-696.

58. Frankel, A.D. and C.O. Pabo, *Cellular uptake of the tat protein from human immunodeficiency virus.* Cell. **55**, 1189-1193.

59. Green, M. and P.M. Loewenstein, *Autonomous functional domains of chemically synthesized human immunodeficiency virus tat trans-activator protein.* Cell. **55**, 1179-1188.

60. Joliot, A., C. Pernelle, H. Deagostini-Bazin, and A. Prochiantz, *Antennapedia homeobox peptide regulates neural morphogenesis.* Proceedings of the National Academy of Sciences, 1991. **88**, 1864-1868.

61. Green, M., M. Ishino, and P.M. Loewenstein, *Mutational analysis of HIV-1 Tat minimal domain peptides: Identification of trans-dominant mutants that suppress HIV-LTR-driven gene expression.* Cell, 1989. **58**, 215-223.

62. Vivès, E., P. Brodin, and B. Lebleu, *A Truncated HIV-1 Tat Protein Basic Domain Rapidly Translocates through the Plasma Membrane and Accumulates in the Cell Nucleus.* Journal of Biological Chemistry, 1997. **272**, 16010-16017.

63. Derossi, D., A.H. Joliot, G. Chassaing, and A. Prochiantz, *The third helix of the Antennapedia homeodomain translocates through biological membranes.* Journal of Biological Chemistry, 1994. **269**, 10444-50.

64. Bechara, C. and S. Sagan, *Cell-penetrating peptides: 20 years later, where do we stand?* FEBS letters, 2013. 587, 1693-1702.

65. Heitz, F., M.C. Morris, and G. Divita, *Twenty years of cell-penetrating peptides: from molecular mechanisms to therapeutics.* British Journal of Pharmacology, 2009. 157, 195-206.

66. Stewart, K.M., K.L. Horton, and S.O. Kelley, *Cell-penetrating peptides as delivery vehicles for biology and medicine.* Organic & Biomolecular Chemistry, 2008. 6, 2242-2255.

67. Vivès, E., J. Schmidt, and A. Pèlegrin, *Cell-penetrating and cell-targeting peptides in drug delivery.* Biochimica et Biophysica Acta (BBA) - Reviews on Cancer, 2008. 1786, 126-138.

68. Marx, V., *Cell biology: delivering tough cargo into cells.* Nat Meth, 2016. 13, 37-40.

69. Milletti, F., *Cell-penetrating peptides: classes, origin, and current landscape.* Drug Discovery Today, 2012. 17, 850-860.

70. Johansson, H.J., S. El-Andaloussi, T. Holm, M. Mae, J. Janes, T. Maimets, and U. Langel, *Characterization of a Novel Cytotoxic Cell[hyphen]penetrating Peptide Derived From p14ARF Protein.* Mol Ther, 2007. 16, 115-123.

71. Copolovici, D.M., K. Langel, E. Eriste, and Ü. Langel, *Cell-Penetrating Peptides: Design, Synthesis, and Applications.* ACS Nano, 2014. 8, 1972-1994.

72. Kauffman, W.B., T. Fuselier, J. He, and W.C. Wimley, *Mechanism Matters: A Taxonomy of Cell Penetrating Peptides.* Trends in Biochemical Sciences. 40, 749-764.

73. Nakase, I., H. Akita, K. Kogure, A. Gräslund, Ü. Langel, H. Harashima, and S. Futaki, *Efficient Intracellular Delivery of Nucleic Acid Pharmaceuticals Using Cell-Penetrating Peptides.* Accounts of Chemical Research, 2012. 45, 1132-1139.

74. Reissmann, S., *Cell penetration: scope and limitations by the application of cell-penetrating peptides.* Journal of Peptide Science, 2014. 20, 760-784.

75. Fonseca, S.B., M.P. Pereira, and S.O. Kelley, *Recent advances in the use of cell-penetrating peptides for medical and biological applications.* Advanced Drug Delivery Reviews, 2009. 61, 953-964.

76. Wang, F., Y. Wang, X. Zhang, W. Zhang, S. Guo, and F. Jin, *Recent progress of cell-penetrating peptides as new carriers for intracellular cargo delivery.* Journal of Controlled Release, 2014. 174, 126-136.

77. Santra, S., H. Yang, J.T. Stanley, P.H. Holloway, B.M. Moudgil, G. Walter, and R.A. Mericle, *Rapid and effective labeling of brain tissue using TAT-conjugated CdS[ratio]Mn/ZnS quantum dots.* Chemical Communications, 2005, 25, 3144-3146.

78. Olson, E.S., T. Jiang, T.A. Aguilera, Q.T. Nguyen, L.G. Ellies, M. Scadeng, and R.Y. Tsien, *Activatable cell penetrating peptides linked to nanoparticles as dual probes for in vivo fluorescence and MR imaging of proteases.* Proceedings of the National Academy of Sciences, 2010. 107, 4311-4316.

79. Bozym, R.A., R.B. Thompson, A.K. Stoddard, and C.A. Fierke, *Measuring Picomolar Intracellular Exchangeable Zinc in PC-12 Cells Using a Ratiometric Fluorescence Biosensor.* ACS chemical biology, 2006. 1, 103-111.

80. Madani, F., S. Lindberg, Langel, #220, lo, S. Futaki, Gr, #228, and A. slund, *Mechanisms of Cellular Uptake of Cell-Penetrating Peptides.* Journal of Biophysics, 2011. 2011.

81. Gruenberg, J., *The endocytic pathway: a mosaic of domains.* Nat Rev Mol Cell Biol, 2001. 2, 721-730.

82. Lindgren, M., M. Hällbrink, A. Prochiantz, and Ü. Langel, *Cell-penetrating peptides.* Trends in Pharmacological Sciences, 2000. 21, 99-103.

83. Di Pisa, M., G. Chassaing, and J.-M. Swiecicki, *Translocation Mechanism(s) of Cell-Penetrating Peptides: Biophysical Studies Using Artificial Membrane Bilayers.* Biochemistry, 2015. 54, 194-207.

84. Sébastien, D., C.M. May, D. Gilles, and H. Frederic, *Interactions of Cell-Penetrating Peptides with Model Membranes*, in *Handbook of Cell-Penetrating Peptides, Second Edition,* 2006, CRC Press. p. 139-160.

85. Gräslund, A. and L.E.G. Eriksson, *Biophysical Studies of Cell-Penetrating Peptides*. Cell-Penetrating Peptides: Processes and Applications ed. U. Langel; 2002: CRC Press.

86. Holm, T., H. Johansson, P. Lundberg, M. Pooga, M. Lindgren, and U. Langel, *Studying the uptake of cell-penetrating peptides.* Nat. Protocols, 2006. 1, 1001-1005.

87. Armstrong, V.T., M.R. Brzustowicz, S.R. Wassall, L.J. Jenski, and W. Stillwell, *Rapid flip-flop in polyunsaturated (docosahexaenoate) phospholipid membranes.* Archives of Biochemistry and Biophysics, 2003. 414, 74-82.

88. Messina, P., G. Hallais, E. Labbé, M. Béranger, G. Chassaing, S. Lavielle, C. Mansuy, O. Buriez, and C. Amatore, *Electrochemistry of a ferrocene-grafted cell-penetrating peptide.* Electrochimica Acta, 2012. 80, 180-186.

Second Chapter:

Contribution of electrochemistry to detect cell-penetrating peptides in confined environments

2. Second Chapter: Contribution of electrochemistry to detect cell-penetrating peptides in confined environments

2.1. Introduction

As shown in the previous chapter, the electrochemical detection of a cell-penetrating peptide (CPP) tagged with a ferrocenyl moiety has already been investigated in the group [1]. However, these experiments required large CPP amounts due to the electrochemical device used (milliliter electrochemical cell and millimetric sized electrodes). Within this context, we implemented of a simple three-electrode micro-cell equipped with a conventional reference saturated calomel electrode (SCE) based on micro-volume droplets suspended by capillary forces to the fritted glass of the SCE bridge. Under these conditions, working and counter electrodes were simply introduced through the droplet surface, allowing classical electrochemistry to be readily performed in minute samples. In parallel to the development of this micro-electroanalytical cell, an alternative strategy for the electrochemical detection of a CPP crossing a suspended artificial membrane was attempted via combination of the patch-clamp principle and amperometric detection. These two electrochemical approaches will be presented in this second chapter. Before developing these aspects, it will be recalled how electrochemistry can contribute to the analysis in small volumes and to the detection of peptides.

2.2. Contribution of electrochemistry to the analysis in small volumes

From a general point of view, miniaturization of analytical techniques is an important issue for samples of low availability and for the development of portable devices, as well as for evident economic and ecological reasons (consumption of small amounts of precious and/or expensive reagents, waste production). Within this framework, electrochemistry brings a significant contribution to the analysis in small volumes, notably through the miniaturization of electrodes and thanks to the development of microfabrication techniques (photolithography, screen printing, plasma etching, and laser ablation).

2.2.1. Miniaturization of electrodes

2.2.1.1. Miniaturization of the working electrode

Miniaturization of working electrodes is a continuously growing trend in the field of electro-analysis [2]. The development of ultramicroelectrodes, which are electrodes with diameters less than 25 µm, offers practical advantages, but also opened new fundamental possibilities [3]. Their small sizes offer unique electrochemical characteristics such as minimization of solution resistance effects and rapid response times. Moreover, they exhibit excellent signal-to-background characteristics [3]. Due to these characteristics, such electrode can be advantageously used in local concentration profiles measurements [4], for detection in microflow systems [5], and the analysis of very small (microliter) sample volumes [2]. Furthermore, they can be used in investigations aimed at time-resolved probing of dynamic processes in single cells (secretion of chemical messengers), the in vivo monitoring of neurochemical events (stimulated dopamine release), and the in vivo detection of nitric oxide [6], the use of nanoscopic electrode tips for single-molecule detection [7]. Electrodes can be fabricated in the low µm diameter range by sealing etched platinum or gold microwires, or carbon fibers in glass [8].

On the other hand, the development of micro-fabrication techniques such as photolithography [8-14], screen printing [15, 16], plasma etching [17], and laser ablation [18, 19] allowed the preparation of volume-limited structures.

(i) Screen printing

This technology is a widely used technique for the production of economical, portable, and disposable electrochemical sensors [15]. In procedure (Figure 2.1A), a thixotropic fluid is printed through a mesh screen, which defines the shape and the size of the desired electrode. The thixotropic fluid is composed of substances such as graphite, carbon blank, solvents and polymeric binder. This ink is very viscous but even so can be forced through the screen mesh by a roller or squeegee. This step allows the ink penetrate across the open areas of the mesh, defining thus the final shape/design. When the ink touches the substrate (normally a ceramic or plastic material) [20], it returns to its viscous state forming the shape/design. These shapes/designs have thickness of about 20 to 100 µm, a thickness bigger than those obtained by other printing methodologies. Figure 2.1B shows a scheme of a screen printed device involving a working, a counter and a reference electrode.

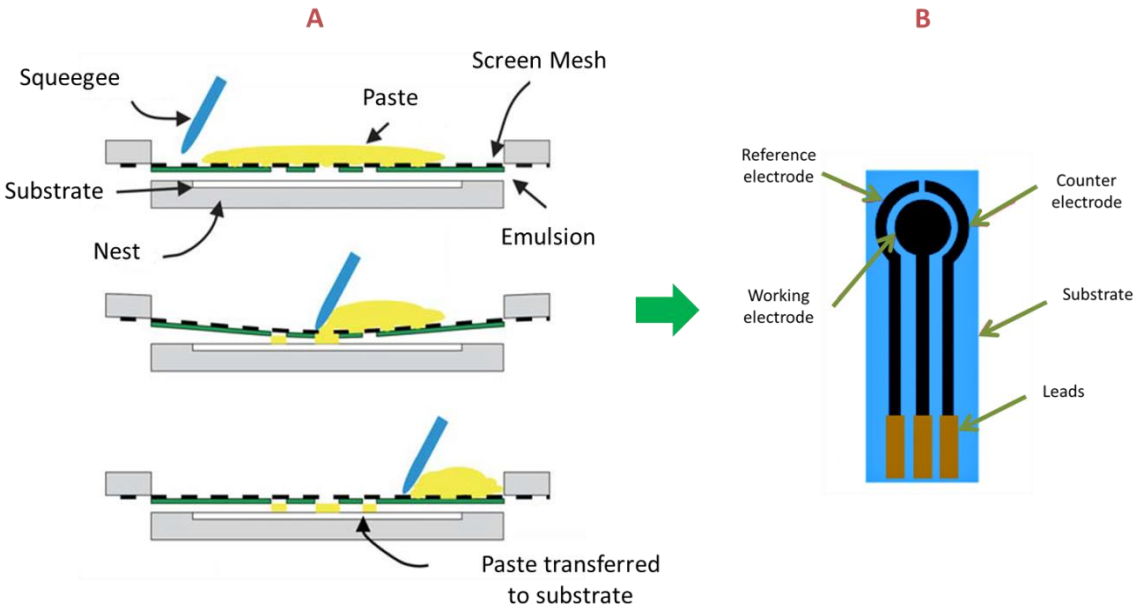

Figure 2.1 (A) Cross-sectional side view of the main steps allowing fabrication of electrodes by screen printing method. Adapted from Ref [20]. (B) Scheme of a screen printed electrode.

(ii) Photolithography

Photolithography is a readily employed microfabrication technique to create patterns into a material. Such pattern is generated on a substrate through exposure of regions of a light-sensitive material to ultraviolet (UV) light. The overall process is depicted in Figure 2.2A. The fabrication starts by coating a substrate material (i. e. silicone or glass) with a layer of a photoresist, or light-sensitive polymer. A photomask, made by patterning with an opaque material the desired shape on a transparent material, is thus placed on top of the substrate and the photoresist. This assembly is then irradiated with UV light, which exposes the sections of the photoresist not covered by the opaque regions of the photomask. Depending on the type of photoresist utilized, it will undergo one of two possible transformations upon exposure to light. For instance, when light illuminates a positive photoresist the exposed regions break down and become more soluble in a developing solution. Conversely, after illumination, a negative photoresist becomes crosslinked and thus insoluble in the developing solution. As a result, only parts not exposed to light will be removed upon contact with the developing solution. After the desired process is completed, the photoresist can be removed, leaving the pattern design on the substrate [21]. Figure 2.2B shows a scanning electron micrograph of: a platinized working electrode (Figure 2.2B, 1), a platinum counter electrode (Figure 2.2B, 2) and a silver reference electrode, all of them patterned by UV exposure and using a negative photoresist [12].

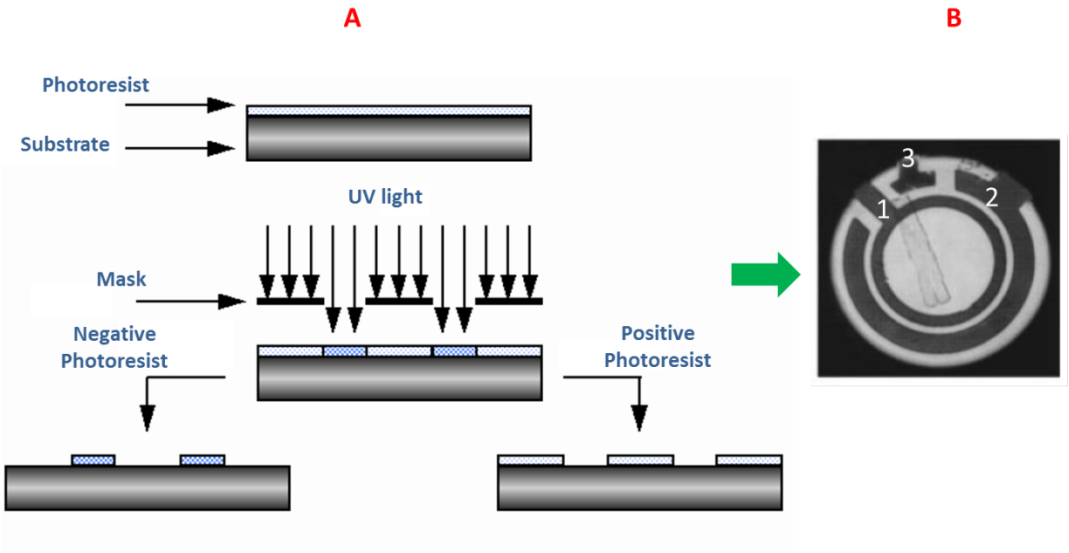

Figure 2.2 (A) Process of photolithography. A mask with opaque regions in the desired pattern is used to selectively illuminate a light-sensitive photoresist. Depending on the type of photoresist utilized, it will become more soluble (positive photoresist) or crosslinked (negative photoresist) after UV light exposure, thus generating the appropriate pattern upon developing. Figure adapted from [21]. (B) Scanning electron micrograph showing (1) working, (2) counter and (3) reference electrodes patterned by photolithography. Picture adapted from Ref [12].

(iii) Etching

Etching is a process that aims at creating topographical features on a surface by selective removal of material through physical or chemical means. Etching can be isotropic if it acts equally in all directions or anisotropic if it proceeds in one specific direction. Isotropic etching occurs not only in the direction of the depth, but also laterally, and results in a curved profile (Figure 2.3-A). Anisotropic etching occurs in only one direction, usually selectively increasing the depth of the cavity (Figure 2.3-B/2.3-C). The mechanisms used for etching utilize liquid chemicals or gas-phase physicochemical-processes (for instance, reactive ion etching, which utilizes oxygen or fluorine plasma). These methods are more commonly known as wet etching or dry etching. Dry anisotropic etching results in a flat profile, while wet anisotropic etching results in cavities with inclined side-walls. The characteristic slanted profile of wet anisotropic etching is a result of the interaction of the etching reagent with the crystalline structure of the material being etched. The crystal structure determines the rate of etching that occurs at crystal plane [21]. Figure 2.3D shows a 52 µm diameter electrode patterned by plasma etching [17]. The round shape of the pattern is typical for isotropic etching by plasma (Figure 2.3-A).

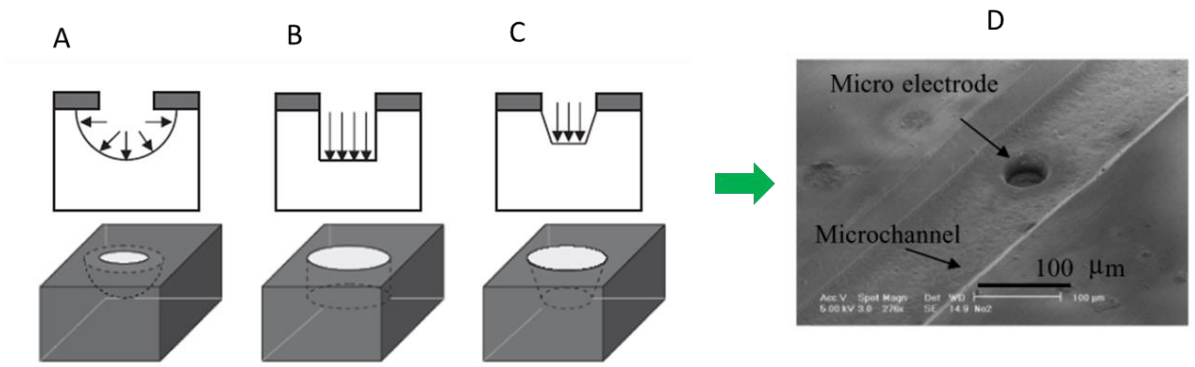

Figure 2.3 Etching profiles generated with (A) isotropic etching, (B) dry anisotropic etching, and (C) wet anisotropic etching. (D) Scanning electronic micrograph of a 52 µm diameter electrode patterned by plasma etching. Adapted from Ref [17].

(iv) Laser ablation

Laser ablation provides a relatively simple, direct, and rapid mean to make nano/micro-structures. In this technique, a laser pulse causes the ejection of highly excited particles and neutral atoms from the target material surface in the form of nonequilibrium highly-energy and very dense plasma cloud. Evaporated particles (atoms, ions, electron, and clusters) are ejected from the target surface, which causes the ablation of the target (Figure 2.4-A). The properties of the fabricated structure such as its shape and size, depend on the laser characteristics adjusted for ablation (radiation wavelength, pulse length and repetition rate, and pulse energy) and surrounding conditions (vacuum, fixed gas pressure, or liquid) [22]. In electrochemistry, this technique is generally coupled with screen printing or sputter deposition to make nanovials with “built-in” working and reference electrodes.

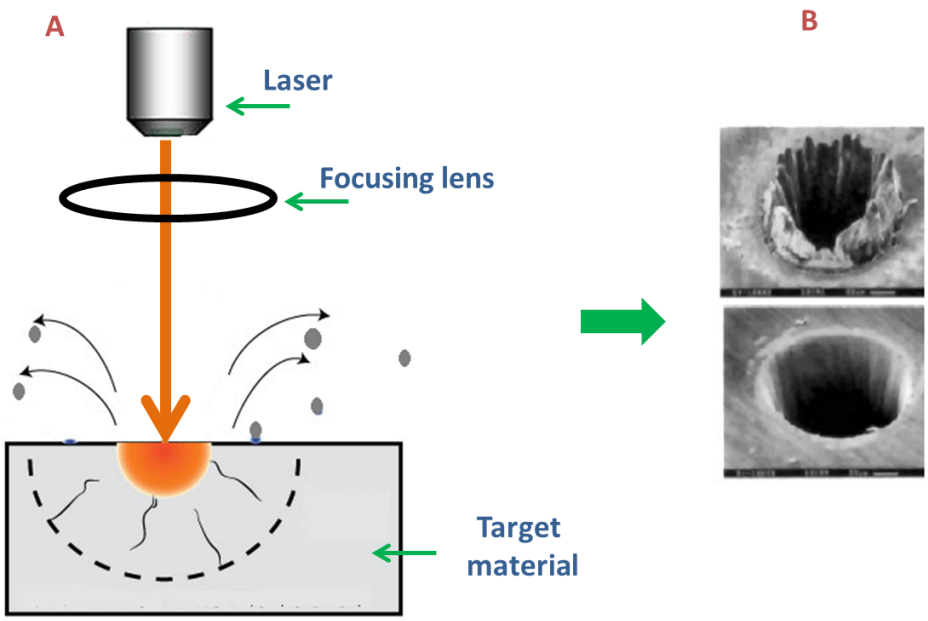

Figure 2.4 Scheme of the fabrication of a microstructure by laser ablation. (A) The laser beam vertically irradiates the target which causes the ablation of this structure. (B). Hole drilled in a 100-µm thick steel foil by laser pulses each 3.3 ns at λ = 780 nm. Figure adapted from reference [22].

2.2.1.2. Miniaturization of reference electrodes

Microscale reference electrodes (µRE) are typically miniaturized versions of conventional macroscale reference electrode (See appendix 6.2). In this case, even if all the electrode components are miniaturized, the µRE conserves the same function principle of the classical RE [23]. Attempts to fabricate miniaturized RE can be classified in three categories. The first category deals with the miniaturization of the entire equivalent RE, preserving its basic structure and operational principle. One challenge with this approach relies in the construction of the liquid-junction cavity [23]. The second category keeps the active component of a reference electrode, but replaces the liquid inner electrolyte with a solid one. This is generally carried-out by coating the active component with a polymer, a NAFION membrane or a gel [23]. The third category lies in the use of pseudo-reference wire-shaped electrodes such as Ag, Ag/AgCl, or Pt, which are placed directly into the solution. The requirements for an ideal RE, methods of construction, and examples of miniaturized RE are discussed below.

The scaling-down of a RE requires of particular attention in controlling factors such as potential drift, liquid junction effects and solution concentrations [24]. Overlooking the control of these factors can lead to misleading results. The following features are required to build functional and robust μRE [25]:

- Non-polarizability
- A sample-independent potential value maintained over a wide temperature range
- Good short-term and long-term stability without contaminating the sample by leaching
- Short equilibration time
- Low susceptibility to junction contamination
- Fast activation after storage
- Easy fabrication

These requirements may ensure the proper device operation and reliability of the results [24]. Above all, it is imperative to have an electrode with a long lifetime. This is a serious problem faced in miniaturization, due to the rapid dissolution of small electrode volumes during operation. Thin electrode layers get depleted faster exposing the underlying support directly to the solution, creating mixed potentials [24]. To avoid this downside, the electrode layers are protected with a sort of diffusion barrier, which usually is a gel or a polymer film [23].

The μREs are generally fabricating employing technologies as thin film deposition, electroplating, and screen printing [24]. They are described below.

(i) Thin film deposition. This is achieved by evaporation, sputter or chemical vapor deposition (CVD) of the electrode material onto a metallic lead patterned by lithography.

(ii) Electroplating. Here, the substrate is electrochemically treated into a bath containing cations of the required material.

(iii) Screen printing. This involves pressing the electrode metal “ink” on a surface using a blocking meshed stencil. The present technique can produce the highest thickness of the electrode material, but is normally done as a manual step and not integrated with automated processing techniques.

After its deposition, the metal is coated with a layer of a salt having a cation of the same nature of the metal used previously. For instance, a silver (Ag) layer is chlorinated to produce the coating silver chloride (AgCl). In calomel electrodes, a layer of mercury (I) chloride (Hg_2Cl_2, known as calomel) is introduced along the mercury drop. The standard hydrogen electrodes using platinum substrates are generally coated with platinum black to enhance charge transfer dynamics [24]. The coating procedure depends on the type of chemistry needed and on the resulting surface geometry. Some coating technologies are [24]:

a. Direct mixture deposition. Here, a paste of a metallic salt compound is directly deposited onto the metal's surface. Although this step is easy to accomplish, some problems appear when there in an incorrect adhesion of the layer. Moreover, the reliability of the electrode is affected by the homogeneity of the employed paste.

b. Ion exchange reaction. In this approach the coating film is formed by a chemical reaction between the metal substrate and another compound. For instance, a deposit of Ag reacts with a solution of $FeCl_3$ to form an AgCl layer.

c. Electrochemical coating. Here, the preparation of the metallic salt layer is carried-out by the electrochemical reduction of dissolved metal cations present in an electrolytic bath.

The final step of designing is the fabrication of the electrolyte solution container. Indeed, in miniaturized electrodes, the container acts as both a reservoir of the electrolytic material and as a diffusion barrier to decrease the electrode dissolution. Some of these barriers are constructed by:

- Porous materials: natural porous materials such as agarose gel; these are placed between the reference and test solutions.

- Gel: synthetic gels such as polyacrylamide.

- Nano-porous membranes: these materials are polymer membranes containing Nano-channels across their structure. The channels are made using laser ablation. The sizes of the Nano-pores are adjusted to achieve the required junction resistance.

The former technologies are tested to fabricate a reliable electrode that works as similar as possible to its macro-sized version. But in practice, as the designing of a µRE depends on the application and the availability of specific ionic species in the sample, most of the time the construction cannot include all the features of a classical RE. AS a consequence, a given µRE that serves as a good reference electrode in a particular environment might be unsuitable for others. Moreover, as certain µRE are complicated to build, there are a few electrodes types that appear more frequently than others [24]. Some of them are described below.

(i) Microfabricated solid-state Silver/Silver chloride

The most popular type of µRE is the miniaturized version of the silver-silver chloride RE (Ag/AgCl). The classical Ag/AgCl RE consists of a silver wire coated by a substantial layer of silver chloride and immersed in solution rich in chloride ion (i. e. KCl 3 M) [26]. The electrode reaction in aqueous media is:

$$AgCl(s) + e^- \rightleftarrows Ag(s) + Cl^-(aq) \qquad (1)$$

The potential is calculated as shown in Eq (2):

$$E_{Ag/AgCl} = E^{\circ}_{Ag/AgCl} - \frac{RT}{F} ln a_{Cl^-} \qquad (2)$$

According to equation (2), the chlorine ion activity defines the electrode potential. In a rich chloride filling solution, negligible changes in the chloride activity are caused for a flow of current hence will not affect significantly its chemical potential. That is the origin of the electrode stability [26]. The Ag/AgCl RE has advantages such as simple and inexpensive design, involves non-toxic components, and importantly, lends itself to microfabrication as well as incorporation into sensors [23]. Based on these advantages, researchers have developed µAg/AgCl REs that vary in size and design. However, they hold a similar feature: the filling solution is replaced with a solid state-exchange membrane doped with the ions required for the electrode equilibrium. These “novel sources of chloride” create a diffusion barrier to slow down the rate at which the AgCl dissolves and simultaneously provide a relatively constant activity of chloride ion [24]. The used doped membranes are electrolyte gels and polymer films [23]. The first type, are mixtures of agar gel and saturated KCl (Figure 2.5 -1) which are deposed over the µAg/AgCl thin films by spin coating or screen printed techniques.

Last modification makes the reference electrode insensitive to pH in the range of 4 – 10 and Cl- ion concentration from the range of 10^{-6} M to 0.3 M [24].

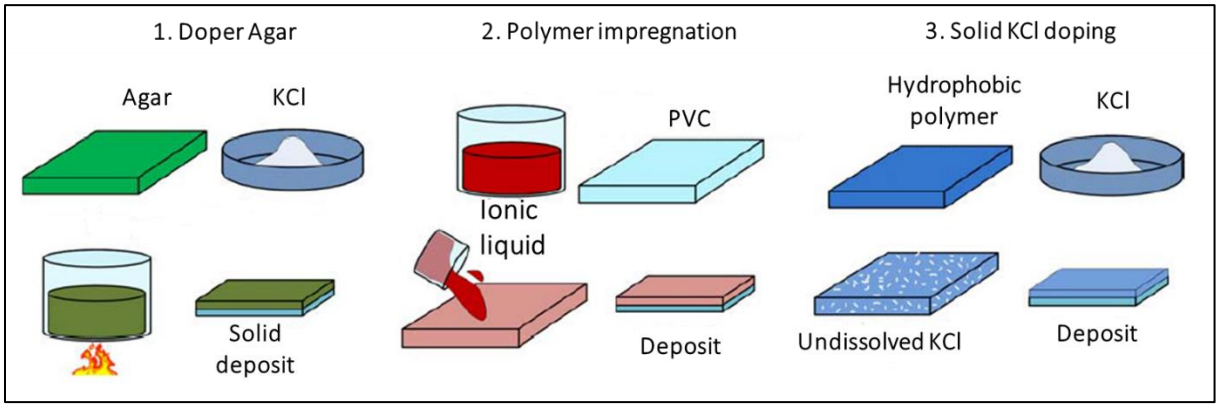

Figure 2.5 Different methods for synthesis of a solid – state membrane. Figure from Ref [24].

Another possibility to integrate the electrolyte-gel into a µAg/AgCl consists in immobilizing KCl over a hydrophobic material (Figure 2.5-3) such as polyurethane, nafion, or silicone. This strategy avoids the problem of variation of the KCl concentration, as occurs with agar gel [24]. The variation comes principally from two sources, KCl dilution over the agar, and drying process due to long storing times. These processes bring as a consequence an instability of the electrode potential [24]. To avoid the former problem, it is possible to incorporate an ionic liquid as the 1 – dodecyl – 3 – methylimidazolium chloride into a matrix of polyvinyl chloride (PVC, Figure 2.5-2). The ionic liquid replaces the KCl in the solid matrix and maintains the ion-chloride concentration constant in the internal solid electrolyte. Moreover, as ionic liquids have low vapor pressure and thus volatility, the drying issue is not a problem after long times of storage [24]. Although the above strategies improve the Ag/AgCl stability, the problems associated with coating dissolution and inadequate diffusion of the internal electrolyte remain at different degree, prone to affect the electrode performance [27] and utilization [24].

(ii) Miniaturized mercury electrodes

Other examples of µRE are given by the miniaturized Mercury Sulfate Reference Electrode (MSRE), which are developed following the method of agar-based µRE [28]. This approach corresponds to a reference electrode of second type in which the electrolyte is directly determining the concentration of the anions via their solubility product. µMSRE are formed by an amalgamated mercury-gold (AuHg) coated with a layer of either Hg_2SO_4 or $Hg_2(CH_3COO)_2$. The mercurous salts are deposited by electroplating. The reference potential is calculated by Equation (3):

$$E^{Hg/Hg_2^{2+}} = E_0^{Hg/Hg_2^{2+}} + \frac{RT}{2F} ln \frac{[Hg_2^{2+}]}{[Hg]^2} \quad (3)$$

The µMSRE approach replaces the SO_4^{2-} filling solution founded in the MSRE, by an agar gel matrix saturated with a common ion to that of the salt (i.e. $NaSO_4$, $NaCH_3COO$). The $AuHg/(Hg_2)nX_m$ wire is immersed into the agar matrix and contained in a glass capillary that provides a structural support to the electrode [29]. Although the device shows a long time and potential stability, the incorporation of the agar electrolyte is not readily compatible with microfabrication techniques [24].

As the MSRE, the conventional calomel electrode has also been miniaturized [30]. This approach was developed to record DC potentials changes from the brain of freely moving rats. The design of the miniaturized electrode was done following the same scheme adopted for usual calomel electrodes. It means a drop of pure mercury is placed in contact with a layer of calomel. An important feature here is that the layer is formed by immersing a cotton or paper matrix saturated with calomel in a 10 % of NaCl solution. Both the mercury drop and the calomel layer are encapsulated in the upper part of a pulled-glass capillary. The capillary tip is filled with an agar gel matrix, composed of 10 % of NaCl solution in 2 % of agar.

The described approaches attempt to realize reference electrodes preserving the whole function of macroscopic reference electrodes. However, they all suffer of potential instability, undesired cross – sensitivity towards anions, and shorter lifetimes compared to their macroscopic versions. This limits their application to specific analysis. On the other hand, approaches as the “quasi-reference” electrodes are only usable under well-defined environments due to their sensitivity towards activity changes of their primary anion. For instance, silver-silver chloride wires immersed in solutions with poor content of chloride ion could lead to potential drifts. In this work, we proposed a new approach operating with a real reference electrode.

2.2.3. Electrochemistry in small volumes

Two main approaches have been developed aimed at running electrochemistry in small volumes. The first one, essentially developed in view of the detection of small numbers of molecules released by single cells, consists either in the immersion of needle-type micro-electrodes in small chambers, or vials, prepared by micro-fabrication techniques [9, 10, 31, 32], or the microfabrication of vials whose electrodes are formed in situ in the chambers by photolithography techniques [33].

a) Microvials

Microvials are devices developed to perform electrochemical experiments using volumes ranging from few microliters to nanoliters [33]. These devices are fabricated with photolithography, laser ablation, hot press method, screen printed and ink jet printing techniques, or a combination of them [33]. For instance, a vial template was first prepared with a technique such as photolithography, and then transferred into a substrate with a hot press method. There are two prominent ways of working with these containers. The simplest one involves micromanipulators to position the working and the reference electrode into the vial. The second one is preparing structures with integrated functional electrodes [34]. These electrodes are formed by techniques such as electrochemical deposition, microfabrication and photolithography or by the combination of screen printing and laser ablation [33]. However, an important drawback of such fabricating methods is that the materials forming the sides and bottom of the vials are not always the same. This could lead to different adsorption of analytes and therefore erroneous voltammograms [33] (Figure 2.6).

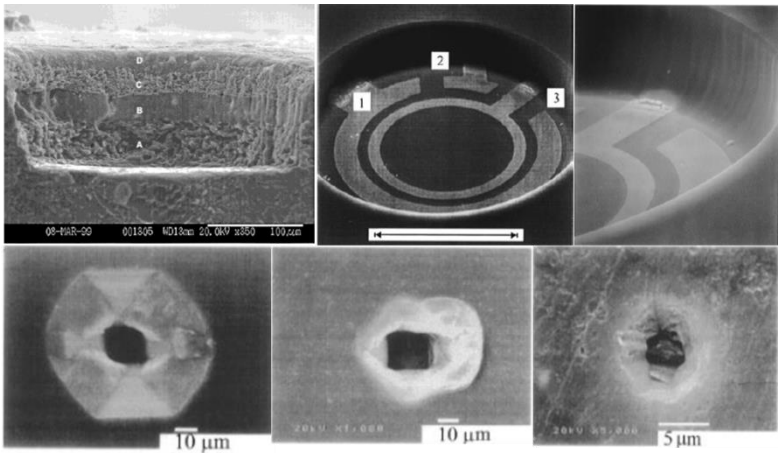

Figure 2.6. Scanning-electron micrographs of three types of microvials. The leftmost images are polystyrene microvials fabricated with photolithography and hot press method. The center images are vials photolithographically defined polyimide wells. The rightmost image is a vial prepared by ink jet printing followed by laser ablation. From Ref [33].

Another approach is the preparation of transparent containers from, for instance, fused-silica capillaries, which are suitable for the observation and manipulation of both electrodes and sample [34]. In this system, an electrochemically chlorined silver wire is inserted into the capillary and acts as a reference electrode. The volume of the container is determined by the insertion depth of the silver wire, which normally leaves a void space of picoliters. A better way to control the container volumes is achieved by lithography. This technique is used to fabricate templates that are imprinted in

polystyrene [34]. The final transparent microvial ranging from 300 to 0.4 pL can be easily viewed with transmission light microscopy.

Alternatively, the second route deals with the immersion of needle-type micro-electrodes within droplets, or meniscus, thus avoiding the preparation of containers [34, 35]. This approach has been implemented with micro-, nano-, pico- and femto-liter droplets deposited either on a substrate or onto the electrode itself.

b) Microscopic droplets

Micro volume droplets are generally deposited onto the working electrode surface [25, 27]. However, comparatively large liquid-solid reference electrode (e.g. SCE) cannot be immersed in such drops. Instead, pseudo-reference wire-shaped electrodes such as Ag, Ag/AgCl, or Pt are used though they suffer from potential instability with some species [28, 36, 37].

Droplets enable the encapsulation of small volumes without the need of a solid container [23]. They can be stably formed using appropriate substrates and experimental conditions [34]. Since performing electrochemistry in small volumes does not require that the sample container is defined by solid boundaries, droplets can be used as micro-electrochemical cells. When droplets are formed directly over a substrate different from an electrode surface, the electrochemical analysis requires both the working and reference electrode to be positioned into the sample by micromanipulation [23]. On the other hand, when droplets are placed over an electrode surface (electrode surface modification), the sample does not have to contain any added supported electrolyte as the droplet-coated electrode is inserted in an immiscible conductive solution to perform the analysis [38]. Some interesting advantages when working with droplets are: (i) every single droplet represents an electrochemical cell or micro-reactor, since the analysis can be realized separately; (ii) small sample requirements, then low reagent costs; and (iii) the possibility to analyze samples existing only in scarce quantities. However, droplet systems involve practical parameters: the difficulty of handling low volumes, the whole miniaturization of the involved tools, and the occurrence of evaporation process. The last one is a common phenomenon due to the high surface-to-volume ratio inherent to droplets. Evaporation can causes important modifications on physicochemical properties like analytical concentration, solubility, pH, density and viscosity. Strategies to suppress them include sample isolation and moisture control. Sample isolation consists on covering the droplet either with a special chamber or with immiscible liquids as mineral oil, glycerol [9] or heptane [35]. Moisture control is achieved using water reservoirs or streaming water vapor.

Although the above described solutions are fabricated holding the configuration of a three electrode electrochemical cell, they are not used with conventional reference electrode. Instead, the approaches involve “pseudo-reference electrodes”, due to the difficulty of miniaturizing large liquid-solid reference electrodes. Considerable effort have been done to fabricate miniaturized “conventional reference electrodes” for being used in biological applications [24]. A literature overview of the topic of miniaturized reference electrodes has been presented earlier in this chapter.

2.2.4. Electrochemical response in small volume samples

Briefly, an ultramicroelectrode (UME) is an electrode whose diffusion layer can reach a comparable or even less size than the dimension of electrode surface at infinite time during experiments [3] (Figure 2.7). Although UMEs properties are not directly related to their dimension, the critical size of these devices under usual conditions is about 25 µm classical electrochemical solvents and reagents [3].

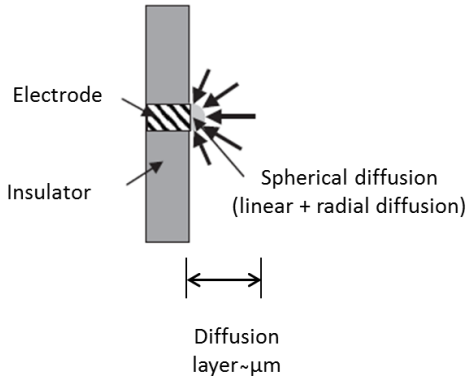

Figure 2.7 Scheme of a diffusion layer for an ultramicroelectrode.

An UME is working in bulk solution in which the amount of electroactive species consumed due to the passage of current will not be drastically changed during an experimental time of a few minutes. This happens when the electrode surface area (A)/volume solution (V) ratio is small, thus the sample is not altered by the electrochemical experiment [6]. The typical voltammetric behavior of UMEs at steady-state and transient conditions (Figure 2.8; A and B, respectively) in bulk solution is:

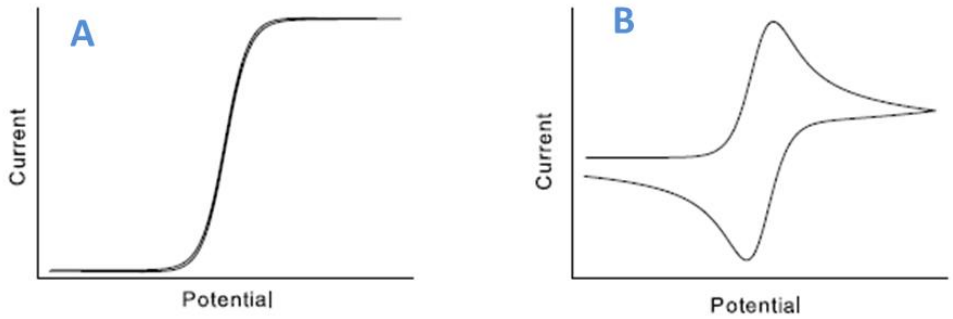

Figure 2.8 Typical voltammetric behaviors of UMEs in bulk solution at different scan rates. (A) Sigmoidal-shaped response that characterized steady-state mass transfer in slow scan-rate cyclic voltammetry. (B) Peak-shaped response observed at short experimental time scales (high scan rates).

However, if the A/V ratio is changed to higher values, the bulk concentrations of electroactive species will be dramatically affected, given place to an experiment similar to preparative-scale electrolysis. This can be problematic when performing electrochemistry in small volumes, as those found in microvials and droplets. For instance, Clark and co-workers analyzed the voltammetric behavior at 5 µm carbon fiber electrode as a function of sample volume, voltammetric scan rate, and analyte concentration [10]. In their work, they found that a voltammogram of 1 mM ferrocenecarboxylic acid in a 16 pL vial obtained at the highest scan rate (10 V/s, Figure 2.9-A) was not significantly different from that observed in bulk solution. Then, at an intermediate scan rate (1 V/s, Figure 2.9-B) the voltammogram was sigmoidal, similar to bulk solution voltammograms at the same scan rate with UMEs. However, a significant deviation from bulk solution was apparent when the voltage was scanned slowly (0.1 V/s, Figure 2.9-C). Unlike in bulk solution where voltammograms are sigmoidal for disks UMEs at low scan rates, voltammograms in picoliter vials at very slow-scan rates are peak-shaped and display a large current increase on the reverse (reduction) wave. This result for low scan rates can be described as a quasi-thin layer behavior.

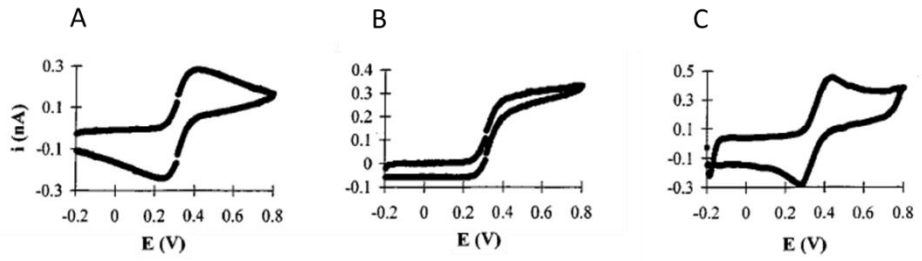

Figure 2.9 Cyclic voltammograms of 0.1 mM ferrocenecarboxylic acid in a 16-pL vial. The scan rates are (A) 0.1, (B) 1.0, and (C) 10 V/s. Carbon fiber working electrodes are 5 µm in diameter. Figure adapted from Ref. [10].

Peak-shaped voltammograms at slow scan rates only appeared in smaller vials (16 pL or less) and can be explained comparing diffusion in bulk solution and in microvials. In such recipients, the diffusion profile to the electrode is altered due to the vial boundaries. Thus, depletion of electroactive species near small electrodes can be achieved in the smallest vials. As described above, in bulk solution the amount of molecules reduced at a UME is negligible compared to the bulk analyte concentration. But, in a 16-pL vial the data show that 21 % of the total analyte in solution is oxidized by a 5 µm electrode scanned at 0.1 V/s. This data suggests that bulk electrolysis in microvials can be easily implemented to determine the total amount of analyte present in a vial [10], if the electrolytic process does not stop due to the changed conditions inside the microvial.

The increase in the current corresponding to the reverse peak in a 16 pL vial means that the oxidized species cannot diffuses away from the electrode surface. Thus, unlike experiments in bulk solution where the oxidation product at a UME diffuses away prior to the reverse scan, in a microvial, the oxidation product restricted by the vial boundaries and forms a depletion layer that can be re-reduced. Therefore, the study demonstrates that the characteristics of the diffusion/depletion layer, which is dependent on the ratio of the sizes of the sample microvial and the electrode, is the largest determining factor on the voltammetric response [10].

2.3. Electrochemical detection of peptides

Diverse peptides have a broad range of useful properties in human health, including antimicrobial, antifungal, antiviral and antitumor activities [39]. Moreover, some of them participate in the process of signaling between nerve cells, these molecules are called neuropeptides. On the other hand, peptides released in the intracellular and extracellular medium are specific to some kind of diseases, so they can be used as biomarkers or indicators of that state [40]. Thus, their detection and quantitative determination is particularly interesting for future biomedical applications. Within this framework, electrochemistry provides a powerful method for the determination of peptides. Basically, these fall into two categories: labeled [41] and label-free detection systems [40]. The latest one conducted by direct or redox mediated detection, and by electrochemistry at modified electrodes or liquid interface systems [3]. The direct electrochemistry of peptides can be carried-out at bare electrodes; this approach is based on either their redox reactions or on adsorption at the electrode surface. Indeed, the electrode material has a major impact, and an amino acid can undergo unique redox reactions at different materials. The electrochemistry of peptides requires that amino acids such as cysteine, tyrosine and tryptophan (Figure 2.10) are part of the peptide structures [42, 43]. These

amino acids are redox active and improve the electrochemical signal due to their adsorption on the electrode surface. Other amino acids are oxidized at much higher potentials, resulting in high background currents that prevent determination of traces levels of peptides without tryptophan, tyrosine and cysteine [44].

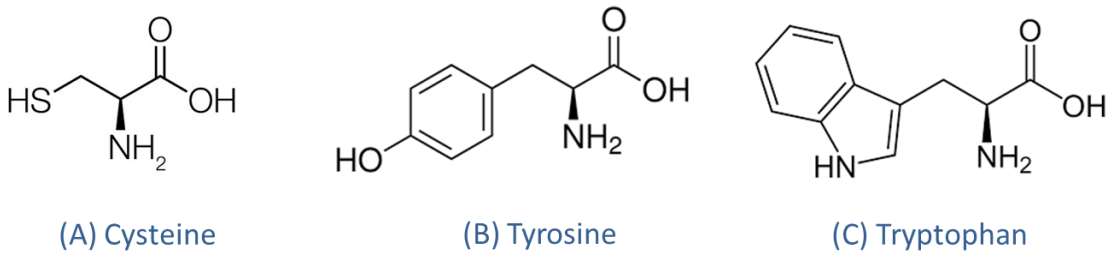

(A) Cysteine (B) Tyrosine (C) Tryptophan

Figure 2.10 Structures of (A) cysteine, (B) tyrosine and (C) tryptophan.

The oxidation of free tyrosine, tryptophan and cysteine at a paraffin wax-impregnated graphite electrode at pH 4 and 8.4 are given in Table 2.1 These oxidation potential are strongly dependent on parameters such as pH and electrode material. Moreover, the oxidation potentials of such amino acids in peptides can be shifted towards more positive or negative values than those potentials of free amino acids [44].

Table 2.1 Oxydation Peak potentials for tyrosine, Tryptophan and Cysteine at paraffin – wax impregnated graphite electrode.

	Oxidation peak potential (V vs SCE)*		
	Tyrosine	Tryptophan	Cysteine
pH 4	0.90	0.92	1.23
pH 8.4	0.65	0.70	1.00

*Data from linear sweep voltammetry (scan rate of 8.3 mV/s for tryptophan and tyrosine, and 16.7 for cysteine).

On the other hand, peptides not containing such molecules can be monitored due to their ability to adsorb on a surface and disrupt the electrical double layer, resulting in a change of the electrochemical signal. The corresponding methods are not very sensitive or selective and are more suited to study surface interactions rather than direct analytical measurements. Other approaches of determination are: amperometry detection of peptides and following their separation by high-performance liquid chromatography (HPLC) or capillary electrophoresis; the use of boron-doped

diamond electrodes; the use of noble electrodes and pulsed amperometric methods; carbon nanotube arrays and carbon disk electrodes integrated into a capillary electrophoresis system [40].

The detection of peptides via redox mediation relies on the complexation of metal ions by peptides, which produces redox active complexes. That is performed by complexing mixtures of oligopeptides with Cu(II) ions in alkaline pH [40]. The process is based on the Biuret reaction, a colorimetric method for the protein quantification [45]. In this reaction, Cu(II) first coordinates with the amine terminus and then with the carbonyl of the amide bond (Figure 2.11). Such coordination with the carbonyl draws electron density away from the amino nitrogen, thereby lowering the amide pK_a. This process enables the Cu(II) to coordinate to successive amido nitrogens. The strategy allows the detection at lower potentials than the ones observed for oxidation of adsorbed amino acids and oligopeptides [44].

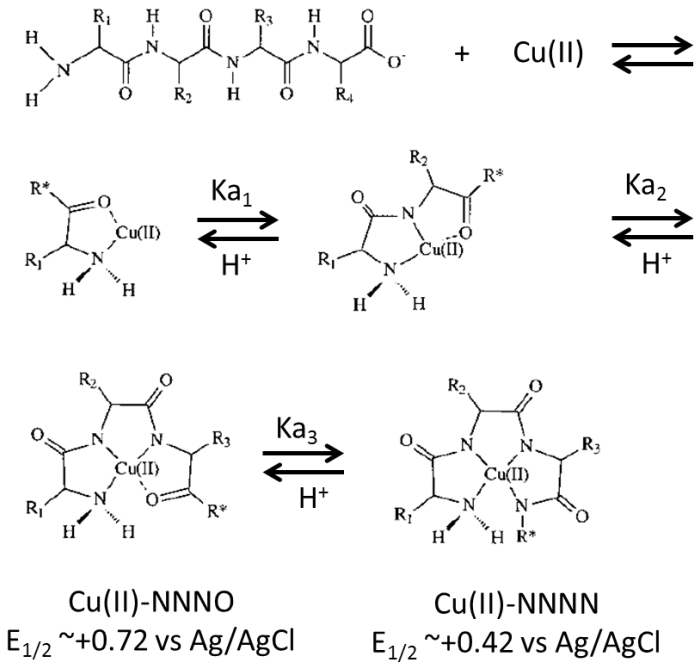

Figure 2.11 Scheme of a generic complexation reaction of Cu(II) with a tetrapeptide. Figure adapted from Ref [44]. Note that in each structure R* as defined in Ref [44], represent the pectidic

In other examples of peptide detection, polymer film modified electrodes are suitable for measuring Gly-Trp, Trp-Ala and Tyr-Gly peptides. The presence of the polymer film improves the electrocatalytic properties of surface, increasing the oxidation peak current and reducing the peak potential of the above peptides. Immobilized redox active species such as cobalt phthalocyanine, cobalt hexacyanoferrate, ruthenium cyanide, ferrocene derivatives and pyrroloquinoline quinone successfully

detect glutathione at the micromolar range. Moreover, it is possible to couple these modified electrodes with separating techniques [40].

Finally, for the case of detection using liquid interface systems, the ion selective potentiometric method is able to perform the direct detection of protamine. Protamine is an arginine rich cationic peptide with a sequence of 30 amino acids and 20 positive charges at physiological pH. In the approach, heparin, a sulfonated polysaccharide used as anticoagulation agent, interacts with its antidote protamine. This method works directly in the blood without requiring any separation or washing steps [40]. Protamine can also be detected by cyclic voltammetry and chronoamperometry, by measuring the protamine transfer across water-oil microinterfaces [46]. Here, the transfer is facilitated by dinonylnaphthalene sulfonate ionophore (DNSS) present in the organic phase, which forms complexes with the protamine polyions (Figure 2.12).

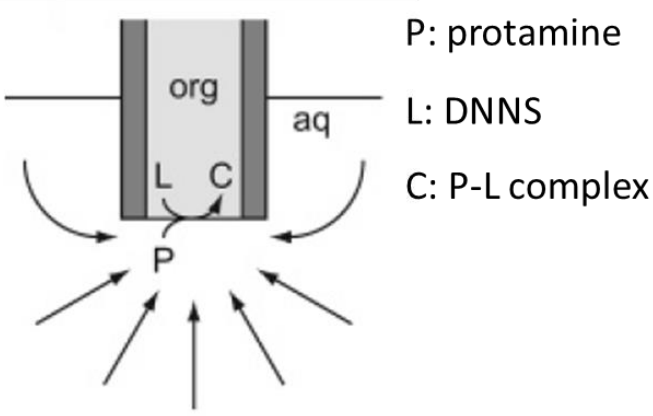

Figure 2.12 Experimental scheme at organic-filled micropipette electrode. In this experiment, a voltammogram is obtained by scanning the interfacial potential ($\Delta_W^0\emptyset$) to the negative potential. Here, the protamine is transferred from the aqueous phase into the organic phase. Protamine (P) and DNNS (L) are present initially in the water and organic phases, respectively. When the DNNS concentration is much higher than the protamine concentration, mass transfer is controlled by protamine diffusion in the outer solution. Figure adapted from Ref [46].

In general, label-free strategies are suitable for peptide analysis due to the advantages of sensitivity, no labeling step requirement, and compatibility with a range of electrodes. However, the use of these approaches often results in currents with high background signals, making difficult analytical interpretations; also possible sample alteration may result extremely inconvenient when analyzing scarce and precious samples. In contrast, the electrochemical labeling is a rapid, simple and non-destructive sample method [47]. The electrochemical labeling involves the conjugation of bioactive molecules with electroactive moieties. Although an analyzed species possess intrinsic electrochemical

activity, the binding of a suitable label results in a better distinction between the target molecule and the probe, improving sensitivity and selectivity of the analysis. Labeling with organic chelates of transition metal such as ferrocene, ruthenium, or osmium complexes is highly convenient due to their stability and well-defined one electron system (i. e. Fc/Fc^{+}), and solvent-independent redox potential [48]. For example, these complexes have been successfully used for the detection of DNA. Here, organic chelates of transition metal such as ferrocene, ruthenium, or osmium complexes are used to label oligonucleotides present in the DNA structure [47]. In the case of peptides, the assembling of these molecules with redox active groups gives them specific electronic properties that may be exploited as biosensors and biomolecular wires applications [49]. Some examples are given by ferrocene-peptide derivatives prepared by solid or solution phase synthesis. Former methods have led to the preparation of a number of monosubstituted Fc-peptide derivatives. The main interest for such structures is their utilization as molecular wires rather than pure detection [1]. As far we know, the group where I did my Ph D Work has pioneered on successfully performing the electrochemical detection of peptides (specifically, CPPs) via the redox-probe labeling method (Addressed in section 1.2.7 [1]).

Although above approaches are feasible for the electroanalysis of peptides, their application requires of large amounts of samples (milliliter electrochemical cell and millimetric sizes electrodes). This is problematic when dealing with precious or poorly available molecules, like the Cell-Penetrating Peptides. Hence, it is imperative the development of electrochemical systems able to handle small sample volumes, as is the case of miniaturized electrochemical cells. In the following section, some examples of such electrochemical systems are given, for knowing how is possible to work with small amounts of products.

2.4. How to use electrochemistry to analyze and detect cell-penetrating peptides in confined environment

2.4.1. Electro-analysis and detection of a cell-penetrating peptide in minute samples

The electro-analysis of precious/poorly available molecules such as cell-penetrating peptides requires the use of a small electrochemical cell. As described in the bibliography section, electrochemistry can bring a significant contribution to the analysis in small volumes, notably through the miniaturization of electrodes [34]. Nevertheless, the use of conventional reference electrodes is generally not compatible with miniaturized devices. Instead, pseudo-reference wire-shaped electrodes such as Ag, Ag/AgCl, or Pt are used though they suffer from potential instability with some species [24, 50, 51]. Within this context, we developed a new approach for real three-electrode operation with a commercial SCE (Saturated Calomel Electrode) in micro-volume droplets combined to smaller counter and working electrodes.

2.4.1.1. Design of the cell

As shown in Figure 2.13, a three-electrode micro-cells equipped with a conventional-reference electrode (SCE) may easily be constructed based on micro-volume droplets (50 µL) suspended by capillary forces to the fritted glass of the SCE bridge. Working and counter electrodes may simply be inserted through the droplet surface. Actually, the novelty of this device relies on the fact that droplets are deposited neither on a substrate nor on the working electrode surface, but suspended to the fritted glass of a bridge compartment in which the SCE is placed (Figure 2.13). The bridge was aimed at preventing any contamination of the reference electrode from the solution and vice versa. On the other hand, the bridge can also play the role of a “tank” avoiding thus solvent evaporation contained in the droplet. The counter electrode was a 1 cm length platinum wire (0.5 mm in diameter). Two kinds of working electrodes were tested: either a platinum wire (25 µm in diameter) or a carbon fiber microelectrode (25 µm in diameter).

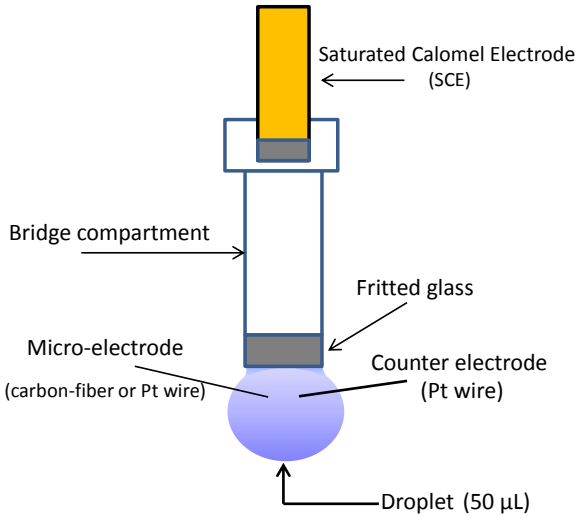

Figure 2.13 Experimental device used to perform cyclic voltammetry and controlled-potential electrolysis in 50 µL hanging droplets.

2.4.1.2. Validation of the cell

In order to validate this original cell, cyclic voltammetry experiments were first performed in water and in organic media.

a) In water

Cyclic voltammograms of ferrocenemethanol were first recorded at a carbon-fiber electrode immersed in a suspended 50 µL water droplet to test and validate the device under steady-state and transient conditions. Usual sigmoidal- and peak-shaped voltammograms were obtained at slow and high scan rates, respectively (Figure 2.14). Importantly, identical voltammograms were obtained in a bulk solution (3 mL) of same composition upon using the same electrodes demonstrating that, in microliter volumes, voltammetric responses were not affected by depletion phenomena as observed in pico-liter cells [35]. Furthermore, it was calculated that 4.82 mC would be required to completely electrolyze 50 µL of 1 mM ferrocenemethanol. Considering a steady-state current of ca. 4 nA flowing during 25 seconds, i.e., ca. 0.1 µC passed, only about 3 % of the analyte was oxidized during one slow scan. This confirms that depletion of ferrocenemethanol in the drop can be disregarded even at slow scan experiments.

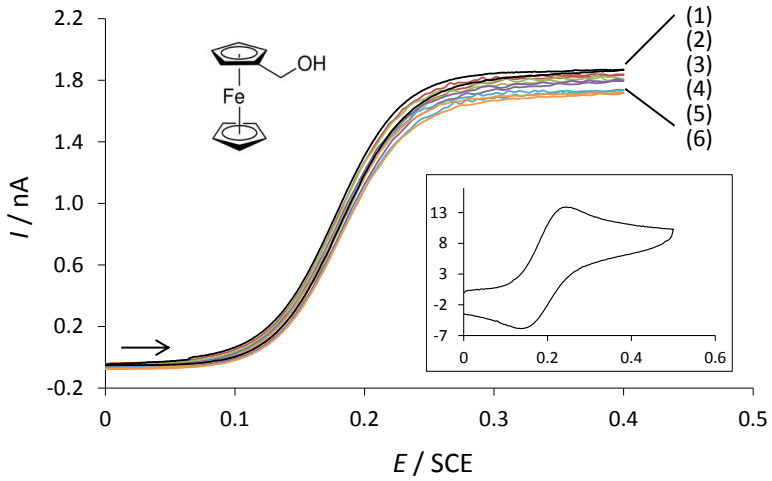

Figure 2.14 Voltammetry of ferrocenemethanol (0.5 mM) in H_2O + KCl (0.1 M) at a 10 µm diameter carbon-fiber electrode (v=20 mV/s). The same curve (1) was obtained in the droplet or in bulk solution or after cleaning the electrode surface. Curves (2) to (6) corresponded to successive scans run after 2, 3, 8, 13, and 15 minutes, respectively, in the micro-volume cell. Inset shows a voltammogram obtained at 20 V/s in the droplet.

Another important point to test was related to evaporation. It was already reported that evaporation from an air-exposed 1 µL aqueous droplet was significant after around 60 seconds (peak currents increased by more than 5%) [52]. Since relative evaporation rate is proportional to the surface-to-volume ratio of the sample, no evaporation, and therefore no peak current increase, was expected under our conditions within tens of minutes. Conversely, a very slight peak current decrease was observed with time (Figure 2.14). This was due to the fouling of the working electrode surface. Indeed, the initial peak current value was recovered after polishing the electrode, and no evidence of evaporation was observed after 15 minutes exposure to air.

b) In organic media

Interestingly, organic solvent droplets could be suspended as well to the bridge fritted glass. Cyclic voltammetry of ferrocene was therefore performed in dimethylformamide or acetonitrile with a platinum micro-electrode, because it was found that the polymer isolating the carbon fiber (poly(oxyphenylene)) can be dissolved in some organic solvents. To prevent solvent evaporation, a "chamber" was added to the device (Figure 2.15) and a tissue soaked with the same organic solvent was placed inside. Such a chamber is also useful for running experiments under inert atmospheres.

Besides, an argon stream saturated with solvent was also gently blown before starting each experiment, for five minutes, to remove oxygen from the chamber.

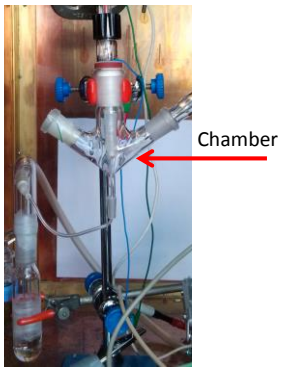

Figure 2.15 Picture showing the "chamber" allowing electrochemical investigations under inert atmosphere and/or in organic solvents.

Transient and stationary voltammograms were recorded at high (20 V/s) and slow (20 mV/s) scan rates, respectively (Figure 2.16). As observed in water, the electrochemical responses were identical to those obtained in a bulk solution (3 mL) and no solvent evaporation was noted during 15 minutes at least, in agreement with previous reports [52].

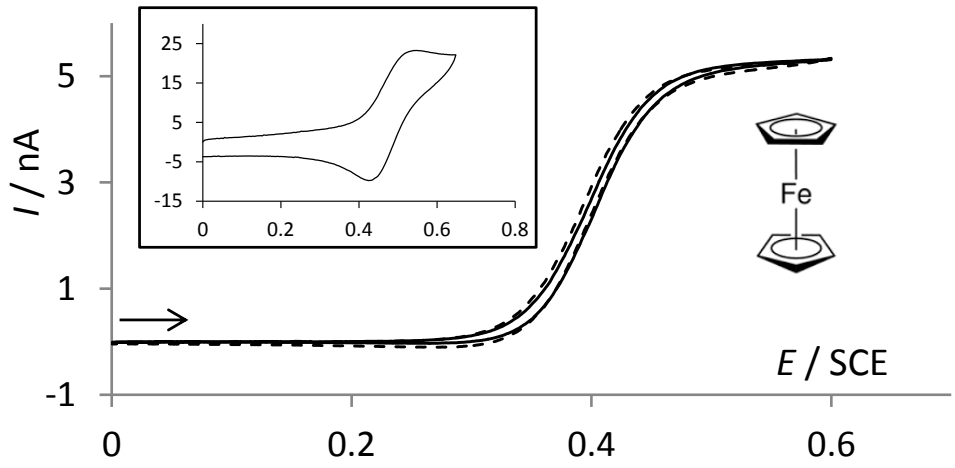

Figure 2.16 Voltammetry of ferrocene (1 mM) in DMF + nBu_4PF_6 (0.1 M) at a platinum electrode after 15 minutes in the droplet (dotted line) and in a bulk solution (solid line). v= 20 mV/s. Inset shows a voltammogram obtained in the droplet at 20 V/s.

c) Utilization of the cell to detect a cell-penetrating peptide

Owing to its minute volume, the above described cell appeared perfectly suited for electroanalysis of precious/poorly available molecules such as cell penetrating peptides (CPP). In view of this, the electrochemical detection of a CPP composed of nine arginines and tagged with a ferrocenyl unit (noted as Fc-$(Arg)_9$) was investigated at a carbon fiber electrode immersed in a micro-volume suspended water droplet. The modification of CPP with a ferrocenyl moiety was performed in collaboration with the group of Prof. S. Lavielle (peptide synthesis section 4.3.1-c). The molecular structure of Fc-$(Arg)_9$ is given in Figure 2.17.

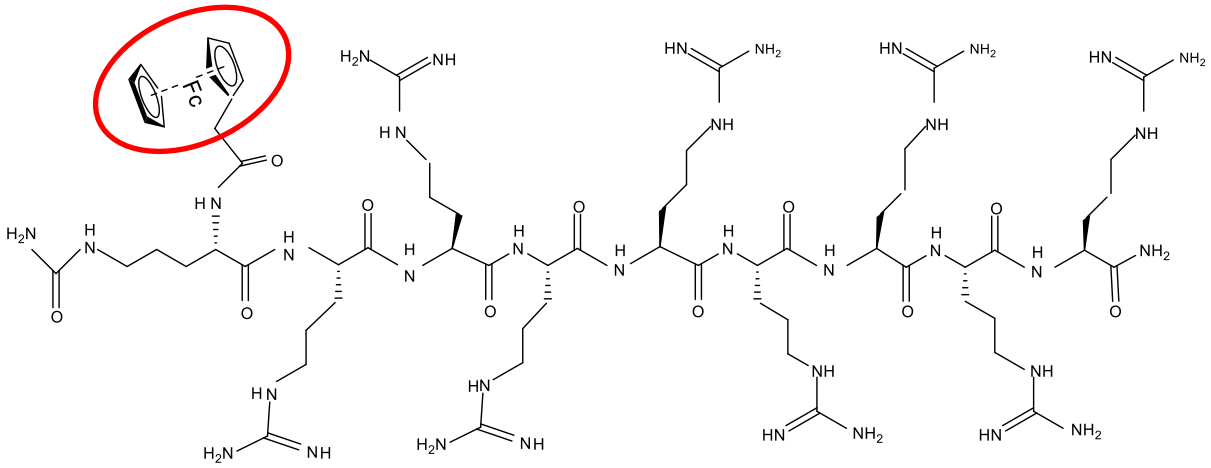

Figure 2.17 Molecular structure Fc-$(Arg)_9$ used in this work to investigate the electro-analysis of a CPP in a micro-volume hanging droplet.

As shown in Figure 2.18, a well-defined sigmoidal voltammogram was obtained at slow scan rate in the presence of micromolar concentration of the Fc-$(Arg)_9$ peptide. Also, the Fc-$(Arg)_9$ oxidation appeared at a more positive potential value than that of ferrocenemethanol illustrating an electron-withdrawing effect of the amino acids [41].

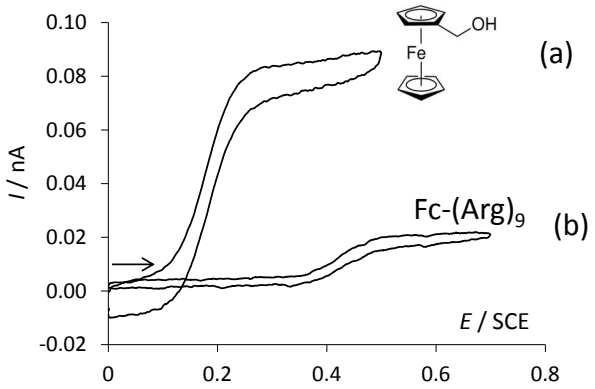

Figure 2.18 Voltammetry of (a) ferrocenemethanol (25 µM) and of (b) Fc-(Arg)9 (50 µM) in PBS at a 10 µm diameter carbon-fiber electrode in the droplet (v=20 mV/s).

Compared to already reported investigations in which large CPP amounts, milliliter electrochemical cell, and millimetric sized electrodes were used [1], the result shown in Figure 2.18 illustrates the analytical interest of the three-electrode droplet cell approach. This cell opens new perspective not only for the CPP analysis, but also for any precious/poorly available compounds. This result prompted us to extend the use of this original device towards other electrochemical techniques such as controlled-potential electrolysis.

d) Utilization of the cell in controlled-potential electrolysis

The presence of a saturated calomel electrode in our device can be indeed particularly relevant to perform accurate controlled-potential electrolysis in micro volumes. Since the anode and cathode were in close proximity (few millimeters) any electrolysis of a reversible redox soluble couple should have led to redox cycling (Figure 2.19). This is produced if the product of the working electrode reaction is insoluble.

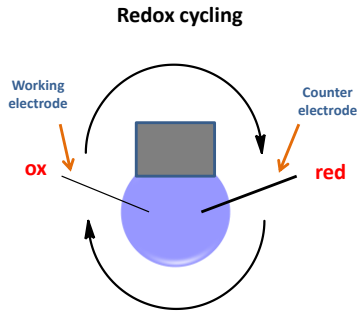

Figure 2.19 When the anode and the cathode are in close proximity, any electrolysis of a reversible redox soluble couple can lead to a redox cycling process.

For this reason, we considered the reduction of H_2PtCl_6 or $KAuCl_4$ in aqueous solutions as test experiments to modify carbon fiber electrodes with platinum and gold, respectively. Preparation of such electrodes, usually performed in milliliter volumes [53], are indeed of high interest in the analytical detection of biological species and of reactive oxygen species.

e) Platinization

Accordingly, series of controlled-potential electrolyses were run in suspended 50 µL water droplets as a function of the charge passed and analyzed by SEM (Figure 2.20). Platinization of the carbon-fiber microelectrode was successfully achieved. SEM images show that platinization occurred only on the active surface but not on the insulated one. Also, no interference of the counter electrochemical reaction was observed within the short time-scale electrodeposition (estimated maximum diffusion layer thickness c.a.: 0.5 mm). A typical variation of the amperometric current following the reduction of hydrogen hexachloroplatinate (IV), in the presence of lead acetate, on the carbon-fiber active surface is shown in Figure 2.20 (B), being compatible with a regular increase of the electrode surface with time after an initial reading period.

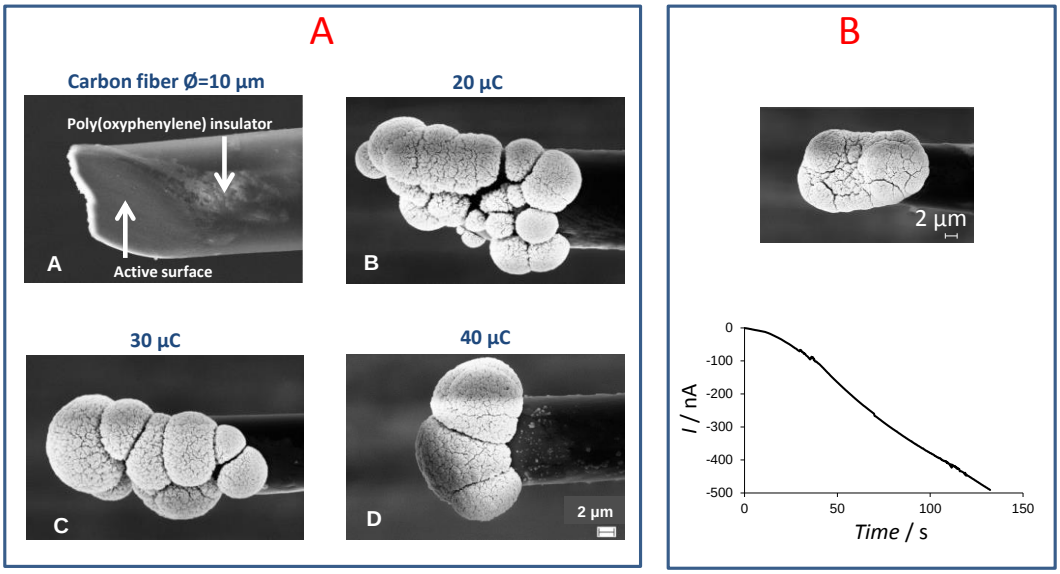

Figure 2.20 (A) Scanning electron microscopy images of a carbon fiber (10 µm in diameter) electrode obtained before (A) and after a platinization charge of 20 µC (B), 30 µC (C), and 40 µC (D) within the droplet. In (B) is shown a typical evolution of the amperometric current recorded during the reduction (E = - 65 mV/SCE) of hydrogen hexachloroplatinate(IV) (28 mM) in the presence of lead acetate (0.57 mM). The electrodeposition started at t = 0 and was pursued until reaching a platinization deposit (30 µC in this case).

f) Electrodeposition of gold

Similarly, electrodeposition of gold nanocrystals could be also achieved onto carbon-fiber electrode surfaces. In Figure 2.21 are shown the SEM images obtained after reduction of potassium tetrachloroaurate for 30 seconds at either + 400 or – 500 mV / SCE corresponding to the plateau and the foot of $KAuCl_4$ reduction wave, respectively. As already demonstrated on glassy carbon electrodes [54], the size, structure, and distribution of gold nanocrystals depended on the overpotential, illustrating the benefit of the three-electrode cell operation.

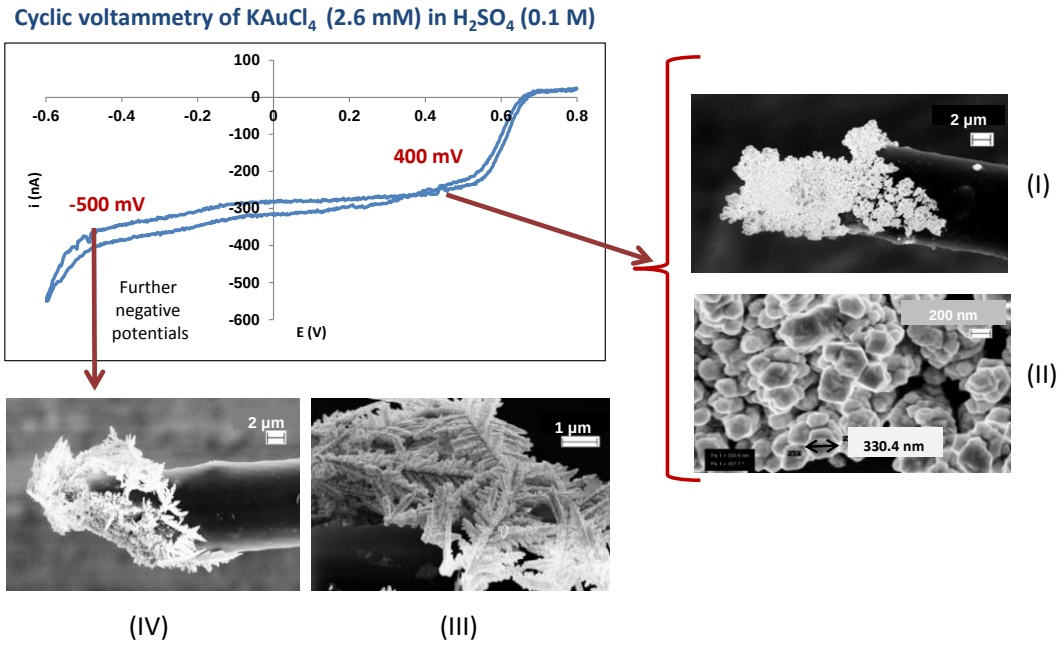

Figure 2.21 Scanning electron microscopy images of a 10 µm gold modified carbon fiber electrode by reduction of potassium tetrachloroaurate(III) (2.6 mM) dissolved in sulfuric acid (0.1 M). Images (I) and (II) were obtained after reduction at + 400 mV/SCE for 30 seconds. (III) and (IV) were obtained after reduction at - 500 mV/SCE for 30 seconds. Cyclic voltammetry of $KAuCl_4$ 1mM in H_2SO_4 (0.1 M) at 10 µm carbon fiber electrode (v = 100 mV/s).

2.4.2. Conclusion and perspectives

This work established the validity of electrochemical investigations performed in micro-volume hanging droplets, in the presence of a conventional reference electrode. This original approach is simple, low-cost, easy to implement and versatile. As demonstrated, this cell is perfectly suited for electroanalysis of precious compounds such as cell-penetrating peptides. Moreover, the use of this device can be extended to perform accurate controlled-potential electrolysis in micro-volumes, but only in the case of irreversible redox soluble couple due to the close proximity of both the anode and the cathode. To run "classical" preparative electrolyses, the working and counter electrodes should be separated. In Figure 2.22 is shown an alternative device allowing separation of these electrodes and which should be useful to perform preparative electrolyses of high added value compounds.

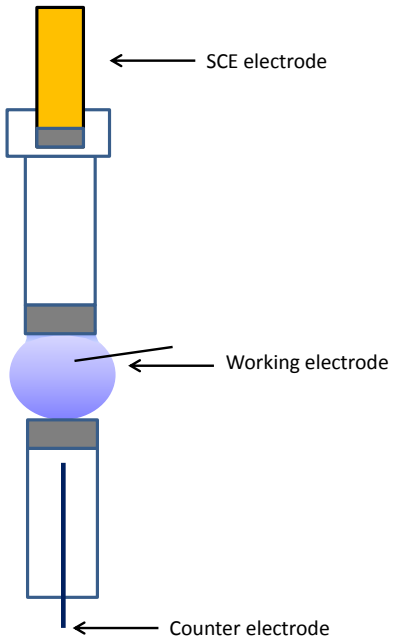

Figure 2.22 Separation of the working and counter electrodes, which should allow the achievements of preparative electrolyses of high added value compounds in micro-volume hanging droplets.

2.5. Electrochemical detection a cell-penetrating peptide via combination of the patch-clamp technique and amperometric method

After the development of an electrochemical device allowing the electroanalysis of cell-penetrating peptides in minute samples, the second objective of the work presented in this chapter was aimed at monitoring the passive transport of CPP through patch-clamp suspended model membranes. For such investigations, the idea was based on the use of an original approach recently developed in the group of electrochemistry and which combines the patch-clamp principle with amperometric detection for monitoring, in real time, fluxes of redox-tagged molecular species across real and model cell membranes [55].

2.5.1. "Historical" context

Transport of active molecules across biological membranes is a central issue for the success of many pharmaceutical strategies. Despite this crucial importance, most approaches, included these aimed to pharmacological issues, rely on the measurement of partition coefficients between water and hydrophobic solvent models. However, this thermodynamic method is "blind" to any kinetics between the two phases and assumes that the stack-lipid rails can be modeled by a fluid hydrophobic phase.

On the other hand, transport through artificial membranes is a well-developed field. Accordingly, the preparation of suspended micro-meter sized artificial membranes, which can be used for electrochemical investigations, can be achieved according to three main different methods: (i) the painting technique [56], (ii) the Langmuir Blodgett technique [57], and (iii) the tip dip technique [58] (Figure 2.23).

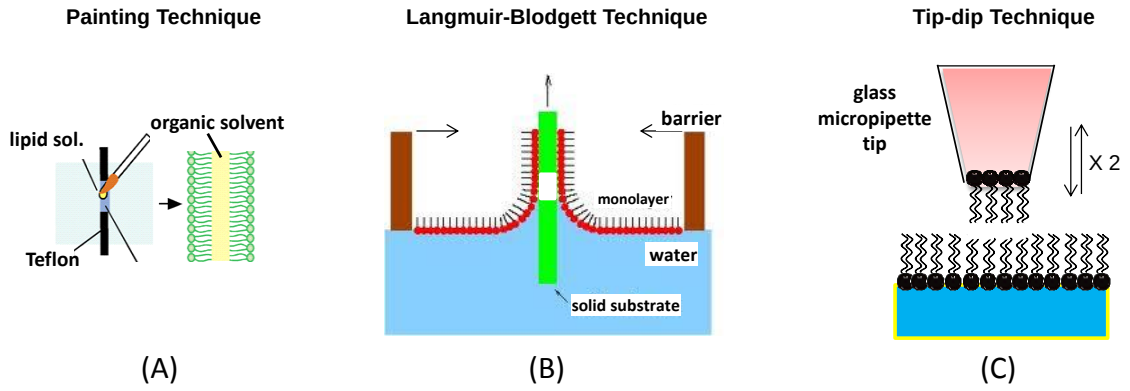

Figure 2.23 Three main techniques allowing preparation of suspended micro-meter sized artificial membranes.

However, none of these methods can be transposed to be used with real cell membranes, whose complexity is extremely high. Alternatively, the preparation of real suspended cell membranes can be achieved by the patch-clamp technique. The patch-clamp technique is an electro-physiological procedure used in biology, especially for the identification of ionic channels in real cell membranes. This method consists in sealing a patch of real cell membrane at the tip of a glass micropipette similar to that used in the tip-dip technique. Neher and Sakmann who developed this technique in the seventies received the Nobel Prize in 1991 [59].

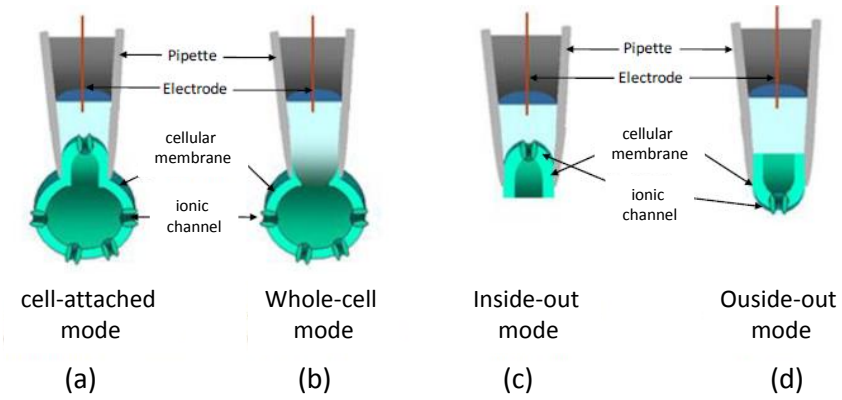

Figure 2.24 Patch-Clamp configurations which are accessible with a micropipette. Configurations (c) and (d) are also called "excised configurations" [60].

Among the patch-clamp configurations, the "inside-out" one ((c) in Figure 2.24) was found to be very interesting to prepare suspended membranes. In this case, after the formation of a gigaseal between the cell and the micropipette, the latter is quickly withdrawn from the cell, thus ripping a patch of membrane off the cell and leaving the patch of membrane attached to the micropipette. The name "inside-out" comes from the fact that the intracellular surface of the membrane becomes exposed to the external media (Figure 2.25 -(A)).

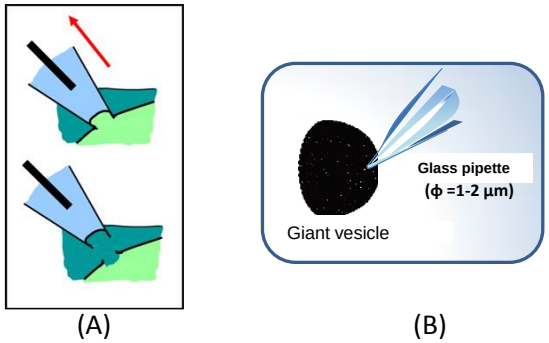

Figure 2.25 (A) Principle of the "inside-out" patch-clamp configuration. (B) Patch of a giant vesicle.

Based on this technique, real suspended membranes as well as protein- and solvent-free suspended membranes were successfully obtained *via* the patch of macrophage cells and of artificial giant vesicles, respectively (10-70 µm range in diameter) (Figure 2.25-(B)). This patch-clamp technique was then combined with an amperometric detection where a carbon-fiber electrode (10 µm in diameter) was placed in front of the glass micropipette tip containing a redox probe and at the tip of which was attached the suspended membrane (Figure 2.26).

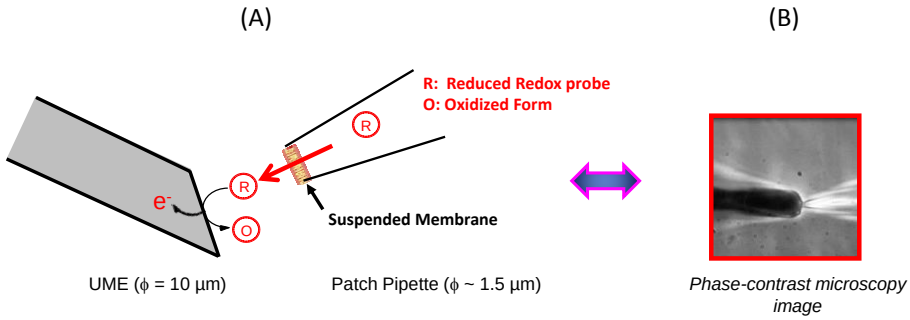

Figure 2.26 (A) Device allowing the electrochemical detection of redox probes crossing a suspended membrane (real or artificial). (B) Typical amperometric configuration showing a carbon-fiber microelectrode (left) positioned in the vicinity of an artificial patched membrane held by the micropipette (right) [55] .

2.5.2. Passive transport of ferrocene-methanol through a suspended artificial membrane

Before to attempt monitoring of the passive transport of CPP through patch-clamp suspended model membranes, I have trained myself to several important aspects of the method: (i) preparation of giant vesicles by electroformation, (ii) patch of giant vesicles with home-made patch pipette under an inverted microscope, (iii) preparation of carbon-fiber ultra-micro electrodes, (iv) utilization of micromanipulators to position the suspended membrane in front of the carbon fiber as well as to patch vesicles.

To achieve this training, my objective was to investigate the electrochemical detection of ferrocene-methanol crossing an artificial suspended membrane made of DPhPC (1,2-diphytanoyl-sn-glycero-3-phosphocholine). It was indeed shown that the patch success rate obtained for pure DPhPC vesicles was about of 90%. Moreover, DPhPC is one of the most commonly used lipids for electro-

physiologically significant measurements as well as for experiments involving peptide-lipid interactions [61-63] (Figure 2.27).

Note that phospholipids characteristics and properties will be presented in the next chapter. In the following, I will therefore only describe the most important aspects allowing the preparation of suspended membranes in view of an electrochemical detection.

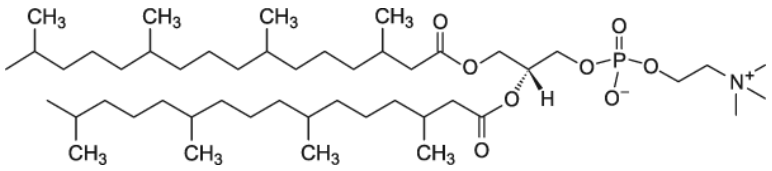

Figure 2.27 1,2-diphytanoyl-sn-glycero-3-phosphocholine (DPhPC).

2.5.2.1. Electroformation of Giant Unilamellar Vesicles (GUVs) made of DPhPC lipids

The procedure allowing the preparation of giant vesicles was similar to that described elsewhere [64]. Typically, 5-10 µL of a 10-25 mg/mL DPhPC phospholipid solution in chloroform was spread at a constant speed with a micropipette tip on an ITO-coated glass (surface resistivity: 30-60 Ω/sq) previously cleaned with acetone and isopropyl alcohol, and let dried for 30 minutes. The lipid film was then dried under vacuum for 90 min., and the electroformation chamber was assembled (Figure 2.28).

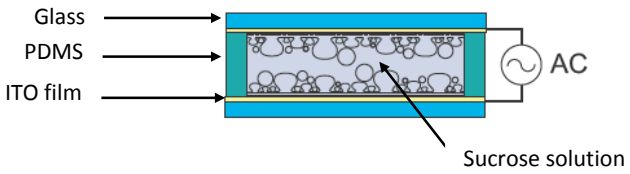

Figure 2.28 Electroformation chamber involving two ITO-coated coverslips facing each other and separated by a 2 mm thick silicon rubber square (PDMS: polydiméthylsiloxane) sealing the chamber.

This chamber consisted of two ITO-coated coverslips facing each other and separated by a 2 mm thick silicon rubber square sealing the chamber. The assembled vesicle electroformation chamber was slowly filled with 500 µL of a water solution containing sucrose (0.5 M) and NaN_3 (4.6 mM) with an osmolarity of ca. 650 mOsm. Then, a sinusoidal AC electric field of 2 V and 10 Hz was applied for 4 h. to form GUVs. To detach the vesicles from the surface an additional AC field was applied (3 V and 5 Hz) for 1h.

2.5.2.2. Patch of a DPhPC GUV

The vesicle suspension (5-10 µL) was added in a 2 mL solution containing glucose (0.32 M), NaCl (C=0.15M) and NaN_3 (C=4.6 mM) with the same osmolarity that the solution used for the preparation of GUVs (650 mOsm). Giant vesicles (20-50 µm diameters) were then visualized using an inverted microscope, placed into a Faraday cage, under phase contrast and selected for patching based upon their size, position and morphology. The patch micro-pipette (1.5-2 µm in diameter, as measured by microscopy) was pressed against the GUV (diameters in the 15 to 40 µm range) allowing the formation of a high resistance seal (1-10 GΩ range) between the glass pipette and the vesicle membrane (giga seal). After formation of the giga seal, the micropipette was quickly withdrawn from the vesicle, ripping off the sealed patch of lipid bilayer attached to the micropipette. The patch success rate of pure DPhPC vesicles was about of 90 %.

2.5.2.3. Amperometric detection

Amperometric detections were then performed by positioning the patch clamp pipette (at the tip of which was attached the DPhPC suspended membrane) previously filled with the electroactive substance (ferrocenemethanol in the present case), in front of a carbon-fiber microelectrode (10 µm in diameter) with a micromanipulator. The microelectrode potential was set at a value located on the plateau of the probe oxidation wave (+ 400 mV vs. Ag/AgCl) to detect, in real time, the substrate flux (ferrocenemethanol) crossing the lipid membrane (Figure 2.29).

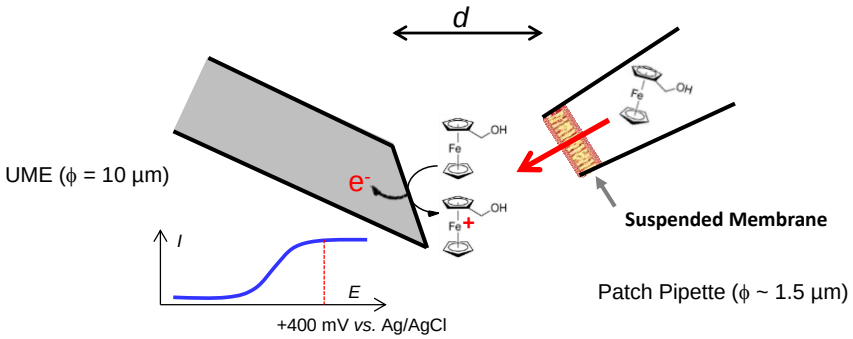

Figure 2.29 Configuration used for the electrochemical detection of ferrocenemethanol crossing a DPhPC suspended membrane.

The current response was investigated, in real time, as a function of the electrode/membrane distance (Figure 2.30).

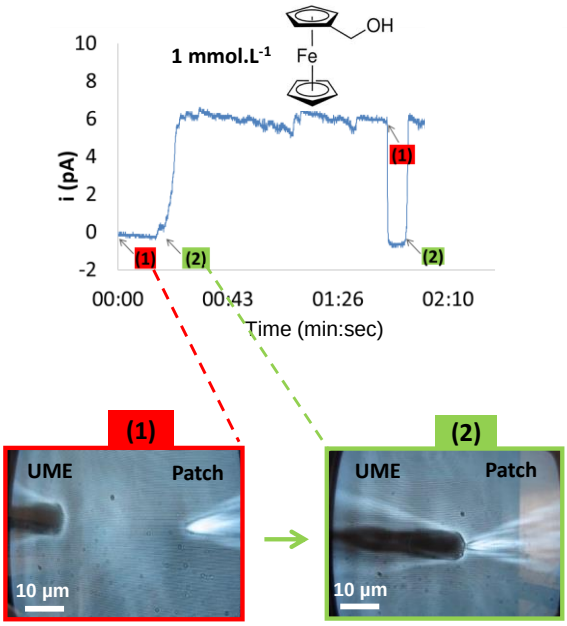

Figure 2.30 Typical current/time response obtained for ferrocenemethanol (C = 1 mM) as a function of the electrode/membrane distance *d* (*d* > 100 µm (1); *d* < 1 µm (2)). The arrows and labels 1 or 2 refer to the beginning of signal after the repositioning at the selected value.

As shown in Figure 2.30, and in agreement with already reported results [55] no current response was observed when the membrane was too far away from the electrode to detect a possible molecular species flux. However, as soon as the membrane was in the vicinity of the electrode (typically less than 5 µm) the current (due to the oxidation of ferrocene methanol) increased rapidly and reached a steady-state reflecting the spontaneous steady state diffusion of ferrocene methanol through the suspended membrane. Under these conditions, the collection efficiency was nearly quantitative. Conversely, the current decreased very rapidly as the pipette was moved away from the electrode.

2.5.2.4. Preparation of DOPG suspended artificial membranes

In order to investigate the passage of CPPs through suspended membrane, the next objective was the preparation of a DOPG (Dioleoylphosphatidylglycerol)-suspended membrane. DOPG that bears a negatively charged head-group is an interesting phospholipid notably for the investigation of CPPs that are positively charged. However, in contrast with DPhPC, it was impossible to patch pure DOPG

vesicles, presumably because of the electrostatic repulsions between the negative DOPG heads and the negatively charged surface of the glass patch-pipette [65]. We found that this drawback could be overcome after addition of dicationic species such as Ca^{2+} and/or Mg^{2+} (at 10 mM and 0.5 mM, respectively) in the glucose solution before patching vesicles.

2.5.2.5. Detection of a CPP going outside a micropipette

Before the investigation of CPP crossing the suspended-DOPG membrane, it was important to have a "blank" experiment in which the CPP detection was achieved in the absence of suspended membrane. Accordingly, the CPP already used in the previous part of this chapter (Fc-$(Arg)_9$) – see Figure 2.17) and labeled with a ferrocenyl unit (synthesized in the group of Prof. Solange Lavielle) was placed in the patch-pipette for detection. Note that the concentration of Fc-$(Arg)_9$ could not be higher than 50 µM to avoid peptide agregation. Unfortunately, under these conditions, it was impossible to detect any current related to the oxidation of the Fc moiety. Nevertheless, when the same carbon electrode was immersed in a solution containing the Fc labeled peptide at the same concentration (50 µM) as that used in the micropette an electrochemical response could be obtained (Compare a) and b) in Figure 2.31). Contrary to the previous experiment in which ferrocenemethanol was use at a concentration of 1 mM, this demonstrates that at 50 µM the flux of Fc-$(Arg)_9$ going outside the patch pipette is too small to be electrochemically detected using a patch configuration.

As expected, no detection of Fc-$(Arg)_9$ could be obtained when a DOPG membrane was suspended at the tip of the patch pipette. Nevertheless, this does not mean that Fc-$(Arg)_9$ is unable to diffuse inside the DOPG membrane. Indeed, it was recently shown (results not published yet) that when Fc-$(Arg)_9$ (at a concentration of 50 µM) is in the presence of a glassy carbon electrode modified with a supported DOPG membrane, it can be electrochemically detected demonstrating the diffusion of the Fc-CPP until the electrode surface through the artificial membrane.

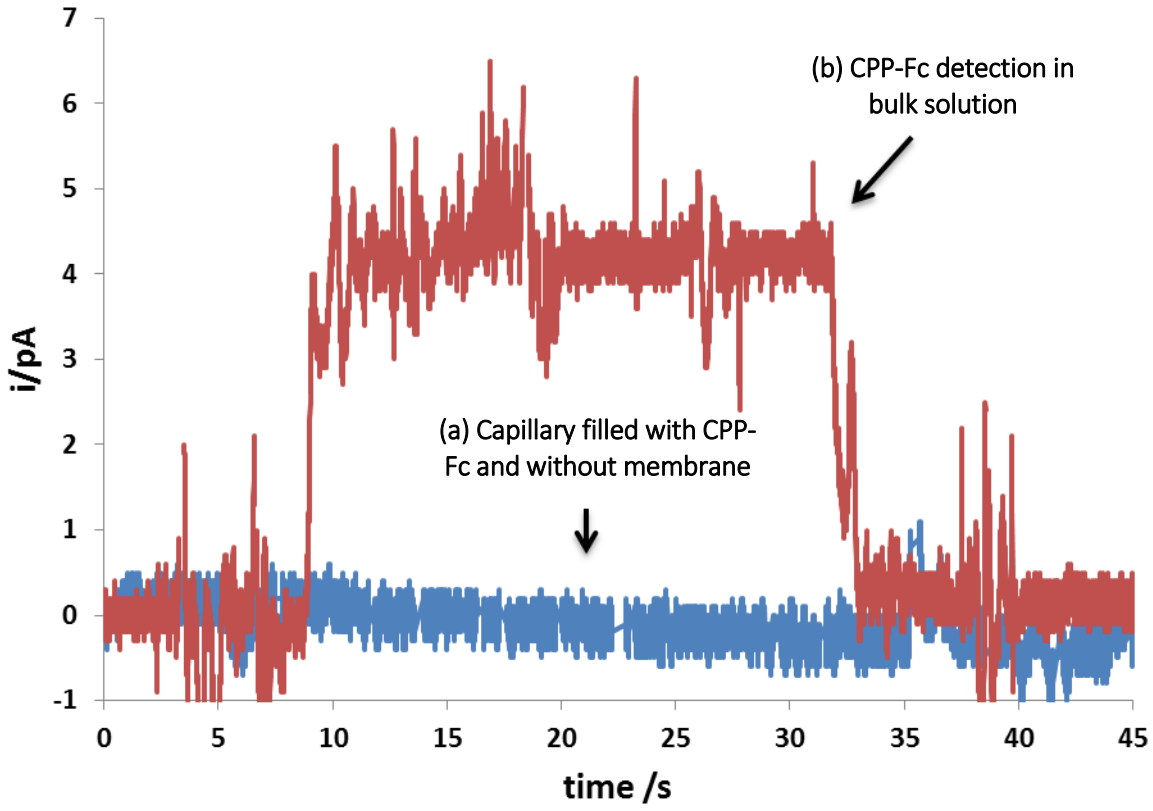

Figure 2.31 Current/time response obtained at a carbon fiber microelectrode (10 µm in diameter) positioned either (a) in front of a glass micropipette tip filled with a solution of Fc-$(Arg)_9$ (C = 50 µM), or (b) immersed in a PBS (10 µM) solution containing Fc-$(Arg)_9$ at a concentration of 50 µM.

2.5.3. Conclusion and Perspectives

So far, the patch of giant vesicles made of DOPG as the phospholipid was impossible due to electrostatic repulsions between the lipid heads and the glass patch pipette which are both negatively charged. Here, we showed that the patch of DOPG vesicles is possible provided that dicationic species such as Ca^{2+} or Mg^{2+} were also present in solution. Though the use of electrochemistry to detect micromolar concentrations of CPPs going outside a micrometric pipette was found to be impossible due to a too small outflow, the device combining the patch-clamp principle and amperometry could be however used for the investigation of antimicrobial peptides (AMPs). Antimicrobial peptides, which are implied in the innate immune systems of living organisms is another important class of cationic peptides. These peptides have been demonstrated to kill numerous bacteria including some being resistant to conventional antibiotics and also cancerous cells. Contrary to CPPs, AMPs do not cross cellular membranes, but cause their lysis *via* the formation of pores. In such a case, the detection of a concentrated redox species crossing a "perforated" suspended membrane should be possible in the

presence of AMPs. Combination of the patch-clamp and amperometry techniques could be thus useful to screen peptides families and to differentiate therefore the translocation of cationic peptides through membranes (CPPs) and the alteration of membrane permeability *via* the formation of pores (AMPs).

2.6. Chapter Conclusion

This chapter was devoted to the electrochemical detection of cell-penetrating peptides in confined environments. In the first part of the work, an original three-electrode micro-cell equipped with a conventional reference saturated calomel electrode (SCE) was easily constructed based on micro-volume droplets suspended by capillary forces to the fritted glass of the SCE bridge. This original approach which is simple, low-cost, easy to implement and versatile is perfectly suited for electroanalysis of precious compounds such as cell-penetrating peptides. Importantly, the use of this device can be extended to perform accurate controlled-potential electrolysis in micro-volumes notably when non-reversible redox soluble couples are involved. Otherwise, the working and counter electrode should be separated.

In the second part of the work, the electrochemical detection of a CPP crossing a suspended artificial membrane was attempted via combination of the patch-clamp principle and amperometric detection. Though the preparation of suspended artificial membranes made of DOPG, a negatively charged phospholipid, was successfully achieved provided the presence of dications, it was impossible to detect any CPP crossing the membrane. As confirmed in the presence of an open pipette tip (i.e., in the absence of a suspended membrane) this result is due to a too weak outflow of CPP.

In conclusion, though electrochemistry can be useful to run electro-analysis of CPPs in small volumes, this technique was demonstrated to be not enough sensitive to detect small CPP fluxes crossing a suspended membrane. This unexpected result led us to turn to a more sensitive technique such as fluorescence whereas electrochemistry was rather used to control fluorescence (See Chapter 3).

References

1. Messina, P., G. Hallais, E. Labbé, M. Béranger, G. Chassaing, S. Lavielle, C. Mansuy, O. Buriez, and C. Amatore, *Electrochemistry of a ferrocene-grafted cell-penetrating peptide.* Electrochimica Acta, 2012. **80**, 180-186.
2. Dawson, K. and A. O'Riordan, *Electroanalysis at the Nanoscale.* Annual Review of Analytical Chemistry, 2014. **7**, 163-181.
3. Amatore, C., *Electrochemistry at ultramicroelectrodes.* Physical Electrochemistry: Principles, Methods and Applications, 1995. **4**, 131-208.
4. Wightman, R.M., P. Runnels, and K. Troyer, *Analysis of chemical dynamics in microenvironments.* Analytica Chimica Acta, 1999. **400**, 5-12.
5. Li, Y., C. Sella, F. Lemaître, M. Guille Collignon, L. Thouin, and C. Amatore, *Highly Sensitive Platinum-Black Coated Platinum Electrodes for Electrochemical Detection of Hydrogen Peroxide and Nitrite in Microchannel.* Electroanalysis, 2013. **25**, 895-902.
6. Christian, A., G.-C. Manon, and L. Frédéric, *Recent Investigations of Single Living Cells with Ultramicroelectrodes*, in *Nanoelectrochemistry.* 2015, CRC Press. p. 439-468.
7. Yeh, J.I. and H. Shi, *Nanoelectrodes for biological measurements.* Wiley Interdisciplinary Reviews: Nanomedicine and Nanobiotechnology, 2010. **2**, 176-188.
8. Forster, R.J. and T.E. Keyes, *Ultramicroelectrodes,* in *Handbook of Electrochemistry, Cynthia G. Zoski.* 2007, Elsevier: Amsterdam. p. 155-171.
9. Clark, R.A., P.B. Hietpas, and A.G. Ewing, *Electrochemical Analysis in Picoliter Microvials.* Analytical Chemistry, 1997. **69**, 259-263.
10. Clark, R.A. and A.G. Ewing, *Characterization of Electrochemical Responses in Picoliter Volumes.* Analytical Chemistry, 1998. **70**, 1119-1125.
11. Bratten, C.D.T., P.H. Cobbold, and J.M. Cooper, *Micromachining Sensors for Electrochemical Measurement in Subnanoliter Volumes.* Analytical Chemistry, 1997. **69**, 253-258.
12. Bratten, C.D.T., P.H. Cobbold, and J.M. Cooper, *Single-Cell Measurements of Purine Release Using a Micromachined Electroanalytical Sensor.* Analytical Chemistry, 1998. **70**, 1164-1170.
13. Andrew, F.D., D. Gregor, V. Vicente, G.Y. Ming, D.J. Conrad, G.C. Harold, and L. Manfred, *An electrochemical detector array to study cell biology on the nanoscale.* Nanotechnology, 2002. **13**, 285.
14. Chen, P., B. Xu, N. Tokranova, X. Feng, J. Castracane, and K.D. Gillis, *Amperometric Detection of Quantal Catecholamine Secretion from Individual Cells on Micromachined Silicon Chips.* Analytical Chemistry, 2003. **75**, 518-524.

15. Hayat, A. and J. Marty, *Disposable Screen Printed Electrochemical Sensors: Tools for Environmental Monitoring.* Sensors, 2014. **14**, 10432.
16. Li, M., Y.-T. Li, D.-W. Li, and Y.-T. Long, *Recent developments and applications of screen-printed electrodes in environmental assays—A review.* Analytica Chimica Acta, 2012. **734**, 31-44.
17. Rossier, J.S., C. Vollet, A. Carnal, G. Lagger, V. Gobry, H.H. Girault, P. Michel, and F. Reymond, *Plasma etched polymer microelectrochemical systems.* Lab on a Chip, 2002. **2**, 145-150.
18. Ball, J.C., D.L. Scott, J.K. Lumpp, S. Daunert, J. Wang, and L.G. Bachas, *Electrochemistry in Nanovials Fabricated by Combining Screen Printing and Laser Micromachining.* Analytical Chemistry, 2000. **72**, 497-501.
19. Ball, J.C., J.K. Lumpp, S. Daunert, and L.G. Bachas, *Effect of Fabrication Factors on Performance of Screen-Printed/Laser Micromachined Electrochemical Nanovials.* Electroanalysis, 2000. **12**, 685-690.
20. Metters, J.P., R.O. Kadara, and C.E. Banks, *New directions in screen printed electroanalytical sensors: an overview of recent developments.* Analyst, 2011. **136**, 1067-1076.
21. Betancourt, T. and L. Brannon-Peppas, *Micro- and nanofabrication methods in nanotechnological medical and pharmaceutical devices.* International Journal of Nanomedicine, 2006. **1**, 483-495.
22. Makarov, G.N., *Laser applications in nanotechnology: nanofabrication using laser ablation and laser nanolithography.* Physics-Uspekhi, 2013. **56**, 643.
23. Smith, T.J. and K.J. Stevenson, *4 - Reference Electrodes A2 - Zoski, Cynthia G*, in *Handbook of Electrochemistry*2007, Elsevier: Amsterdam. p. 73-110.
24. Shinwari, M.W., D. Zhitomirsky, I.A. Deen, P.R. Selvaganapathy, M.J. Deen, and D. Landheer, *Microfabricated Reference Electrodes and their Biosensing Applications.* Sensors, 2010. **10**, 1679.
25. Ciobanu, M., J.P. Wilburn, N.I. Buss, P. Ditavong, and D.A. Lowy, *Miniaturized Reference Electrodes Based on Ag/AgiX Internal Reference Elements. I. Manufacturing and Performance.* Electroanalysis, 2002. **14**, 989-997.
26. Oldham, K.B., J.C. Myland, and A.M. Bond, *Electrodes*, in *Electrochemical Science and Technology.* 2011, John Wiley & Sons, Ltd. p. 105-124.
27. Polk, B.J., A. Stelzenmuller, G. Mijares, W. MacCrehan, and M. Gaitan, *Ag/AgCl microelectrodes with improved stability for microfluidics.* Sensors and Actuators B: Chemical, 2006. **114**, 239-247.
28. Hassel, A.W., K. Fushimi, and M. Seo, *An agar-based silver|silver chloride reference electrode for use in micro-electrochemistry.* Electrochemistry Communications, 1999. **1**, 180-183.

29. Lill, K.A. and A.W. Hassel, *A combined μ-mercury reference electrode/Au counter-electrode system for microelectrochemical applications.* Journal of Solid State Electrochemistry, 2006. 10, 941-946.
30. Shibata, M., B. Siegfried, and J.P. Huston, *Miniature calomel electrode for recording DC potential changes accompanying spreading depression in the freely moving rat.* Physiology & Behavior, 1977. 18, 1171-1174.
31. Troyer, K.P. and R.M. Wightman, *Dopamine Transport into a Single Cell in a Picoliter Vial.* Analytical Chemistry, 2002. 74, 5370-5375.
32. Gao, N., M. Zhao, X. Zhang, and W. Jin, *Measurement of Enzyme Activity in Single Cells by Voltammetry Using a Microcell with a Positionable Dual Electrode.* Analytical Chemistry, 2006. 78, 231-238.
33. Wittenberg, N.J. and A.G. Ewing, *Electrochemistry in and at single biological cells,* in *Handbook of Electrochemistry. Cynthia G Zoski, Ed.,* 2007, Elsevier: Amsterdam. p. 719-749.
34. Li, T. and W. Hu, *Electrochemistry in nanoscopic volumes.* Nanoscale, 2011. 3, 166-176.
35. Kashyap, R. and M. Gratzl, *Electrochemistry in Microscopic Domains. 1. The Electrochemical Cell and Its Voltammetric and Amperometric Response.* Analytical Chemistry, 1998. 70, 1468-1476.
36. Lee, H.J., U.S. Hong, D.K. Lee, J.H. Shin, H. Nam, and G.S. Cha, *Solvent-Processible Polymer Membrane-Based Liquid Junction-Free Reference Electrode.* Analytical Chemistry, 1998. 70, 3377-3383.
37. Simonis, A., H. Lüth, J. Wang, and M.J. Schöning, *New concepts of miniaturised reference electrodes in silicon technology for potentiometric sensor systems.* Sensors and Actuators B: Chemical, 2004. 103, 429-435.
38. Banks, C.E., T.J. Davies, R.G. Evans, G. Hignett, A.J. Wain, N.S. Lawrence, J.D. Wadhawan, F. Marken, and R.G. Compton, *Electrochemistry of immobilised redox droplets: Concepts and applications.* Physical Chemistry Chemical Physics, 2003. 5, 4053-4069.
39. Perez Espitia, P.J., N. de Fátima Ferreira Soares, J.S. dos Reis Coimbra, N.J. de Andrade, R. Souza Cruz, and E.A. Alves Medeiros, *Bioactive Peptides: Synthesis, Properties, and Applications in the Packaging and Preservation of Food.* Comprehensive Reviews in Food science and Food Safety, 2012. 11, 187-204.
40. Herzog, G. and D.W.M. Arrigan, *Electrochemical strategies for the label-free detection of amino acids, peptides and proteins.* Analyst, 2007. 132, 615-632.

41. Kraatz, H.-B., D.M. Leek, A. Houmam, G.D. Enright, J. Lusztyk, and D.D.M. Wayner, *The ferrocene moiety as a structural probe: redox and structural properties of ferrocenoyl-oligoprolines Fc-Pro$_n$-OBzl (n = 1 – 4) and Fc-Pro$_2$-Phe-Bzl.* Journal of Organometallic Chemistry, 1999. **589**, 38-49.

42. MacDonald, S.M. and S.G. Roscoe, *Electrochemical oxidation reactions of tyrosine, tryptophan and related dipeptides.* Electrochimica Acta, 1997. **42**, 1189-1200.

43. Yeo, I.-H. and D.C. Johnson, *Electrochemical response of small organic molecules at nickel–copper alloy electrodes.* Journal of Electroanalytical Chemistry, 2001. **495**, 110-119.

44. Mader, P., *Brajter-Toth, A., Chambers, J.Q. (ed.): Electroanalytical Methods for Biological Materials.* Photosynthetica, 2002. **40**, 90-90.

45. Boyer, R.F., *Modern Experimental Biochemistry.* 2000, Benjamin Cummings.

46. Yuan, Y. and S. Amemiya, *Facilitated Protamine Transfer at Polarized Water/1,2-Dichloroethane Interfaces Studied by Cyclic Voltammetry and Chronoamperometry at Micropipet Electrodes.* Analytical Chemistry, 2004. **76**, 6877-6886.

47. Drummond, T.G., M.G. Hill, and J.K. Barton, *Electrochemical DNA sensors.* Nat Biotech, 2003. **21**, 1192-1199.

48. Kahlert, H., *Reference Electrodes*, in *Electroanalytical Methods: Guide to Experiments and Applications*, F. Scholz, et al., Editors. 2010, Springer Berlin Heidelberg: Berlin, Heidelberg. p. 291-308.

49. Kraatz, H.-B., *Ferrocene-Conjugates of Amino Acids, Peptides and Nucleic Acids.* Journal of Inorganic and Organometallic Polymers and Materials, 2005. **15**, 83-106.

50. Da Silva, R.A.B., A.C. Rabelo, R.A.A. Munoz, and E.M. Richter, *Three-Electrode-Integrated Sensor into a Micropipette Tip.* Electroanalysis, 2010. **22**, 2167-2171.

51. Clark, M.E., J.L. Ingram, E.E. Blakely, and W.J. Bowyer, *Effects of cell design on electrochemical measurements in submicroliter volumes.* Journal of Electroanalytical Chemistry, 1995. **385**, 157-162.

52. Bowyer, W.J., M.E. Clark, and J.L. Ingram, *Electrochemical measurements in submicroliter volumes.* Analytical Chemistry, 1992. **64**, 459-462.

53. Amatore, C., Arbault, S., Y. Bouret, B. Cauli, M. Guille, A. Rancillac, J. Rossier, *In situ electrochemical monitoring of reactive oxygen and nitrogen species released by single MG63 osteosarcoma cell submitted to a mechanical stress.* ChemPhysChem, 2006. **7**, 181-187.

54. Finot, M.O., G.D. Braybrook, and M.T. McDermott, *Characterization of electrochemically deposited gold nanocrystals on glassy carbon electrodes.* Journal of Electroanalytical Chemistry, 1999. **466**, 234-241.

55. Messina, P., F. Lemaître, F. Huet, K.A. Ngo, V. Vivier, E. Labbé, O. Buriez, and C. Amatore, *Monitoring and Quantifying the Passive Transport of Molecules Through Patch–Clamp Suspended Real and Model Cell Membranes.* Angewandte Chemie International Edition, 2014. **53**, 3192-3196.

56. Mueller, P., D.O. Rudin, H. Ti Tien, and W.C. Wescott, *Reconstitution of Cell Membrane Structure in vitro and its Transformation into an Excitable System.* Nature, 1962. **194**, 979-980.

57. Zasadzinski, J., R. Viswanathan, L. Madsen, J. Garnaes, and D. Schwartz, *Langmuir-Blodgett films.* Science, 1994. **263**, 1726-1733.

58. Hanke, W., C. Methfessel, U. Wilmsen, and G. Boheim, *Ion channel reconstitution into lipid bilayer membranes on glass patch pipettes.* Bioelectrochemistry and Bioenergetics, 1984. **12**, 329-339.

59. Neher, E. and B. Sakmann, *Single-channel currents recorded from membrane of denervated frog muscle fibres.* Nature, 1976. **260**, 799-802.

60. Meunier, A., Thèse, Ecole Normale Supérieure, 2011.

61. O'Connell, A., R. Koeppe, and O. Andersen, *Kinetics of gramicidin channel formation in lipid bilayers: transmembrane monomer association.* Science, 1990. **250**, 1256-1259.

62. Hung, W.C., F.Y. Chen, and H.W. Huang, *Order–disorder transition in bilayers of diphytanoyl phosphatidylcholine.* Biochimica et Biophysica Acta (BBA) - Biomembranes, 2000. **1467**, 198-206.

63. Andersson, M., J. Jackman, D. Wilson, P. Jarvoll, V. Alfredsson, G. Okeyo, and R. Duran, *Vesicle and bilayer formation of diphytanoylphosphatidylcholine (DPhPC) and diphytanoylphosphatidylethanolamine (DPhPE) mixtures and their bilayers' electrical stability.* Colloids and Surfaces B: Biointerfaces, 2011. **82**, 550-561.

64. Le Berre, M., A. Yamada, L. Reck, Y. Chen, and D. Baigl, *Electroformation of Giant Phospholipid Vesicles on a Silicon Substrate: Advantages of Controllable Surface Properties.* Langmuir, 2008. **24**, 2643-2649.

65. Corey, D.P. and C.F. Stevens, *Single Channel Recordings, B. Sakmann, E. Neher (Eds.).* Plenum Press, New York 1983. **Chapter 3**: p. 53-68.

Third Chapter:

Selective Electrochemical Bleaching of Fluorescence Emitted by NBD-labelled Phospholipids or Peptides

3. Third Chapter: Selective Electrochemical Bleaching of Fluorescence Emitted by NBD-labelled Phospholipids or Peptides

1.1. Introduction

In the previous chapter, we showed that the use of electrochemistry to detect micromolar concentrations of Cell-Penetrating Peptides crossing a micrometric suspended lipid bilayer membrane is rather difficult for sensitivity reasons. On the other hand, fluorescence-based methods, which are known for their high sensitivity, have been intensively used to monitor and quantify the amount of internalized peptides within liposomes used, as cell models, in order to understand mechanisms involved during CPPs translocation through membranes. Today, endocytosis and direct translocation are the two major described processes, but they are still under debate [1]. Actually, this controversy comes from the fact that fluorescence-based techniques (spectroscopy and microscopy), which are the most common exploited approaches to assess the uptake of these peptides, are unable to discriminate between internalized and surface-bound CPPs due to their poor resolutions with respect to the lipid bilayer membrane thickness (4 nm). Typically, the most common method to evaluate peptide uptake is the coupling of a peptide to a fluorophore and the monitoring of fluorescence on treated cells. It is a convenient method for the determination of both the localization and the amount of uptake of peptides. Nevertheless, drawbacks to this method are that uptake does not always correlate with bioavailability, and care must therefore be taken when interpreting the translocation process. Furthermore, cationic peptides are known to bind to the external face of the cell membrane and can thereby give false positive results, again because fluorescence cannot easily discriminate between internalized and surface-bound peptides. To overcome this difficulty, protocols have been developed to reduce signals from surface-bound peptides. The most popular one consists in fluorescence quenching of surface-bound CPPs tagged with 4-nitrobenzo-2-oxa-1,3-diazol-4-yl (NBD), a very common used small neutral fluorescent probe. Under these conditions, fluorescence is generally quenched by dithionite ($S_2O_4^{2-}$), which act as a chemical reducing agent [2-6]. However, this physiologically compatible chemical quencher has recently been found to permeate membrane vesicles [7]. This permeation property could therefore severely affect translocation investigations based on the fluorescence monitoring after dithionite quenching.

These considerations prompted us to develop a non-chemical strategy to quench the fluorescence emitted by NBD. Indeed, considering the redox nature of the reaction between dithionite and NBD, an electrochemical reduction could bring a significant benefit in several aspects: (i) it avoids the

introduction of exogenous chemical agents like dithionite and (ii) the heterogeneous nature of electron transfers achieved at solid electrodes allows an electrochemical reduction to only effect species dissolved outside the vesicles or aggregated in the outer phospholipid leaflet of vesicles. Electrochemical activation/deactivation of fluorescent probes is not a new concept *per se*. Indeed, Miomandre et al. have described the electrochemically controlled switching of chloromethoxytetrazine [8] and other dyes have also been switched on/off electrochemically [9-12]. Generally such approaches make sense if the fluorescence is confined and examined (through microscopy) in a thin layer which fits the dimension of an electrode diffusion layer thickness. In order to develop an electrochemical approach allowing the quantitative fluorescence extinction of surface-bound NBD-labelled peptides, we first focused on the development of an original electrochemical approach able to quench selectively the outer leaflet of NBD-labeled giant liposomes. In this third chapter, we will show notably how confocal fluorescence microscopy and potentiometry were combined to monitor the selective fluorescence extinction of outer leaflet fluorophore-labeled giant liposomes, allowing discrimination between the inside and the outside of membranes (Section 3.5). This original electrochemical approach was then tested in the presence of NBD-labelled peptides localized on the outer leaflet of giant liposomes (Section 3.6). Before addressing these two important contributions, relevant information will be presented not only on fluorescence (principle, fluorescent probes, fluorescence microscopy – Sections 3.2 and 3.3), but also on model membranes (vesicles, phospholipids – Section 3.4) allowing thus a better understanding of the work presented in this chapter.

3.2. Fluorescence

3.2.1. Fluorescence principle

Fluorescence, as well as phosphorescence, is a particular case of luminescence [13-16]. More specifically, generation of luminescence through excitation of a molecule by absorption of light (photons) is a phenomenon termed photoluminescence, which is formally divided into two categories, fluorescence and phosphorescence, depending upon the electronic configuration of the excited state and the emission pathway. Compared to phosphorescence in which photoluminescence results from a triplet–singlet electronic relaxation (typical lifetime: milliseconds to hours), fluorescence involves a singlet–singlet electronic relaxation leading therefore to a shorter emission rate (typical lifetime: nanoseconds). Fluorescence can therefore provide information on dynamic processes on the nanosecond time-scale.

Typically, fluorescence emission can be divided in three main steps: 1) absorption of light, 2) internal conversion, and 3) emission of light. In summary and as illustrated in the Jablonski diagram (Figure 3.1), when an electron leaves the ground state S_0 (electronic singlet), due to the absorption of a quantum of light (single photon), it moves to a higher electronic states (Figure 3.1 - green arrows). Then, the electron undergoes an internal conversion leading to a non-radiative de-excitation during a very short time (around 10^{-12}s). Finally, returning to the ground state (S_0) makes the electron dissipate the remaining energy by emitting a photon with a longer wavelength (fluorescence emission; see blue arrows in Figure 3.1) [14].

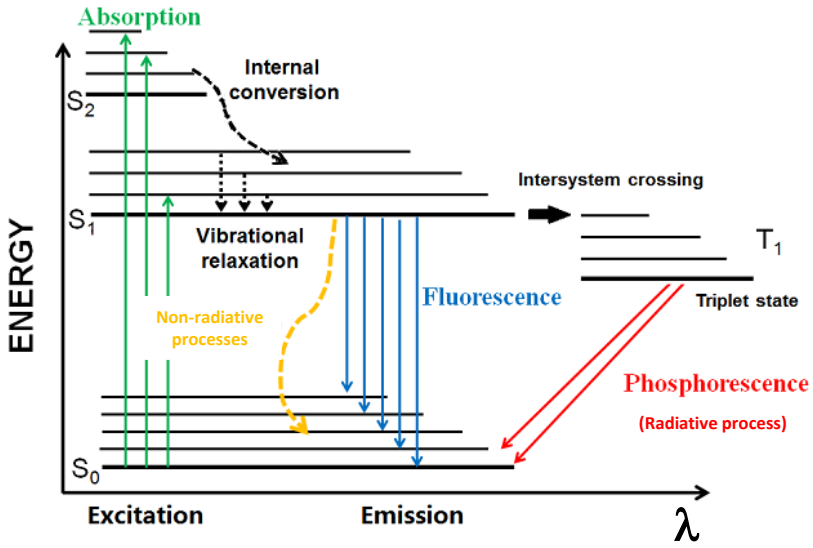

Figure 3.1 Jablonski diagram (adapted from : http://www.ibs.fr)

Though an excited molecule can return to the ground state with emission of fluorescence, many other pathways, either radiative or non-radiative, are also possible. For instance, phosphorescence is the most known radiative de-excitation. In this case, the absorbed photon energy undergoes an intersystem crossing into an energy triplet state. As a result, the energy can become trapped in the triplet state with only "forbidden" transitions available to return to the lower energy state. These transitions are kinetically unfavored and thus progress at significantly slower time scales compared to fluorescence. Concerning the non-radiative de-excitation, the most common are (i) the photo-induced electron transfer, (ii) the quenching by FRET (Förster Resonance Energy Transfer), and (iii) photo-induced reactions such as fluorophore photo-bleaching. In the latter case the fluorescence loss is due

to the irreversible degradation of the fluorescent probe. Interestingly, this process can be also deliberately used in microscopy to visualize and to quantify some dynamic phenomenon. This will be discussed later in this chapter when FRAP (Fluorescence Recovery After Photobleaching) and FLIP (Fluorescence Loss In Photobleaching) techniques will be described.

On the other hand, the success of fluorescence, as an investigative tool in studying the structure and dynamics of matter or living systems, arises from the high sensitivity of fluoro-metric techniques, the specificity of fluorescence characteristics due to the microenvironment of the emitting molecule, and the ability of the latter to provide spatial and temporal information. As shown in Figure 3.2, numerous physical and chemical parameters which characterize the microenvironment can affect the fluorescence characteristics of a fluorescent probe.

Besides, an interesting feature of the NBD probe used in this work is its sensitivity to the environment in which the fluorophore is placed. Indeed, the NBD group exhibits a high degree of environmental sensitivity [17-21] and its fluorescence lifetime displays remarkable sensitivity to environmental polarity [20, 22]. It was also recently described that a fast pH jump has an effect on the fluorescence quenching of NBD. This property was notably used to evaluate the intra-vesicular accumulation of NBD-labelled peptides [6]. The physicochemical properties of the NBD probe will be described in the following paragraph.

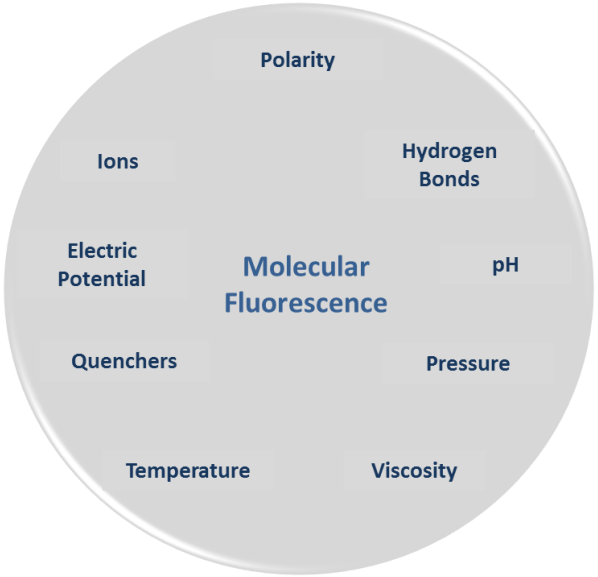

Figure 3.2 Parameters influencing the emission of fluorescence [16].

3.2.2. Fluorescent probes

3.2.2.1. General

Fluorescent probes are molecules that absorb light (photon) at a specific wavelength and emit light at a different, typically longer, wavelength. These molecules, also called fluorophores, typically contain several combined aromatic groups, or plane or cyclic molecules with several π bonds. Though they can be used alone (e.g. as a tracer in fluids), fluorophores are generally covalently bonded to a macromolecule, serving as a marker (or dye, or tag, or reporter) for bioactive reagents (antibodies, peptides, nucleic acids). Fluorophores are notably used to stain tissues, cells, or materials in a variety of analytical methods including fluorescent imaging and spectroscopy. Fluorophores are generally classified into four categories: proteins (e.g. Green Fluorescent Protein) and peptides, small organic compounds, synthetic oligomers and polymers, and multi-component systems [23]. In the following, we will especially focus on small organic compounds such as fluorescein, rhodamine and NBD derivatives since they are commonly used in CPPs investigations.

3.2.2.2. Properties and characteristics

Fluorescent probes are generally characterized by various parameters. Here are the most important ones:

- **Extinction Coefficient ($Mol^{-1}cm^{-1}$):** the first characteristic of a fluorophore is its capacity to absorb a photon to reach the excited state. The light absorption efficiency is determined by the molar extinction coefficient (ε). This links the quantity of absorbed light, at a given wavelength, to the concentration of fluorophore in solution.

- **Quantum yield:** the second most important characteristic of a fluorophore is its capacity to emit a photon efficiently. This is given by the quantum yield which reflects the efficiency of the energy transferred from incident light to emitted fluorescence (= number of emitted photons per absorbed photons)

- **Maximum excitation and emission wavelength (expressed in nanometers (nm)):** corresponds to the peak in the excitation and emission spectra (usually one peak each). This point must be particularly considered when living systems (cells, animals) are investigated. Under these

conditions, “auto-fluorescence” coming from endogen entities (e.g. tryptophan, tyrosine, NADH, etc.) may indeed interfere with the intrinsic fluorescence of a fluorophore tag.

- **Fluorescence Lifetime (in picoseconds):** duration (from 0.1 to 100 ns) of the excited state of a fluorophore before returning to its ground state. It refers to the time taken for a population of excited fluorophores to decay to 1/e (≈0.368) of the original amount. This is an important parameter for time-resolved measurements [24] and applications involving fluorescence polarization [25].

- **Stokes shift:** difference between the maximum excitation and maximum emission wavelengths. From a practical point of view, the detection of fluorescent species is easier when the Stokes shift is larger. Some fluorescent probes such as rhodamine and fluorescein derivatives have a small Stokes shift ($\Delta\lambda$ = 20-30 nm); in this case, these probes usually undergo “self-quenching” phenomenon [13].

Other important “obvious” characteristics of fluorophores which may be also taken into account are (i) brilliance, (ii) stability, (iii) solubility, and (iv) chemical accessibility.

3.2.3. Florescent probes and Cell-Penetrating Peptides (CPPs)

Visualization of CPPs *via* the fluorescence emitted by some intrinsically fluorescent amino-acids such as tryptophan is unfortunately impossible especially in living cells in which other biomolecules are present. This drawback is overcome by grafting an organic fluorescent probe on the CPP. Among the numerous existing organic fluorescent probes (Figure 3.3), fluorescein, rhodamine, and NBD [26-29] are the most used derivatives to visualize the internalization of CPPs inside Giant Unilamellar Vesicles (GUVs) by confocal fluorescence microscopy [30-37].

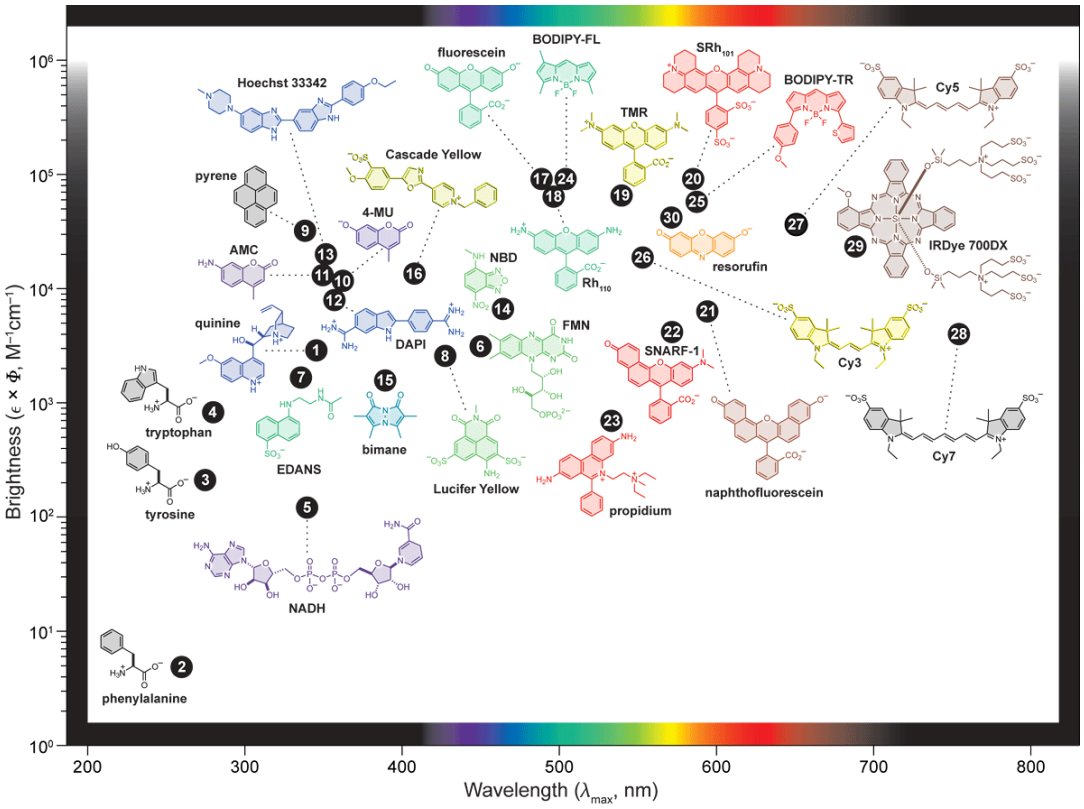

Figure 3.3 Main organic fluorophores classified according to their brilliance and as a function of their emission wavelengths. From Ref [38].

However, compared to fluorescein and rhodamine, the NBD probe (4-nitrobenz-2-oxa-1,3-diazol-4-yl) appeared more adapted for the investigation of CPPs translocation through membranes (Figure 3.4). This was due to several reasons. First of all, it was recently shown that fluorescence of fluorescein- and rhodamine-labelled CPPs was quenched in close proximity of membranes due to a fluorescence self-quenching process which does not exist for NBD [39, 40]. Moreover, compared to fluorescein and rhodamine, the NBD probe (i) is smaller in size (not bigger than a tryptophan amino acid), (ii) is less hydrophobic, and (ii) has no charge at the physiological pH; these three characteristics make NBD a tag that should not significantly affect the translocation properties of CPPs.

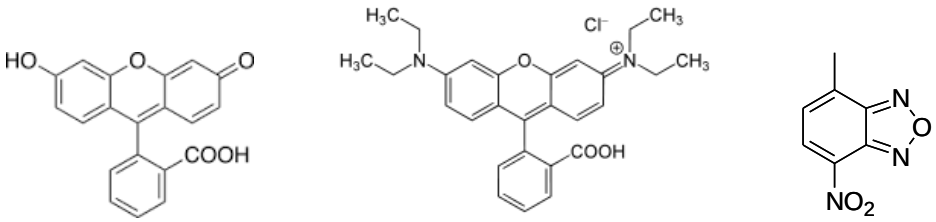

Fluorescein Rhodamine B NBD

Figure 3.4 Three typical organic fluorescent probes used to tag CPPs.

On the other hand, the fluorescence emitted by NBD is highly sensitive to the environment in which it is placed. This also explains why the NBD group is a widely used fluorophore in biophysical, biochemical, and cell biological investigations [41, 42]. Actually, NBD fluorescence lifetime displays a remarkable sensitivity to the surrounding polarity. This is reflected by an increase of its quantum yield in low polar media. Actually, the NBD fluorescence is a decreasing function of the dielectric permittivity. This sensitivity comes from the fact that the NBD fluorescence is due to an intramolecular charge transfer associated to a strong dipole moment change (4 Debye) [19, 21, 43]. This is illustrated in Figure 3.5 that depicts the quantum yield variation of the *n*-propylamino-NBD derivative as a function of the medium dielectric permittivity [44]. As a consequence, it was demonstrated that the fluorescence intensity of NBD-labeled peptides increases by around a factor of ten when they are in contact of vesicles. This is easily explained by the fact that the interface between water and the lipid bilayer has a lower polarity ($\varepsilon = 40$) than that of water ($\varepsilon = 78$).

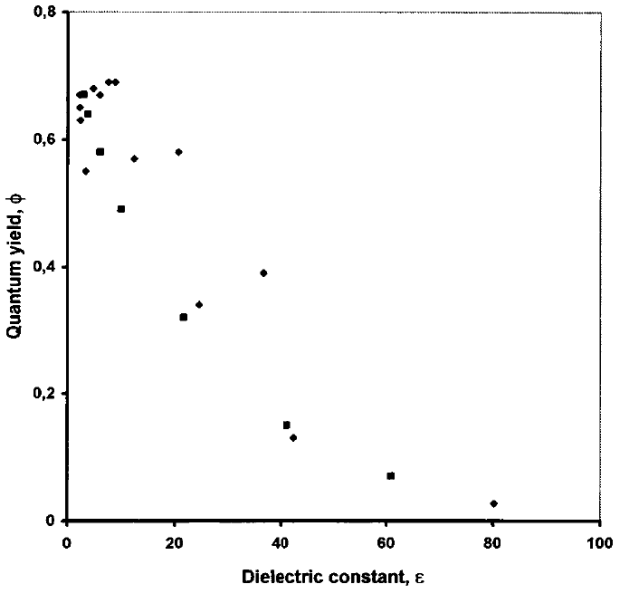

Figure 3.5 Plot of the fluorescence quantum yield ϕ of *n*-propylamino-NBD as a function of the organic solvent polarity (♦) and water/dioxane mixtures (■) versus the solvent dielectric constant ε [44].

Another interesting feature of the NBD probe is that its fluorescence emission can be suppressed by dithionite, a chemical reducing agent (*vide infra*). This property is very useful to localize molecules that are labeled with this fluorophore [17].

Importantly, NBD can be not only grafted onto peptides, but also onto phospholipids. Moreover, numerous NBD-phospholipids are commercially available (with the NBD localized either on the polar phospholipid head or on an alkyl chain). We have notably used these NBD-labelled lipids to develop

the electrochemical approach allowing the selective quenching of fluorescent outer leaflet vesicles which is described in the paragraph 3.5. The chemical structures of phospholipids used here are shown in Section 3.4.3.1.

3.2.4. Redox properties of the NBD fluorescent probe

As mentioned above, the NBD fluorescent probe is also interesting from the electrochemical point of view since its fluorescence can be quenched by reduction. This redox property made the NBD probe popular to investigate the CPP uptake in the presence of vesicles. Indeed, based on this property, protocols have been developed to allow a better discrimination between internalized and surface-bound peptides. In this case, the NBD fluorescent probes are quenched by dithionite ($Na_2S_2O_4$). Actually, the active species allowing the reduction of the NBD nitro group into the corresponding amine derivative is the anion radical $^{\bullet}SO^{2-}$ [45]. However, dithionite must be used in excess due to its instability in water and in the presence of oxygen. In water, dithionite undergoes a fast disproportionation reaction whereas oxygen is able to oxidize it. Moreover, this physiologically compatible chemical quencher has recently been found to permeate membrane vesicles [7]. This permeation property could therefore severely affect translocation investigations based on the fluorescence monitoring after dithionite quenching.

Alternatively, the NBD probe can be reduced by electrochemistry. Recently, we investigated the NBD-glycine (NBD-G) as a test compound to collect information on the electrochemical behavior of the NBD probe covalently bonded to an amino acid. The cyclic voltammogram recorded in PBS is presented in Figure 3.6.

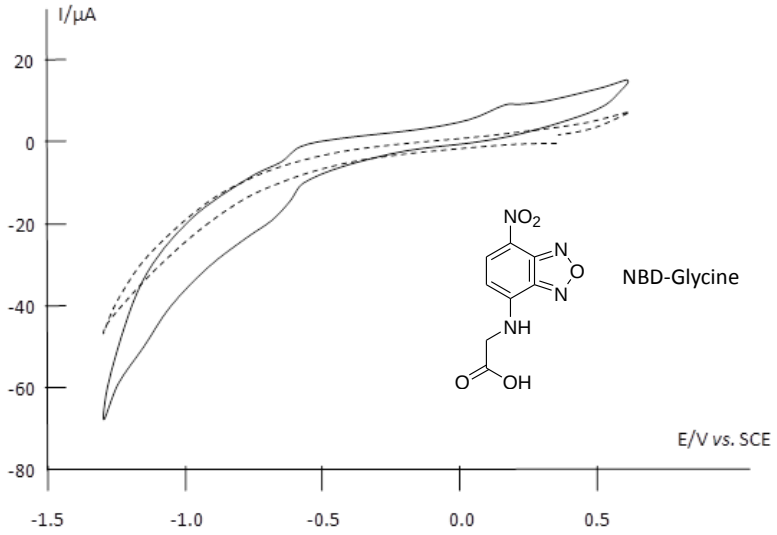

Figure 3.6 Cyclic voltammogram of NBD-G at a 1 mm diameter glassy carbon electrode in PBS aqueous buffer (50 mmol.L^{-1}). Dashed line: background CV before addition of NBD-G. Straight line: NBD-G 4 mmol.L^{-1}. Scan rate: 0.1 V.s^{-1}

The residual cathodic current observed is ascribed to the slow electrochemical reduction of water according to:

$$H_2O + e^- \rightarrow ½\ H_2 + OH^- \quad (1)$$

For a fast reduction process, the reduction of water would be expected to proceed at its thermodynamic potential value, i.e. -0.42 V vs. SHE or -0.67 V vs. SCE at pH = 7.2. In Figure 3.6, the sluggish evolution of the cathodic residual current (dashed line) recorded at a glassy carbon electrode (electrode material known for its large proton/water reduction overpotential) is consistent with a slow reduction process as expected. In the presence of NBD-G, a broad, partially reversible reduction wave is observed at -0.65 V. Since glycine alone does not show any faradaic process in the potential window explored, this wave accounts for the electrochemical reduction of the NBD probe.

The electrochemical reduction of aliphatic and aromatic nitro compounds has been extensively reviewed [46, 47]. The reduction may engage as much as 6 electrons to yield the parent amino compound. Actually, in water and more generally in protic solvents the cyclic voltammograms display two successive reduction steps, the first one producing a hydroxylamino intermediate:

$$Ar\text{-}NO_2 + 4e^- + 4\ H^+ \rightarrow Ar\text{-}NHOH + H_2O \quad (2)$$

This reduction step is observed at a potential values which strongly depends on several factors, namely the pH of the medium. At neutral pH values like in Figure 3.6, reaction (2) is observed at -0.9 V vs. SCE [48], i.e. similar to the reduction potential value of NBD-G in Figure 3.6. Therefore, the wave at -0.65 V observed in Figure 3.6 most likely represents the reduction of the NBD nitro group.

3.3. Fluorescence Microscopy

3.3.1. Introduction / Principle

Microscopy is one of the numerous applications of fluorescence especially in life sciences. Typically, in fluorescence microscopy, the sample is first illuminated with a light of specific wavelength which is absorbed by the fluorophore. After this excitation, light is emitted at a different, typically longer, wavelength (i.e., of a different color than the absorbed light). The illumination light is separated from the much weaker emitted fluorescence through the use of a spectral emission filter. Typical components of a fluorescence microscope are a light source (xenon arc lamp, lasers), the excitation filter, the dichroic mirror, and the emission filter (Figure 3.7).

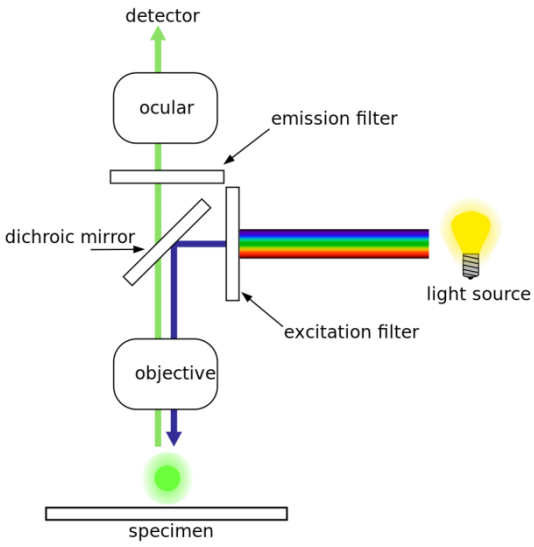

Figure 3.7. Principle of excitation and emission in fluorescence microscopy.

Most fluorescence microscopes in use are epifluorescence microscopes in which the fluorescence emitted by the specimen is focused onto the detector by the same objective than that used for the excitation. These microscopes are widely used in biology and are the basis for more advanced microscope designs, such as the total internal reflection fluorescence microscope (TIRF) and the confocal microscope.

3.3.2. Confocal Microscopy

In a conventional wide-field fluorescence microscope (as described above), the entire specimen is flooded evenly in light from a light source. All parts of the sample in the optical path are excited at the same time and the resulting fluorescence is detected by the microscope's photodetector including a large unfocused background part. In contrast, a confocal microscope uses a pinhole in an optically conjugate plane in front of the detector to eliminate out-of-focus signal (the name "confocal" stems from this configuration). The principle of confocal microscopy is depicted in Figure 3.8.

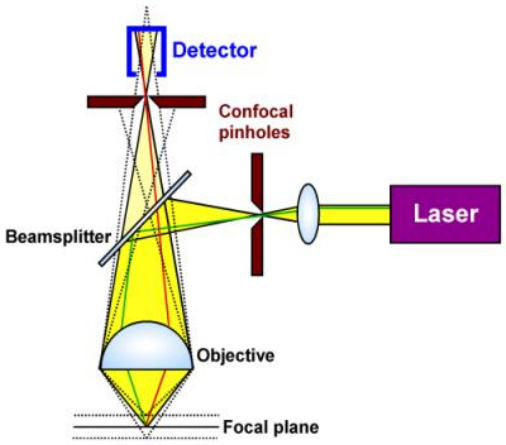

Figure 3.8 Principle of confocal microscopy.

As only light produced by fluorescence very close to the focal plane can be detected, the image's optical resolution, particularly in the sample depth direction, is much better than that of wide-field microscopes (around 400 nm in the axial direction and 200 nm in the lateral direction versus 500-700 nm and 200-300, respectively in a conventional fluorescence microscope) [49]. Therefore, confocal microscope enables the reconstruction of three-dimensional structures from the obtained images by collecting sets of images at different depths within a thick object. This technique has gained popularity in the scientific and industrial communities and wide applications can be found in life sciences. As we will see later in the chapter, the use of a confocal microscope was particularly relevant to visualize giant vesicles (several tenths µm in diameter) and to follow their fluorescence quenching in real time.

3.3.3. Advanced Fluorescence Microscopy Techniques

As mentioned in the first paragraph of this chapter, photo-induced reactions such as photo-bleaching are generally considered as drawbacks in fluorescence because these processes lead to a non-

radiative de-excitation of fluorophores. However, photo-bleaching can be deliberately used to visualize and to quantify some dynamic phenomena. In this case, photo-bleaching consist in switching off the fluorescence by high intensity illumination with a focused laser beam. Within this context, five main techniques have been developed: (i) fluorescence recovery after photobleaching (FRAP), fluorescence loss in photobleaching (FLIP), fluorescence localization after photobleaching (FLAP), Förster or fluorescence resonance energy transfer (FRET), and fluorescence lifetime imaging microscopy (FLIM). In this paragraph we will focus on FRAP and FLIP techniques which are the most used procedures. Moreover, these techniques are directly connected to the electrochemical quenching of NBD fluorescence described in this chapter.

• Fluorescence Recovery after Photo-Bleaching (FRAP) was developed in the 1970s by Axelrod to investigate protein mobility in living cells by measuring the rate of fluorescence recovery at a previously bleached area [14]. In a typical FRAP experiment (Figure 3.9), fluorescent molecules are irreversibly photo-bleached in a small region of interest (ROI) of the cell by high intensity illumination with a focused laser beam. Subsequently, diffusion of the surrounding non-bleached fluorescent molecules into the bleached area leads to recovery of fluorescence with a specific rate, which is recorded at low laser power.

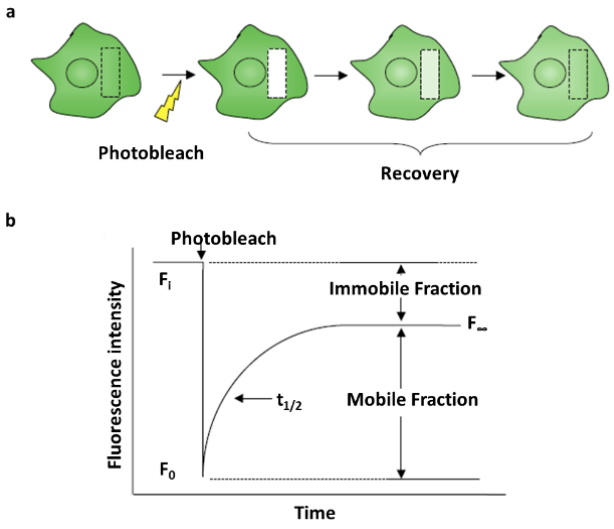

Figure 3.9 Principle of Fluorescence Recovery After Photobleaching. (a) A region of interest (ROI) is selected (dashed rectangle), bleached with an intense laser beam, and the fluorescence recovery in the ROI is measured over time. (b) Corresponding plot of the fluorescence recovery revealing the mobile and immobile fractions of the fluorophore in the cell. Adapted from reference [50].

Originally the FRAP technique was utilized as a method to measure diffusion in cellular membranes [51, 52] using organic dyes such as fluorescein. However, with the development of both fluorescent protein technology and confocal microscopy, FRAP became popular for studying protein mobility in the cell interior. Nowadays, the FRAP technique is used not only to address diffusion rates, but protein dynamics and interactions with other cellular components [53-57]. Most importantly, FRAP has been shown to be a good approach to study nuclear protein dynamics in living cells and was further developed by researchers such as Adriaan Houtsmuller [58, 59].

• Fluorescence Loss In Photobleaching (FLIP), is a complementary technique to FRAP. The FLIP method is usually used to investigate the exchange of molecules between two compartments separated by lipid bilayers [60-62]. In FLIP experiments the illumination of the region of interest (ROI) is applied continuously so that fluorescence cannot be recovered. The loss in fluorescence in the ROI defines the mobile fraction of the fluorescently labeled molecule. Conversely, the incomplete loss in fluorescence defines the immobile fraction of fluorescently-labeled molecules that do not move into the continuously photo-bleached area [14] (Figure 3.10).

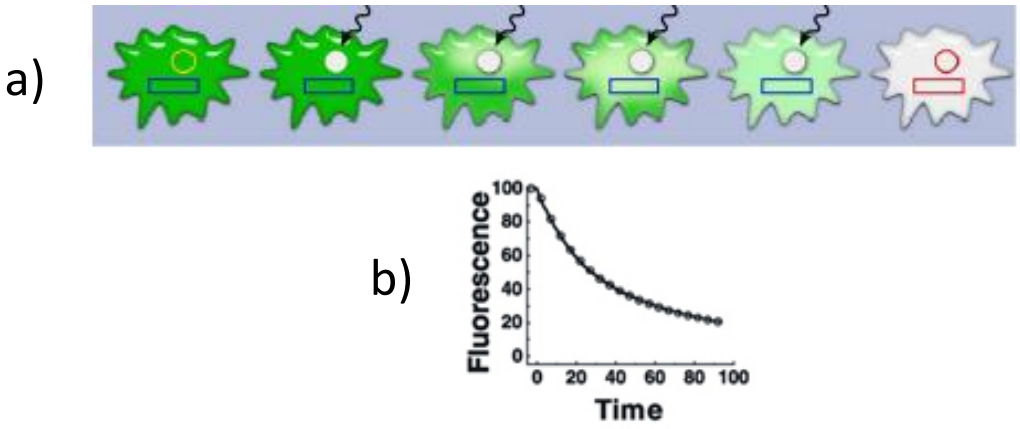

Figure 3.10 Principle of Fluorescence Loss In Photobleaching (FLIP). (a) FLIP experiments involve repetitive bleaching of a selected region of interest (ROI; orange circle in a)) during the entire monitoring period and the fluorescence intensity in regions outside the selected bleached area is measured (rectangle). (b) Corresponding fluorescence intensity decay measured in the surrounding regions (rectangular area). The fluorescence loss is due to bleaching of fluorophores that move through the ROI during the repetitive bleaching process. The drop in fluorescence intensity outside the bleached region is caused by a steadily increasing population of bleached, non-fluorescent molecules within the cell and thus provides quantitative data on their molecular mobility. Figure adapted from reference [14].

3.4. Model Membranes

3.4.1. Introduction / Choice of the model membrane

Artificial membrane bilayers are attractive models of natural membranes notably for the analysis of energy-independent processes. Supported lipid bilayers, suspended lipid bilayers and vesicles are the most used artificial membranes. Nevertheless, within the context of the transport of (bio)-molecules only suspended lipid bilayers and vesicles are interesting since both the inner and outer leaflet of artificial membranes are accessible under these configurations. For instance, suspended protein-free lipid bilayers can be used to investigate the transport of molecules [63]. Unfortunately, we showed in the previous chapter that such suspended membranes were not suitable, at least when they are combined with an electrochemical detection, to follow small fluxes of CPPs.

On the other hand, since translocation of CPPs is usually investigated in the presence of vesicles we then decided to use these artificial/model membranes. Vesicles, or liposomes, are spherical lipid assemblies having an aqueous core enclosed by one or more phospholipid bilayers or lamellae [64]. According to their size, liposomes can be divided in three different kinds of unilamellar vesicles: small (SUV, 20-50 nm), large (LUV, 50-100 nm) and giant (GUV, 1-100 µm) (Figure 3.11) [65]. Though LUVs and GUVs are the most used vesicles to investigate CPP translocation, we decided to work with giant unilamellar vesicles because their size enables the use of confocal fluorescence microscopy to monitor and to quantify fluorescence extinction in real time.

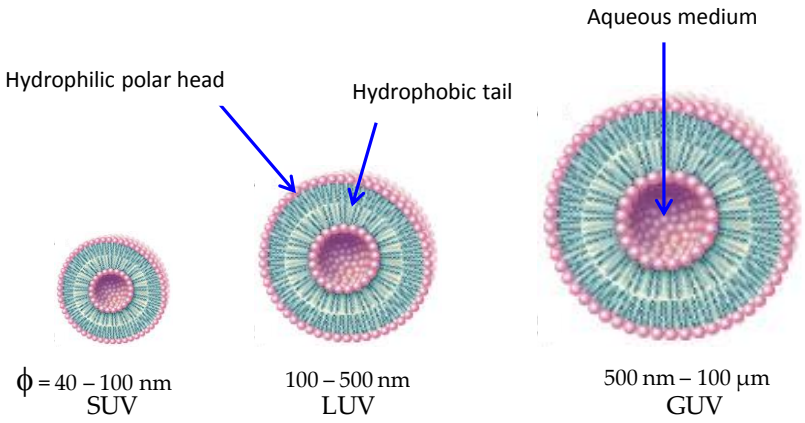

Figure 3.11 Different types of vesicles as a function of their diameter.

3.4.2. Giant unilamellar vesicles (GUVs)

Giant unilamellar vesicles (GUVs) have been extensively used as model system to investigate membrane behaviors [66]. They are employed not only for the quantitative characterization of physicochemical properties of lipid membranes, but also to investigate membrane related process like cell adhesion, phase separation, and domain formation, protein sorting in lipid rafts, endo and exocytosis, uptake of various molecules, and protein mobility [66]. GUVs are also a very practical tool to study the response of membranes to external perturbations like hydrodynamic flows, locally applied forces, micromanipulation, and electric fields [66]. Indeed, in terms of shape, structure, and membrane curvature (close to zero), GUVs are similar to cell and organelles membranes [66]. Moreover, thanks to their micrometer range size, GUVs are easily observable under an optical microscope using various enhanced techniques like phase contrast, differential interference contrast, or confocal and conventional fluorescence microscopy.

3.4.2.1. Preparation of Symmetric GUVs

Three main methods have been developed for preparing symmetrical GUVs i.e., that both the outer and the inner leaflet of the vesicle possess the same phospholipid: either by (i) gentle hydration of a phospholipid film, or (ii) electroformation, or (iii) coalescence of small vesicles [64]. These methods are briefly described below:

Gentle hydration of a phospholipid film. This method involves deposition of phospholipids, from a solution in an organic solvent such as chloroform or ethanol, onto a substrate. The film consisting of staked phospholipid bilayers is subsequently hydrated during a couple of days in the absence of hydrodynamic flow to obtain an aqueous suspension of GUVs. However, the gentle hydration method which is especially used to prepare GUVs containing charged phospholipids produces also a significant fraction of multilamellar vesicles [66].

Electroformation. In this method, the phospholipid film is deposited on electrodes, consisting in ITO-coated glass coverslips, and subsequently hydrated for a couple of hours in the presence of electric fields [67]. With this method, 80 % of the electroformed vesicle population is unilamellar and free from defects [66].

Coalescence of small vesicles. Coalescence of small vesicles that are stored in suspension for several days, results in the formation of GUVs. Fusion of LUVs may be induced by various means including subjecting them to freeze-thaw cycles in concentrated solutions of electrolytes, using oppositely charged phospholipids, addition of poly(ethylene glycol), or fusogenic peptides, and incorporating divalent cations into negatively charged phospholipids [66].

3.4.2.2. Asymmetric vesicles

Though the above-described methods are interesting for the preparation of symmetrical GUVs, they are unsuitable to prepare vesicles having different lipid composition on each leaflet. Yet, and as it will be described later, the selective electrochemical quenching of the outer leaflet of NBD-labeled giant liposomes requires the use of asymmetric lipid bilayers. The challenging preparation of asymmetric GUVs was first successfully demonstrated in 2003 by S. Pautot (Figure 3.12) [68].

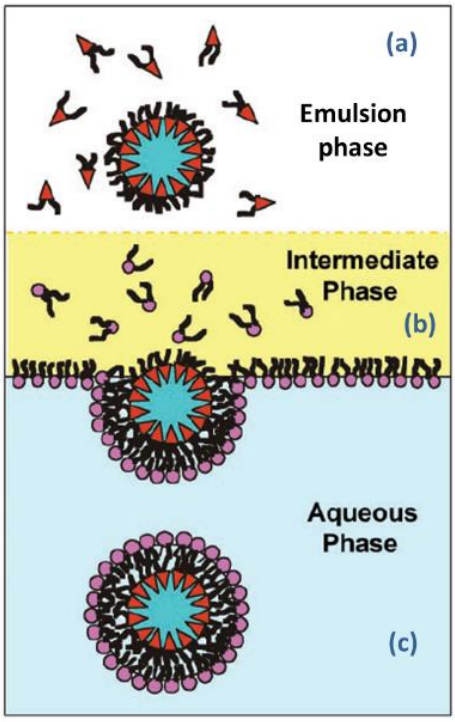

Figure 3.12 Illustration of the technique used to prepare asymmetric vesicles. In this method, the sample is composed of three parts: an inverted emulsion where water droplets in lipid-saturated oil are stabilized by lipid molecules destined for the inner leaflet; an intermediate phase of lipid-saturated oil heavier than the inverted emulsion phase, and whose lipids form a monolayer at the oil water interface; and the bottom aqueous phase, which receives the final asymmetric vesicles. The lipids in the intermediate phase are completely different from those in the inverted emulsion and form the outer leaflet of the bilayer; the final structure is an asymmetric vesicle. From Ref. [68].

The preparation begins with an inverted emulsion of water droplets disperse in dodecane and stabilized by the lipids intended for the inner leaflet (Figure 3.12-a, emulsion phase). This phase is placed over an intermediate phase (Figure 3.12-b) of the same oil containing the lipids for the outer leaflet. The intermediate phase is placed over a final aqueous phase, and a monolayer of the second lipid forms at the interface. The water droplets in the emulsion are heavier than oil and thus sediment, pulling the second monolayer from the interface to complete the bilayer, resulting in the formation of asymmetric vesicles in the final aqueous phase (Figure 3.12-c). The construction of asymmetric vesicles was confirmed using a fluorescence quenching assay (dithionite) to identify the location of the molecules in the bilayers [68].

However, in this method, an external force such as centrifugation had to be used due to the density of silicon oil (1.05) which makes the intermediate phase slightly denser than the emulsion. In this context, an alternative preparation of asymmetric GUVs was more recently developed [69, 70]. The authors reported the spontaneous formation of giant liposomes (ranging from 1 to 100 µm) in a biphasic (oil/water) environment without applying any external driving force. In summary, and as depicted in Figure 3.13, a water–oil emulsion is first prepared with lipid A dissolved in the oil phase, encasing droplets in a monolayer. The emulsion is added to a water–oil (W/O) well with lipid B dissolved in the oil phase, assembling as a monolayer at the interface. Droplets cross the column under gravity (represented by the thick green arrow), and are enveloped by a second monolayer. Asymmetric GUVs are thus formed, with lipid A in the inner leaflet and lipid B in the outer leaflet.

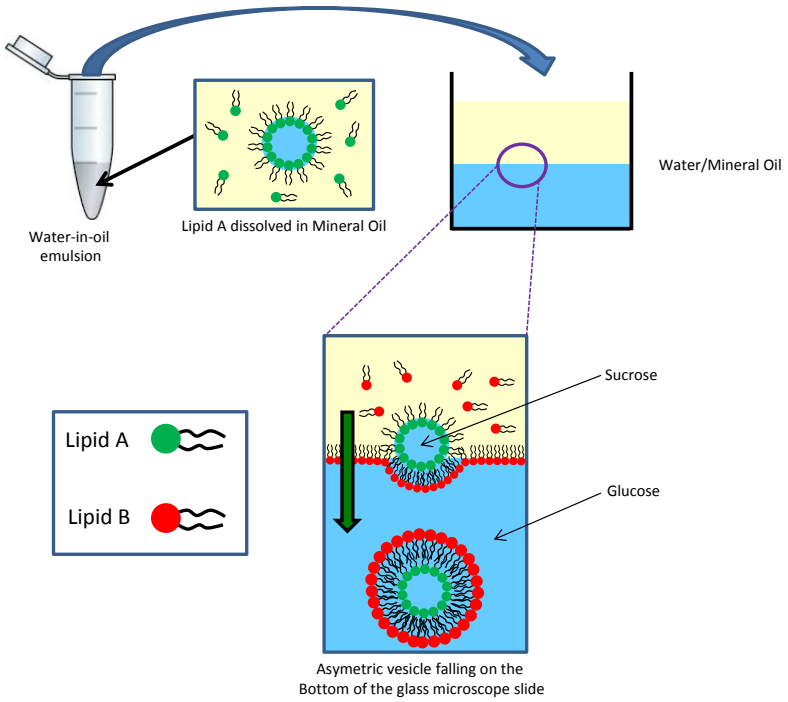

Figure 3.13. Asymmetric GUV preparation via phase transfer. Adapted from reference [68].

3.4.3. Choice of the phospholipids

3.4.3.1. Structure and properties

Phospholipids are basic components of cellular membranes. The structure of the phospholipid molecule generally consists of two hydrophobic fatty acid "tails" and a hydrophilic phosphate "head", joined together by a glycerol molecule. Note that hydrophobic alkyl chains which can be saturated or not have between 12 and 24 carbon atoms [71]. The third alcohol function of the glycerol nucleus is associated to a polar group (the hydrophilic head of the phospholipid) via a phosphoric acid. Acronyms are usually used to simplify the reading of phospholipids. These acronyms give information on the nature of both the alkyl chain and the phospholipid head. The two first letters give thus information on fatty acids. For instance, DP means Di-Palmitoyl (twice 16 carbons) whereas PO corresponds to 1-Palmitoyl-2-Oleoyl (2 alkyl chains possessing 16 and 18 carbons, respectively). The two last letters relate to the “head” linked to the glycerol moiety. Main heads are (i) phosphatidylcholine (PC); (ii) phosphatidylethanolamine (PE); (iii) phosphatidylserine (PS), and (iv) phosphatidylglycerol (PG). Note that PC and PE heads are switterionic whereas PS and PG are negatively charged.

Within the framework of this chapter, we used DOPG and DPPG as phospholipids. Their structures are given in Figure 3.14.

DOPG
Tm = -18°C

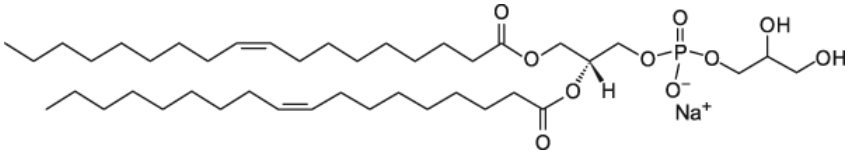

1,2-dioleoyl-*sn*-glycero-3-phospho-(1'-*rac*-glycerol) (sodium salt)

DPPG
Tm = 41°C

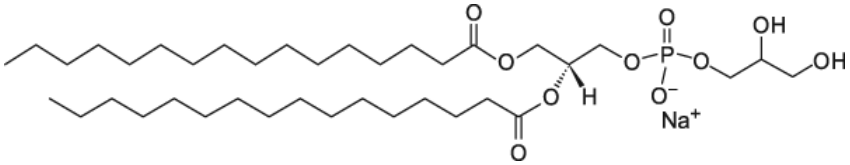

1,2-dipalmitoyl-*sn*-glycero-3-phospho-(1'-*rac*-glycerol) (sodium salt)

NBD-PE

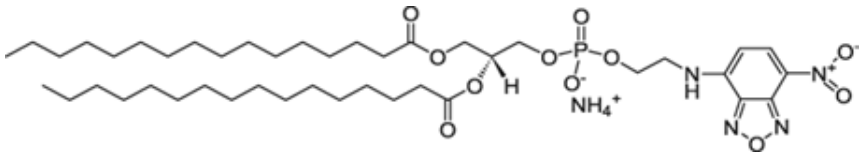

1,2-dipalmitoyl-*sn*-glycero-3-phosphoethanolamine-N-(7-nitro-2-1,3-benzoxadiazol-4-yl) ammonium salt

Figure 3.14 Phospholipids used in this work.

DOPG and DPPG are negatively charged phospholipids and are non-fluorescent. Conversely, NBD-PE is a fluorescent phospholipid due to the presence of the NBD molecule. Importantly, fluorescent lipids must be used at low concentrations to avoid the self-quenching (concentration quenching) of the fluorescent probe. In self-quenching, the fluorophore quenches its own fluorescence owing to the close proximity of identical molecules at high concentration. Various mechanisms underlie self-quenching, including radiationless energy transfer (this occurs particularly in fluorochromes with small Stokes shifts) or formation of molecular aggregates. Self-quenching occurs especially in biomembranes, where the lipid bilayer behaves as a two dimensional fluid with different domains of fluidity where fluorochromes can be concentrated. Accordingly, DOPG vesicles used in this work were tagged with only few percent of NBD-PE (5 mol. %).

One of the most important properties of the lipid bilayer is the relative fluidity and mobility of each individual lipid molecule in the bilayer. The mobility of lipids changes with the temperature. Depending on the phase transition temperature (Tm) the lipid bilayer will be either in a solid (gel) phase (T < Tm) or liquid (fluid) phase (T > Tm). In both phases lipid molecules are constrained to the two dimensional plane of the membrane but in liquid phase the lipid molecules can diffuse much more freely within the plane. Phase transition temperature (Tm) of phospholipids and lipid bilayers depends on: (i) the length of the acyl chain in the lipid, (ii) the degree of saturation of the hydrocarbon chains in lipid, (iii) the ionic strength of the suspension medium, and (iv) the type of the polar head group. Accordingly, at room temperature, DOPG and DPPG will be in fluid and gel phase, respectively.

Importantly, when they are organized in lamellar phase (e.g. vesicules) and whatever the temperature at which they are investigated, phospholipids are subjected to various diffusion/movement: (i) lateral diffusion (D_L), rotational diffusion (D_R), and (iii) translocation also called “flip-flop” that corresponds to the passage of phospholipids from a monolayer to the other one (Figure 3.15) [72].

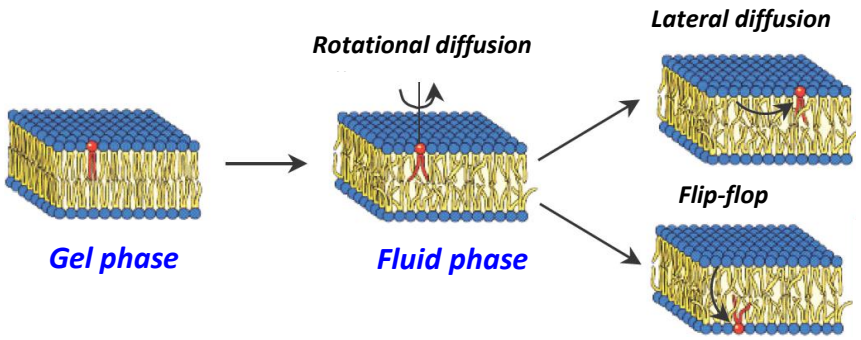

Figure 3.15 Schematic representation of the lipid dynamic inside membranes. Adapted from Ref. [73].

Obviously, diffusion coefficients of each dynamic type are depending on the phase transition temperature (Tm). Accordingly, D_L and D_R which are in the order of 10^{-11} $cm^2.s^{-1}$ et de 10^{-7} $cm^2.s^{-1}$ in gel phase (T < Tm), respectively, are in the order of 10^{-7} $cm^2.s^{-1}$ et de 10^{-9} $cm^2.s^{-1}$ in fluid phase (T > Tm) [72].

Note that lateral and rotational diffusions are rather rapid phenomena with respect to translocation. From the thermodynamic point of view, the latter is an unfavorable phenomenon because the polar head of the phospholipid must cross a hydrophobic zone made of alkyl chains ("tails") of other phospholipids. The time-scale of such a process is of several hours or even days according to the nature of the phospholipid. Interestingly, the "flip-flop" process is faster for phospholipids possessing at least one unsaturated alkyl chain.

3.5. Selective electrochemical bleaching of the outer leaflet of NBD – labeled giant liposomes

3.5.1. Introduction

The mechanisms involved in the internalization of CPPs into cells are still under debate. As already said in the main introduction part of this chapter, this controversy comes from the fact that fluorescence-based techniques (spectroscopy and microscopy), which are the most common exploited approaches to assess the uptake of these peptides, are unable to discriminate between internalized and surface-bound CPPs due to their poor resolutions with respect to the lipid bilayer membrane thickness (4 nm). Within this context, protocols have been developed to reduce signals from surface-bound peptides. The most popular one consists in fluorescence quenching of surface-bound CPPs tagged with 4-nitrobenzo-2-oxa-1,3-diazol-4-yl (NBD), a very common used small neutral fluorescent probe. Under these conditions, fluorescence is generally quenched by dithionite ($S_2O_4^{2-}$), which act as a chemical reducing agent. However, as said above, this physiologically compatible chemical quencher has recently been found to permeate membrane vesicles [7]. This permeation property could therefore severely affect translocation investigations based on the fluorescence monitoring after dithionite quenching.

These considerations prompted us to develop a non-chemical strategy to bleach selectively the fluorescence emitted by NBD located in the outer leaflet of GUV membranes. This original approach was first tested to quench fluorescence emitted by giant unilamellar vesicles (GUVs) tagged with NBD. Both the qualitative and quantitative validations of this approach led us then to test it to quench fluorescence emitted by NBD-labelled peptides localized on the outer leaflet of giant liposomes.

3.5.2. Design and development of the electrochemical cell

First of all, we had to develop an original and specific cell allowing not only the *in situ* preparation and observation of GUVs by fluorescence confocal microscopy, but also the electrochemical reduction of fluorescent probes borne by NBD-PE phospholipids. Based on the work reported by Yamada et al [74], a millimetric-scale well made of poly(dimethyloxane) (PDMS) was bound onto a glass microscope cover slide that was previously coated with a thin layer of ITO (10 nm thickness), a commonly used material in spectro-electrochemistry experiments (Figure 3.16). Details of this fabrication are given in the experimental part.

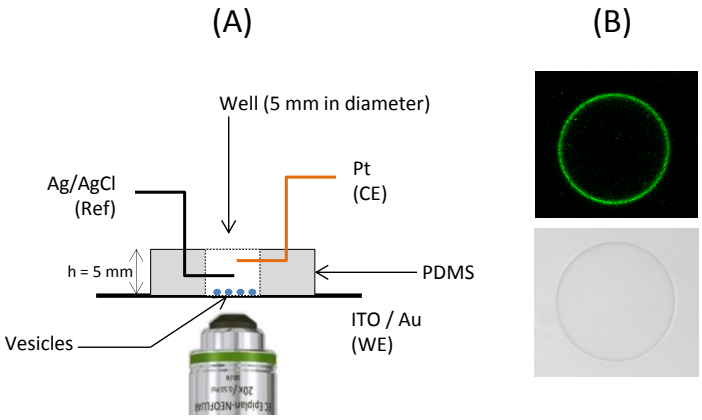

Figure 3.16 A) Scheme of the experimental device allowing preparation as well as visualization of giant vesicles before and during their electrochemical fluorescence extinction. B) Typical confocal fluorescence (top) and transmission (bottom) microscopy images focused at the equatorial plane of a giant unilamellar vesicle (50 µm in diameter) made of DOPG and of NBD-PE on its outer leaflet (5 mol. %) and settled at the bottom of the PDMS well as sketched in A).

Nevertheless, it was observed that electrochemical properties of ITO were modified after prolonged polarizations (500 seconds) at a cathodic potential of -0.9 V/Ag/AgCl corresponding to the value at which the NBD nitro group is reduced (*vide infra*) (Figure 3.17). According to recent reported works [75-77], the cathodic polarization of ITO thin films would indeed lead to morphological, optical, and

conductivity changes of the material due to the reduction of its metallic sites. We found this drawback could be overcome by covering the ITO surface with a thin gold layer (20 nm thickness). Chronoamperograms obtained in the presence of such ITO/Au surfaces remained much more stable than those obtained in the absence of the gold layer (Figure 3.17).

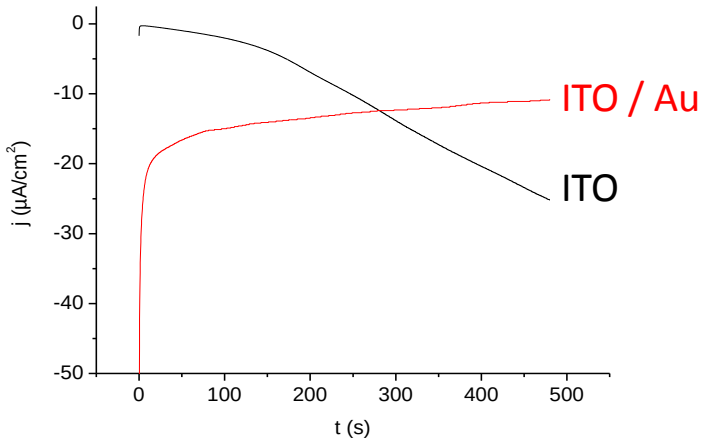

Figure 3.17 Polarization of ITO and ITO / Au electrodes (5 mm in diameter) at E = -0.9 V/Ag/AgCl in PBS for 500 seconds.

Importantly, fluorescence transmission of the NBD probe through the ITO/Au bilayer was only divided by a factor of two compared to that transmitted through a non-modified glass microscope cover slide (Figure 3.18).

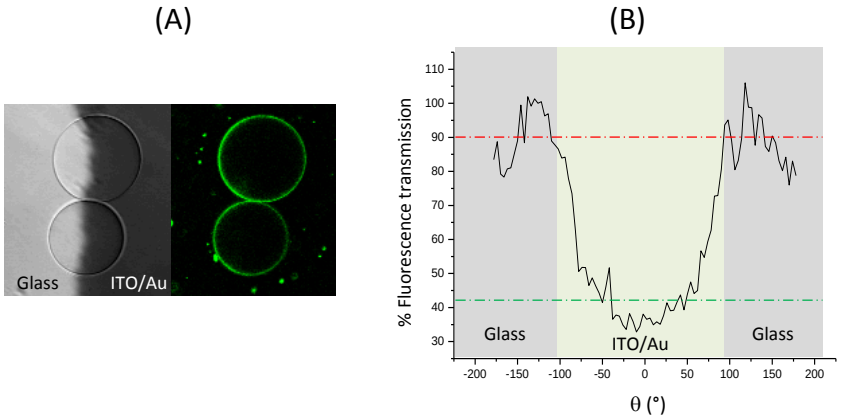

Figure 3.18 Comparison of fluorescence transmission through glass and ITO / Au surfaces. (A) Transmission (left) and confocal fluorescence (right) microscopy images, focused at the equatorial plane, of DOPG vesicles (55 and 48 µm in diameter) containing NBD-PE (3 mol %) and lying on both glass and ITO/Au surfaces. (B) Corresponding fluorescence transmission normalized with respect to glass.

This was still high enough to visualize NBD-tagged GUVs (Figure 3.16-B). As sketched in Figure 3.16-A, a Pt wire and an Ag/AgCl wire (0.5 mm in diameter each) used as the counter and the reference electrodes, respectively, were inserted into the well to complete the electrochemical device. The latter was used to perform a cyclic voltammetry of NBD-glycine derivative, used as model, to determine the reduction potential value of the fluorescent probe under the same conditions as that used to quench fluorescence of NBD-tagged giant vesicles. Accordingly, and in agreement with similar nitro derivatives [48, 78, 79], the first reduction wave of NBD appeared at -0.7 V/Ag/AgCl (Figure 3.19).

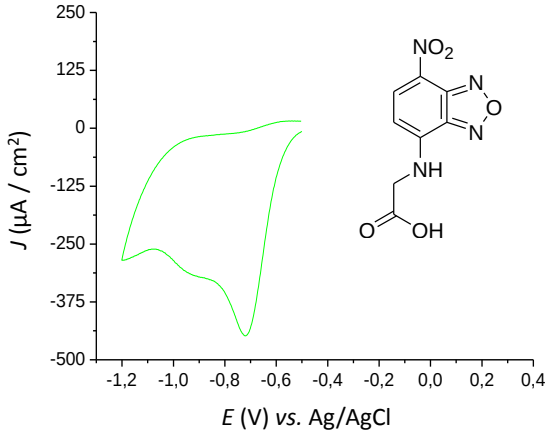

Figure 3.19 Cyclic voltammogram of NBD-Gly (100 µM) performed at an ITO/Au electrode (5 mm in diameter) in PBS solution and at v = 100 mV/s.

3.5.3. Preparation of giant unilamellar vesicles (GUVs)

Our approach devoted to the electrochemical reduction of GUVs tagged with NBD, used as the fluorescent probe, required the preparation of different kind of vesicles. Actually, three families of giant vesicles had to be prepared and tested as a function of the fluorescent probe localization: (a) either on the outer, (b) or on the inner, (c) or both on inner and outer leaflets. Vesicles were made of 1,2-dioleoyl-sn-glycero-3-phosphoglycerol (DOPG) phospholipids, a classical anionic phospholipid used to prepare endosome models, and a small fraction (5 mol. %) of 1,2-dipalmitoyl-sn-glycero-3-phosphoethanolamine-N-(7-nitro-2-1,3-benzoxadiazol-4-yl) (NBD-PE) to avoid self-quenching (Figure 3.20).

DOPG
Tm = -18°C

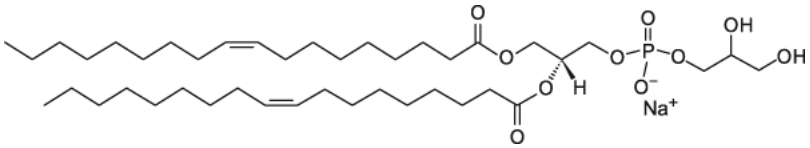

1,2-dioleoyl-*sn*-glycero-3-phospho-(1'-*rac*-glycerol) (sodium salt)

NBD-PE

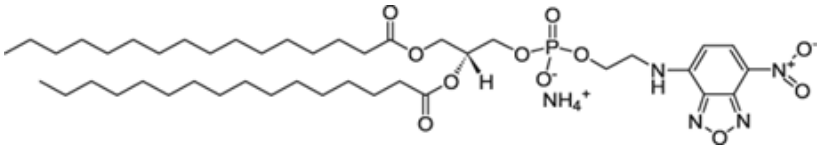

1,2-dipalmitoyl-*sn*-glycero-3-phosphoethanolamine-N-(7-nitro-2-1,3-benzoxadiazol-4-yl) ammonium salt

Figure 3.20 Non-fluorescent and fluorescent phospholipids used for the preparation of fluorescent giant vesicles.

The preparation of unsymmetrical and symmetrical liposomes was based on the work reported by Yamada et al who developed a protocol to generate giant liposomes from an oil/water interface [74]. Giant vesicles were prepared directly in the electrochemical device described in the previous paragraph limiting thus their possible deterioration before electrochemical experiments (Figure 3.13).

3.5.4. Visualization of fluorescent giant unilamellar vesicles (GUVs) by confocal microscopy

Once prepared in the well described in Figure 3.16, giant vesicles were observed by confocal fluorescence microscopy to verify their integrity as well as their contact with the conductive well surface of the well. In Figure 3.21 are shown typical confocal fluorescence microscopic images focused at either the equatorial plane or at the ITO/Au electrode surface of GUVs made of DOPG and of a small fraction (5 mol. %) of NBD-PE fluorescent phospholipids on their outer leaflet. It is shown that vesicles A and B are partially and fully-opened, respectively, at the electrode surface (see the red arrows). Conversely, the vesicle C (right part of Figure 3.21) is closed.

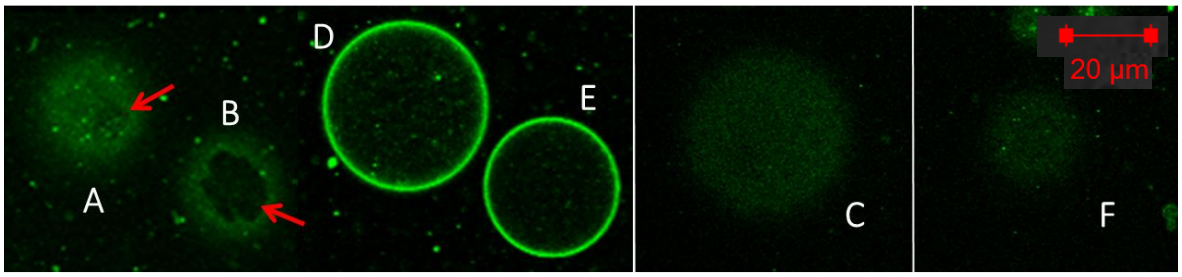

Figure 3.21 Fluorescence confocal images of both inner- and outer-leaflet NBD-tagged GUVs. The focal plane is set either (A, B, C, F) at the interface formed by the ITO/Au electrode and the bottom of the vesicle or (D, E) at the equatorial plane of the GUV. Images A, B and C show a partially opened, completely opened and closed membrane, respectively. Images at the equator plane correspond to vesicles A and B. Image F corresponds to a vesicle not touching the electrode surface.

Actually, we noted that vesicles are rather unstable onto the gold substrate. Only few of them were totally closed. To improve the vesicle stability the gold surface was covered with a biotin monolayer avoiding thus a direct contact between the vesicle and the metallic material [80] (see protocol in section 5.1.7). As already reported, Biotin (a water-soluble B-vitamin) can be easily adsorbed onto gold surfaces via its sulfur atom [80] (Figure 3.22). Importantly, this modification affected neither the fluorescence transmission nor the electrochemical properties of the gold layer.

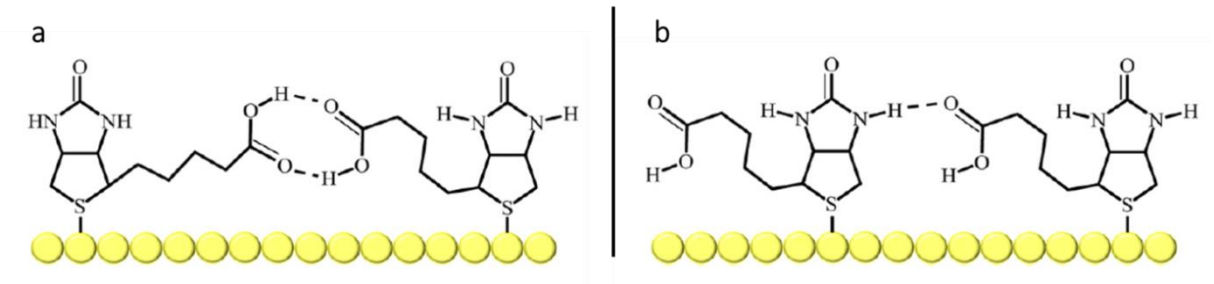

Figure 3.22 Possible molecular arrangements of biotin onto a gold surface. Two molecules can be held together through either (a) double hydrogen bond formed between their carboxylic groups, or (b) single hydrogen bond formed between a carboxylic group on one molecule and the tetrahydroimidizalone ring in another molecule. The representations are a simply description of the chemical nature of the absorbed layer, without any conviction about the orientations of the chains [80].

3.5.5. Qualitative electrochemical fluorescence extinction of outer leaflet NBD-labeled giant vesicles

To qualitatively validate our concept, a first series of experiments was performed in the presence of outer leaflet NBD-labeled vesicles. Usually, after verifying the integrity of the vesicle as well as the contact with the electrode surface (some vesicles did not reach the bottom of the well) a fluorescent confocal image was taken at the equatorial plane of the GUV. The working electrode was then polarized at a constant cathodic potential value of -0.9V/Ag/AgCl (i.e. 200 mV more negative than the reduction peak of the NBD nitro group). The potential pulse was stopped after 30 seconds and a new confocal fluorescence microscopy image of the equatorial plane of the vesicle was taken. This sequence was repeated about 20 times on the same vesicle to follow fluorescence variations at the vesicle equatorial plane as a function of the polarization time. At this stage it is important to note that the charge passed during 30 seconds was around 1 mC. This value resulted far higher than that expected for reducing the small fraction of NBD fluorescent probes present in the investigated vesicle, but one has to consider that i) NBD reduction may not be the only electrochemical reaction (hydrogen evolution may also occur at -0.9 V) and ii) the electrolysis proceeds at the whole ITO surface, hence many GUVs, while microscopy only focuses on a specific region.

In Figure 3.23 is shown a typical series of confocal fluorescence microscopy images obtained as a function of the reduction time and focused at the equatorial plane of a giant unilamellar vesicle containing DOPG phospholipids and a small fraction (5 %) of fluorescent phospholipids (NBD-PE) on the outer leaflet.

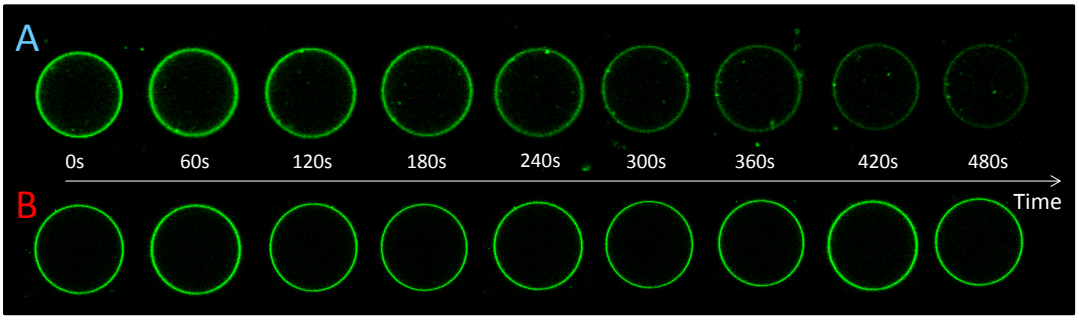

Figure 3.23 Typical series of confocal fluorescence microscopy images focused at the equatorial plane of a giant unilamellar vesicle (50 µm in diameter) containing DOPG phospholipids and a small fraction of fluorescent phospholipids (NBD-PE; 5 mol. %) on the outer leaflet obtained in (A) the presence and (B) the absence of cathodic polarization (-0.9 V/Ag/AgCl) of the ITO/Au surface. For simplification, only pictures that have been taken every minute (until 8 minutes) are shown in (A) and (B).

Clearly, the fluorescence intensity decreased with the number of potential pulses, or in other words with the reduction time. Importantly, the fluorescence extinction was not due to a possible photo-bleaching process in agreement with the fact that constant fluorescence intensities were obtained without applying a cathodic potential value (compare A and B in Figure 3.23). Furthermore, this demonstrates also that fluorescence extinction was not due to a possible electrogenerated reducing species and/or pH variation in the well. In agreement with this statement, it was impossible to quench a vesicle which was not in contact with the electrode surface, a parameter which is easily verified through z stacking in confocal microscopy. Note also that in case water reduces concomitantly with NBD to yield H_2 and OH^-, the pH evolution possibly triggered through the production of hydroxyl anion would be compensated by the generation of proton at the anode through water oxidation since the auxiliary and working electrodes are not separated in the well.

Under these conditions, the global fluorescence decrease observed at the GUV equatorial plane can be ascribed to the electrochemical reduction of the NBD probe at the electrode surface. By analogy with FRAP and FLIP techniques, this process can be related to an electrochemical bleaching where the laser beam is replaced by an electrode. Similarly, this electrochemical bleaching created a concentration gradient triggering a diffusion of fluorescent phospholipids towards the fluorophore-depleted region of the GUV, i.e. the one in contact with the electrode. Moreover, when the polarization of the electrode was performed continuously as in FLIP experiments the fluorescence intensity decay overlapped the one obtained for successive polarizations. Taking into account (i) the electrobleached area size and (ii) the size of the GUV (two crucial parameters – vide infra), this indicates that the fluorescence observed at the equatorial plane does not undergo strong variation during the time elapsed to record one picture. Besides, this time (several seconds) is much shorter than the characteristic electrobleaching time (roughly 100 seconds, see hereinafter).

3.5.6. Quantitative electrochemical fluorescence extinction of NBD-labeled giant vesicles

The fluorescence extinction was then quantitatively investigated as a function of the NBD fluorescent probe localization: (a) either mainly on the outer, (b) or mainly in the inner, (c) or on both inner/outer leaflets. Fluorescence variations at the equatorial plane of GUVs were quantified and corrected from background signals and photo-bleaching (see details in section 5.1.10) as a function of the number of potential pulses and the total time elapsed for the electrochemical reduction. Results are summarized in Figure 3.24, where F^0 and F are the corrected fluorescence intensities at time 0 and at time t, respectively.

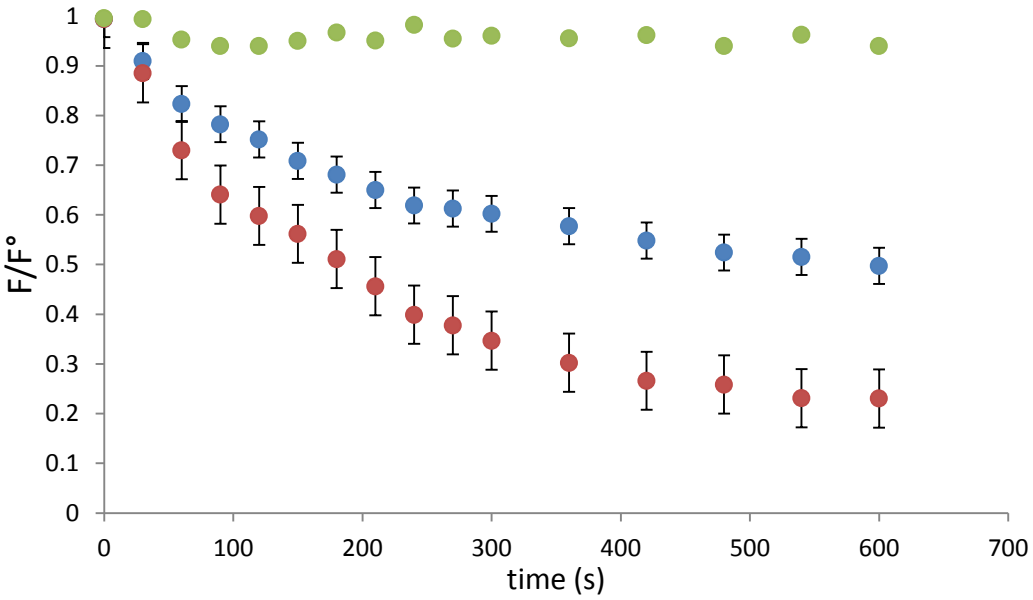

Figure 3.24 Fluorescence variations as a function of polarization time (*E* = -0.9 V/Ag/AgCl) obtained at a biotinylated electrode surface for 5 inner (●), 13 inner/outer (●, 50/50), and 5 outer (●) leaflet NBD-labelled DOPG giant vesicles. The studied vesicles had an equatorial diameter between 42 to 120 µm.

Three different behaviors were obtained depending on the fluorescent probe localization. First, almost no fluorescence extinction was obtained in the presence of inner-leaflet NBD-labeled vesicles demonstrating that electrochemical reduction of fluorescent probes that are inside the vesicle cannot be achieved. As already verified, the slight fluorescence loss (around 10 %) was not due to a possible photobleaching process. Actually, some fluorescent phospholipids may have been trapped on the outer leaflet of the vesicle during their preparation and then be reduced. Conversely, a significant fluorescence intensity decrease was observed in the presence of outer-leaflet NBD-labeled vesicles. On average, almost 80 % of the fluorescence was indeed quenched after 600 seconds of electrochemical reduction/bleaching. This means that, on average 20 % of the tagged phospholipids were inserted in the inner leaflet which is consistent with reported values [68].

Contrary to the two previous series of experiments, where some discrepancies were noted due to non-specific staining of single leaflets, fluorescence extinction of vesicles with both inner- and outer-leaflet NBD-labeled led to a an average fluorescence extinction of 50 %. Similarly to the two previous types of experiments some dissymmetry in the NBD-PE repartition between the two leaflets happened. Nevertheless, they compensate. Indeed, the normalized fluorescence intensity at time 600 s lay in the range 0.32-0.69 with a mean value of 0.5 ±0.12 (std). Importantly, these results confirmed

that electrochemical bleaching of fluorescent phospholipids concerns only those which are localized on the outer-leaflet of vesicles allowing thus discrimination between both sides of lipid bilayers.

3.5.7. Comparison with FLIP experiment

The strong analogy existing between our electrochemical bleaching assay and the FLIP technique led us to compare both approaches. In FLIP experiments, focus was made on the top of the vesicle (radius a), where it appears as a uniform disk. The region to be bleached was defined (disk with radius a_{bleach}), and focus was then made at the equatorial plane of the GUV allowing subsequent fluorescence loss monitoring during bleaching. The bleaching was performed with sequences of 20 laser pulses (3 s, total duration). The vesicle equator was imaged between successive sequences of laser pulses. A typical fluorescence decay obtained under these conditions is shown in Figure 3.25. Fluorescence loss at the equator was well fitted with the numerical solution of the diffusion equation solved on the surface of oblate spheroidal vesicles. We checked that similar behavior was observed with a bleached region located at the bottom of the vesicle, on the electrode surface.

Initial conditions were F/F0(0,θ) =1, where θ is the latitude angle. Imposed boundary conditions were F/F0(t,θ_0) = 0, with θ_0 the latitude of the bleached region edge, and zero flux d\dθ[F/F0(t,π/2]=0. This fitting procedure yielded a diffusion coefficient value of D = 4 $\mu m^2/s$, consistent with reported valued obtained with other methods like fluorescence correlation spectroscopy [81], or FRAP [82] for phospholipid similar to DOPG.

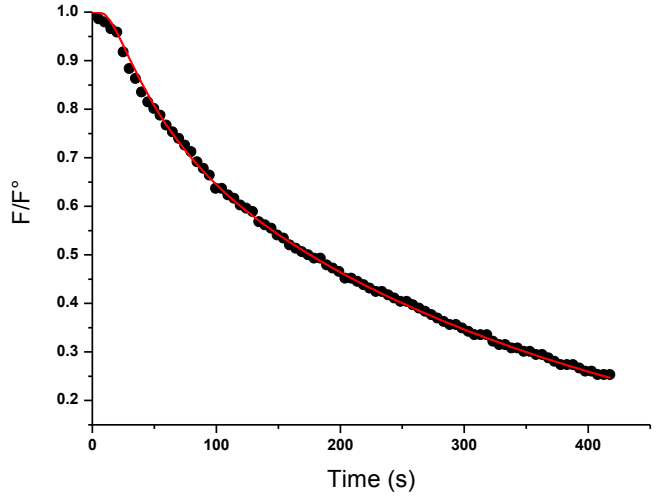

Figure 3.25 Fluorescence intensity decay obtained during a FLIP experiment of a both outer/inner leaflet NBD-labeled giant vesicle (65 µm in diameter – a_{bleach}/a = 1.5 – black points - with error bars corresponding to point size) and corresponding modelization (red solid line).

The data corresponding to the bleaching of fluorescence by electrochemical reduction could not be fitted using the same procedure due to dissymmetry in phospholipids partitioning between the two leaflets. In order to compare the electrochemical bleaching assay and FLIP kinetics, we performed a FLIP assay on a vesicle with a_{bleach}/a=1.5 ratio close to the mean a_{bleach}/a= 1.4 ±.1 (std) ratio of the five outer labeled GUV investigated through FLIE and presented in Figure 3.26.

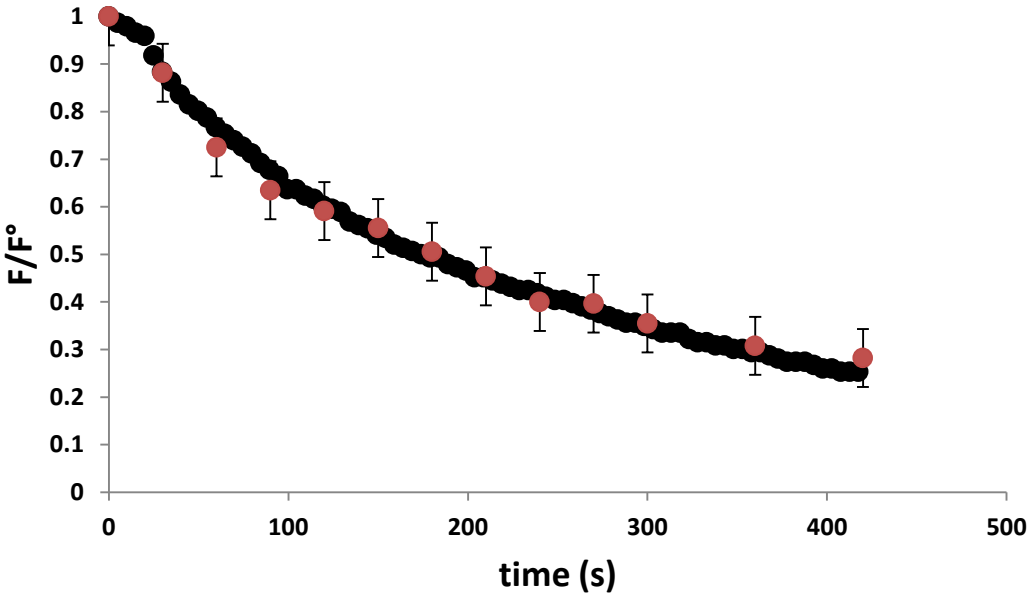

Figure 3.26 Comparison between the fluorescence intensity decay obtained through a FLIP assay with an outer/inner leaflet NBD-labeled giant vesicle (a_{bleach}/a = 1.5 – blue points) and the fluorescence intensity decay resulting from electrochemical reduction (continuous applied voltage) of five outer-leaflet NBD-labeled giant vesicles (a_{bleach}/a=1.4 ± 0.1 (std) – red point).

Interestingly, our results show that FLIP and electrochemical bleaching performed on vesicles can be used as a quantitative method of diffusion coefficient measurement. Nevertheless, the preparation step of vesicles should be improved, decreasing the dissymmetry in partitioning. A way to do so is proposed in ref [68], relying on the use of a second oil during preparation of the GUVs. It is also worth noting that FLIP and the electrochemical assay described here allow measuring the diffusion coefficient without requiring fast acquisition like FRAP or single tracking methods.

3.5.8. Conclusion

Electrochemistry is a powerful tool to bleach the fluorescence emitted by fluorophores possessing redox properties and localized on the outer leaflet of lipid bilayer. Compared to typical photobleaching techniques such as FRAP and FLIP, the electrochemical process does not affect the fluorescent probes localized inside vesicles allowing thus discrimination between the outer and the inner membrane leaflet. The use of an electrochemical process also discards the use of chemical reducing agents that may undergo slow internalization within vesicles. Furthermore, combination of electrochemistry and confocal fluorescence microscopy was found useful for monitoring and quantifying the fluorescence loss in real time. This procedure appears versatile and perfectly adequate to investigate and quantify the transport of active molecules at the membrane level offering thus relevant insights on such important biological and pharmacological issues.

3.6. Selective electrochemical quenching of fluorescence emitted by NBD-labelled peptides localized on the outer leaflet of giant liposomes

3.6.1. Back to Cell-penetrating peptides

In this section, the electrochemical-bleaching assay is tested to bleach the fluorescence emission coming from NBD-labeled peptides. To carry out this strategy, non-labeled vesicles made of DPPG are incubated with NBD-R6/W3 at micromolar concentrations. The electrochemical assay is performed in GUVs in both fluid and gel phase. The obtained results demonstrate that the electrochemical bleaching could be applied in the future in CPP translocation studies.

3.6.2. Chemical quenching of fluorescence emitted by NBD-labeled peptides localized on the outer leaflet of large unilamellar vesicles (LUV)

Before going further, it is important to remind here how are typically evaluated the internalization of cell-penetrating peptides into large unilamellar vesicles (LUV). As already reported, the internalization of peptides into LUVs is generally quantified *via* the quenching of NBD that is covalently attached on the *N*-terminus of peptides. Treatment of the incubation medium (LUVs and NBD-labeled peptides are mixed for 5 minutes) with dithionite rapidly reduces the NBD probe, and consequently quenches its fluorescence. The residual fluorescence after dithionite treatment therefore corresponds to the intravesicular CPP, which is supposed to be protected from the reducing agent (Figure 3.27).

Importantly, the concentrations ratio [peptide] / [lipid] is generally equal to 1/100 for two main reasons: (i) to avoid a possible damage of the plasma or the artificial membrane which would facilitate the peptide internalization [1], and (ii) to avoid a self-quenching of fluorescence due to peptide accumulation around the membrane [39]. This protocol can be used with a large variety of both peptides and lipids [6].

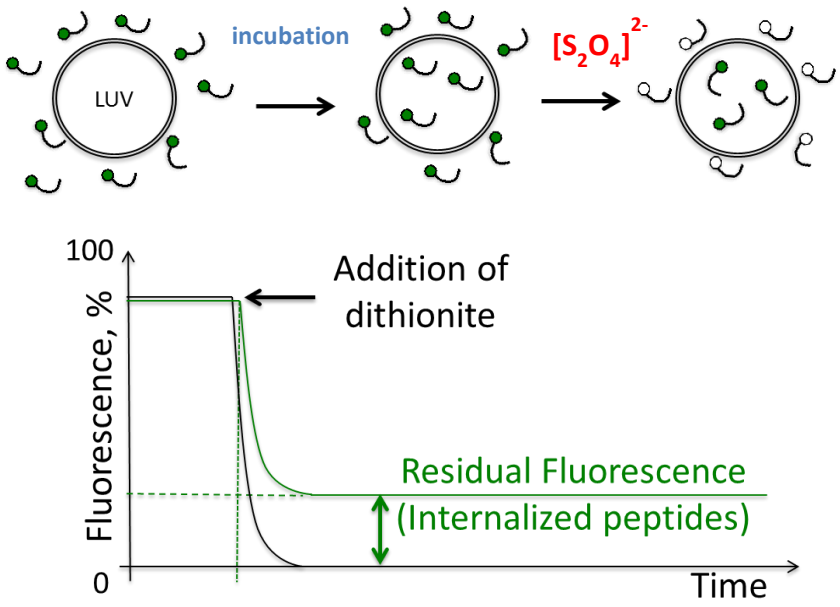

Figure 3.27 Schematic representation of the assay set-up for measuring the internalization of NBD-labeled peptides inside LUVs (100 nm in diameter). Typically, LUVs (10 µM in phospholipids) are incubated for 5 minutes with the NBD-labeled peptide (100 nM). Then, dithionite (final concentration 10 mM) is added to reduce the external NBD-labeled peptides, and the fluorescence quenching is recorded for 25 min. The residual fluorescence corresponds to the NBD-labeled peptides that have been internalized into the LUVs. Figure adapted from reference [6] .

3.6.3. Towards the electrochemical quenching of fluorescence emitted by NBD-labeled peptides in the presence of giant vesicles

Based on the protocol described above, our electrochemical approach (which replaces the chemical reduction by dithionite) was then attempted in the presence of both NBD-labeled peptides and unlabeled GUVs. The first step was the selection of both the phospholipid and the peptide.

3.6.3.1. Phospholipid selection

According to the literature, the anionic lipid 1,2-dipalmitoyl-*sn*-glycero-3-phospho-(1'-*rac*-glycerol) (DPPG) is a typical phospholipid employed to investigate CPP translocation and notably to understand the role of electrostatic interactions between peptides and lipids. DPPG belongs to the family of phosphatidylglycerols (PGs), a class of lipids found in mammalian membranes in low amounts (1 to 2 % of total phospholipids). Though PGs are minor components of animal membranes, they are the main constituent of some bacterial membranes [81]; therefore, they are a good model for CPPs and antimicrobial peptides (AMP) investigations. The charge on the phosphate group means that this lipid is anionic at neutral pH. The DPPG lipid possesses two C_{16} saturated alkyl chains lipids (Figure 3.28).

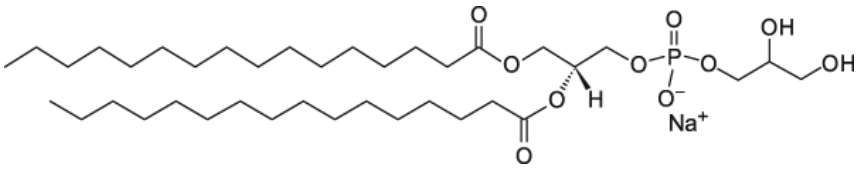

Figure 3.28 Molecular structure of the 1,2-dipalmitoyl-*sn*-glycero-3-phospho-(1'-*rac*-glycerol) (DPPG) phospholipid. Phase transition temperature: 41 °C.

Interestingly, the phase transition temperature of DPPG is equal to 41°C. Compared to DOPG which was always used in fluid phase at room temperature (T_m = - 18°C), DPPG vesicles can be therefore advantageously used either in fluid phase or in gel phase. More interestingly, incubation of peptides and vesicles can be performed in fluid phase (to favor internalization) then analyzed in gel phase (to trap the internalized peptides).

3.6.3.2. Peptide selection

Various CPPs have been investigated in the presence of LUVs made of DPPG in a PBS buffer [6]. However, preparation of giant vesicles in our home-made electrochemical device requires that GUVs must be loaded with a high sucrose concentration (700 mM) for density reasons. Nevertheless, such a high sucrose concentration may affect the internalization of CPPs. In this context, we first investigated the internalization of various peptides into LUVs made of DPPG loaded with sucrose (details are given in the experimental section). Accordingly, the protocol described in paragraph 3.6.2, which is based on a chemical reduction of the NBD probe by dithionite, was achieved. Results are summarized in Table 3.1.

Table 3.1 Internalization of various peptides in LUVs made of DPPG and loaded with a sucrose solution (700 mM in PBS buffer). a) The NBD probe was incorporated at the *N*-terminus of the peptide, leading to the corresponding fluorescent peptides. b) Values obtained from [6].The extent of internalization was determined after a time of incubation LUVs/NBD-CPP of 10 minutes.

Peptides [a]	Referred in text as	% internalization in the presence of sucrose	% internalization in the absence of sucrose [b]
RRRRRRRRR-NH_2	R9	23	4.0 ± 0.2
RRWWRRWRR-NH_2	R6/W3	47	39 ± 3
YGRKKRRQRRR-NH_2	Tat	15	6.5 ± 1.5

As shown in Table 3.1, the presence of sucrose inside vesicles does not prevent CPP internalization. However, the percentage of internalized peptide seems to be dependent on the presence of sucrose. Though our results were obtained from only one experiment for each investigated peptide, we decided to test the electrochemical quenching approach in the presence of the NBD-labeled R6/W3 peptide owing to its high internalization percentage whatever the experimental conditions.

The R6/W3 peptide is an amphipathic peptide in which R and W represent the arginine and tryptophan amino acids, respectively (Figure 3.29). This peptide bears a net charge of +6 due to the arginine residues present in its structure. This peptide is considered as a very efficient CPP due to its both cationic and hydrophobic nature [6].

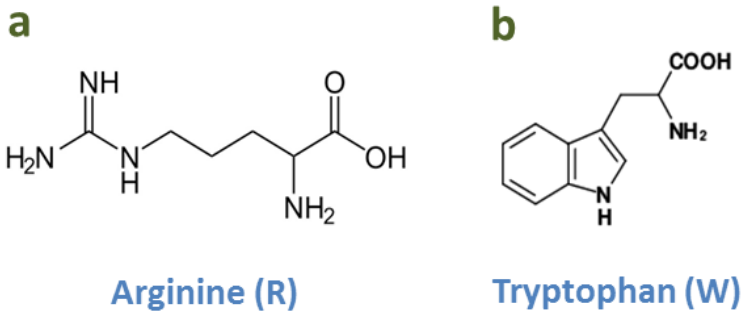

Figure 3.29 Molecular structures of the amino acids arginine (R) and tryptophan (W).

3.6.3.3. Preparation of giant unilamellar vesicles made of DPPG

After selection of both the phospholipid and the peptide, the next step was the preparation of giant unilamellar vesicles made of DPPG as the phospholipid. Symmetrical DPPG vesicles were prepared *via* the same protocol as that used for the generation of unsymmetrical fluorescent DOPG vesicles, i.e., through an oil/water interface. Importantly, the preparation of DPPG vesicles was performed at 45 °C (T_m = 41 °C) in order to obtain a fluid phase. Interestingly, DPPG vesicles were found to be stable on the gold working electrode (no membrane disruption was observed by phase-contrast microscopy). Compared to DOPG vesicles, the electrode was therefore not pre-treated with biotin in the present case.

3.6.3.4. Optimization of the R6/W3 peptide concentration

Typically, the internalization of CPPs into LUVs are investigated for peptide/phospholipid ratios of 1/100 ([CPP] = 100 nM and [phospholipid] = 10 µM) to avoid fluorescence self-quenching and membrane damage. This ratio is easily controlled when working with LUV due to the mode of preparation which produces vesicle populations that are homogeneous in size. However, this homogeneity cannot be obtained with GUVs notably when they are prepared *via* the double emulsion process. Moreover, it is not possible to control the repartition of NBD-labeled peptides around vesicles during the incubation period. Based on this, it was decided to start our investigations with concentrated NBD-labeled peptide solutions (2.5 µM).

On the other hand, several important points must be taken into account when working at high CPP concentrations: (i) care must be taken to keep isotonic conditions in our experimental device (Figure 3.16) especially when NBD-labeled peptides are added in the well containing giant vesicles, (ii) due to the non-homogeneous repartition of CPP on GUVs that are present in the well, it is important to check not only the membrane integrity before running the electrochemical experiment, but also the fluorescence stability.

Accordingly, a first experiment consisted in the confocal fluorescence microscopy observation of GUVs made of DPPG in the presence of NBD-R6/W3 (final concentration in the well: 2.5 µM) added at room temperature (gel phase) (Figure 3.30).

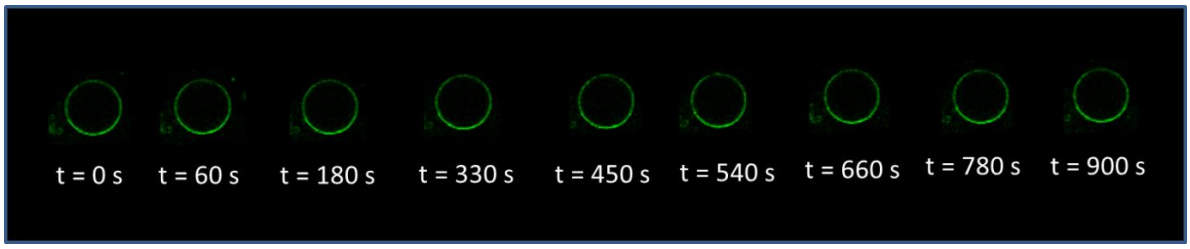

Figure 3.30 Typical series of confocal fluorescence microscopy images focused at the equatorial plane of a giant unilamellar vesicle (35 µm in diameter) containing DPPG phospholipids and incubated for 5 minutes in the presence of NBD-R6/W3 (final concentration in the well: 2.5 µM).

As shown in Figure 3.30, the observed DPPG vesicle remained stable after addition of NBD-R6/W3 at a concentration of 2.5 µM (both the shape and the size of the GUV remained constant). On the other hand, and as shown in Figure 3.31, no photo-bleaching was evidenced.

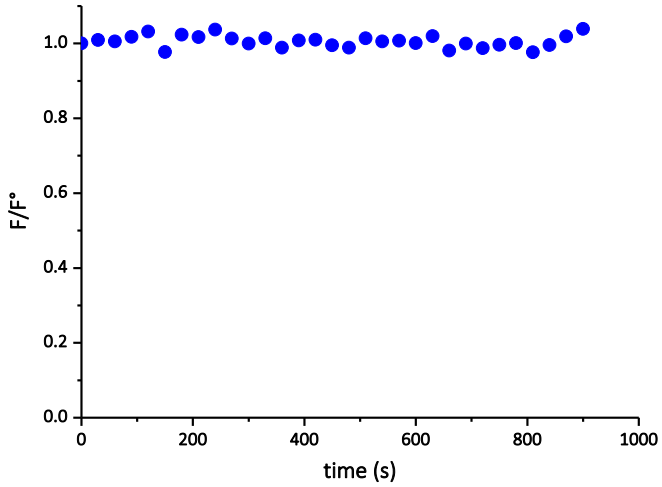

Figure 3.31 Normalized fluorescence intensity (F° corresponds to fluorescence at time 0) as a function of time, measured from the series of confocal fluorescence microscopy images shown in Figure 3.30.

3.6.3.5. Electrochemical quenching of fluorescence emitted by NBD-labeled peptides in the presence of giant vesicles

According to the results reported in the previous paragraph, the electrochemical quenching of fluorescence emitted by NBD-R6/W3 peptides in the presence of giant vesicles made of DPPG was finally performed and visualized by confocal microscopy fluorescence. This was done in gel-phase at two peptide concentrations (2.5 and 0.63 µM) and in fluid-phase at 2.5 µM.

• In gel-phase

In this case, vesicles were first incubated with NBD-R6/W3 (final concentration in the well: 2.5 µM) at 22 °C for five minutes. After incubation, it was observed that most of the vesicles became fluorescent owing to the strong affinity of the cationic peptides for the negatively charged DPPG phospholipids. After verifying the membrane integrity of the selected vesicle as well as its contact with the electrode surface a fluorescent confocal image was taken at the equatorial plane of the GUV. The gold surface of the well was then continuously polarized at a constant cathodic potential value of -0.9V/Ag/AgCl i.e., 200 mV more negative than the reduction peak of the NBD nitro group. A fluorescent confocal image was taken every 30 seconds at the equatorial plane of the GUV to follow fluorescence variations as a function of the polarization time.

In Figure 3.26 is shown typical fluorescence variations obtained for two different vesicles where F^0 and F are the corrected fluorescence intensities at time 0 and at time t, respectively. As already shown in the presence of NBD-labeled vesicles, the fluorescence intensity decrease demonstrates the electrochemical quenching of NBD-labeled peptides being on the outer leaflet of vesicles.

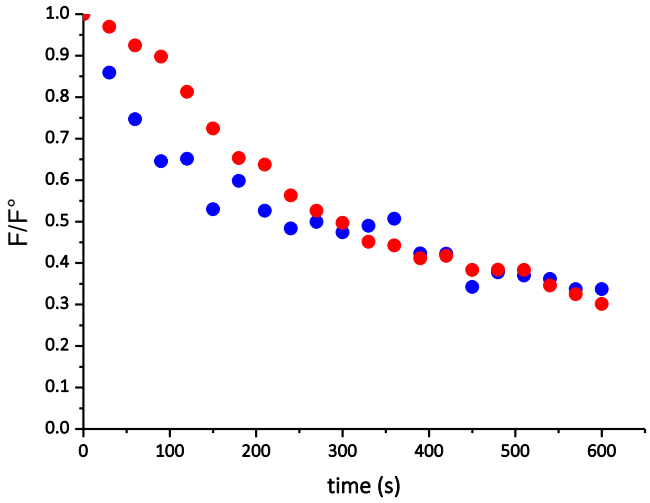

Figure 3.26 Typical fluorescence variations of two different DPPG vesicles with surface-bound NBD-labelled peptides during polarization of the gold electrode at E = -0.9 V vs Ag/AgCl. Experiments realized at 22 °C (gel-phase). GUVs and peptides (final concentration in the well: 2.5 µM) were incubated together in the electrochemical cell for 5 minutes before polarization. Blue and red dots correspond to two vesicles having equatorial diameters of 12 µm and 40 µm, respectively.

Interestingly, until about 200 seconds, the fluorescence decrease was faster for the smaller vesicle (compare the blue and red dots in Figure 3.26). Also, in both case, about 70 % of the initial fluorescence was electrochemically quenched in 600 seconds indicating that such experiments may be also conducted in gel-phase.

Note that it was difficult to extend the electrochemical experiment above 600 seconds for two main reasons: (i) most of vesicles became unstable beyond this period (most of them collapsed), and (ii) treatment/measurements of fluorescence intensities using the software ImageJ became difficult to accomplish (see e.g. in Figure 3.27 the fluorescence intensity obtained at 600 seconds). At this stage, it is therefore impossible to tell that the 30 % remaining fluorescence was due to internalized peptides.

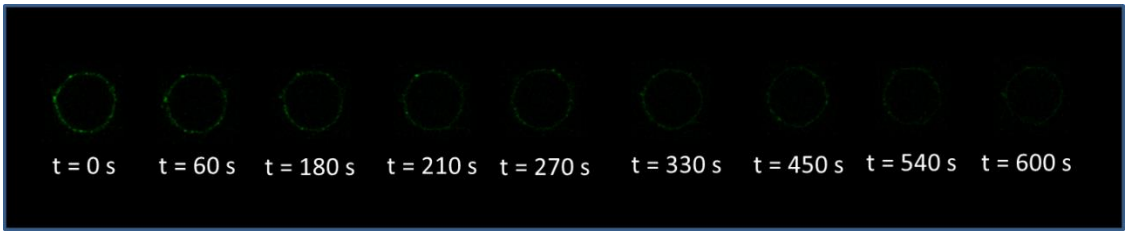

Figure 3.27 Typical series of confocal fluorescence microscopy images focused at the equatorial plane of a DPPG giant unilamellar vesicle (12 µm in diameter) that was incubated with NBD-R6/W3 peptides (final concentration in the cell: 2.5 µM) for 5 minutes. Experiment performed at 22 °C (gel-phase).

The instability of GUV observed above 600 seconds could be due to a too strong accumulation of peptides around the vesicle. To test this hypothesis, another experiment was still performed at 22°C, but the incubation was performed with a diluted peptide solution (0.63 µM instead of 2.5 µM).

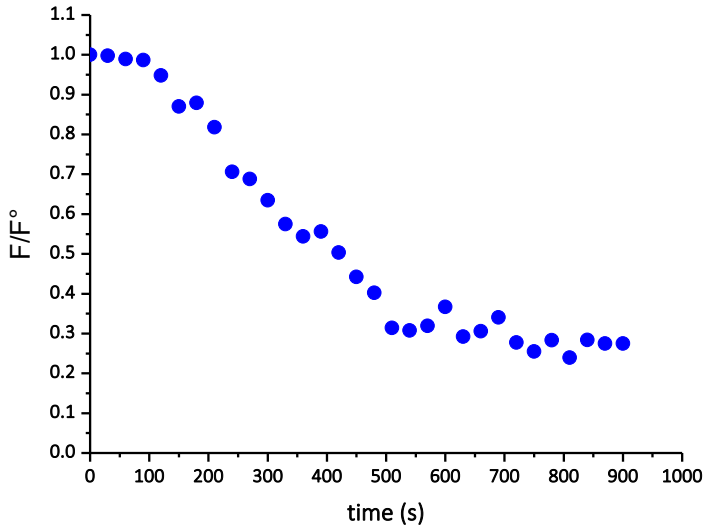

Figure 3.28 Fluorescence variations of a DPPG vesicle (12 µm in diameter) with surface-bound NBD-labelled peptides during polarization of the gold electrode at E = -0.9 V vs Ag/AgCl. Experiment performed at 22 °C (gel-phase). GUVs and peptides (final concentration in the well: 0.63 µM) were incubated together in the electrochemical cell for 5 minutes before polarization.

As shown in Figure 3.28, and as expected, longer experiments could be run when the peptide concentration was decreased. Nevertheless, here again, a maximum of around 70 % of the initial fluorescence was quenched, suggesting strongly that 30 % of the NBD-labeled peptide was really internalized in the vesicle.

• <u>In fluid-phase</u>

DPPG phospholipids are interesting because their phase transition temperature is 41 °C. This gives the possibility to work not only in gel-phase, but also in fluid phase. Accordingly, the above-described experiments performed at 22 °C were then repeated at 45 °C in the presence of a peptide concentration of 2.5 µM (Figure 3.29). At 45°C it was indeed not possible to work at a peptide concentration of 0.63 µM due to quite weak fluorescence intensity under these conditions.

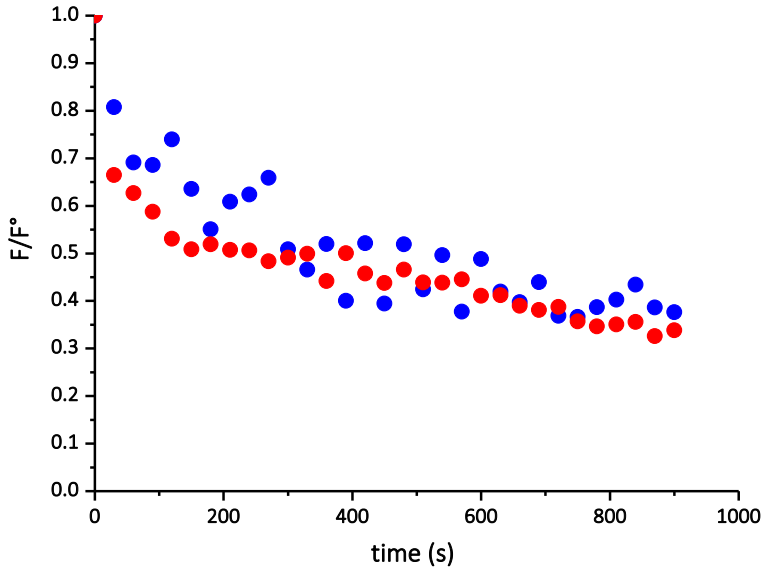

Figure 3.29 Typical fluorescence variations of two different DPPG vesicles with surface-bound NBD-labelled peptides during polarization of the gold electrode at E = -0.9 V vs Ag/AgCl. Experiments realized at 45 °C (fluid-phase). GUVs and peptides were incubated together in the electrochemical cell for 5 minutes before polarization. Blue and red dots correspond to two vesicles having equatorial diameters of 12 µm and 80 µm, respectively.

Here again, the fluorescence intensity decrease demonstrates the electrochemical quenching of NBD-labeled peptides. However, and in agreement with a faster diffusion coefficient of phospholipids in fluid phase, the fluorescence intensity decay was faster at 45°C than at 22°C at least during the first

100 seconds (compare figures 3.29 and 3.26). Nevertheless, whatever the temperature, 70 % of the initial fluorescence was quenched from 600 seconds. This may indicate that 30% of the peptide was internalized in the GUV.

3.6.3.6. Conclusion

Combination of confocal fluorescence microscopy and chronoamperometry appeared successful to monitor, in real time, the selective fluorescence extinction of either outer leaflet NBD-labeled giant liposomes (GUV) or NBD-labeled CPP localized on the outer leaflet of GUVs. Compared to typical photo-bleaching techniques such as FRAP and FLIP, the electrochemical process does not affect the fluorescent probes localized inside vesicles allowing thus discrimination between the outer and the inner membrane leaflet. The use of an electrochemical process also discards the use of chemical reducing agents that may undergo slow internalization within vesicles. This original procedure appears versatile and perfectly adequate to monitor the internalization of active molecules (not only of CPPs but also of any biomolecules) at the membrane level offering thus relevant insight on such important biological and pharmacological issue.

References

1. Bechara, C. and S. Sagan, *Cell-penetrating peptides: 20 years later, where do we stand?* FEBS letters, 2013. **587**, 1693-1702.
2. Swiecicki, J.M., M. Di Pisa, F. Lippi, S. Chwetzoff, C. Mansuy, G. Trugnan, G. Chassaing, S. Lavielle, and F. Burlina, *Unsaturated acyl chains dramatically enhanced cellular uptake by direct translocation of a minimalist oligo-arginine lipopeptide.* Chemical Communications, 2015. **51**, 14656-14659.
3. Swiecicki, J.-M., A. Bartsch, J. Tailhades, M. Di Pisa, B. Heller, G. Chassaing, C. Mansuy, F. Burlina, and S. Lavielle, *The Efficacies of Cell-Penetrating Peptides in Accumulating in Large Unilamellar Vesicles Depend on their Ability To Form Inverted Micelles.* ChemBioChem, 2014. **15**, 884-891.
4. Di Pisa, M., G. Chassaing, and J.-M. Swiecicki, *Translocation Mechanism(s) of Cell-Penetrating Peptides: Biophysical Studies Using Artificial Membrane Bilayers.* Biochemistry, 2015. **54**, 194-207.

5. Di Pisa, M., G. Chassaing, and J.-M. Swiecicki, *When cationic cell-penetrating peptides meet hydrocarbons to enhance in-cell cargo delivery.* Journal of Peptide Science, 2015. **21**, 356-369.
6. Swiecicki, J.-M., M. Di Pisa, F. Burlina, P. Lécorché, C. Mansuy, G. Chassaing, and S. Lavielle, *Accumulation of cell-penetrating peptides in large unilamellar vesicles: A straightforward screening assay for investigating the internalization mechanism.* Peptide Science, 2015. **104**, 533-543.
7. Moreno, M.J., L.M.B.B. Estronca, and W.L.C. Vaz, *Translocation of Phospholipids and Dithionite Permeability in Liquid-Ordered and Liquid-Disordered Membranes.* Biophysical journal, 2006. **91**, 873-881.
8. Madani, F., S. Lindberg, U. Langel, S. Futaki, Gräslund, A., *Mechanisms of Cellular Uptake of Cell-Penetrating Peptides.* Journal of Biophysics. 2011, **2011**, 1-10.
9. Mi, S., J. Wu, J. Liu, Z. Xu, X. Wu, G. Luo, J. Zheng, and C. Xu, *AIEE-Active and Electrochromic Bifunctional Polymer and a Device Composed thereof Synchronously Achieve Electrochemical Fluorescence Switching and Electrochromic Switching.* ACS Applied Materials & Interfaces, 2015. **7**, 27511-27517.
10. Seo, S., C. Park, X. Yang, J. You, Y. Kim, and E. Kim. *Reversible multi-color electrofluorescence switching*. SPIE Proceedings, 2012, 8258
11. Kuo, C.P., Y.S. Lin, and M.K. Leung, *Electrochemical fluorescence switching properties of conjugated polymers composed of triphenylamine, fluorene, and cyclic urea moieties.* Journal of Polymer Science Part A: Polymer Chemistry, 2012. **50**, 5068-5078.
12. Shin, I.-S., T. Hirsch, B. Ehrl, D.-H. Jang, O.S. Wolfbeis, and J.-I. Hong, *Efficient Fluorescence "Turn-On" Sensing of Dissolved Oxygen by Electrochemical Switching.* Analytical Chemistry, 2012. **84**, 9163-9168.
13. Lakowicz, J.R., *Principles of fluorescence spectroscopy.* Springer, 2010. Third edition.
14. Ishikawa-Ankerhold, H.C., R. Ankerhold, and G.P.C. Drummen, *Advanced Fluorescence Microscopy Techniques—FRAP, FLIP, FLAP, FRET and FLIM.* Molecules, 2012. **17**, 4047.
15. Sauer, M., J. Hofkens, and J. Enderlein, *Basic Principles of Fluorescence Spectroscopy*, in *Handbook of Fluorescence Spectroscopy and Imaging*. 2011, Wiley-VCH Verlag GmbH & Co. KGaA. p. 1-30.
16. Valeur, B., *Introduction*, in *Molecular Fluorescence.* 2001, Wiley-VCH Verlag GmbH. p. 3-19.
17. Chattopadhyay, A., S. Mukherjee, and H. Raghuraman, *Reverse Micellar Organization and Dynamics: A Wavelength-Selective Fluorescence Approach.* The Journal of Physical Chemistry B, 2002. **106**, 13002-13009.

18. Chattopadhyay, A. and E. London, *Spectroscopic and ionization properties of N-(7-nitrobenz-2-oxa-1,3-diazol-4-yl)-labeledlipidsinmodelmembranes.* Biochimica et Biophysica Acta (BBA) - Biomembranes, 1988. **938**, 24-34.
19. Fery-Forgues, S., J.-P. Fayet, and A. Lopez, *Drastic changes in the fluorescence properties of NBD probes with the polarity of the medium: involvement of a TICT state?* Journal of Photochemistry and Photobiology A: Chemistry, 1993. **70**, 229-243.
20. Lin, S. and W.S. Struve, *Time-Resolved Fluorescence of Nitrobenzoxadiazole-aminohexanoic acid: effect of intermolecular hydrogen-bonding on non-radiative decay.* Photochemistry and Photobiology, 1991. **54**, 361-365.
21. Mukherjee, S., A. Chattopadhyay, A. Samanta, and T. Soujanya, *Dipole moment change of NBD group upon excitation studied using solvatochromic and quantum chemical approaches: Implications in membrane research.* The Journal of Physical Chemistry, 1994. **98**, 2809-2812.
22. Rawat, S.S. and A. Chattopadhyay, *Structural Transition in the Micellar Assembly: A Fluorescence Study.* Journal of Fluorescence, 1999. **9**, 233-244.
23. Liu, J., C. Liu, and W. He, *Fluorophores and Their Applications as Molecular Probes in Living Cells.* Current Organic Chemistry, 2013. **17**, 564-579.
24. Bright, F.V. and C.A. Munson, *Time-resolved fluorescence spectroscopy for illuminating complex systems.* Analytica Chimica Acta, 2003. **500**, 71-104.
25. Owicki, J.C., *Fluorescence Polarization and Anisotropy in High Throughput Screening: Perspectives and Primer.* Journal of Biomolecular Screening, 2000. **5**, 297-306.
26. Richard, J.P., K. Melikov, E. Vives, C. Ramos, B. Verbeure, M.J. Gait, L.V. Chernomordik, and B. Lebleu, *Cell-penetrating Peptides: A REEVALUATION OF THE MECHANISM OF CELLULAR UPTAKE.* Journal of Biological Chemistry, 2003. **278**, 585-590.
27. Wender, P.A., D.J. Mitchell, K. Pattabiraman, E.T. Pelkey, L. Steinman, and J.B. Rothbard, *The design, synthesis, and evaluation of molecules that enable or enhance cellular uptake: Peptoid molecular transporters.* Proceedings of the National Academy of Sciences, 2000. **97**, 13003-13008.
28. Vivès, E., C. Granier, P. Prevot, and B. Lebleu, *Structure–activity relationship study of the plasma membrane translocating potential of a short peptide from HIV-1 Tat protein.* Letters in Peptide Science, 1997. **4**, 429-436.
29. Fuchs, S.M. and R.T. Raines, *Pathway for Polyarginine Entry into Mammalian Cells.* Biochemistry, 2004. **43**, 2438-2444.
30. Thorén, P.E.G., D. Persson, E.K. Esbjörner, M. Goksör, P. Lincoln, and B. Nordén, *Membrane Binding and Translocation of Cell-Penetrating Peptides.* Biochemistry, 2004. **43**, 3471-3489.

31. Ciobanasu, C., J.P. Siebrasse, and U. Kubitscheck, *Cell-Penetrating HIV1 TAT Peptides Can Generate Pores in Model Membranes.* Biophysical journal, 2010. **99**, 153-162.
32. Takechi, Y., H. Yoshii, M. Tanaka, T. Kawakami, S. Aimoto, and H. Saito, *Physicochemical Mechanism for the Enhanced Ability of Lipid Membrane Penetration of Polyarginine.* Langmuir, 2011. **27**, 7099-7107.
33. Persson, D., P.E.G. Thorén, E.K. Esbjörner, M. Goksör, P. Lincoln, and B. Nordén, *Vesicle size-dependent translocation of penetratin analogs across lipid membranes.* Biochimica et Biophysica Acta (BBA) - Biomembranes, 2004. **1665**, 142-155.
34. Bárány-Wallje, E., J. Gaur, P. Lundberg, Ü. Langel, and A. Gräslund, *Differential membrane perturbation caused by the cell penetrating peptide Tp10 depending on attached cargo.* FEBS letters, 2007. **581**, 2389-2393.
35. Wheaten, S.A., F.D.O. Ablan, B.L. Spaller, J.M. Trieu, and P.F. Almeida, *Translocation of Cationic Amphipathic Peptides across the Membranes of Pure Phospholipid Giant Vesicles.* Journal of the American Chemical Society, 2013. **135**, 16517-16525.
36. Marks, J.R., J. Placone, K. Hristova, and W.C. Wimley, *Spontaneous Membrane-Translocating Peptides by Orthogonal High-Throughput Screening.* Journal of the American Chemical Society, 2011. **133**, 8995-9004.
37. Thorén, P.E.G., D. Persson, M. Karlsson, and B. Nordén, *The Antennapedia peptide penetratin translocates across lipid bilayers : the first direct observation.* FEBS letters, 2000. **482**, 265-268.
38. Lavis, L.D. and R.T. Raines, *Bright Ideas for Chemical Biology.* ACS chemical biology, 2008. **3**, 142-155.
39. Swiecicki, J.-M., F. Thiebaut, M. Di Pisa, S. Gourdin -Bertin, J. Tailhades, C. Mansuy, F. Burlina, S. Chwetzoff, G. Trugnan, G. Chassaing, and S. Lavielle, *How to unveil self-quenched fluorophores and subsequently map the subcellular distribution of exogenous peptides.* Scientific Reports, 2016. **6**, 20237.
40. Baldini, F., *Alexander P. Demchenko: Introduction to fluorescence sensing.* Analytical and Bioanalytical Chemistry, 2009. **395**, 1195-1196.
41. Haldar, S. and A. Chattopadhyay, *Application of NBD-Labeled Lipids in Membrane and Cell Biology* Fluorescent Methods to Study Biological Membranes, 2013. **13**, 37-50.
42. Chattopadhyay, A., *Chemistry and biology of N-(7-nitrobenz-2-oxa-1,3-diazol-4-yl)-labeled lipids: fluorescent probes of biological and model membranes.* Chemistry and Physics of Lipids, 1990. **53**, 1-15.
43. Paprica, P.A., N.C. Baird, and N.O. Petersen, *Theoretical and experimental analyses of optical transitions of nitrobenzoxadiazole (NBD) derivatives.* Journal of Photochemistry and Photobiology A: Chemistry, 1993. **70**, 51-57.

44. Mazères, S., V. Schram, J.F. Tocanne, and A. Lopez, *7-nitrobenz-2-oxa-1,3-diazole-4-yl-labeled phospholipids in lipid membranes: differences in fluorescence behavior.* Biophysical journal, 1996. 71, 327-335.

45. Wasmuth, C.R., C. Edwards, and R. Hutcherson, *Participation of the SO2- Radical Ion in the Reduction of p-Nitrophenol by Sodium Dithionite.* The Journal of Physical Chemistry, 1964. 68, 423-425.

46. Lund, H. and M.M. Baizer, *Organic Electrochemistry: An Introduction and a Guide*. 1991, Marcel Dekker.

47. Jan, S.J., *Aromatic Nitrogen Containing Compounds*, in *Organic Electrochemistry, Fifth Edition.* 2015, CRC Press. p. 1121-1148.

48. Squella, J.A., S. Bollo, and L.J. Nunez-Vergara, *Recent Developments in the Electrochemistry of Some Nitro Compounds of Biological Significance.* Current Organic Chemistry, 2005. 9(6): p. 565-581.

49. Pawley, J.B., *Fundamental Limits in Confocal Microscopy*, in *Handbook Of Biological Confocal Microscopy*, B.J. Pawley, Editor 2006, Springer US: Boston, MA. p. 20-42.

50. Goodwin, J.S. and A.K. Kenworthy, *Photobleaching approaches to investigate diffusional mobility and trafficking of Ras in living cells.* Methods, 2005. 37, 154-164.

51. Liebman, P.A. and G. Entine, *Lateral Diffusion of Visual Pigment in Photoreceptor Disk Membranes.* Science, 1974. 185, 457-459.

52. Poo, M.-m. and R.A. Cone, *Lateral diffusion of rhodopsin in the photoreceptor membrane.* Nature, 1974. 247, 438-441.

53. Reits, E.A.J. and J.J. Neefjes, *From fixed to FRAP: measuring protein mobility and activity in living cells.* Nat Cell Biol, 2001. 3, E145-E147.

54. Carrero, G., D. McDonald, E. Crawford, G. de Vries, and M.J. Hendzel, *Using FRAP and mathematical modeling to determine the in vivo kinetics of nuclear proteins.* Methods, 2003. 29, 14-28.

55. Kimura, H., M. Hieda, and P.R. Cook, *Measuring Histone and Polymerase Dynamics in Living Cells*, in *Methods in Enzymology.* 2003, Academic Press. p. 381-393.

56. Houtsmuller, B.A. and W. Vermeulen, *Macromolecular dynamics in living cell nuclei revealed by fluorescence redistribution after photobleaching.* Histochemistry and Cell Biology, 2001. 115. 13-21.

57. White, J. and E. Stelzer, *Photobleaching GFP reveals protein dynamics inside live cells.* Trends in Cell Biology, 1999. 9, 61-65.

58. Denk, W., J. Strickler, and W. Webb, *Two-photon laser scanning fluorescence microscopy.* Science, 1990. 248, 73-76.

59. Monetta, P., I. Slavin, N. Romero, and C. Alvarez, *Rab1b Interacts with GBF1 and Modulates both ARF1 Dynamics and COPI Association.* Molecular Biology of the Cell, 2007. **18**, 2400-2410.

60. Lippincott-Schwartz, J., E. Snapp, and A. Kenworthy, *Studying protein dynamics in living cells.* Nat Rev Mol Cell Biol, 2001. **2**, 444-456.

61. Ellenberg, J., E.D. Siggia, J.E. Moreira, C.L. Smith, J.F. Presley, H.J. Worman, and J. Lippincott-Schwartz, *Nuclear Membrane Dynamics and Reassembly in Living Cells: Targeting of an Inner Nuclear Membrane Protein in Interphase and Mitosis.* The Journal of Cell Biology, 1997. **138**, 1193-1206.

62. Cole, N.B., C.L. Smith, N. Sciaky, M. Terasaki, M. Edidin, and J. Lippincott-Schwartz, *Diffusional Mobility of Golgi Proteins in Membranes of Living Cells.* Science, 1996. **273**, 797-801.

63. Messina, P., F. Lemaître, F. Huet, K.A. Ngo, V. Vivier, E. Labbé, O. Buriez, and C. Amatore, *Monitoring and Quantifying the Passive Transport of Molecules Through Patch–Clamp Suspended Real and Model Cell Membranes.* Angewandte Chemie International Edition, 2014. **53**, 3192-3196.

64. Patil, Y.P. and S. Jadhav, *Novel methods for liposome preparation.* Chemistry and Physics of Lipids, 2014. **177**, 8-18.

65. Walde, P., K. Cosentino, H. Engel, and P. Stano, *Giant Vesicles: Preparations and Applications.* ChemBioChem, 2010. **11**, 848-865.

66. Fidorra, M., A. Garcia, J.H. Ipsen, S. Härtel, and L.A. Bagatolli, *Lipid domains in giant unilamellar vesicles and their correspondence with equilibrium thermodynamic phases: A quantitative fluorescence microscopy imaging approach.* Biochimica et Biophysica Acta (BBA) - Biomembranes, 2009. **1788**, 2142-2149.

67. Angelova, M.I. and D.S. Dimitrov, *Liposome electroformation.* Faraday Discussions of the Chemical Society, 1986. **81**, 303-311.

68. Pautot, S., B.J. Frisken, and D.A. Weitz, *Engineering asymmetric vesicles.* Proceedings of the National Academy of Sciences, 2003. **100**, 10718-10721.

69. Yamada, A., T. Yamanaka, T. Hamada, M. Hase, K. Yoshikawa, and D. Baigl, *Spontaneous Transfer of Phospholipid-Coated Oil-in-Oil and Water-in-Oil Micro-Droplets through an Oil/Water Interface.* Langmuir, 2006. **22**, 9824-9828.

70. Yamada, A., M. Le Berre, K. Yoshikawa, and D. Baigl, *Spontaneous Generation of Giant Liposomes from an Oil/Water Interface.* ChemBioChem, 2007. **8**, 2215-2218.

71. Heimburg, T., *Membrane Structure*, in *Thermal Biophysics of Membranes*2007, Wiley-VCH Verlag GmbH & Co. KGaA. p. 15-27.

72. Schwenen, L.L.G., R. Hubrich, D. Milovanovic, B. Geil, J. Yang, A. Kros, R. Jahn, and C. Steinem, *Resolving single membrane fusion events on planar pore-spanning membranes.* Scientific Reports, 2015. **5**, 12006.
73. Coste, V., *Thèse, Université Pierre et Marie Curie - Paris VI.* 2006.
74. Liu, Y.-J., G.P.R. Hansen, A. Venancio-Marques, and D. Baigl, *Cell-Free Preparation of Functional and Triggerable Giant Proteoliposomes.* ChemBioChem, 2013. **14**, 2243-2247.
75. Senthilkumar, M., J. Mathiyarasu, J. Joseph, K.L.N. Phani, and V. Yegnaraman, *Electrochemical instability of indium tin oxide (ITO) glass in acidic pH range during cathodic polarization.* Materials Chemistry and Physics, 2008. **108**, 403-407.
76. Matveeva, E., *Electrochemistry of the Indium-Tin Oxide Electrode in 1 M NaOH Electrolyte.* Journal of The Electrochemical Society, 2005. **152**, H138-H145.
77. Cid, C.C.P., E.R. Spada, and M.L. Sartorelli, *Effect of the cathodic polarization on structural and morphological proprieties of FTO and ITO thin films.* Applied Surface Science, 2013. **273**, 603-606.
78. Bollo, S., P. Jara-Ulloa, G. Zapata-Torres, E. Cutiño, J.C. Sturm, L.J. Núñez-Vergara, and J.A. Squella, *Voltammetric reduction of 4-nitroimidazole derivatives: Influence of the N-1 substitution in protic and aprotic media.* Electrochimica Acta, 2010. **55**, 4558-4566.
79. Manuscript in preparation, 2016.
80. Laborde, H.M., A.M.N. Lima, F.C.C.L. Loureiro, C. Thirstrup, and H. Neff, *Adsorption, kinetics and biochemical interaction of biotin at the gold–water interface.* Thin Solid Films, 2013. **540**, 221-226.
81. Sterling, S.M., E.S. Allgeyer, J. Fick, I. Prudovsky, M.D. Mason, and D.J. Neivandt, *Phospholipid Diffusion Coefficients of Cushioned Model Membranes Determined via Z-Scan Fluorescence Correlation Spectroscopy.* Langmuir, 2013. **29**, 7966-7974.
82. Baumgart, T. and A. Offenhäusser, *Polysaccharide-Supported Planar Bilayer Lipid Model Membranes.* Langmuir, 2003. **19**, 1730-1737.
83. Stillwell, W., *Chapter 1 - Introduction to Biological Membranes*, in *An Introduction to Biological Membranes.* 2013, Elsevier, pp: 1-12.

General Conclusion and Outlook

As written in the General Introduction of this manuscript, I had two main objectives when I started my PhD work in 2013.

The first one was the development of a small electrochemical cell allowing analysis of poorly available compounds such as CPPs. In this context, an original three-electrode micro-cell equipped with a conventional reference electrode was developed. Though important for the analytical investigation of CPPs, this original approach which is simple, low-cost, easy to implement and versatile is also significant for evident economic and ecological reasons (consumption of small amounts of precious and/or expensive reagents, waste production). Though not developed in the present work, the experimental device could be also easily modified to separate the working and counter electrodes. Such modification would be of high interest to perform preparative electrolysis of high added value compounds.

The second objective was the use of the approach combining the patch-clamp principle and amperometry to monitor the transport of CPPs through suspended artificial membranes. Unfortunately, we found that this combination was not adapted to the characterization of CPP translocation. Nevertheless, though patches of pure DOPG vesicles are difficult to realize, the presence of di-cationic species (Ca^{2+}, Mg^{2+}) in solution introduced adequate electrostatic interactions to stabilize the DOPG membrane on the glass pipette. Although not reliable in CPP monitoring, this amperometric + patch clamp setup may offer new perspectives for the investigation of antimicrobial peptides (AMPs) which do not cross cellular membranes, but cause damages to cells via pore formation. In such a case, the detection of a concentrated redox species crossing a suspended membrane should be possible in the presence of AMPs. Combination of the patch-clamp and amperometry techniques could be thus useful to screen peptides families and to differentiate therefore the translocation of cationic peptides through membranes (CPPs) and the alteration of membrane permeability *via* the formation of pores (AMPs).

Considering the difficulty in probing micromolar concentrations of CPP crossing a micrometric suspended lipid bilayer membrane through direct amperometric detection, an alternative approach combining fluorescence and electrochemistry was developed. Compared to combined fluorescence/electrochemical devices developed so far, quantitative investigation could not be achieved using only an electrochemical setup, but implied resulting simultaneously to fluorescence

measurements. Indeed, the of confocal fluorescence microscopy with an electrochemical command appeared successful to selectively bleach, the fluorescence of either outer leaflet NBD-labeled giant liposomes (GUV) or NBD-labeled CPP localized on the outer leaflet of GUVs. Compared to classical photo-bleaching techniques such as FRAP and FLIP, the electrochemical process does not affect the fluorescent probes localized inside the vesicles allowing the discrimination between the outer and the inner membrane leaflet, a selectivity photobleaching techniques cannot offer. The use of an electrochemical process also discards the use of chemical reducing agents that may cause ionic strength variations and undergo slow internalization within vesicles. This original procedure appears versatile and perfectly adequate to undertake a more accurate tracking of active molecules (not only of CPPs) along the internalization process. Finally, the determination of passive transport mechanisms concerning the distribution, internalization and release of fluorescently-labelled drugs and other bioactive compounds may substantially benefit from the introduction of an electrochemical command in the switching of fluorescence. In our view, an important contribution of this PhD work was to establish the possibility to perform an electrochemical reduction of NBD-tagged phospholipids. This entry in the key-issue of the control of fluorescence is intrinsically "reversible", i.e. a fluorophore precursor could be electrochemically switched on, provided such precursors can be synthesized, opening avenues in complex imaging strategies.

Experimental Sections

4. Experimental section of the Second Chapter

4.1. Three-electrode analytical electrochemistry in micro-volume hanging droplets

4.1.1. Chemicals

Tetra-n-butylammonium hexafluorophosphate (Acros Organics) and potassium chloride (Sigma Aldrich) were used as supporting electrolytes and in highly purified water (HPW; resistivity = 18 MΩ cm; Millipore, Billerica, MA, USA), respectively. Acetonitrile (Sigma Aldrich), N,N-dimethylformamide (Acros Organics), ferrocene (Fluka), ferrocenemethanol (Aldrich), potassium tetrachloroaurate (Aldrich), and lead (II) acetate trihydrate (Sigma) were used as received. Phosphate-buffered saline (PBS) pH 704 (Gibco, Invitrogen Co.) was prepared with HPW.

4.1.2. Instrumentation

Cyclic voltammetry and controlled-potential electrolysis experiments were performed in a Faraday Cage using a Princeton Applied Research potentiostat (PARSTAT 2273). The quality of gold and platinum depositions was monitored by scanning electron microscopy (Eline model by RAITH).

4.1.3. Fabrication of disk-shaped ultramicroelectrodes

The fabrication of ultramicroelectrodes involves several steps. These include the carbon fiber or metal wire insertion into a glass capillary, sealing, electrode polishing and characterization. For this final step, cyclic voltammetry experiments are recorded to obtain the electrochemical behavior of the fabricated electrode. The procedure of fabrication for the employed electrodes in this thesis is depicted below.

a) Carbon fiber electrodes

(i) Isolation of carbon fibers

The carbon fiber electrodes are totally fabricated in our laboratory, following the procedure described by Arbault and co-workers [1]. Briefly, the electrodes are made from individuals carbon fibers of 10 µm (Cytec, Thornel, P-55S, Blacksburg USA), which are composed of 99 % of carbon and 1 % of epoxy resin. These fibers are wound onto bobbins whose strand contains about 10, 000 filaments.

Figure 4.1 Carbon fiber bobbin. The roving is of a bundle of parallel strands without twisting. Picture adapted from Cong Lu thesis, Electrochimie UMR 8640.

To select an individual fiber, a piece of strand with a length of 15 cm is cut and then placed over a white paper, which facilitates the visualization with the naked eye. After, the fibers are softly split out on individual filaments over the paper.

(ii) Carbon fiber insertion within a glass capillary

The electrode body is a Pyrex glass capillary of 1,2 mm outer diameter and 0,7 mm inner diameter (Clark Electrochemical Instruments, GC-120F-10, Pangbourne, UK). Such capillary has an inner filament for enabling exchange of air inside and outside the capillary. Then, a previously isolated fiber is inserted into the glass capillary by aspiration. In this step, the glass capillary is first connected at one end to a water trap which creates a pressure drop. Then, the opened end is approached to the fiber, which is aspired inside the glass capillary (Figure 4.3-a). Finally, the exceeding parts of the carbon fiber are cut with the help of scissors.

(iii) Capillary sealing

To begin the sealing process, the capillary/ carbon fiber assembly is centered in the middle of a coil of an upright pipette puller (Figure 4.2, Narishige, PB-7, NY, USA). One capillary extremity is fixed into the upper part of the holder and another one is fixed to a counterweight. By heating the coil, the glass is tapered around the fiber. Two pipettes are obtaining after the pulling, which remain linked by an exposed carbon fiber (Figure 4.3-b). This fiber is then cut with a scissors two separate the electrodes. The electrical contact is then made between the carbon fiber and a wire through a small mercury pool injected inside the capillary (Figure 4.3-c).

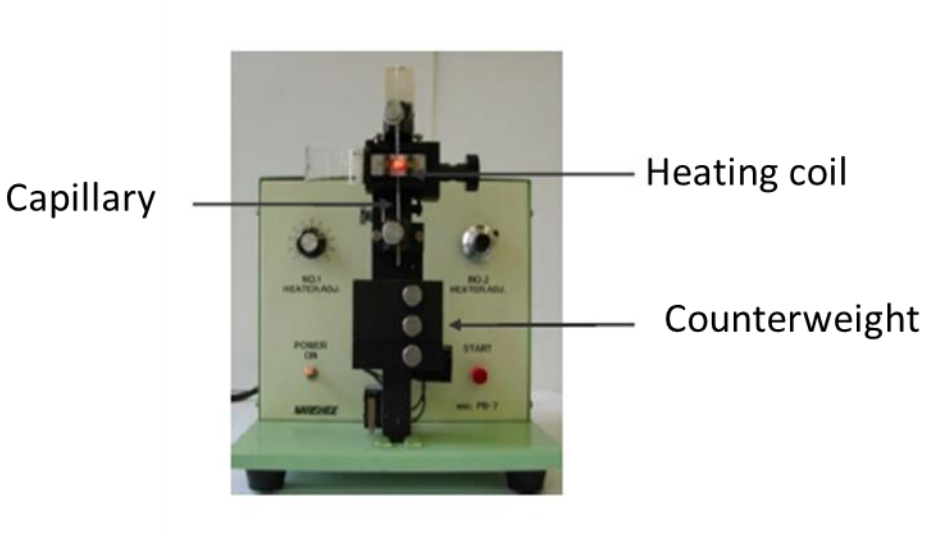

Figure 4.2 Narishige micropipette puller for vertical pulling action. Picture adapted from Cong Lu thesis, Electrochimie UMR 8640.

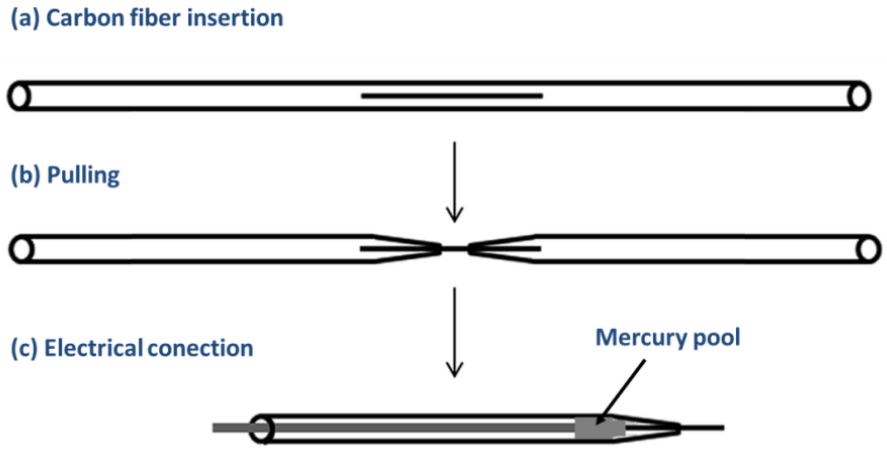

Figure 4.3 Aspiration, pulling and electrical procedure for fabricating carbon fiber ultramicroelectrodes.

(iv) Carbon fiber coating by electropolymerization

So far, the active surface of the electrode is the carbon fiber non-encapsulated for the capillary glass. Thus, the area is a cylinder which length is uncertain. To have a better control of such surface, the carbon fiber is coated with a film of polyoxyphenylene. Then, the conductive surface is delimited at carbon fiber tip.

In this method, the electropolymerization solution is prepared using the reagents: 2-allylphenol (0.23 M, monomer), allylamine (0.4 M, co-monomer), and 2-butoxyethanol (0.23 M, surfactant), all dissolved in a water/methanol mixture (1:1), Table 4.1.

Table 4.1 Component volumes added to 100 mL of a water/methanol mixture (1:1).

Reagents	Volumes (mL)
2-allylphenol	3
allylamine	3
2-butoxyethanol	3

For preparing the solution for electropolymerization, it is imperative to follow the next steps: first, about 10 mL of mixture water/methanol are added into a 100 mL glass beaker. Then, the volumes of 2-allylphenol, allylamine and 2-butoxyethanol are added to the baker. Finally, the remaining 90 mL of water/methanol are added.

The electropolymerization is carry-out applying a voltage of 4 V for 3 minutes. This potential captures the monomers and releases the radicals triggering the polymerization. Thus, a film of polymer coating the carbon fiber is obtained having a thickness of 1 µm. In this setup, a platinum wire is used as both counter and reference electrode. In practice, a group of around 5 to 7 electrodes are prepared simultaneously. The employed reagents are toxic, so it is necessary to manipulate them under a fume hood. After, each electrode is rinsed with highly pure water and the structure is observed under microscope. If there are some bubbles around the carbon fiber, it means that the polymerization process was well-achieved.

To ensure that the coating is a well electric insulating, the polymer should be promoted to a cross-linking reaction. For that, it is employed a thermal treatment, placing the electrodes (without containing the mercury pool) inside an oven at 150 °C during 3 hours. In this manner, the solvent is evaporated, and the mechanical rigidity is enhanced.

(v) Electrode polishing

To expose the active surface from the polymer coating, the electrode is polished using a polishing wheel is used as that shown on Figure 4.4. Such surface should be identical for all the electrodes and plane. Thus, the electrode is placed in the pipette holder and then beveled at 45 °, using a speed of 80

rpm for 5 minutes. Moreover, the fiber length can be controlled by cutting the part of it with a scalpel. When the beveling process is complete, the active surface is indicated by marking the capillary face.

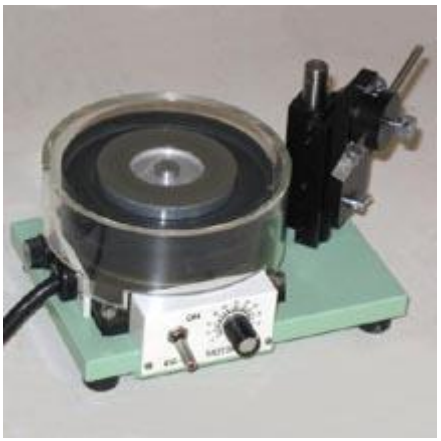

Figure 4.4 Narishige beveller EG-4.

After accomplishing the former steps, a 45° beveled carbon fiber electrode is obtained as show in Figure 4.5.

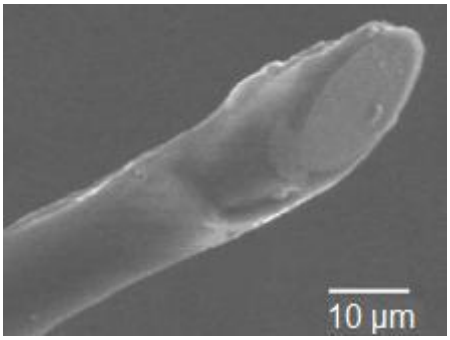

Figure 4.5 Electron microscopy micrograph of a 45° beveled carbon fiber electrode. Picture adapted from Cong Lu thesis, Electrochimie UMR 8640.

b) Microfabrication of glass-sealed metal electrodes

The procedure for fabricating metal disk-shaped UMEs involves the pulling of Pyrex glass capillaries (HARVARD APPARATUS, 10 cm long, 1.2 mm outer diameter, 0.6 mm inner diameter) using a laser puller apparatus (P-2000, Sutter Instrument Co). In this step, two capillaries having the shape of a micropipette are obtained. Then, the capillary tip is sealed by heating with a tungsten coil of a home-made current source. Once the tip is completely closed, a 25 µm platinum wire is inserted inside the capillary through the opened end. It should be ensured that the platinum wire reaches the closed tip. Then, the unsealed end is connected to a vacuum line and the tip is gently heated until the platinum

wire is encapsulated by the glass. The electrical junction is made by inserting an iron wire (30 AWG, 0.25 mm, PRO POWER) covered of silver epoxy (Circuit Works conductive epoxy, Chemtronics). Here, the capillary tip is again heated for one minute. The iron wire is stuck at the opened end with epoxy. After this, the electrode is placed vertically over a micromanipulator and the tip is polished for 1 minute with a polisher machine (MINITECH 233 by PRESI) and polisher cloths (200 Ø, PRESI 200 MM NT). Finally, the electrode is sonicated for 10 minutes on highly pure water dried under air stream.

4.3. Device configuration

The device for performing electrochemical experiments in a hanging drop is built as following:

1. A platinum wire of 0.5 mm (counter electrode) and a rubber cap are placed over a liquid junction protection tube, as depicted in Figure 4.6:

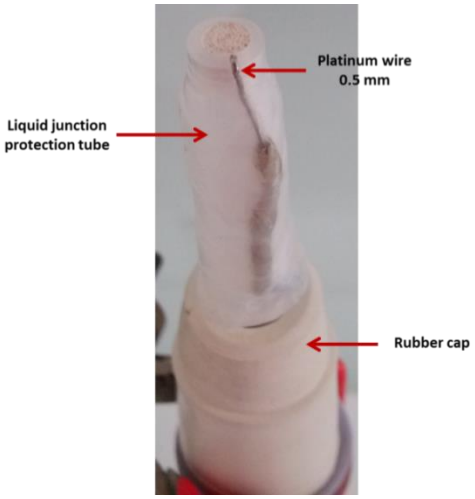

Figure 4.6 Platinum wire and rubber cap placed over the liquid junction protection tube.

2. The salt bridge tube is filled with the electrolyte solution used for the electrochemical experiments (i. e. 0.1 M KCl solution or 0.1 M DMF + nBu_4PF_6). A KCl saturated calomel reference electrode is immersed within the junction tube and in turn, such tube is placed in a glass chamber. The rubber cap allows sealing the tube to the chamber (Figure 4.7).

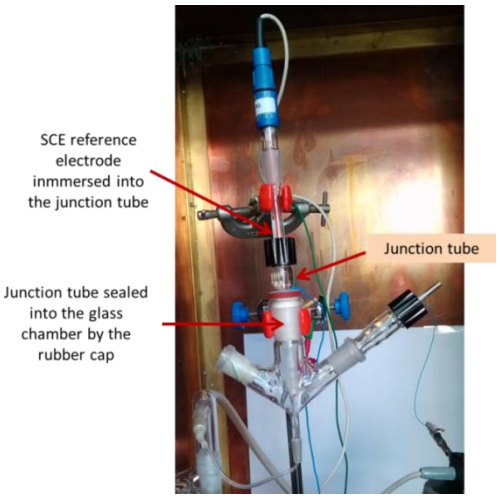

Figure 4.7 SCE reference electrode and liquid junction placed into the glass chamber.

3. For complete the three electrode electrochemical cell, the working electrode is placed into an electrode holder then both of them are set into the glass chamber. In this step, it must be ensure that the electrode surface is correctly immersed within the drop.

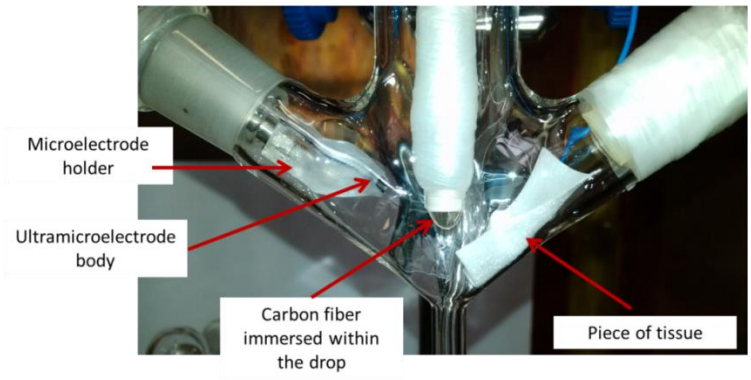

Figure 4.8 Working electrode placement and immersion within the drop.

For experiments in organic solvent, the evaporation is avoided by placing a piece of tissue (TX 604 cellulose/polyester, ~ 2 cm^2) wetted with the employed organic solvent and by blowing saturated argon for five minutes inside the glass chamber before starting each set of experiments.

4. When the electrochemical cell is already completed, the three electrodes are connected to a PAR potentiostat (PARSTAT 2273) and the electrochemical experiments are driven with the software PowerSuite.

4.3.1. Validation of the cell

a. Cyclic voltammetry in water and organic solvent

Solutions for cyclic voltammetry experiments were prepared at 1 mM of ferrocenemethanol used as electroactive specie, and 0.1 M of potassium chloride as supported electrolyte, dissolved in highly purified water. Similarly, solutions at 1 mM of ferrocene and 0.1 M of tetra-*n*-butylammonium hexafluorophosphate (redox and electrolyte species, respectively) were prepared in either acetonitrile or N, N-dimethylformamide.

b. Utilization of the cell in controlled-potential electrolysis

b.1 Platinized carbon fiber electrodes

Depositions of black-platinum are generated over the active surface of carbon fiber electrodes. Such procedure was reported by Ikariyama and co-workers [2]. The solution for electrodeposition is prepared by mixing 1 mL of hydrogen hexachloroplatinate (IV) (ALDRICH, 8 % *wt* solution in water) and 1.6 mL of lead (II) acetate trihydrate (99 %, 1.6 mg) in 6.4 mL of PBS. The presence of a small quantity of lead ion in the solution promotes the process of nucleation. The hydrogen hexachloroplatinate undergo a four electrons reaction:

$$Pt^{IV}Cl_6^{2-} + 2e^- \rightarrow Pt^{II}Cl_4^{2-} + 2Cl^- \quad (1)$$

$$Pt^{II}Cl_4^{2-} + 2e^- \; Pt^0 + 4Cl^- \quad (2)$$

The hexachloroplatinic acid follows a four electrons reduction after applying a constant potential of -65 mV vs SCE. The deposits were growing using the charges from 30 to 50 µC.

b.2 Gold particles deposition

Deposition of gold metal at the surface of a carbon fiber UME was achieved by reduction of potassium tetrachloroaurate (III) 2.6 mM dissolved in sulfuric acid 0.1 M. The applied voltages were 400 and -500 mV for 30 s.

c. Utilization of the cell for detecting a cell-penetrating peptide

c.1 Peptide preparation by solid phase synthesis

All standard chemicals and protected amino acids were purchased from Sigma (Saint Quentin Fallavier, France), Merck chemicals Ltd. (Nottingham, UK), Carlo Erba (Val de Reuil, France) or Iris Biotech AG (Marktredwitz, Germany). Rink amide MBHA resin was from Merck chemicals Ltd. The chemicals were used as commercially available without further purification.

The crude peptide was purified by RP-HPLC (Waters) on a VP 250x16 mm NUCLEODUR® C18 HTec 5 µm column working at 14mL/min, UV detection at 220 and 280 nm. The solvent systems used were: A (0.1% TFA in H_2O) and B (0.1% TFA in CH_3CN). The peptide characterization was carried out by RP-HPLC (Dionex) working at 1mL/min using a Proto 200 C18-3 µm 100x4.6 mm column (Higgins Analytical), UV detection at 220 and 280 nm, and by MALDI-TOF MS (DE-Pro, ABI) in positive ion reflector mode using the matrix CHCA. The m/z of the protonated molecules is given as experimental and calculated. Proteomix 4 (Laserbio Labs) [500–3500 Da] was used for calibration.

The ferrocene-$(Arg)_9$-NH_2 peptide was obtained as follows. The linear nonarginine sequence was synthesized by conventional *t*Boc/Bzl SPPS starting from a MBHA-Resin (0.54 mmol/g loading) on an ABI model 431A synthesizer (Applied Biosystem), 0.1 mmol scale. All $^{\alpha}$N-Boc-amino acids (1mmol) were coupled with N,N'-Diisopropylcarbodiimide (DIC)/1-hydroxybenzotriazole (HOBt) (1 mmol, 1:1). The dried $^{\alpha}$N-terminus Boc-deprotected peptidyl resin was then transferred to a fritted syringe, swollen in NMP and then reacted with ferrocene carboxylic acid (0.5 mmol), HBTU (0.45 mmol), and DIPEA (1 mmol), in NMP for 30 minutes. The ferrocene peptidyl-resin was then washed with NMP, DCM, MeOH, and dried overnight under vacuum. The peptide was cleaved from the using HF at 0°C, in the presence of anisole as scavenger (1.5 µL/mg of resin), for 2 hours. Filtration and precipitation with a 10% CH_3COOH aqueous solution afforded the crude peptide. After lyophilisation the peptide was purified by RP-HPLC using a linear gradient, 05-30% B in 30 minutes. Finally, the ferrocene-$(Arg)_9$-NH_2 peptide was characterized analytical RP-HPLC, Rt =8.48min, 05-30% B in 10 minutes linear gradient, and by MALDI-TOF MS (m/z): $[M+H]^+$ calcd 1635.73; found, 1635.09. Peptide purity was higher than 95%.

4.4. Monitoring and quantifying the passive transport of CPPs trough suspended model membranes

In this section, the experimental part corresponding to Patch clamp experiments is detailed. It comprises the giant unilamellar vesicles preparation by electroformation, employed solutions and capillary fabrication.

4.4.1. Preparation of DPhPC vesicles by electroformation

Giant unilamellar vesicles (GUVs) were prepared by the method of electroformation developed by M. Angelova [3, 4] and optimized by Le Berre et al [5]. The method consists in applying an alternative current (AC) over lipid layers deposited on ITO glass surfaces (ITO, Aldrich; surface resistivity: 30-60 Ω/sq) (Figure 4.9). Application of an external electric field leads to a better control in the hydration process.

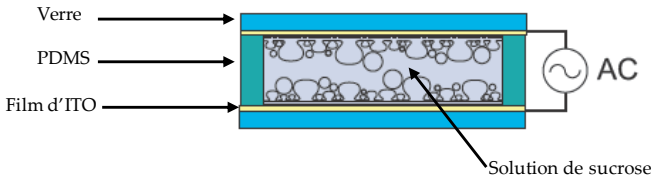

Figure 4.9 Schematic of a chamber for the electroformation of giant unilamellar vesicles.

4.4.2. Solution preparation

Two stock solutions were prepared:

- A glucose solution (0.32 M) in highly pure water (mQ water, resistivity=18 MΩ cm; Milli-Q system, Millipore, Billerica, MA, USA) and also containing NaCl (0.150 M) and NaN_3 (4.6 mM) (Solution 1).

- A sucrose solution (0.51 M) in mQ water and also containing NaN_3 (4.6 mM). (Solution 2).

The osmolarity of each solution is measured by using an osmometer VAPRO® (WESCOR). The osmolarity of each solution corresponded to about 650 milliosmoles (mOsm). Both solutions must have the same osmolarity to avoid differences on osmotic pressure between the inside and outside of the vesicle. Moreover, both solutions are filtered using and 0.2 µm Nylon filter (VWR) and such solutions are used for two weeks as maximum. They are stored in the fridge at a temperature between 2 and 8 °C.

4.4.2. Lipids

The lipid used for preparing giant unilamellar vesicles was the 1,2-diphytanoyl-sn-glycero-3-phosphocholine (DPhPC, Figure 4.10), dissolved in chloroform 10 mg/mL Avanti Polara Lipids. This phospholipid is used as purchased and stored at -20 °C

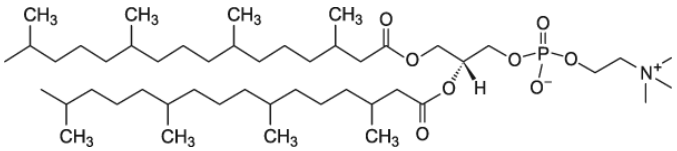

Figure 4.10 Structure of the phospholipid DPhPC, MW= 846, 252 g/mol.

4.4.3. ITO slides

The electroformation of giant vesicles is carried-out using two indium tin oxide (ITO) coated glass slides (Sigma Aldrich, surface resistivity = 8-12 Ω/sq, 25 mm x 25 mm x 1.1 mm). These ITO slides are cleaned respectively with Milli-Q water, isopropanol and acetone. Then, they are dried in a vacuum chamber for 30 minutes.

4.4.4. Phospholipid deposition and drying

In this step, the phospholipids are deposited over the cleaned and dried ITO slides. This is achieved using an automatic micropipette and an organic solvent resistant tip. Thus, 10 µL of phospholipid solution are deposed over each ITO slide. Then, these are spread out over the electrode surfaces. If the deposition step is well-done, it should reflect a violet light. Conversely, if such deposition is non-well done, it will reflect a yellow light and the electroformation process will be difficult to happen.

After the deposition, the solvent contained within the phospholipid films is dried by placing the ITO slides in the vacuum chamber for two hours.

4.4.5. Preparation of the electroformation cell

Here, the two slides are placed in front each other but split them out by a piece of PDMS having a thickness of 2 mm. This allows forming a hermetic-electroformation chamber of about 500 µL of volume. Then, the cell is filled with 500 µL of sucrose solution a closed with a small piece of PDMS. Here, the chamber is ready for starting the electroformation process.

4.4.6. Electroformation process

Both ITO slides are connected to an AC generator and a sinusoidal voltage of 2 or 3 V and 10-15 Hertz for at least 4 hours. The electric field allows growing spherical-like shape vesicles. After the 4 hours or swelling, it is necessary to set the generator at 3 V and 5 Hz for one hour for taking the vesicles off from the surface.

Then, 50 µL of GUVs/sucrose solution is mixed with 2 mL of glucose solution (solution 1) over a Petri dish. The presence of sucrose inside and glucose outside the vesicles allows the observation of these with a contrast phase microscope (Axiovert-135, Carl Zeiss, Germany) (Figure 4.11). Moreover, the difference in density helps to sediment the GUVs.

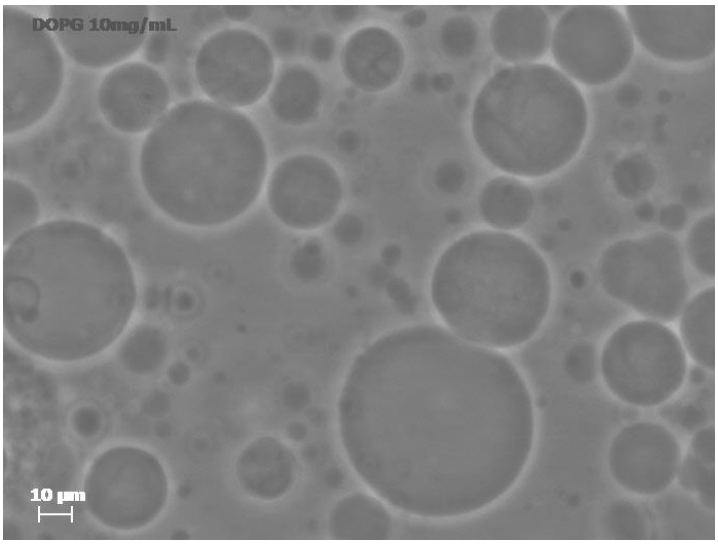

Figure 4.11 Giant unilamellar vesicles obtained at the end of the electroformation method.

4.4.7. Fabrication of patch clamp pipettes

This section describes the procedure for fabricating patch clamp pipettes for inside-out experiments. The geometry for such patch experiments requires of pipettes having long tapers and relatively small tips (Figure 4.12). The fabrication is achieved using Borosilicate capillaries GC120-10 (Harvard Apparatus LTD; 1.2 mm OD x 0.69 mm ID) and a laser based micropipette puller (Sutter Instruments, Model P-2000) (Figure 4.13). To assure the most reproducible results the puller should be warm up for 15 minutes before pulling pipettes.

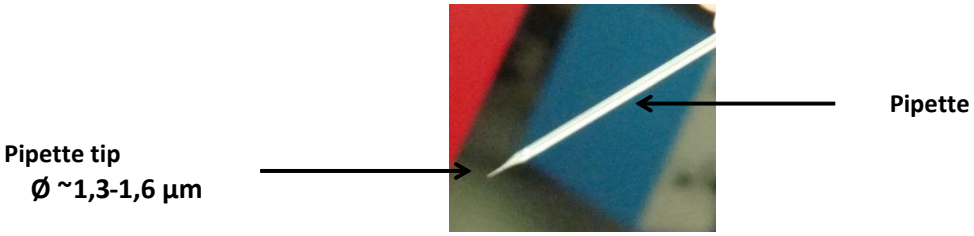

Figure 4.12 Patch clamp pipette obtained after the puller procedure.

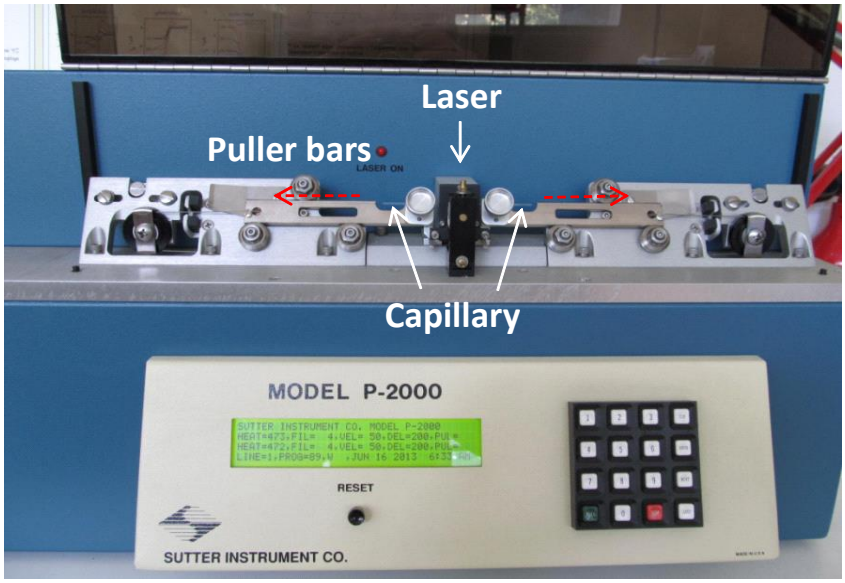

Figure 4.13 Laser Pipette Puller, P-2000.

The protocol starts thus loading a glass capillary into the puller bars. The required shape for inside-out pipettes is accomplished using the two-line program depicted on Table 4.2:

Table 4.2 Two-line micropipette program for pulling borosilicate capillaries.

Program	Heat	Filament	Velocity	Delay	Pull
1	473	4	50	200	0
2	473	4	50	200	0

Where HEAT specifies the output power of the laser, and consequently the amount of energy supplied to the glass; FILAMENT specifies the scanning pattern of the laser beam that is used to supply HEAT to the glass; VELOCITY determines the speed of the glass carriage system; PULL controls the force of the hard pull (in general, the higher the pull the smaller the pipette's tip diameter and the longer tapper); DELAY controls the time between when the HEAT turns off and when the hard PULL is activated (the higher the delay value, the cooler the glass will be when the hard PULL is executed).

Once pipettes are pulled, they are kept in a box with a lid (a 16 mm in diameter Petri dish). This ensures that pipettes are clean, so fresh pipettes are pulled every day.

4.4.8. Patching GUVs and electrochemical detection

The experiments of patch clamp are achieved using a contrast phase microscope (Axiovert-135, Carl Zeiss, Germany) cover for a Faraday cage and an EPC 10 amplifier.

The excising of giant vesicles by patch clamp starts by loading the pipettes with a solution of glucose (solution 1). This step is achieved as follows:

1. A tube of 1.5 mL is filled with the solution 1.

2. The pipette is connected to a vacuum pump by plastic tubing.

3. The pipette tip is then dived into the solution contained in the tube (Figure 4.14).

4. The vacuum pump is turned on, like that; the pipette tip is filled with solution 1.

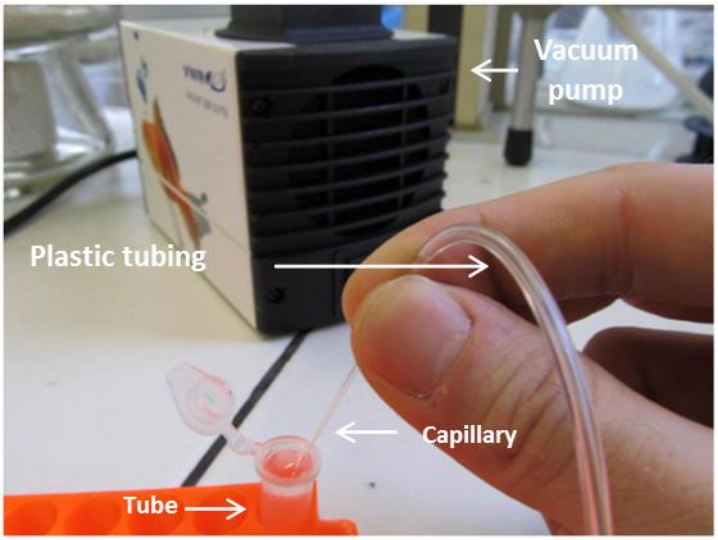

Figure 4.14 Process for loading the pipettes with glucose solution using a vacuum pump.

5. Then, the filling is completed using a microloader (Eppendorf Femtotips Capillary Tips), which allows loading about 15 µL of solution 1 in the another end. It is important do not overfilling the capillary, otherwise this can bring electric noise during measurements.

6. The bubbles inside the capillary are removed by kindly hitting the pipette body with one finger.

7. The whole procedure should be repeated for preparing at least 10 pipettes.

When the pipettes are already filled with glucose solution, they can be used to excise patch from giant unilamellar vesicles. This is described below:

1. A Petri dish of 8 cm of diameter is placed over the stage of the inverted microscope. Then, 2 mL of solution 1 are added in such dish.

2. One of the filled pipettes is inserted into the capillary holder which is connected to the amplifier. Inside of such holder there is an Ag/AgCl reference electrode (Figure 4.17, Electrode 1). This one will be in contact with the solution inside the capillary. The pipette is connected, through the holder, to a syringe which helps to apply a little pressure to the pipette.

3. A volume of 5 or 10 µL of solution containing GUVs is added over the Petri dish. Some minutes after, the vesicles sediment out to the bottom. The vesicles may be large enough (about 25 to 30 µm) for being well attached to the dish surface.

4. A little positive pressure is applied to the pipette solution before crossing the bath surface and approaching to the vesicle. The pressure keeps the tip clean from any debris in the bath. The capillary resistance is controlled by an amplifier system EPC 10.

5. The pipette is approached to the GUV by using micromanipulators (Model MHW-103, Narishige Co., London, UK) (Figure 4.15). The pipette comes in at an angle toward the vesicle of 45 degrees. Due to the imposed positive pressure, the vesicle moves away from the pipette. So, a little negative pressure is applied to bring the vesicle towards the pipette tip.

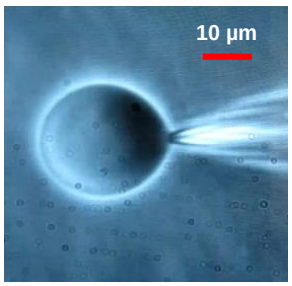

Figure 4.15 Patching of a giant vesicle.

The contact pipette/GUV causes the formation of a giga-seal, which is characterized by the increasing of the pipette resistance until values in the order of gigaohms. For the GUVs made of DPhPC the giga-seal is formed just after the simple contact pipette/GUV.

6. After a seal is stablished, the pipette is quickly pulled apart for excising a patch of membrane.

Thus, in this manner a suspended membrane is formed at the pipette tip. This is shown by the steady increase of the resistance (between 1 to 5 gigaohms) and by a transient current having an exponential decay:

$$i(t) = (I_0 - I_{SS})exp\left(-\frac{t}{\tau}\right) + I_{SS}$$

Where I_0 represents the initial transient current which relaxes towards a value of stationary-residual current I_{ss} (Figure 4.16 B_1) and τ represents the time constant RC of the studied system. The current response to a small potential ±5 mV through the electrode Ag/AgCl, is an important aid to guide and check the process of making a seal (Figure 4.16). This potential allows controlling (by a resistance change) the formation of a membrane at the pipette tip. A successful seal is indicated by a virtual absence of current response to a test pulse.

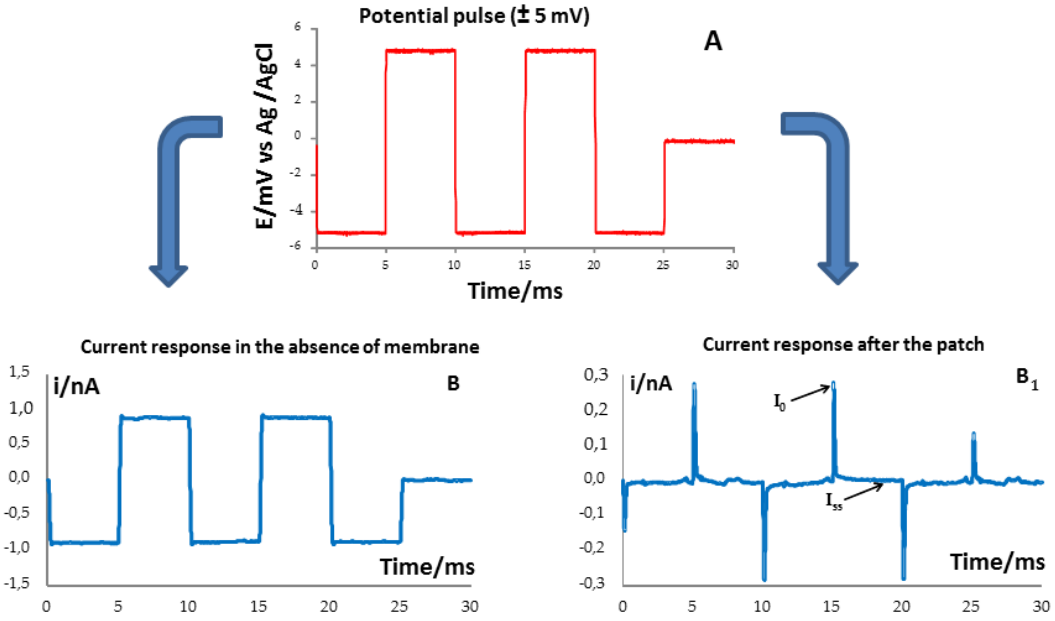

Figure 4.16 Characteristic current responses to a ±5 mV (spectrum A) before (spectrum B) and after (spectrum B_1) the formation of a bilayer at the pipette tip.

4.5. Electrochemical detection of ferrocene methanol through DPhPC suspended bilayers

4.5.1. Solutions

For study the passive transport of molecules across suspended bilayer we tested the redox-probe ferrocenemethanol ($FcCH_2OH$) at 1 mM. This molecule is dissolved in solution 1 (glucose 0.32 mM + NaCl 0.15 mM + NaN_3 4.6 mM).

4.5.2. Electrochemical detection

The half-wave potential was determined by a carbon fiber UME and a Picostat (EDAQ, E-corder®) as follows:

1. A Petri dish containing 1 mL of solution 1 (glucose 0.32 mM + NaCl 0.15 M + NaN_3 4.6 mM) is placed over the microscope stage.
2. A carbon fiber UME (10 µm) is placed over a holder for microelectrodes installed in a micromanipulator arm. An Ag/AgCl wire of 0.5 mm of diameter is used as reference electrode. Both electrodes are connected to the picostat.
3. A cyclic voltammetry at a speed rate of 0.1 V/s is performed as a Blanc.

4. Then, 1 mL of ferrocenemethanol 1 mM is added to the Petri dish to reach a final concentration of 0.5 mM.
5. A second voltammetry is performed at the same speed rate and the oxidation pick is identified:

Molecule	$FcCH_2OH$
Half-wave potential	
$E_{1/2}$/V vs Ag/AgCl	0.15

After the half-wave potential of ferrocenemethanol was identified, it was proceeded to perform the electrochemical detection the passive transport of such molecule across a DPhPC suspended membrane. The experiments were carried out using a pico-ammeter (AMU-130, Radiometer Analytical Instruments, Copenanhagen, DK) and a 10 µm carbon fiber electrode placed in front of the suspended membrane. All the experiments were performed at 22 ±1 °C.

Two systems are installed next to the microscope. One systems corresponds to the patch clamp experiments (Figure 4.17, description in blue) and the another one for the electrochemical experiments (Figure 4.17, description in red). Thus, a 10 µm carbon fiber electrode is used for detecting the diffusion of the redox probe, which is placed in a micromanipulator system at the left-side of the microscope. Here, the reference electrode is the external Ag/AgCl wire immersed in the bath solution (patch clamp system). The use of such shared reference (and not two difference reference for each system) allows decreasing the electrical noise during the electrochemical measurements. Both the carbon fiber electrode and the Ag/AgCl wire are connected to the pico-ammeter. The patch clamp pipette and the carbon fiber electrode are positioned at 45° degrees perpendicular to the pipette and electrode longitudinal axis.

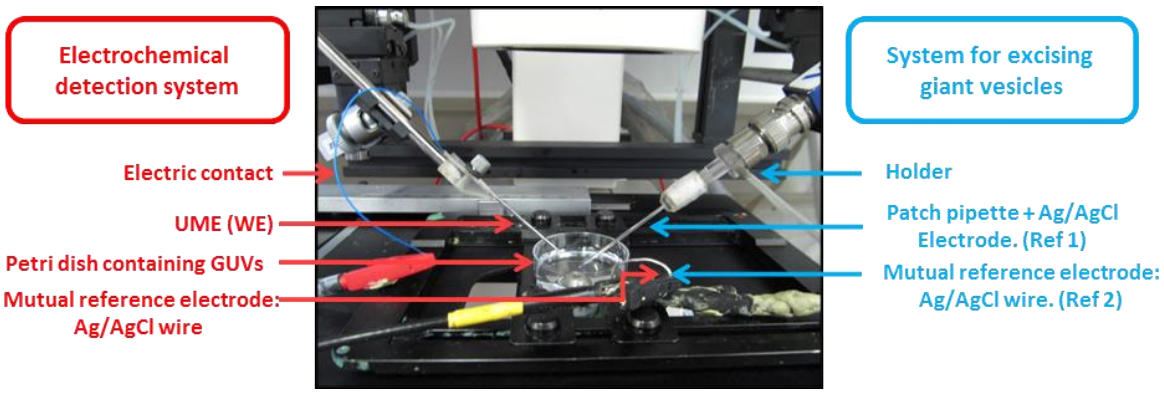

Figure 4.17 Experimental setup to detect the passive transport of redox probes across artificial-suspended membranes.

The patch of a vesicle for forming a suspended membrane is carried out using a pipette previously loaded with the sample solution. After the membrane patch excising, the electrochemical detection is accomplished as follows:

1. The electrode is quickly positioned at the bottom of the Petri dish and held at a distance of about 100 µm from the pipette tip.
2. The chronoamperometry is performed at a potential of 400 mV vs Ag/AgCl. When the electrode is far from the pipette, no current is detected.
3. The pipette is positioned near to the electrode surface, until a distance of 1 µm. The current increase if the redox-probe crosses the membrane.
4. After the measurement is accomplished (about 2 minutes), the suspended membrane is broken by imposing an overpotential between 500 to 1000 mV vs Ag/AgCl. Thus, the current increases, meaning that the barrier has already disappeared, and the pipette resistance drops to MΩ values. Sometimes occurs that the current decays to zero due a pressure drop.

4.6. Electrochemical detection of Fc-Arg_9 through DOPG suspended bilayers

4.6.1. Preparation of DOPG vesicles by electroformation

The preparation of DOPG vesicles follows the electroformation method described in section 4.4.6. Here, vesicles are diluted in a glucose solution (Solution 1) prepared at 0.32 M and containing NaCl 0.150 M, NaN_3 4.6 mM, $CaCl_2$ 10 mM and $MgCl_2$ 0.5 mM.

References

1. Arbault, S., P. Pantano, J.A. Jankowski, M. Vuillaume, and C. Amatore, *Monitoring an oxidative stress mechanism at a single human fibroblast.* Analytical Chemistry, 1995. **67**, 3382-3390.
2. Ikariyama, Y., S. Yamauchi, T. Yukiashi, and H. Ushioda, *Electrochemical Fabrication of Amperometric Microenzyme Sensor.* Journal of The Electrochemical Society, 1989. **136**, 702-706.
3. Angelova, M.I. and D.S. Dimitrov, *Liposome electroformation.* Faraday Discussions of the Chemical Society, 1986. **81**, 303-311.

4. Dimitrov, D.S. and M.I. Angelova, *Lipid swelling and liposome formation on solid surfaces in external electric fields*, in *New Trends in Colloid Science*, H. Hoffmann, Editor 1987, Steinkopff: Darmstadt. p. 48-56.
5. Le Berre, M., A. Yamada, L. Reck, Y. Chen, and D. Baigl, *Electroformation of Giant Phospholipid Vesicles on a Silicon Substrate: Advantages of Controllable Surface Properties.* Langmuir, 2008. **24**, 2643-2649.

5. Experimental Section of the Third Chapter

5.1. Selective Electrochemical Quenching of Fluorescence Emitted by NBD-labelled Phospholipids or Peptides

5.1.1. Lipids

1,2-dioleoyl-*sn*-glycerol-3-phospho-(1'-rac-glycerol) sodium salt (DOPG, 10 mg / mL in chloroform), 1,2-dipalmitoyl-*sn*-glycero-3-phosphoethanolamine-N-(7-nitro-2-1,3-benzoxadiazol-4-yl) ammonium salt (NBD-PE, 1 mg / mL in chloroform, λ_{ex}=460 nm, λ_{em}=535 nm) and 1,2-dipalmitoyl-*sn*-glycero-3-phospho-(1'-*rac*-glycerol) (DPPG, 10 mg/mL in chloroform) were purchased from Avanti Polar Lipids.

5.1.2. Chemicals

Mineral oil Bio-ultra, D-(+)-Glucose, Sucrose, and Biotin were obtained from Sigma Aldrich. Phosphate buffer saline (PBS) tablets (10 mM phosphate, 150 mM sodium chloride; pH 7.4) were purchased from GIBCO Invitrogen Corporation. All chemicals were used without further modification.

5.1.3. Solutions

a) Preparation of phosphate buffered saline pH 7.4

Phosphate buffered saline solution was prepared by dissolving 1 PBS tablet on 500 mL of highly purified water (resistivity = 18 MΩ.cm; Milli-Q system; Millipore, Billerica, MA, USA) for reaching a concentration of 10 mM on phosphate and 150 mM in sodium chloride. The final pH is 7.4.

b) Preparation of sucrose and glucose solution

To have an efficient sedimentation of giant vesicles at the ITO/Au substrate, GUVs are prepared with a high concentrated sucrose solution (0.7 M) encapsulated at the interior of their aqueous core. This concentration has an osmolarity value of about 990 mOs L^{-1}. Thus, the osmolarity of the glucose solution which is the surrounding medium incubating the vesicles should match such osmolarity. The diffraction index asymmetry of both solutions inside and outside the vesicles, enhance the image obtained with phase contrast microscopy. Moreover, the two solutions have to be isotonic to prevent vesicles from collapsing, i. e. bursting or shrinking because of the osmotic difference across the membrane.

Glucose and sucrose solutions were prepared by dissolving 6.3 g and 12 g of each compound, respectively, in 50 mL of PBS, to reach a final concentration of 0.7 M and an osmolarity around 990 mOsm. To ensure isotonic conditions, the osmolarity had to be sometimes adjusted by adding small amounts of PBS solution [1, 2]

5.1.4. Phospholipid suspensions

Oil suspensions of DOPG/NBD-PE (95/5 molar ratio) was prepared as follows: first, DOPG (52 µL; 10 mg/mL in chloroform) and NBD-PE (26.5 µL; 1 mg/mL in chloroform) were mixed in a 2 mL glass vial that was then placed under vacuum for 2 hours to evaporate chloroform. Mineral oil (650 µL) was then added to dried phospholipids and the suspension was sonicated (1.5 hours at 70°C). Pure DOPG oil suspensions were prepared similarly.

5.1.5. Osmolarity measurement

The osmolarity is measured by using a vapor pressure osmometer VAPRO 5520 (WESCOR, INC; Figure 5.1) and SS-033 sample discs.

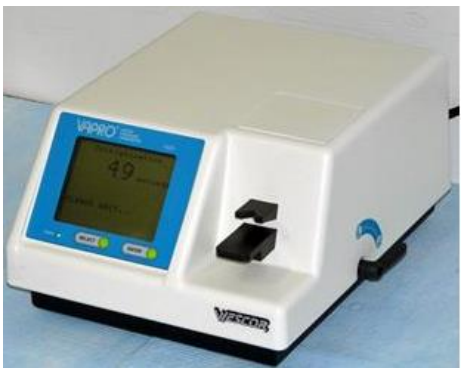

Figure 5.1 Vapor pressure osmometer VAPRO 5520.

The procedure for recording the value of osmolarity is the depicted below:

1. A single sample disc is placed in the central depression of the sample holder by using a forceps.

2. 10 µL of sucrose or glucose solution are taken with a pipettor. This is the optimum sample volume for obtaining repeatable results. Samples greater than 11 microliters can contaminate the thermocouple.

3. The 10 µL sample is loaded onto the sample disc. The pipettor tip must briefly contact the sample disc to press it flat against the holder. The paper disc should appear fully saturated, with a slight liquid meniscus on its surface.
4. The sample holder is closed by gently pushing it into the instrument. The measurement stars when the sample chamber is sealed.
5. When the measurement is completed the chimed sounds and the screen displays the osmolality of the specimen.

5.1.6. Device fabrication

The experimental device is based on a "home-made chamber" previously reported by Yamada et at [2] In our work, the device allows not only the fabrication and microscopy observation of NBD-labeled giant vesicles, but also the electrochemical bleaching of the latter. The steps involved in the fabrication are detailed below. A schematic of the procedure is depicted on Figure 5.2.

1. First, a microscope glass slide (50 x 24 x 0.13-0.16 mm-VWR) is rinsed two times with isopropanol and dried with filtered compresses air.

2. The already dried optical glass-slide is then covered with adhesive tape to pattern six 5 mm x 8 mm – sized uncovered bands.

3. A thin film of ITO (10 nm of thickness) is sputtered onto the six free adhesive tape glass parts. This step is achieved using a sputtering system EMITECH K675X, applying a current of 145 mA for 90 s.

4. Then, the ITO film is covered with a thin film of gold (20 nm thickness), by applying a coating current of 60 mA for 30s.

5. The adhesive tape is then removed, letting thus six rectangular ITO/Au electrodes (Figure 5.2-a).

6. Afterwards, three pieces of poly(dimethyloxane) (PDMS, RTV-615; Momentive Performance Materials) are made with the help of a 15 mm diameter hole-like punch. Then, two 4 mm diameter holes are punched in each 15 mm diameter hole as shown in Figure 5.2-b.

7. The ITO/Au modified glass slide and the PDMS pieces are then stuck together by treatment with oxygen plasma at 400 mTorr (100 W) (Harrick Plasma, NY, USA) for 3 minutes leading thus to six identical wells possessing ITO/Au working electrodes in the bottom (Figure 5.2-b).

8. Finally, a metallic wire is stock onto each working electrode with conductive silver paste and epoxy adhesive to ensure further connection with the potentiostat (Figure 5.2-c).

9. The electrochemical device is completed by inserting, through the PDMS well, a Ag/AgCl wire (0.5 mm in diameter) and a platinum wire (0.5 mm in diameter) used as the reference and the counter electrode, respectively.

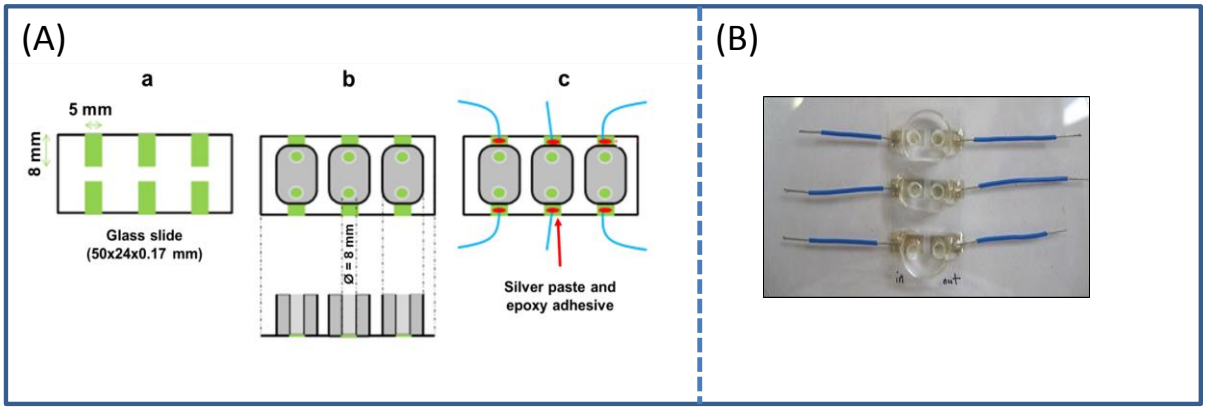

Figure 5.2 (A) Schematic illustration of the different components of the experimental device developed in this work. Note that six wells could be positioned on each glass microscope slide. (a) Glass microscope slide coated with ITO/gold bands; (b) punched and stuck PDMS pieces onto the bands; (c) connection of the working electrode surface. (B) Picture corresponding to step (c) in (A).

5.1.7. Preparation of giant unilamellar vesicles

As shown in Figure 3.21, some giant vesicles suffered physical damage on their membranes when they contacted the ITO/gold substrate. Thus, to improve the stability of GUVs, each gold working electrode was first modified with a biotin monolayer as already described elsewhere [3]. Accordingly, a biotin solution (C= 8 mM – 20 µL) was introduced in each well. After 5 hours, the biotin solution was removed and each well was rinsed twice with a PBS solution then once with the glucose solution to avoid multi-layers of biotin [3]. A glucose solution (C= 0.7 M; 30 µL) was then added in every hole and covered with a thin layer of mineral oil containing DOPG phospholipid (20 µL oil suspension prepared as described above). This phase aimed at forming the outer leaflet of the giant vesicle was put aside overnight to let time for phospholipid self-reorganization. In case of fluorescent outer leaflet preparation, a small fraction (5 % molar ratio) of NBD-PE fluorescent phospholipid was added in the previous suspension. To prepare the inner leaflet of the vesicle, an inverted emulsion was prepared by mixing a sucrose solution (C= 0.7 M; 5 µL) with an unlabeled phospholipid-mineral oil suspension (100 µL) (in case of unlabeled inner leaflet) with a vortex mixer for 60 seconds. The emulsion (20 µL) was then deposited at the well surface that corresponds to an Oil/Water (O/W) phase. The different molar

densities between sucrose (MW=342.30) and glucose (MW=180.16), allowed the W/O droplets crossing the O/W phase, forming thus giant vesicles at the bottom surface of the chamber (Figure 5.3) [2, 4]. Three kinds of NBD-PE labeled vesicles were prepared according to this method: (i) both inner and outer labeled leaflets, (ii) inner-labeled leaflet, and (iii) outer-labeled leaflet.

In the case of unlabeled giant vesicles made of DPPG phospholipid, the above procedure is followed with some modifications. First, the modification of the ITO/gold surface with biotin is not performed. So, 30 µL of glucose solution is added in each well and covered with 20 µL of unlabeled DPPG phospholipids mineral-oil suspension. Thus, the device is incubated at 45 °C for 4 hours to stabilize the layer which will form the outer leaflet. After the incubation, 20 µL of a sucrose/unlabeled phospholipid-mineral oil suspension is added into the former layer. This procedure should be done inside the incubator (at 45 °C) to keep the phospholipids in the fluid phase. Then, the device with the final emulsion is incubated at 45 °C for one hour.

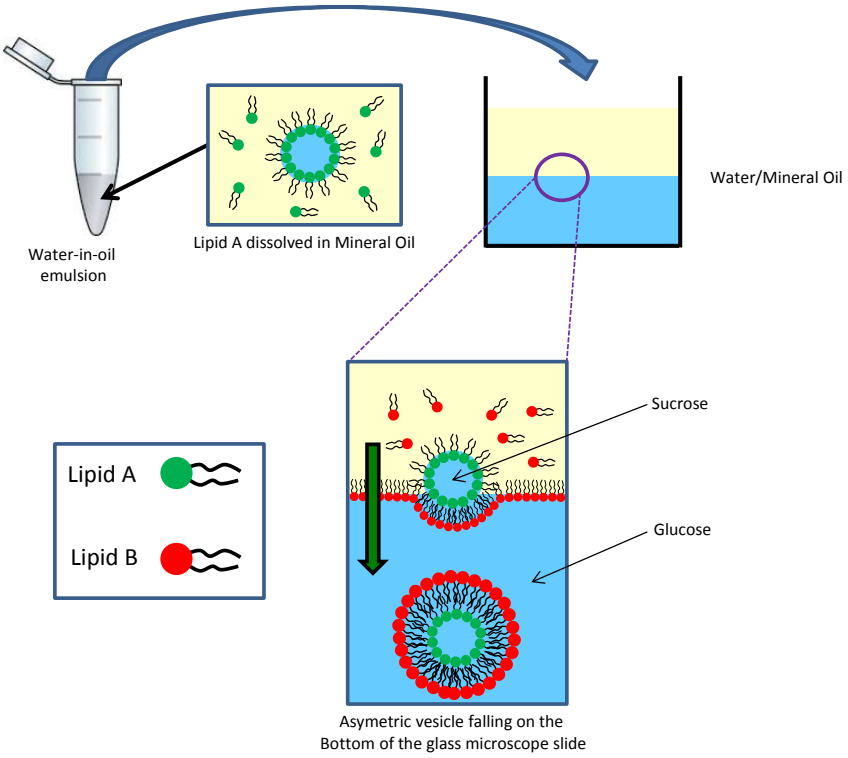

Figure 5.3 Asymmetric GUV preparation *via* phase transfer. A water–oil emulsion is first prepared with lipid A dissolved in the oil phase, encasing droplets in a monolayer. The emulsion is added to a water–oil (W/O) well with lipid B dissolved in the oil phase, assembling as a monolayer at the interface. Droplets cross the column under gravity (represented by the arrow), and are enveloped by a second monolayer. Asymmetric GUVs are thus formed, with lipid A in the inner leaflet and lipid B in the outer leaflet. Adapted from reference [5].

5.1.8. Microscopy observation of GUVs

The giant vesicles were observed by phase-contrast and confocal fluorescence microscopy (Zeiss LSM 710), using 10x and 20x lenses. Vesicles were chosen as a function of their bilayer integrity (some of them can be open) as well as their morphology. This was done by setting the focal plane at the interface formed by the biotin-modified gold electrode and the bottom of the vesicle. In case of a well-structured surface, an image is acquired (Figure 5.4-a). The focal plane is then moved to the equatorial plane of the GUV to take a second picture (Figure 5.4-b). The fluorescence intensity at time 0 (F^0), i.e. before running any FLIP or electrochemical experiments was determined from this image. Concerning of DPPG vesicles in fluid phase, the temperature is controlled at 45 °c by a confocal microscope stage incubator which must be shut it on two hours before imaging.

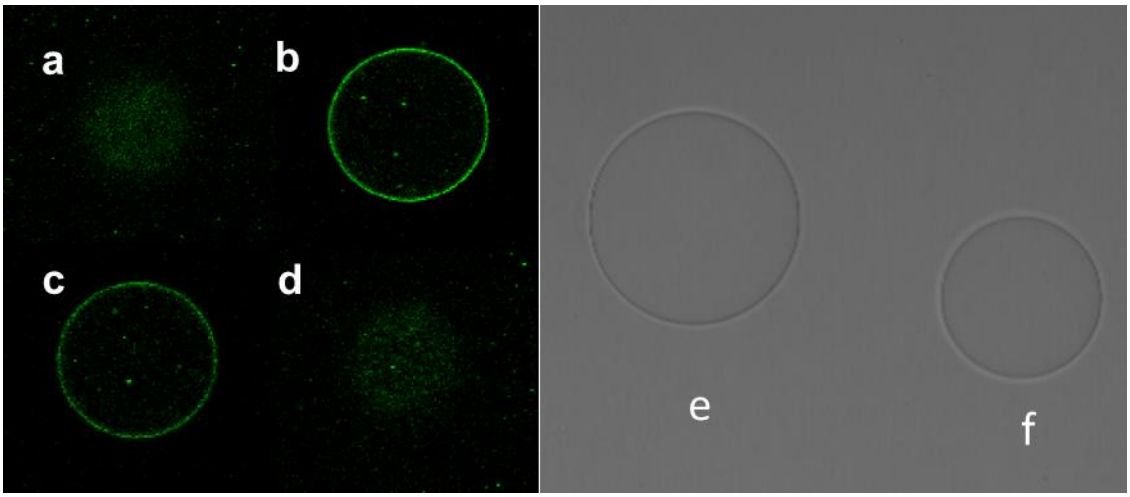

Figure 5.4 Fluorescent confocal images of both inner- and outer-leaflet NBD-tagged GUV. (a) Focal plane set at the interface formed by the biotin-modified gold electrode and the bottom of the vesicle; (b) focal plane set at the equatorial plane of the GUV; (c) same than (b), but after 600 seconds of electrochemical reduction (compare with (b); (d) image showing the integrity of the vesicle after the electrochemical reduction (compare with (a)). Giant vesicles (e) and (f) observing by phase contrast at the equatorial focal plane.

5.1.9. Electrochemical experiments

Just before each experiment, and after the vesicle preparation, the electrochemical device shown in Figure 5.2-(B) was completed by inserting, through the PDMS well, a Ag/AgCl wire (0.5 mm in diameter) and a platinum wire (0.5 mm in diameter) used as the reference and the counter electrode, respectively. This step was facilitated after making a “channel” within the PDMS well with the help of a needle. Then, a series of electrochemical reduction were performed by applying a potential value of -

0.9 V (µAUTOLAB Type III). A picture of the remaining fluorescence at the equatorial plane of the GUV was taken after every 30 seconds until 300 s then every 60 seconds until 600 seconds (Figure 5.4-b,c). After the end of each experiment, the vesicle integrity was verified as shown in Figure 5.4-d. Time lapse-experiments are performed by applying a continuous potential pulse of -0.9 V for 600 s and imaging each 30 s in the equatorial plane of the GUV.

5.1.10. Image analysis and fluorescence quantification

Images were analyzed with the ImageJ software (http://rsb.info.nih.gov/ij/). Integrated intensities obtained from equatorial planes of the GUVs, as a function of time, were measured using the Azimuthal Average plugin. Fluorescence intensities (F) were corrected from background signals (F_{BG}) and photo-bleaching (F_{Ph}) according to equation (1).

$$F_{corr} = \left(\frac{F - F_{BG}}{F^0 - F_{BG}^0}\right)\frac{1}{F_{Ph}} \quad (1)$$

Background fluorescence (F_{BG}) was determined from a squared region localized near to GUV perimeters. The amount of photobleaching (F_{Ph}) was determined from control images obtained in the absence of electrochemical of FLIP experiments.

Fluorescence intensity variations (F/F^0) observed at the equatorial plane of GUVs were plotted as function of *time,* where F^0 and F are corrected fluorescence intensities at time 0 and at time t, respectively.

5.1.11. FLIP experiments

FLIP experiments were performed with the same confocal fluorescence microscope used as for the observation of GUVs (Zeiss LSM 710). Photo-bleaching experiments were carried out with a circular spot using the 458 nm lines from a 40 mW argon laser operating at 100 % power. The bleached region, also called "Region Of Interest" (ROI) was located at 5 µm below the top of GUVs that corresponds to the optical pinhole section. The radius of the ROI depends on the size of the GUV; the ROI size was chosen as being equal to one third of the total vesicle surface. The bleach pulse was optimized on 20 iterations of around 3 – 3.5 seconds duration depending on the ROI size. Fluorescence images were acquired at the GUVs equatorial plane as a function of time, at a low laser

intensity (0.2 % laser power) under the following conditions: Frame Scan Mode, 2 or 3x optical zoom, 512 x 512 pixel resolution, depth 8 bits, nominal speed of 9 (total scan speed <1 s). The pinhole was set at 1 Airy, corresponding to an optical section of 5 µm. The detector gain was adjusted to enable the fluorescent signal, but avoiding saturation.

5.1.12. Solution of the diffusion equation governing an oblate spheroid

Vesicles were found to be flattened due to both adhesion of the vesicle on the electrode surface and to higher density of the inner solution compared with the outer one. The corresponding oblate spheroidal system coordinate system was thus chosen to solve numerically the diffusion equation on the surface of the vesicle. Following the circular symmetry around the vertical axis (z), the problem is independent of the azimuthal coordinate and only depends on the variables θ and µ. As illustrated in Figure 5.5, θ is the latitude angle lying in the range $\left[-\frac{\pi}{2},\frac{\pi}{2}\right]$ and µ is a positive real number related to the ratio of the minor axe length to the major axe length.

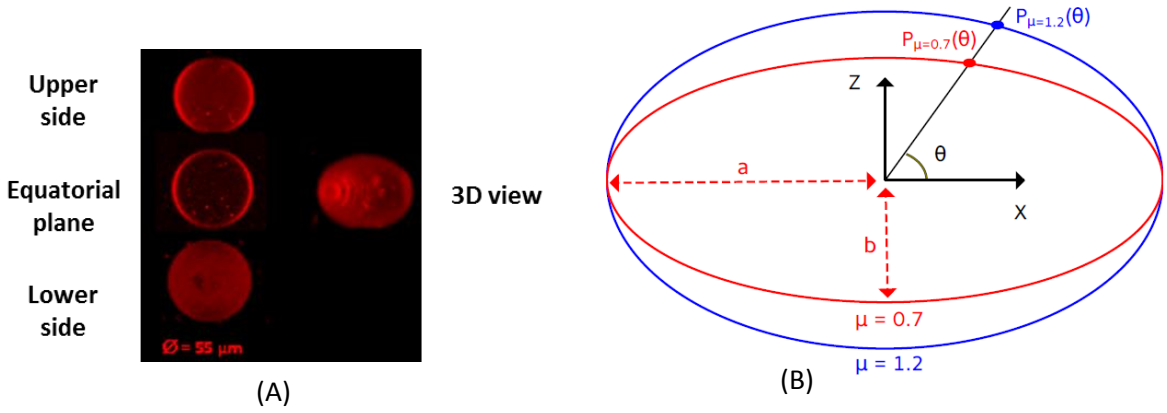

Figure 5.5 (A) Typical confocal microscopy image showing the upper, equatorial, lower sections and 3D reconstruction of a GUV placed in the electrode surface. (B) Cross section of oblates spheroid in the xy plane, with constant µ (ellipsoid); µ measures the deformation with respect to the sphere (tanh µ = *b/a*, with *a* and *b* the semi-major and semi-minor axis lengths respectively) and θ is the latitude angle.

The shape of the vesicles was approximated with ellipsoidal shape, which is spheroid of constant µ as show in Figure 5.5. The diffusion equation then writes

$$\frac{\partial c(t,\theta)}{\delta t} = \frac{D}{r^2(sinh^2\mu + sin^2\theta)cos\theta}\frac{\partial}{\partial\theta}\left(cos\theta\frac{\partial c(t,\theta)}{\partial\theta}\right) \quad (2)$$

Where c is the fluorescence dye concentration, D its diffusion coefficient and r = a/coshμ. The fluorescence intensity measured at the equator (θ=0), the equation (2) was solved with the following initial and boundary conditions: c(0, θ) = 1, $\frac{\partial c(t,\frac{\pi}{2})}{\partial \theta} = 0$ and c(t, θ_0)= the latitude of the bleached surface edge. The Matlab software (MAtlab 2015a, Mathworks) was used to implement the fitting least square method and to calculate numerical solution of equation (2). The value of the parameter D, μ and θ_0 were obtained through this least square method to fit data obtained at the equator (θ=0) of the vesicles. The value of *r* was deduced from vesicle diameter *a* measured on pictures. Note that $\theta_0 = -\arccos\left(\frac{a_{bleach}}{a}\right)$ could be deduced by measuring *a* and a_{bleach}. However, uncertainty in determining a_{bleach} led to introduce a parameter α such that $\theta_0 = -\arccos\left(\alpha\frac{a_{bleach}}{a}\right)$.

An example of fluorescence intensity variation as a function of both time and latitude is shown in Figure 5.6. As expected, a steep decrease is observed with time at latitude angles close to the electrode. On the opposite, in the upper part of the vesicle, a plateau of constant fluorescence (or dye concentration) at short time is followed by a decrease at the longer time.

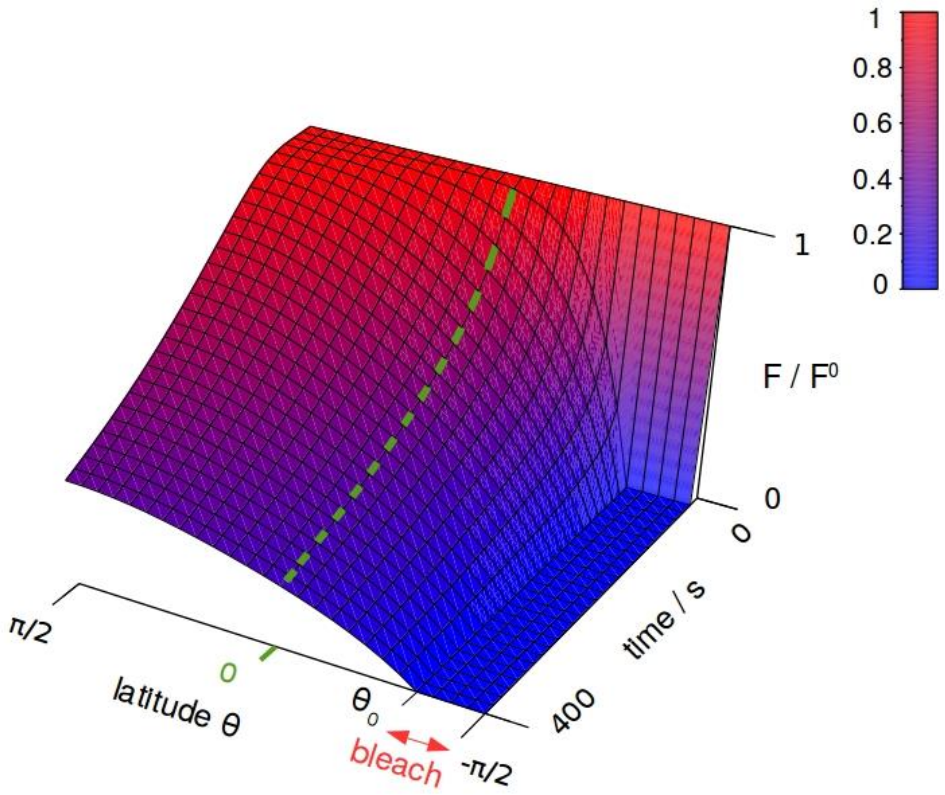

Figure 5.6 Normalized fluorescence intensity on a ellipsoidal vesicle against latitude angle θ and time. Vesicle with diameter 2a = 130 μm and ratio a_{bleach}/a = 1.5. μ=0.8, and D = 4.0 $\mu m^2 \cdot s^{-1}$.

5.1.13. Selection of NBD-R6/W3 experimental concentration

As cited in section 3.6.3.4, studies of CPPs uptake are generally carried out using micro-molar concentrations of peptides (for instance 100 nM). This restriction obeys the following reasons:

- To exclude that peptide internalization is a result of damage of the plasma or artificial membrane [6].
- To avoid a self-quenching of fluorescence due to peptide accumulation over the membrane or intracellular compartments [7].

Nevertheless, we found two main operational constraints for choosing the peptide working concentration:

- The addition of a NBD-R6/W3 solution must not dramatically change the osmolarity of the buffer containing giant vesicles. Thus, it is imperative to keep isotonic conditions.

- The total volume of each well comprised in the device used to extinct the fluorescence was about 80 µL, which 70 µL were already occupied for the glucose and phospholipid suspension. Therefore, it was possible to add just about 10 µL of peptide solution (Figure 5.7). These downsides were overcome as follows:

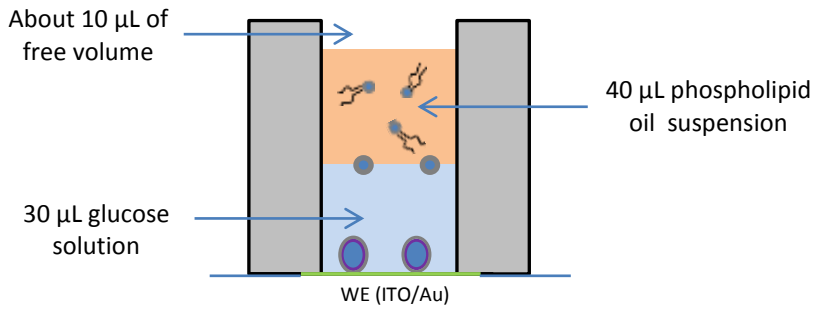

Figure 5.7 Scheme of the side view of a well comprised inside the device used to extinct the fluorescence by electrochemical reduction.

1. A stock solution 100 µM of NBD-R6/W3 buffered in PBS (osmolarity = 300 mOs) was diluted 10 fold in glucose solution 700 mM and 990 mOs. This was done by adding 10 µL of NBD-R6/W3 solution into 90 µL of glucose solution.

2. Like that, the prepared 10 µM NBD-R6/W3 solution had an osmolarity about 990 mOs. The same osmolarity value as the external medium of giant vesicles.

3. Finally, the 10 µM NBD-R6/W3 was diluted four times by adding 10 µL of such solution into the 30 µL of glucose solution contained into the well. Thus, the final concentration of NBD-R6/W3 into the well was 2.5 µM. The addition of peptide solution was achieved by traversing the PDMS block with a 10 µL glass syringe (Hamilton Microliter Syringes). In this manner, the solution is directly added into the glucose solution without crossing the oil phase (Figure 5.8).

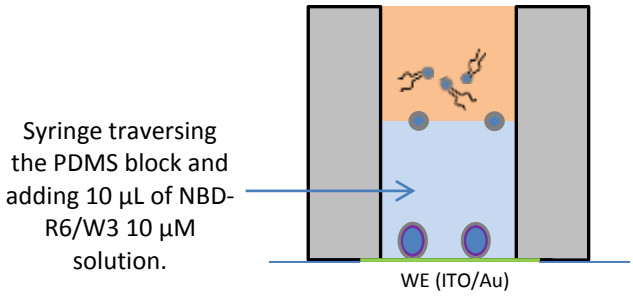

Figure 5.8 Scheme of the addition of 10 µL of NBD-R6/W3 at 10 µM and 990 mOs to reach the final concentration of 2.5 µM.

A similar strategy was followed to obtain an NBD-peptide concentration of 0.63 µM, which was prepared diluting four times a solution 2.5 µM of NBD-R6/W3. This achieved by adding 10 µL of peptide solution into 30 µL of glucose solution contained into well. For concentrations lower to 0.63 M, the fluorescence intensity was difficult to detect. This problem comes from the loss of fluorescence transmission trough the ITO/Au layer.

5.1.14. General procedure for preparation of symmetric LUVs

- For preparing a 10 mL stock-solution of LUVs 1 mM

746.3 µL of DPPG suspension in chloroform was placed in a round-bottomed flask. Chloroform was removed slowly under vacuum at 40 °C with the aid of a rotatory evaporator, and the residue was then placed under high vacuum for 1 h. The lipid was hydrated with 10 mL of sucrose solution 700 mM and 990 mOs, in phosphate-buffered saline pH 7.4 previously prewarmed. The turbid suspension of multilamellar vesicles was subsequently extruded seven times through a 200 nm polycarbonate track-etch membrane and ten times through a 100 nm polycarbonate track-etch membrane (Whatman) with a 10 mL Thermobarrel extruder (Lipix Biomembranes). The extruder was heated at 41 °C using a thermocontrolled circulation bath during the LUVs preparation. The LUVs solution was stored at room temperature [8].

References

1. Liu, Y.-J., G.P.R. Hansen, A. Venancio-Marques, and D. Baigl, *Cell-Free Preparation of Functional and Triggerable Giant Proteoliposomes.* ChemBioChem, 2013. **14**, 2243-2247.
2. Yamada, T.Y., T Hamada, M. Hase, K. Yoshikawa and D. Baigl, *Spontaneous transfer of phospholipid-coated oil-in-oil and water-in-oil micro-droplets through an oil/water interface.* Langmuir, 2006. **22**, 9824-9828.
3. Laborde, H.M., A.M.N. Lima, F.C.C.L. Loureiro, C. Thirstrup, and H. Neff, *Adsorption, kinetics and biochemical interaction of biotin at the gold–water interface.* Thin Solid Films, 2013. **540**, 221-226.
4. Pautot, S., B.J. Frisken, and D.A. Weitz, *Engineering asymmetric vesicles.* Proceedings of the National Academy of Sciences, 2003. **100**, 10718-10721.
5. Elani, Y., S. Purushothaman, P.J. Booth, J.M. Seddon, N.J. Brooks, R.V. Law, and O. Ces, *Measurements of the effect of membrane asymmetry on the mechanical properties of lipid bilayers.* Chemical Communications, 2015. **51**, 6976-6979.
6. Bechara, C. and S. Sagan, *Cell-penetrating peptides: 20 years later, where do we stand?* FEBS letters, 2013. **587**, 1693-1702.
7. Swiecicki, J.-M., F. Thiebaut, M. Di Pisa, S. Gourdin -Bertin, J. Tailhades, C. Mansuy, F. Burlina, S. Chwetzoff, G. Trugnan, G. Chassaing, and S. Lavielle, *How to unveil self-quenched fluorophores and subsequently map the subcellular distribution of exogenous peptides.* Scientific Reports, 2016. **6**, p. 20237.
8. Swiecicki, J.-M., A. Bartsch, J. Tailhades, M. Di Pisa, B. Heller, G. Chassaing, C. Mansuy, F. Burlina, and S. Lavielle, *The Efficacies of Cell-Penetrating Peptides in Accumulating in Large Unilamellar Vesicles Depend on their Ability To Form Inverted Micelles.* ChemBioChem, 2014. **15**, 884-891.

Appendixes

6. Appendixes

6.1. Appendix A: Sputtering for thin film deposition

6.1.1. Film Electrodes

Electrodes based on films of conducting material have made possible numerous experiments that would be difficult or impractical to implement with conventional bulk electrodes [1]. The first applications of thin film electrode were the development of spectroelectrochemical experiments in which the light beam was directed through an optically transparent film electrode [1]. Nowadays, there are a vast number of applications such as the well-known spectroelectrochemistry for characterizing molecules [2-5], development of biological sensors [6-8], development of lithium battery and capacitors [9-11], among others.

Film electrodes are commonly fabricated from conducting or semiconducting materials, which are deposited onto a suitable substrate through either a physical or a chemical process (or both). The substrate is generally an insulator [1]. Factors controlling the desired thickness of the film involve both the electrical resistivity (ρ) and the optical transparency or reflectance of the material (if optical transmission or reflection is desired). The optimum film thickness for an application involving both electrical and optical considerations will require a compromise, since a decrease in resistivity normally is also accompanied by a decrease in light transmission (undesirable for an optically transparent electrode) [1].

The film optical transmission spectrum is important in optically transparent electrode (OTE) when these are applied in spectroelectrochemistry. Thus, it is necessary to make a balance between maximizing transmittance and minimizing sheet resistance. Some parameters to take into account are film thickness (transmittance and resistance decrease with increasing thickness), charge carrier density in the conduction band (transmittance and resistance decrease with increasing carrier density), and the band gap. In case of metals, they generally exhibit strong absorption by the free electron charge carriers in the visible and infrared spectral regions, but may become transparent at wavelengths shorter than a critical edge value defined by the plasma frequency of the metal, usually in the ultraviolet region. On the other hand, semiconductor electrodes have much lower charge carrier densities therefore they typically absorb in the infrared. These electrodes exhibit much lower absorption by charge carriers than metals of comparable film thickness, and frequently show a

transparency window in much of the visible spectrum due to substantial band-gap energy, before absorbing again in the ultraviolet [1].

6.1.2. Preparation of Thin film electrodes

Thin film deposition is a technique to apply coatings of pure materials onto the surface of many different objects. Thin films are fabricated by the deposition of individual atoms on a substrate [12]. This technique have been used for making electronic devices, optical coatings, instrument hard coatings, decorative parts [12] and working electrodes in electrochemistry [12, 13]. The fabrication of thin-film metal electrodes can be achieved on a variety of substrates by vacuum evaporation, DC and RF sputtering, screen printing and chemical vapor deposition (CDV) [13]. Common substrates are glass (soda-lime and quartz), silicon, and mica. The substrates should possess a relatively smooth morphology with low surface roughness. The preparation of the substrate is a crucial step in the formation of well-adhering, electrically conducting and optically transparent films. Cleaning is a critical step in the substrate preparation that is sometimes overlooked. A common procedure for cleaning glass or oxide-coated silicon involves boiling in an aqueous detergent solution, rinsing with ultrapure water, followed by degreasing with clean organic solvents, such as isopropanol or methanol. When the surface is clean, distilled water will run off the surface as a continuous sheet and not bead up in the form of droplets. Mica is best prepared by cleaving the layer planes with tape or a sharp knife, which results in the exposure of a clean basal plane. The cleaning step should be performed immediately prior to film deposition [13]. As mentioned before, there are several methods available to fabricate thin film electrodes which would depend on the film material. In this work, the thin film deposition by plasma sputtering is addressed below.

6.1.3. Sputtering

The sputtering phenomenon occurs when a solid surface is bombarded with energetic particles such as accelerated ions and, as a consequence, surface atoms of the solid are scattered backward due to collisions between the surface atoms and the energetic particles (Figure 6.1) [13].

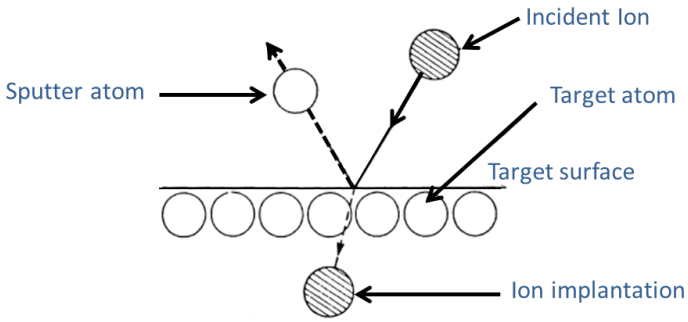

Figure 6.1. The physical sputtering process. Figure adapted from Ref [13].

The simplest kind of sputtering system is the dc diode device (Figure 6.2). The dc sputtering system is composed of two planar electrodes, one working as a cathode and the other as an anode. In the surface of the cathode it is placed the target materials to be deposited. Meanwhile, the substrates are placed on the anode. The sputtering chamber is filled with gas, for instance, argon gas at 5 Pa. The application of dc voltage between the electrodes generates a glow in the gas discharge, which means that the gas has been already ionized. The Ar^+ ions are accelerated at the cathode fall and sputter the target, resulting in the deposition of the thin films on the substrates. In the dc sputtering system, the target is composed of metal since the glow discharge (current flow) is maintained between the metallic electrodes [13].

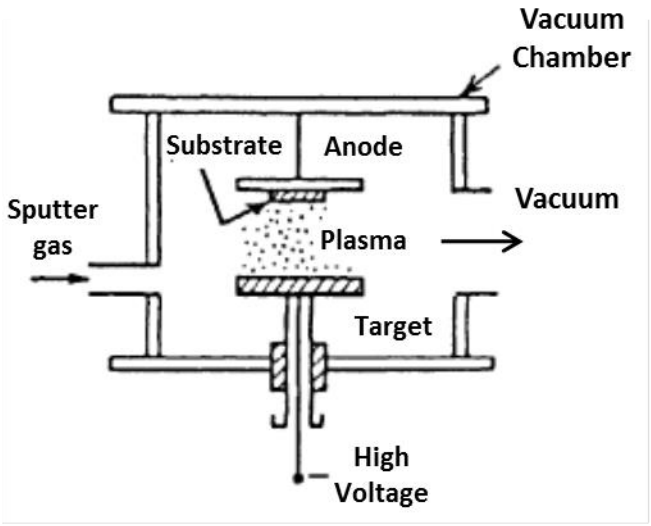

Figure 6.2 DC-diode sputter system. From Ref [13].

When a reactive gas species such as oxygen or nitrogen is introduced into the chamber, thin films of compounds (i.e., oxides or nitrides) are deposited by the sputtering of the appropriate metal targets. This technique is known as reactive sputtering and is used for the high-rate deposition of insulating metal oxide films [13].

Another kind of sputtering system is the magnetron device (Figure 6.3). In magnetron sputtering, a magnetic field is imposed on the cathode and glow discharge, which is parallel to the cathode surface. The electrons in the glow discharge show cycloidal motion, and the center of the orbit drifts in the direction of E×B with the drift velocity of E/B, where E and B denote the electric field in the discharge and the superposed transverse magnetic field, respectively. The magnetic field is oriented such that these drift paths for electrons form a closed loop. This electron trapping effect increases the collision rate between the electrons and the sputtering gas molecules. This allows lowering the sputtering gas pressure until 10^{-5} torr or 10^{-2} torr. In the magnetron sputtering system, the magnetic field increases the plasma density which leads to increases in the current density at the cathode target, effectively increasing the sputtering rate at the target. Due to the low working pressure of the gas, the sputtered particles traverse the discharge space without collisions, which results in a high deposition rate. Nowadays, the planar magnetron is indispensable for the fabrication of semiconductor devices [13].

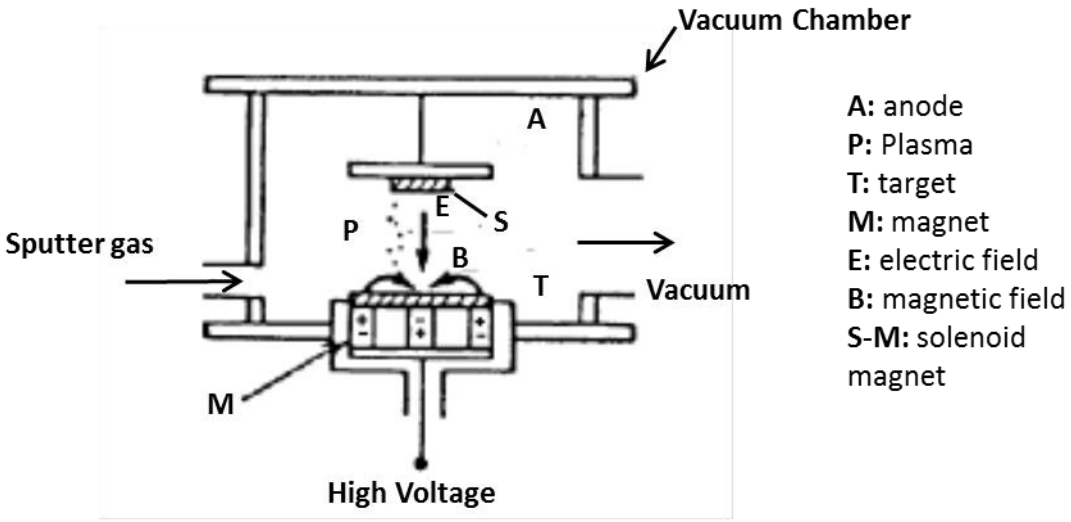

Figure 6.3 Planar Magnetron. From Ref [13].

References

1. Kissinger, P. and W.R. Heineman, *Film Electrodes, In Laboratory Techniques in Electroanalytical Chemistry, Second Edition, Revised and Expanded.* 1996, Taylor & Francis.
2. Gershinsky, G., H.D. Yoo, Y. Gofer, and D. Aurbach, *Electrochemical and Spectroscopic Analysis of Mg^{2+} Intercalation into Thin Film Electrodes of Layered Oxides: V2O5 and MoO3.* Langmuir, 2013. **29**, 10964-10972.
3. Wang, T., D. Zhao, N. Alvarez, V.N. Shanov, and W.R. Heineman, *Optically Transparent Carbon Nanotube Film Electrode for Thin Layer Spectroelectrochemistry.* Analytical Chemistry, 2015. **87**, 9687-9695.
4. Dokko, K., N. Anzue, M. Mohamedi, T. Itoh, and I. Uchida, *Raman spectro-electrochemistry of $LiCo_xMn_2$–xO_4 thin film electrodes for 5 V lithium batteries.* Electrochemistry Communications, 2004. **6**, 384-388.
5. Zhang, Y., S. Kupfer, L. Zedler, J. Schindler, T. Bocklitz, J. Guthmuller, S. Rau, and B. Dietzek, *In situ spectroelectrochemical and theoretical study on the oxidation of a 4H-imidazole-ruthenium dye adsorbed on nanocrystalline TiO_2 thin film electrodes.* Physical Chemistry Chemical Physics, 2015. **17**, 29637-29646.
6. Harrer, S., S. Ahmed, A. Afzali-Ardakani, B. Luan, P.S. Waggoner, X. Shao, H. Peng, D.L. Goldfarb, G.J. Martyna, S.M. Rossnagel, L. Deligianni, and G.A. Stolovitzky, *Electrochemical Characterization of Thin Film Electrodes Toward Developing a DNA Transistor.* Langmuir, 2010. **26**, 19191-19198.
7. Harrer, S., S.C. Kim, C. Schieber, S. Kannam, N. Gunn, S. Moore, D. Scott, R. Bathgate, S. Skafidas, and J.M. Wagner, *Label-free screening of single biomolecules through resistive pulse sensing technology for precision medicine applications.* Nanotechnology, 2015. **26**, 182502.
8. Stefan, H., S.W. Philip, L. Binquan, A.-A. Ali, L.G. Dario, P. Hongbo, M. Glenn, M.R. Stephen, and A.S. Gustavo, *Electrochemical protection of thin film electrodes in solid state nanopores.* Nanotechnology, 2011. **22**, 275304.
9. Maranchi, J.P., A.F. Hepp, and P.N. Kumta, *$LiCoO_2$ and SnO_2 thin film electrodes for lithium-ion battery applications.* Materials Science and Engineering: B, 2005. **116**, 327-340.
10. Yang, Y., Z. Peng, G. Wang, G. Ruan, X. Fan, L. Li, H. Fei, R.H. Hauge, and J.M. Tour, *Three-Dimensional Thin Film for Lithium-Ion Batteries and Supercapacitors.* ACS Nano, 2014. **8**, 7279-7287.
11. Sun, Q., B. Zhang, and Z.-W. Fu, *Lithium electrochemistry of SiO_2 thin film electrode for lithium-ion batteries.* Applied Surface Science, 2008. **254**, 3774-3779.

12. Wasa, K., M. Kitabatake, and H. Adachi, *Thin film materials technology: sputtering of control compound materials.* 2004, William Andrew Pub.
13. Swain, G.M., *Solid Electrode Materials: Pretreatment and Activation,* in *Handbook of Electrochemistry.* Cynthia G, Zoski Ed., 2007, Elsevier, Amsterdam. p. 111-153.

6.2. Appendix B: Reference electrodes

Section 2.4 depicts the development of an original electrochemical device to perform experiments in 50 µL of sample and by using a conventional reference electrode. Because of such electrode is the "heart" of our device, here we present the features that characterize this important tool.

6.2.1. Introduction

Most electrochemical measurements require keeping one of the electrodes in an electrochemical cell at a constant potential [1]. This electrode is called reference electrode (RE) because allows control of the potential of a working electrode (i. e. cyclic voltammetry) or the measurement of an indicator electrode (i. e. potentiometry) [1]. The standard hydrogen electrode (SHE) is the basic reference element in electrochemical systems. It is based in the following reversible equilibrium:

$$H_2 + 2H_2O \rightleftarrows 2H_3O^+ + 2e^- \quad (1)$$

The SHE consists of a platinum wire or a platinum sheet covered with platinum black (platinized) and an electrolyte solution containing hydrogen ions. The hydrogen gas is usually continuously supplied [1]. By convention, the SHE potential (E°) is assigned a value of zero Volts (V) at all temperatures [2]. The potential is calculable using the Nernst equation, expressed in the form:

$$E_{Pt|H_2,H^+} + \frac{RT}{F} ln \frac{a_H}{\sqrt{p_{H_2}}} \quad (2)$$

$$p_{H_2} = P_{barometric} - P_{H_2O} + (4.2 \times 10^{-5})h \quad (3)$$

Where h is the depth of delivery of the H_2 supply to solution (in mm), $P_{barometric}$ the barometric (atmospheric) pressure (in atm), and P_{H2O} the partial pressure of vapor water that can be estimated for dilute solutions as the same as pure water [3]. The ideal experimental conditions for having a SHE require a constant hydrogen pressure of 1 atm, and hydrogen ion activity equal to 1 [3]. These requirements are difficult to attain in practice; thus, either lower concentrations of acid or higher hydrogen pressure are often used [3]. The last provokes the SHE deviates from the defined potential of 0 Volts. As SHE is difficult to handle, other types or reference electrodes are preferred in most experiments, these are called secondary reference electrodes. The chosen secondary RE has to:

(i) Be chemically and electrochemically reversible (i. e. its potential is governed by the Nernst equation and does not change in time).

(ii) Remain its potential must almost constant regardless of current flow through the RE, as well as have a reverse to its original value after the current flow (non-polarizable electrode).

(iii) Have a small thermal coefficient of potential.

Despite there is not RE that fulfills all these properties, some of electrodes are very close to the ideal behavior [1].

The secondary reference electrodes consist of a metal surface coupled to a salt of this metal, such part is known as the active component of a RE (Figure 6.1). That component is placed in contact with an electrolyte solution containing a fixed concentration of the anion of the sparingly soluble salt (known as RE filling solution) [1].

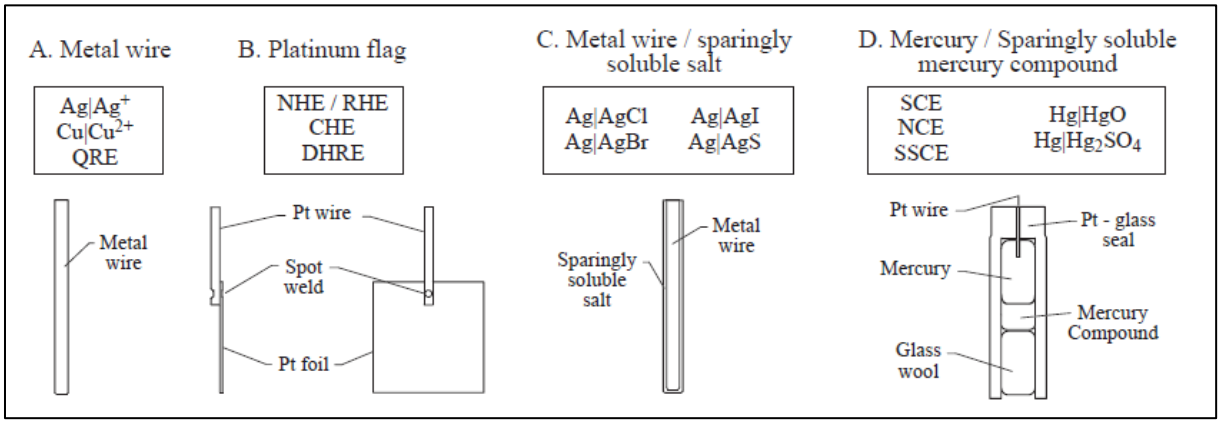

Figure 6.1 Examples of some reference electrode active components: (A) metal wire; (B) platinum flag; (C) metal wire/sparingly salt; (D) mercury/sparingly soluble mercury compound. Figure from reference [3].

It is ideal is both the RE filling solution and the analyzed solution have the same type of electrolytes. However, in many cases this condition is far to be possible, thus, a junction is used to separate both solutions [3]. Some common junctions are (Figure 6.2):

a. **Vycor, polyethylene, or Teflon frit.** The frit material is sealed to the RE body material with heat shrink tubing. The recovery temperature of the heat shrink must be low enough to avoid damage in the frit material.

b. **Ceramic junction.** A ceramic frit is sealed into a glass RE body using standard glass blowing techniques. The ceramic must be held tightly in the glass with no spaces on the sides of the ceramic, otherwise solutions will bypass the ceramic. This type of junction has a very low leak rate.

c. **Glass wool, cellulose pulp; or agar.** These junction materials are filled or wedged into a restricted end of the RE body. The leak rate is adjusted by changing both the type and the density of the material.

d. **Platinum wire, or asbestos fiber.** Here, an imperfect seal is created between the fiber or wire and the RE body. This serve as a leak through which the filling solution interacts with the electrolyte of the electrochemical cell.

e. **Cracked glass bead.** This junction is created fussing a glass bead to a hole in a glass RE body and then initiating a crack at the interface.

f. **Luggin capillary.** A Lugging capillary is constructed by pulling a fine capillary at the end of a glass electrode body. The diameter of such capillary determines the leakage rate of the filling solution.

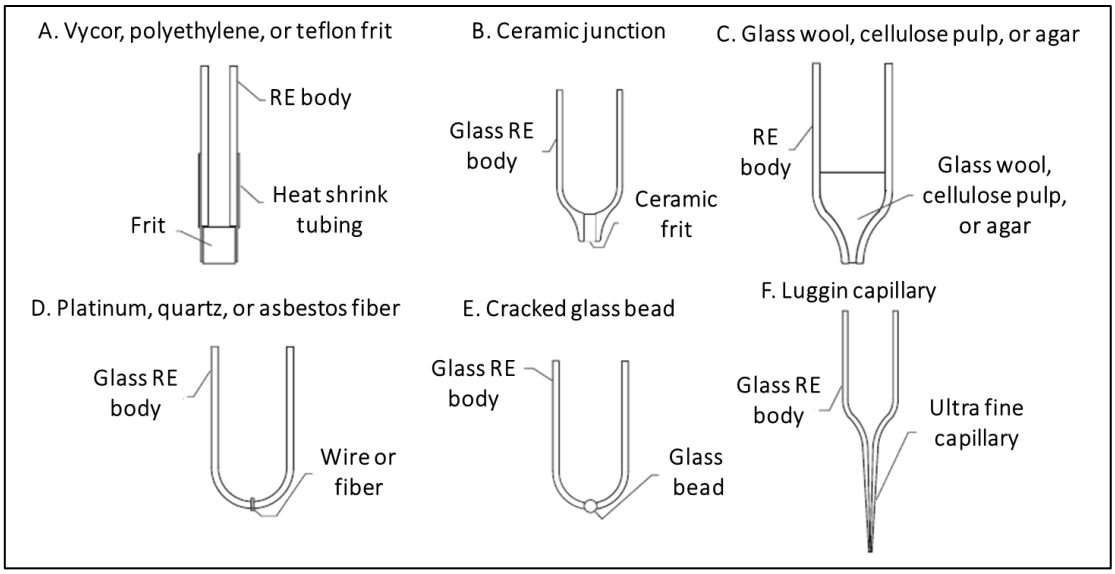

Figure 6.2 Reference electrode junction types: (A) Vycor, polyethylene, or Teflon frit; (B) ceramic junction; (C) glass wool, cellulose pulp, or agar; (D) platinum, quartz, or asbestos fiber; (E) Cracked glass bead; (F) Luggin capillary. Image from reference [3].

There is an important parameter to deal with when using junction systems, this is the junction potential. Such phenomenon appears when two solutions being separated contain either electrolytes with different mobilities, or the same electrolyte in different solvents [3]. The potential drop (ΔV) developed across the junction, is the product of the junction impedance (Z) and the ion flux (or current, *i*) flowing through it. According to the Ohms Law, the potential drop is $\Delta V = iZ$. Thus, it is important to minimize the junction potential, and to ensure that it remains constant during the experiment [3]. As the impedance of junction is controlled by the pore size, the density of the material and the nature of the electrolytes, adjusting these parameters allow minimizing the potential drop [3]. But trying to match the mobilities of anionic and cationic species is not so simple, as occur in highly

acidic or basic solutions due to the high mobilities of hydroxyl and hydronium ions. Because the difficulty of balancing these parameters, alternatives as the employment of high – flow rate junctions or salt bridges are proposed. The use of high – flow rate junctions decreases the impedance, but also increases the amount of filling solution interacting with the sample, which could lead to the mixing of incompatible species [3]. Salt bridges (or double junctions, Figure 6.3) are used to both minimize and stabilize the junction potential between solutions of different compositions as well as minimizing any cross-contamination between them. This second salt bridge may contain in some cases the same electrolyte solution as the reference electrode compartment and the electrochemical cell. But, if the experiment required it, the electrolyte solution may differ from one of the half-cells or both [1]. As salt bridges improve the compatibility between the employed electrolytes, they are often used when working with different solvents [3]. Here, it is important to verify the electrolyte solubility in both solvents, otherwise electrolytes with poor solubility can precipitate in the junction [3]. Indeed, the incorporation of a second junction allows flexibility in the use of a RE in diverse media. Nevertheless, a variety of RE are available to employ in electrochemical experiments. In the following section, we described the function of the calomel electrode, the RE used in the development of our "hanging drop-electrochemical cell".

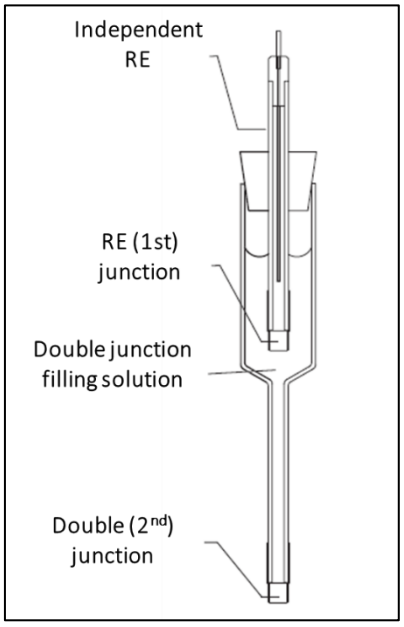

Figure 6.3 Temporary double junction using and independent reference electrode. Image from reference [3].

6.2.2. The calomel electrode

The calomel electrode is the most widely used mercury RE. The preparation of this electrode, in the simplest case, consists on placing a single drop of mercury into a small tube and covering by mercury (I) chloride (calomel Hg_2Cl_2). Another possibility is to fill a small glass tube with a paste of mercury, mercury (I) chloride and potassium chloride solution. The paste is in contact with a potassium chloride solution of constant activity. Mostly, a saturated potassium chloride solution is used and the paste additionally contains solid potassium chloride [9]. Both the preparation method of the RE and the purity of the mercury drop strongly affect the performance and potential exhibited [3]. The electrode controlling process is:

$$Hg^0 + Cl^- \rightleftarrows {}^1/_2 Hg_2Cl_2 + e^- \quad (4)$$

The potential of this electrode against the standard hydrogen electrode is given by the equation:

$$E_{Hg|Hg_2Cl_2} = E^{\circ}_{Hg|Hg_2Cl_2} - \frac{RT}{F} lna_{Cl^-} \quad (5)$$

In equation 5, the potential of the mercury (I) chloride RE is defined by the chloride concentration in the filling solution. For instance, at 25 °C, the potential (mV) displays:

Table 6.1 Electrode potentials of the calomel electrode at different concentrations and at 25 °C [1].

C_{KCl}	0.1 mol L^{-1}	1 mol L^{-1}	Saturated (SCE)
E/mV	333.7	280.1	244.4

The calomel electrode using a saturated potassium chloride solution (saturated calomel electrode, SCE) suffers of a disproportion reaction when is used at temperatures above 35 °C [1]. The reaction takes place according to:

$$Hg_2Cl_2 \rightleftarrows Hg + HgCl_2 \quad (6)$$

The back reaction by cooling down the electrode is very slow so that the electrode displays hysteresis. For this reason the calomel should be used at lower temperatures, in maximum up to 70 °C [1]. The thermal coefficient is smallest for a calomel electrode with 0.1 M KCl, but it is easier to handle the saturated calomel electrode.

References

1. Scholz, F., *Electroanalytical methods, Guide to experiments and applications.* Springer, 2010, 291-308.
2. Oldham, K.B., *Electrochemical science and technology, Fundamental and applications.* Wiley, 2012, 105-123.
3. Smith, T.J. and K.J. Stevenson, *Reference Electrodes,* in *Handbook of Electrochemistry Cynthia G*, *Zoski.* 2007, Elsevier, Amsterdam. p. 73-110.

Résumé

Ce travail de thèse s'intéresse à l'introduction de méthodologies électrochimiques dans la problématique de la caractérisation du transport de peptides pénétrants (CPPs) à travers des membranes phospholipidiques. Malgré leur charge électrique globalement positive, ces peptides sont en effet capables de traverser les bicouches lipidiques de cellules réelles ou artificielles (liposomes) et il n'existe pas à ce jour de mécanisme d'internalisation universellement admis. Dans ce contexte, nous avons dans un premier temps développé des méthodologies visant à détecter des peptides pénétrants marqués par des sondes rédox en optimisant les conditions de volume et de confinement à l'électrode. Parallèlement, nous avons tenté d'observer le passage transmembranaire de ces peptides en utilisant un dispositif dérivé du patch-clamp, dans lequel un morceau (patch)de membrane lipidique est excisé d'une vésicule géante et le suivi du passage assuré par une détection ampérométrique sur ultramicro-électrode à proximité de la membrane. La sensibilité de la technique ampérométrique et le flux de CPP s'avérant faibles, nous nous sommes tournés vers une stratégie associant fluorescence (pour la sensibilité) et commande électrochimique (pour l'extinction de la fluorescence). Dans la mesure où les phospholipides constituent la barrière dynamique à travers laquelle doivent passer les CPPs, nous avons d'abord étudié l'extinction électrochimique de phospholipides marqués par une sonde à la fois rédox et fluorescente, le NBD. Observée sur des vésicules géantes au microscope confocale, la réduction électrochimique a permis l'extinction sélective des phospholipides situés sur le feuillet externe de la vésicule, un résultat que ne permettent ni la réduction par des agents chimiques (dithionite), ni les techniques de « photobleaching ». Cette propriété a été confirmée cette fois-ci pour des CPPs marqués par le NBD qui ont été mis à incuber en présence de vésicules géantes et pour lesquels un essai préliminaire semble confirmer une extinction de fluorescence essentiellement pour les peptides associés au feuillet externe de la vésicule.

Abstract

This PhD work was aimed at introducing electrochemical strategies in the general topic devoted to the characterization of the passage of cell penetrating peptides (CPPs) across phospholipidic membranes. Although positively charged, CPPs are prone to cross lipidic bilayers of real and artificial cells (liposomes) and there is no commonly admitted internalization mechanism so far. Therefore, we first developed electrochemical setups aimed at improving the amperometric detection of redox-tagged CPPs, through optimization of volume and confinement. Additionally, we have made attempts to use patch-clamp inspired setups to monitor the passage of CPPs across a membrane patched from a giant vesicle using ultramicro-electrodes in the close vicinity of the patched membrane. Since the amperometric technique displayed poor sensibility and the flux of CPP was too narrow, we changed our strategy for a methodology coupling fluorescence (for the sensitivity) and an electrochemical command (to achieve fluorescence extinction). Considering that phospholipids are forefront actors of CPP internalization, we first focused on the electrochemical quenching of phospholipids tagged with a probe displaying both redox and fluorescent properties (NBD). Observed on giant unilamellar vesicles (GUVs) with confocal microscopy, the electrochemical reduction of the NBD probe led to the selective extinction of the phospholipids located on the outer leaflet of the vesicle, a selectivity which is not observed using chemical quenchers such as dithionite or photobleaching methods. That property was extended to NBD-tagged CPPs, previously incubated with unlabeled Guvs and that preliminary experiment confirmed that the electrochemical extinction mostly concerned peptides associated to the outer leaflet of the liposome.